Yann Cado

Postdoktor i evolutionen av primordiala magnetfält

Ref nr: SU FV-4638-25-37

Datum för ansökan: 2026-01-20 10:47

Födelsedatum	1991-12-13
E-post	yanncado@ntymail.com
Kön	Man

Frågor

1. *Nuvarande sysselsättning (ange huvudsaklig sysselsättning)*
Anställd vid lärosäte utanför Sverige

2. *Högsta examen*
Doktors-/licentiatsexamen

3. *Från vilket land har du din högsta examen?*
Spanien

4. *Har du din högsta examen från Stockholms universitet?*
Nej

5. *Ange datum när du tog din doktorsexamen*
2023-07-28

6. *NUVARANDE ANSTÄLLNING. Ange arbetsplats och jobbtitel samt när anställningen påbörjades..*
Postdoctoral fellow at the Theoretical High Energy Physics Laboratory (LPTHE) at Sorbonne Université in Paris.
Initiative "Physique des Infinis" grant

7. *REFERENSER. Ange namn, telefon och e-post för 2–3 referenspersoner som kan komma att kontaktas.*
Mariano Quiros, +34634545134, quiros@ifae.es
Christoph Engler, +44 (0) 161 306 6000, christoph.englert@manchester.ac.uk
Tanmoy Modak, +91-680-2227-707, tanmoyy@iiserbpr.ac.in

8. *SPRÅKKUNSKAPER. Beskriv kort dina språkkunskaper.*
English : Fluent (C2)
French : Native
German : Intermediate (B2)
Spanish : Intermediate (B1)

9. *FORSKNINGSPLAN/PROJEKTPLAN. Bifoga din plan som beskriver det tilltänkta projektet.*
Research_statement.pdf

10. *DOKTORSEXAMEN ELLER MOTSVARANDE. Ange doktorsexamen med ämne och lärosäte.*
Degree: Doctor of Science DSc in Physics
Fields of study: high energy physics
Place: Institut de Física d'Altes Energies (IFAE), Universitat Autònoma de Barcelona (UAB), Spain

11. *EXAMENSBEVIS ELLER MOTSVARANDE. Bifoga examensbevis.*
TDR-X7564042-CADO_Yann_David-ECOPIA.pdf

12. *ÅBEROPADE PUBLIKATONER. Publikationer som åberopas till stöd för ansökan kan bifogas här.*
1611.02293v2.pdf

2201.06422v2.pdf

2208.10977v3.pdf

2312.10414v2.pdf

2411.11128v1.pdf

Yann Cado

Postdoktor i evolutionen av primordiala magnetfält

Ref nr: SU FV-4638-25-37

Datum för ansökan: 2026-01-20 10:47

Eget uppladdat CV

Yann Cado
10 rue Pérignon
F-75007 Paris
yanncado@ntymail.com

The Nordic Institute for Theoretical Physics
AlbaNova
Hannes Alfvéns väg 12
114 19 Stockholm, Sweden

Paris, January 20, 2026

Postdoctoral Fellow in Primordial magnetic field evolution

Dear Members of the Search Committee,

I would like to submit my application for the postdoctoral position within the ERC Synergy Grant COSMOMAG. I am currently a postdoctoral researcher at the Theoretical High Energy Physics Laboratory (LPTHE) at Sorbonne Université in Paris. I completed my PhD at IFAE, UAB, in Barcelona, under the supervision of Dr. M. Quirós, following a master's degree at EPFL in Switzerland, in the group of Prof. M. Shaposhnikov.

The scientific expertise and prior work of Profs. A. Brandenburg, C. Caprini, A. Neronov and F. Vazza, which underpin the COSMOMAG project, are closely aligned with my own work. Indeed, a significant part of my research focuses on the generation, evolution and phenomenology of primordial magnetic fields. In particular, I have studied the production of helical (hyper)magnetic fields during inflation through Chern-Simons couplings, and analyzed their survival up to the electroweak phase transition in order to make predictions on baryogenesis. In parallel, I have investigated the non-linear dynamics of gauge-field production during and after inflation, including backreaction effects on the inflaton and fermionic production via the Schwinger effect, with a specific emphasis on preheating. More recently, I carried out a comprehensive analysis of preheating in the R^2-Higgs inflation model, including the full Standard Model $SU(2) \times U(1)$ gauge sector at linear order, showing that the energy transfer during preheating can be dominated by Goldstone modes and identifying the regions of parameter space compatible with the observed baryon asymmetry of the Universe.

All this research has given me a strong familiarity with the magnetohydrodynamic and cosmological framework underlying primordial magnetic fields, from chiral plasma effects and inverse-cascade dynamics to the treatment of primordial fluctuations and their observational signatures. This work relied on the development of an extensive and modular numerical code library I have written to compute multi-field background dynamics, electroweak particle production and Schwinger effects, which I see as a flexible tool that could naturally interface with the theoretical and numerical framework developed within COSMOMAG.

For all these reasons, I believe that joining the group of Prof. Axel Brandenburg would allow me to contribute meaningfully to early-Universe cosmology, while also developing new lines of inquiry at the interface of magnetohydrodynamics, particle physics and cosmology. I would be keen to contribute to COSMOMAG wherever my expertise can be most useful, with a particular interest in the study of primordial magnetic fields at the electroweak scale and their possible observational signatures, including gravitational waves, while remaining fully open to other directions within the project. It would allow me to leverage my experience in particle production in the early-Universe while at the same time giving me the opportunity to interact with researchers outside my current field and to further diversify my research agenda.

I look forward to the possibility of joining your project and pursuing research within the Nordita and Swedish theoretical physics communities. Thank you very much for your consideration.

Yours sincerely,

Yann Cado

Yann Cado

High-energy theorist specializing in particle production after inflation, with expertise in analytical and numerical methods.

Academia

Postdoctoral researcher — *2023-2025*
LPTHE | Sorbonne Université | Paris, France
- Initiative Physique des Infinis grant

Doctor of Science DSc in Physics — *2019-2023*
IFAE | BIST | UAB | Barcelona, Spain
- PREBIST grant, Marie Skłodowska-Curie grant agreement No. 754558

Master of Science MSc in Physics — *2014-2016*
LPPC | EPFL | Lausanne, Switzerland

Bachelor of Science BSc in Physics — *2010-2014*
EPFL | Lausanne, Switzerland
- ERASMUS exchange in Uppsala Universitet, Sweden — *2012-2013*

Teaching

Assistant in General Relativity and Cosmology — *2022-2023*
UAB | Barcelona, Spain

High school teacher — *2018-2019*
Ecole des Arches | Lausanne, Switzerland
- Teaching in mathematics and physics
- Class Responsibility

Assistant in General Physics — *2013-2016*
EPFL | Lausanne, Switzerland

Private tutor — *2007-2023*

Publications

- Y. Cado, M. Gross, Y. Mambrini and K. Olive, Phys. Rev.D **112** (2025) 11, 115027, arXiv:2508.13155 — *2025*
- Y. Cado, C. Englert, T. Modak and M. Quirós, Phys. Rev.D **111** (2025) 2, 023042, arXiv:2411.11128 — *2024*
- Y. Cado, C. Englert, T. Modak and M. Quirós, Phys. Rev.D **109** (2024) 4, 4, arXiv:2312.10414 — *2023*
- Y. Cado and M. Quirós, Phys.Rev.D **108** (2023) 023508, arXiv:2303.12932 — *2023*
- Y. Cado and M. Quirós, Phys.Rev.D **106** (2022) 123527, arXiv:2208.10977 — *2022*
- Y. Cado and M. Quirós, Phys.Rev.D **106** (2022) 055018, arXiv:2201.06422 — *2022*
- Y. Cado, B. von Harling, E. Massó and M. Quirós, JCAP, **07** (2021) 049, arXiv:2102.13650 — *2021*
- Y. Cado and E. Sabancilar, JCAP, **04** (2017) 047, arXiv:1611.02293 — *2017*

Additional

Movie director and screnwriter — *2017-2025*
- Several short films awarded at international festivals

Landscape, portrait and street photographer — *2008-2025*

Pianist — *2002-2025*

Traveler always up for a road trip — *2010-2025*
- 33 countries visited

13.12.1991

Swiss / French

Cat. B

10 rue Pérignon,
75007 **Paris, France**

yanncado@ntymail.com

French ●●●●●
English ●●●●○
Spanish ●●○○○
German ●●○○○

Mathematica ●●●●○
MATLAB ●●●○○
C++ ●●○○○
LaTeX ●●●●○
Office ●●●●○

Research statement

Yann Cado

December 12, 2025

In this document, I give an overview on my past research, carried out during my Master thesis at the *Ecole Polytechnique Fédérale de Lausanne* (EPFL) in Switzerland (2017), my doctoral studies at the *Institut de Física d'Altes Energies* (IFAE) in Barcelona (2019-2023), and my postdoctoral years of research at the *Laboratoire de Physique Théorique et Hautes Energies* (LPTHE) in Paris (since 2023). By now, my work has led to eight papers [1–8], published either by the *Journal of Cosmology and Astroparticle Physics* (JCAP) or by the American Physical Society in *Physical Review D* (PRD) and to a PhD thesis [9].

This document is organized as follows. I begin by providing historical context and an introduction to the problematic, highlighting the main puzzles addressed by my research, namely baryogenesis, inflation and related subjects such as reheating and Higgs physics. Then I briefly explain how helical fields can be generated from inflation, highlighting the main constraints such as the Schwinger effect. This introduction is followed by a discussion of the various models I have developed that connect the inflation paradigm to the need of baryogenesis. I also comment about the light inflaton phenomenology and preheating.

Introduction

The so-called ΛCDM model is today the most elegant and complete model of modern Cosmology. It complements the previous standard model of the Universe's evolution by postulating the existence of Cold Dark Matter (CDM) that accounts for the dynamics of large-scale structures and by adding a tiny cosmological constant Λ that accounts for the actual accelerated expansion detected in 1998 [10, 11]. The theory of Big Bang Nucleosynthesis (BBN), accounting for the birth of the lightest elements, is embedded in this model as well as the description of the Cosmic Microwave Background (CMB) radiation. Last, this model includes a period of tremendous accelerated expansion prior the BBN in order to solve the initial condition problems of the standard model of cosmology and seeds the primordial density perturbations giving rise to the large-scale structure of the Universe that we see today. Denoted as *inflation*, the paradigm was developed in the late 1970s and is today a active field of research [12–17].

By definition the Universe expands adiabatically, therefore a dazzling accelerated expansion, such as inflation, cools it down to absolute zero which is inconsistent with the historic timeline of the Universe as inflation is eventually followed by a thermal plasma leading to BBN. Thus, any inflation model shall come with an explanation on how the Universe reheats afterwards. The reheating details are often overlooked but they can constrain the inflationary model, especially in the perturbative case as it relates the high energy physics of the Universe to the collider phenomenology. If the reheating is non-perturbative, i.e. through an energy transfer that happens at the classical level in the equation of motion before the inflaton decay, we referred to as *preheating*. The inflaton will eventually decay, but in the case of preheating the thermal bath can have much higher temperature that can allow for specific new physics, such as primordial black holes [18], Dark Matter (DM) [19, 20] or baryogenesis [21, 22]. For all these reasons, both reheating and preheating mechanism are nowadays the subject of numerous studies [23–28].

From the point of view of particle physics, the Standard Model (SM) accurately describes particle interactions but does not explain the origin of its content. Its gauge structure implies equal amounts

of matter and antimatter, yet observations show a clear matter dominance. This discrepancy suggests a dynamical early-Universe mechanism creating a matter–antimatter asymmetry, known as *baryogenesis* [29–35].

If the SM Higgs field does not itself play the role of the inflaton, any additional scalar field introduced to drive inflation will generically couple to the Higgs sector, either explicitly at tree level or unavoidably through radiative corrections. As a result, the Higgs field cannot be consistently neglected when studying the cosmological dynamics. This motivates an analysis of inflationary and post-inflationary evolution that includes the Higgs field, while remaining compatible with constraints from collider experiments. In this context, preheating is intrinsically a multi-field phenomenon: interactions between scalar degrees of freedom, including possible non-minimal couplings to gravity, can lead to highly efficient energy transfer after inflation. This remains true even in so-called pure Higgs inflation scenarios, since the dynamics of the Higgs Goldstone modes cannot be ignored, see e.g. Ref. [25].

Therefore, the Higgs field either drives inflation directly, a scenario referred to as Higgs Inflation (HI), or participate in the inflationary dynamics alongside other fields like in one of the best-fitting models of current data [42] which is the R^2-Higgs inflation model where the presence of the R^2 term makes another scalar degree of freedom dynamical and restores up the pure HI model perturbative unitarity to the Planck scale [43–50]. In any case, the models need to address the Higgs *vacuum instability problem* as our current (low-energy) understanding of the Higgs interaction predicts a true vacuum of its potential at an energy scale of $\sim 10^{11}$ GeV that could lead the entire Universe to an unphysical phase. To prevent this catastrophe at such scale, one shall introduce new high-energy physics in the Higgs sector to correct the self-coupling running.

Until now, my research has mainly focused on the computation of the (hyper)magnetic fields generated in such inflationary contexts, either numerically or by simplifying the model to make analytical approximations, in order to find windows of the parameter space for baryogenesis to occur by taking into account the newest observational data and every known constraints.

Baryogenesis during electroweak crossover

It has been shown that a coupling between a pseudoscalar and a gauge field of the form $\phi F_{\mu\nu}\tilde{F}^{\mu\nu}$ generates a magnetic field that is maximally helical at the end of inflation [25,51–54]. On the other hand, helicity in the hypercharge sector can be converted into baryon asymmetry during electroweak (EW) crossover thanks to the chiral anomaly of the SM [55–59]. Putting the pieces together, the observed baryon asymmetry of the Universe (BAU) can be sourced from a $\mathcal{CP}$-violating interaction between the inflaton and the gauge sector. This idea was elaborated in a number of papers, see e.g. [60,61]. In Ref. [1], we apply this mechanism simultaneously to baryonic matter and DM making use of the Asymmetric DM paradigm [62]. We found that both visible and Dark matter present day abundances can be achieved for a wide range of the parameters involved.

Then, in order to stress the possible role of the Higgs in the mechanism of baryogenesis, we coupled, in Refs. [2, 5], the Higgs doublet $\mathcal{H}$ to the ordinary electromagnetic (EM) fields as $|\mathcal{H}|^2 F_{\mu\nu}\tilde{F}^{\mu\nu}$ and we studied the magnetic field generation capabilities during [5] and after [2] inflation. In the former we did a full analytical derivation taking into account the Schwinger effect (see below) and all the other contraints. In the latter, the computation was done numerically in a radiation dominated Universe.

Magnetohydrodynamics

In any case, we must make sure that the helicity produced at the end of inflation survives until the generation of BAU at the electroweak crossover. Soon after inflation, the Universe reheats and a thermal plasma is generated by the decay of the inflaton into the SM particles. Consequently the EW symmetry is

restored until the EW crossover by the appearance of thermal masses and any helicity in the EM sector get converted into hypermagnetic helicity (that will source the chiral anomaly at EW crossover). The latter then interacts with the thermal plasma which, in turn, backreacts on the gauge fields. This system can be described by the so-called magnetohydrodynamics equations [63–65] in which the physical quantities of interest (amplitudes, energy densities, correlation length and helicity) do not scale adiabatically in such an environment, or equivalently their comoving quantities are not constant. Therefore there can be a magnetic diffusion effect leading to the decay of the helicity. If, on the other hand, the magnetic induction is the leading effect, then the helicity can be conserved until the EW crossover and the baryogenesis mechanism can take place. This effect is measured by the magnetic Reynolds number and it is enough to require it bigger than unity at reheating for the helicity to be conserved until the EW crossover. In addition we also have to prevent the chiral plasma instability and the non-Gausiannity issues. The interested reader can find all the constraints and details in Sec. 7 of [3].

The Schwinger effect

The last phenomenon to be under consideration before addressing properly the generation of the BAU is the Schwinger effect. In the presence of strong gauge fields, light fermions charged under the gauge group are produced by the backreaction of gauge fields which source the fermion equations of motion [66–68]. The corresponding currents can then, in turn, backreact on the produced gauge fields. The Schwinger effect hence acts as a damping force in the explosive production of helical gauge fields, and many of the conclusions from the gauge field production should be revised in its presence. In Ref. [3], we considered two semi-analytical methods, namely the Schwinger *maximal estimate* and *equilibrium estimate* [61, 66, 69], and gave the parameter space for successful baryogenesis in both cases. We found a wide range in the axion to gauge field coupling and the reheating temperature for the BAU to be achieved at EWPT.

In a subsequent work, Ref. [4], we performed a deep study of the Schwinger effect by using some numerical methods. We used the fourth order Runge-Kutta algorithm to solve a non trivial integro-differential system that takes into account the backreaction of the produced gauge fields on the inflationary equations of motion, and that of the Schwinger effect on the gauge field production. Our results show that we recover previous analytical results in the slow roll inflation regime by making the same approximations required by an analytical resolution. We then solved the full solution for two classes of inflationary potential, namely the α-attractor and hilltop potentials, and we observed as expected a dampening in the energy density and helicity production. Note that this outcome does not necessarily jeopardize the BAU generation, as a successful baryogenesis does depend on a delicate equilibrium between the amount of helicity, magnetic energy density and magnetic correlation length. Actually, we have found there is still a window in the parameter space for baryogenesis to happen. However, our numerical estimates suggest that the Schwinger effect significantly reduces the share of electromagnetic energy for the considered models and gauge preheating is unlikely to occur. These two comments should be viewed as hints for future studies that address the production of gauge fields at the end of inflation. Of course, a full lattice simulation of the Schwinger effect involving fermions remains to be done.

Light inflaton phenomenology

In Ref. [3] we study a two-field inflation model involving the physical Higgs h and a new scalar ϕ coupled to each other as $\mu\phi h^2$. Like in the Higgs inflation model, where the non-minimal coupling $\xi h^2 R$ induces a flat potential required for slow roll inflation, we study in this work the implication of the coupling $g\phi^2 R$, where R is the Ricci scalar. We show that we can then achieve a slow roll inflation for $g \ll 1$ while preventing the Higgs true vacuum catastrophe at $h \sim 10^{11}$ GeV. Indeed, at low energy scale, when ϕ is integrated out, the Higgs β function gets modified such that a negative self-coupling can be avoided for a

range of values of μ and m_ϕ. On the other hand, at high energy scale, the inflaton dynamics and density perturbation are controlled by the ϕ quartic self-coupling.

An interesting feature of Ref. [3] is that the the mixing ϕ–h can provide a light inflaton candidate that could be detected at the HE-LHC while satisfying all observational constraint and providing a sucessfully inflation epoch. This is because the inflaton mass m_ϕ is decoupled from the inflationary dynamics. With $m_\phi \simeq 1$ TeV, the interaction between both fields, besides solving the vacuum instability, predicts modifications on the trilinear and quartic couplings that could be explored at the HE-LHC, as well as at future colliders, and allows for direct ϕ production at the LHC. Using present results of inclusive cross sections for $\sigma(pp \to H)$ for the leading mechanism of gluon-gluon fusion from CMS and ATLAS (where H stands for the heavy scalar production: in our case the inflaton field), we found a mild bound as $m_\phi \gtrsim 0.55$ TeV at 95% C.L. [70–73], to be improved in the future.

In a subsequent paper [8], we investigated how the interaction $\mu\phi h^2$ constrains the reheating temperature $T_{\rm rh}$. We performed a renormalization group analysis to determine the relative values of μ and m_ϕ such that the Higgs potential remains stable (and perturbative) at high energy. Taking into account the running of the Higgs quartic self-coupling and the experimental constraints from the LHC via the `HiggsTools` public code, we found that 3.4×10^6 GeV $\lesssim T_{\rm rh} \lesssim 3.9 \times 10^{12}$ GeV.

Gravity assisted baryogenesis in R^2-Higgs inflation

In a similar way to prior cases, helical hypermagnetic fields, and therefore the BAU, can also be generated by the dimension-six operator $(R/\Lambda^2)B_{\mu\nu}\widetilde{B}^{\mu\nu}$ in the context of $f(R)$ theories.

In Ref. [6] we adopted the doubly-covariant formalism [23,25,74,75] for both inflationary dynamics and the production of helical gauge fields to show that when the R^2-Higgs inflation model is supplemented by this $\mathcal{CP}$-violating term, the BAU can be obtained for $\Lambda \sim 2 \times 10^{-5}\ M_{\rm Pl}$ with and without the Schwinger effect included. We have primarily focused on the Starobinsky-like (R^2) regime in our linear order analysis. The reheating temperature was left as an open parameter.

In Ref. [7] we studied the implications of the preheating on that model by explicitly computing, for the first time, the reheating time, temperature, and energy without taking them as effective parameters in the model. In addition to the progress done in Ref. [6], we derived the equations of motion and energy densities for the relevant perturbations at linear order which includes the inflationary fields, the $W^\pm$ and Z bosons, the photon, and the three Goldstone fields. The Coulomb gauge was used, as the unitary gauge becomes ill-defined at Higgs zero-crossings, making the Goldstone bosons dynamical. Self-resonance is governed by effective masses that scale differently with non-minimal couplings and evolve over time, influenced by the field-space manifold, metric perturbations, and background spacetime expansion [23,25]. We find the preheating can happen in the scalar, gauge and Goldstone sectors, however, dependent on the value of the nonminimal coupling between the SM Higgs and R.

References

[1] Y. Cado and E. Sabancilar, *Asymmetric Dark Matter and Baryogenesis from Pseudoscalar Inflation*, *JCAP* **04** (2017) 047, [1611.02293].

[2] Y. Cado, B. von Harling, E. Massó and M. Quirós, *Baryogenesis via gauge field production from a relaxing Higgs*, *JCAP* **07** (2021) 049, [2102.13650].

[3] Y. Cado and M. Quirós, *Baryogenesis from combined Higgs – scalar field inflation*, *Phys. Rev. D* **106** (2022) 055018, [2201.06422].

[4] Y. Cado and M. Quirós, *Numerical study of the Schwinger effect in axion inflation*, *Phys. Rev. D* **106** (2022) 123527, [2208.10977].

[5] Y. Cado and M. Quirós, *Baryogenesis from Higgs inflation*, *Phys. Rev. D* **108** (2023) 023508, [2303.12932].

[6] Y. Cado, C. Englert, T. Modak and M. Quirós, *Baryogenesis in R^2-Higgs inflation: The gravitational connection*, *Phys. Rev. D* **109** (2024) 043026, [2312.10414].

[7] Y. Cado, C. Englert, T. Modak and M. Quirós, *Implication of preheating on gravity assisted baryogenesis in R^2-Higgs inflation*, *Phys. Rev. D* **111** (2025) 023042, [2411.11128].

[8] Y. Cado, M. Gross, Y. Mambrini and K. Olive, *Phenomenological constraints on Higgs reheating*, *Phys. Rev. D* **112** (2025) 115027, [2508.13155].

[9] Y. D. Cado, *Baryogenesis and Inflation from the Higgs sector*. PhD thesis, Barcelona, Autonoma U., 2023.

[10] S. Perlmutter, G. Aldering, M. D. Valle, S. Deustua, R. S. Ellis, S. Fabbro et al., *Discovery of a supernova explosion at half the age of the Universe*, *Nature* **391** (1998) 51–54.

[11] P. M. Garnavich, R. P. Kirshner, P. Challis, J. Tonry, R. L. Gilliland, R. C. Smith et al., *Constraints on cosmological models from Hubble Space Telescope observations of high-z supernovae*, *The Astrophysical Journal* **493** (feb, 1998) L53–L57.

[12] A. H. Guth, *The Inflationary Universe: a possible solution to the horizon and flatness problems*, *Phys. Rev. D* **23** (1981) .

[13] A. Linde, *A new inflationary universe scenario: A possible solution of the horizon, flatness, homogeneity, isotropy and primordial monopole problems*, *Phys. Lett. B* **108** (1982) 389.

[14] A. Albrecht and P. Steinhardt, *Cosmology for Grand Unified Theories with radiatively induced symmetry breaking*, *Phys. Rev. Lett.* **48** (1982) 1220.

[15] D. Baumann, *Inflation*, in *Theoretical Advanced Study Institute in Elementary Particle Physics: Physics of the Large and the Small*, pp. 523–686, 2011. 0907.5424. DOI.

[16] D. Langlois, *Lectures on inflation and cosmological perturbations*, *Lect. Notes Phys.* **800** (2010) 1–57, [1001.5259].

[17] B. A. Bassett, S. Tsujikawa and D. Wands, *Inflation dynamics and reheating*, *Rev. Mod. Phys.* **78** (2006) 537–589, [astro-ph/0507632].

[18] M. Riajul Haque, E. Kpatcha, D. Maity and Y. Mambrini, *Primordial black hole reheating*, *Phys. Rev. D* **108** (2023) 063523, [2305.10518].

[19] M. A. G. Garcia, K. Kaneta, Y. Mambrini, K. A. Olive and S. Verner, *Freeze-in from preheating*, *JCAP* **03** (2022) 016, [2109.13280].

[20] S. Clery, Y. Mambrini, K. A. Olive and S. Verner, *Gravitational portals in the early Universe*, *Phys. Rev. D* **105** (2022) 075005, [2112.15214].

[21] P. Adshead, A. J. Long and E. I. Sfakianakis, *Gravitational Leptogenesis, Reheating, and Models of Neutrino Mass*, *Phys. Rev. D* **97** (2018) 043511, [1711.04800].

[22] Y. Cado, T. Modak and E. I. Sfakianakis, *in preparation*, .

[23] M. P. DeCross, D. I. Kaiser, A. Prabhu, C. Prescod-Weinstein and E. I. Sfakianakis, *Preheating after Multifield Inflation with Nonminimal Couplings, I: Covariant Formalism and Attractor Behavior*, *Phys. Rev. D* **97** (2018) 023526, [1510.08553].

[24] M. P. DeCross, D. I. Kaiser, A. Prabhu, C. Prescod-Weinstein and E. I. Sfakianakis, *Preheating after multifield inflation with nonminimal couplings, III: Dynamical spacetime results*, *Phys. Rev. D* **97** (2018) 023528, [1610.08916].

[25] E. I. Sfakianakis and J. van de Vis, *Preheating after Higgs Inflation: Self-Resonance and Gauge boson production*, *Phys. Rev. D* **99** (2019) 083519, [1810.01304].

[26] M. He, R. Jinno, K. Kamada, A. A. Starobinsky and J. Yokoyama, *Occurrence of tachyonic preheating in the mixed Higgs-R^2 model*, *JCAP* **01** (2021) 066, [2007.10369].

[27] F. Bezrukov and C. Shepherd, *A heatwave affair: mixed Higgs-R^2 preheating on the lattice*, *JCAP* **12** (2020) 028, [2007.10978].

[28] M. A. G. Garcia, M. Gross, Y. Mambrini, K. A. Olive, M. Pierre and J.-H. Yoon, *Effects of fragmentation on post-inflationary reheating*, *JCAP* **12** (2023) 028, [2308.16231].

[29] A. Sakharov, *Violation of CP Invariance, C Asymmetry, and Baryon Asymmetry of the Universe*, *Pisma Zh.Eksp.Teor.Fiz.* **5** (1967) 32–35.

[30] A. G. Cohen and D. B. Kaplan, *Spontaneous Baryogenesis*, *Nucl. Phys. B* **308** (1988) 913–928.

[31] A. G. Cohen, D. B. Kaplan and A. E. Nelson, *Progress in electroweak baryogenesis*, *Ann. Rev. Nucl. Part. Sci.* **43** (1993) 27–70, [hep-ph/9302210].

[32] M. Dine and A. Kusenko, *The Origin of the matter - antimatter asymmetry*, *Rev. Mod. Phys.* **76** (2003) 1, [hep-ph/0303065].

[33] J. M. Cline, *Baryogenesis*, in *Les Houches Summer School - Session 86: Particle Physics and Cosmology: The Fabric of Spacetime*, 9, 2006. hep-ph/0609145.

[34] S. Davidson, E. Nardi and Y. Nir, *Leptogenesis*, *Phys. Rept.* **466** (2008) 105–177, [0802.2962].

[35] Planck collaboration, N. Aghanim et al., *Planck 2018 results. VI. Cosmological parameters*, *Astron. Astrophys.* **641** (2020) A6, [1807.06209].

[36] Planck collaboration, Y. Akrami et al., *Planck 2018 results. X. Constraints on inflation*, *Astron. Astrophys.* **641** (2020) A10, [1807.06211].

[37] J. L. F. Barbon and J. R. Espinosa, *On the Naturalness of Higgs Inflation*, *Phys. Rev. D* **79** (2009) 081302, [0903.0355].

[38] C. P. Burgess, H. M. Lee and M. Trott, *Comment on Higgs Inflation and Naturalness*, *JHEP* **07** (2010) 007, [1002.2730].

[39] A. Salvio and A. Mazumdar, *Classical and Quantum Initial Conditions for Higgs Inflation*, *Phys. Lett. B* **750** (2015) 194–200, [1506.07520].

[40] S. Pi, Y.-l. Zhang, Q.-G. Huang and M. Sasaki, *Scalaron from R^2-gravity as a heavy field*, *JCAP* **05** (2018) 042, [1712.09896].

[41] Y. Ema, *Higgs Scalaron Mixed Inflation*, *Phys. Lett. B* **770** (2017) 403–411, [1701.07665].

[42] A. Gundhi and C. F. Steinwachs, *Scalaron-Higgs inflation*, *Nucl. Phys. B* **954** (2020) 114989, [1810.10546].

[43] M. He, A. A. Starobinsky and J. Yokoyama, *Inflation in the mixed Higgs-R^2 model*, *JCAP* **05** (2018) 064, [1804.00409].

[44] D. Gorbunov and A. Tokareva, *Scalaron the healer: removing the strong-coupling in the Higgs- and Higgs-dilaton inflations*, *Phys. Lett. B* **788** (2019) 37–41, [1807.02392].

[45] M. M. Anber and L. Sorbo, *N-flationary magnetic fields*, *Journal of Cosmology and Astroparticle Physics* **0610** (2006) 018, [astro-ph/0606534].

[46] K. Bamba, *Baryon asymmetry from hypermagnetic helicity in dilaton hypercharge electromagnetism*, *Phys. Rev. D* **74** (2006) 123504, [hep-ph/0611152].

[47] K. Bamba, C. Q. Geng and S. H. Ho, *Hypermagnetic Baryogenesis*, *Phys. Lett. B* **664** (2008) 154–156, [0712.1523].

[48] M. M. Anber and L. Sorbo, *Naturally inflating on steep potentials through electromagnetic dissipation*, *Phys. Rev. D* **81** (2010) 043534, [0908.4089].

[49] V. Kuzmin, V. Rubakov and M. Shaposhnikov, *On the Anomalous Electroweak Baryon Number Nonconservation in the Early Universe*, *Phys. Lett. B* **155** (1985) 36.

[50] S. Y. Khlebnikov and M. Shaposhnikov, *The Statistical Theory of Anomalous Fermion Number Nonconservation*, *Nucl. Phys. B* **308** (1988) 885–912.

[51] V. A. Rubakov and M. E. Shaposhnikov, *Electroweak baryon number nonconservation in the early universe and in high-energy collisions*, *Usp. Fiz. Nauk* **166** (1996) 493–537, [hep-ph/9603208].

[52] K. Kamada and A. J. Long, *Baryogenesis from decaying magnetic helicity*, *Phys. Rev. D* **94** (2016) 063501, [1606.08891].

[53] K. Kamada and A. J. Long, *Evolution of the Baryon Asymmetry through the Electroweak Crossover in the Presence of a Helical Magnetic Field*, 1610.03074.

[54] M. M. Anber and E. Sabancilar, *Hypermagnetic Fields and Baryon Asymmetry from Pseudoscalar Inflation*, *Phys. Rev. D* **92** (2015) 101501, [1507.00744].

[55] V. Domcke, B. von Harling, E. Morgante and K. Mukaida, *Baryogenesis from axion inflation*, *JCAP* **10** (2019) 032, [1905.13318].

[56] K. Petraki and R. R. Volkas, *Review of asymmetric dark matter*, *Int. J. Mod. Phys.* **A28** (2013) 1330028, [1305.4939].

[57] M. Giovannini and M. E. Shaposhnikov, *Primordial hypermagnetic fields and triangle anomaly*, *Phys. Rev. D* **57** (1998) 2186–2206, [hep-ph/9710234].

[58] R. Durrer and A. Neronov, *Cosmological Magnetic Fields: Their Generation, Evolution and Observation*, *Astron. Astrophys. Rev.* **21** (2013) 62, [1303.7121].

[59] T. Vachaspati, *Progress on cosmological magnetic fields*, *Rept. Prog. Phys.* **84** (2021) 074901, [2010.10525].

[60] V. Domcke and K. Mukaida, *Gauge Field and Fermion Production during Axion Inflation*, *JCAP* **11** (2018) 020, [1806.08769].

[61] H. Kitamoto and M. Yamada, *Semiclassical analysis of axion-assisted and axion-driven pair production*, *JHEP* **06** (2022) 103, [2109.14782].

[62] T. D. Cohen and D. A. McGady, *The Schwinger mechanism revisited*, *Phys. Rev. D* **78** (2008) 036008, [0807.1117].

[63] E. V. Gorbar, K. Schmitz, O. O. Sobol and S. I. Vilchinskii, *Hypermagnetogenesis from axion inflation: Model-independent estimates*, *Phys. Rev. D* **105** (2022) 043530, [2111.04712].

[64] LHC Higgs Cross Section Working Group collaboration, S. Dittmaier et al., *Handbook of LHC Higgs Cross Sections: 1. Inclusive Observables*, 1101.0593.

[65] LHC Higgs Cross Section Working Group collaboration, D. de Florian et al., *Handbook of LHC Higgs Cross Sections: 4. Deciphering the Nature of the Higgs Sector*, 1610.07922.

[66] ATLAS collaboration, G. Aad et al., *Combination of searches for Higgs boson pairs in pp collisions at $\sqrt{s}$ =13 TeV with the ATLAS detector*, *Phys. Lett. B* **800** (2020) 135103, [1906.02025].

[67] CMS collaboration, A. M. Sirunyan et al., *Combination of searches for Higgs boson pair production in proton-proton collisions at $\sqrt{s}$ = 13 TeV*, *Phys. Rev. Lett.* **122** (2019) 121803, [1811.09689].

[68] J.-O. Gong and T. Tanaka, *A covariant approach to general field space metric in multi-field inflation*, *JCAP* **03** (2011) 015, [1101.4809].

[69] D. I. Kaiser, E. A. Mazenc and E. I. Sfakianakis, *Primordial Bispectrum from Multifield Inflation with Nonminimal Couplings*, *Phys. Rev. D* **87** (2013) 064004, [1210.7487].

Felipe VI, Rey de España

i en nom seu el **y en su nombre el**

Rector de la Universitat Autònoma de Barcelona

UAB Universitat Autònoma de Barcelona

atès que, d'acord amb les disposicions i circumstàncies que preveu la legislació vigent,

considerando que, conforme a las disposiciones y circunstancias previstas por la legislación vigente,

Yann David Cado

que va néixer el dia 13 de desembre de 1991, a Ginebra (Suïssa), de nacionalitat suïssa, ha superat al juliol de 2023 els estudis conduents al títol universitari oficial de

que nació el día 13 de diciembre de 1991, en Ginebra (Suiza), de nacionalidad suiza, ha superado en julio de 2023 los estudios conducentes al título universitario oficial de

Doctor per la Universitat Autònoma de Barcelona

Doctor por la Universitat Autònoma de Barcelona

dins del Programa de Doctorat en Física, establert per Acord de Consell de Ministres de 23 de maig de 2014, expedeix aquest títol oficial amb validesa a tot el territori nacional, que faculta la persona interessada per gaudir dels drets que les disposicions vigents atorguen a aquest títol.

dentro del Programa de Doctorado en Física, establecido por Acuerdo de Consejo de Ministros de 23 de mayo de 2014, expide el presente título oficial con validez en todo el territorio nacional, que faculta a la persona interesada para disfrutar los derechos que a este título otorgan las disposiciones vigentes.

Bellaterra (Cerdanyola del Vallès), 7 de setembre de 2023

Bellaterra (Cerdanyola del Vallès), 7 de septiembre de 2023

La persona interessada,

Yann David Cado

El Rector,

Francisco Javier Lafuente Sancho

El cap de l'Àrea d'Afers Acadèmics,

Joaquín Bernabé Ródenas

022A-095541

Registro Nacional de Títulos	Código de CENTRO	Registro Universitario de Títulos
2023/232686	08071287	274141

SIGNE

Signe M-01/2024

Joaquín Bernabé Ródenas

El cap de l'Àrea d'Afers Acadèmics

amb la qualificació d'EXCEL·LENT,
el dia 28 de juliol de 2023,
que va defensar la seva tesi doctoral
a favor de Yann David Cado,

Anverso del título oficial de Doctor,
expedido en Bellaterra (Cerdanyola del Vallés), el 7 de septiembre de 2023
a favor de Yann David Cado,
que defendió su tesis doctoral
el día 28 de julio de 2023,
con la calificación de SOBRESALIENTE

El cap de l'Àrea d'Afers Acadèmics

Feverso del título oficial de Doctor,
expedit a Bellaterra (Cerdanyola del Vallès), el 7 de setembre de 2023
a favor de Yann David Cado,
que va defensar la seva tesi doctoral
el dia 28 de juliol de 2023,
amb la qualificació d'EXCEL·LENT

CLAVE ALFANUMÉRICA: 022A-095541

Nº REGISTRO NAL. DE TÍTULOS: 2023/232686

CODIGO DE CENTRO: 08071287

REGISTRO UNIV. DE TÍTULOS: 274141

NRO. EXP. UNIV. 1548327079318

Prepared for submission to JCAP

Asymmetric Dark Matter and Baryogenesis from Pseudoscalar Inflation

Yann Cado,[1] **Eray Sabancilar**[1,2]

[1]Laboratory of Particle Physics and Cosmology, Institute of Physics, Ecole Polytechnique Fédérale de Lausanne, CH-1015 Lausanne, Switzerland

[2]Department of Physics, Bielefeld University, D-33615, Bielefeld, Germany

E-mail: yann.cado@epfl.ch, eray.sabancilar@epfl.ch

Abstract. We show that both the baryon asymmetry of the Universe and the dark matter abundance can be explained within a single framework that makes use of maximally helical hypermagnetic fields produced during pseudoscalar inflation and the chiral anomaly in the Standard Model. We consider a minimal asymmetric dark matter model free from anomalies and constraints. We find that the observed baryon and the dark matter abundances are achieved for a wide range of inflationary parameters, and the dark matter mass ranges between 7-15 GeV. The novelty of our mechanism stems from the fact that the same source of CP violation occurring during inflation explains both baryonic and dark matter in the Universe with two inflationary parameters, hence addressing all the initial condition problems in an economical way.

Keywords: asymmetric dark matter, baryogenesis, CP violation, chiral anomaly, pseudoscalar inflation, magnetic helicity

Contents

1 Introduction **1**

2 A Minimal Model of Asymmetric Dark Matter **2**

3 Pseudoscalar Inflation and Asymmetry Generation **3**
- 3.1 Chiral Anomaly 4
- 3.2 Hypermagnetic Fields from Pseudoscalar Inflation 6
- 3.3 Evolution of Hypermagnetic Fields in Plasma 7
- 3.4 Hypermagnetic Helicity 8
- 3.5 Kinetic Equations 8
- 3.6 Results 10

4 Annihilating the Symmetric Component of Dark Matter **11**
- 4.1 Massless γ_D 12
- 4.2 Massive γ_D 13

5 Summary and Discussion **14**

1 Introduction

The curious coincidence between the observed baryon and dark matter abundances lead to the so called asymmetric dark matter (ADM) paradigm, where the dark sector mimics the baryonic one by exhibiting an asymmetry in its abundance of particles over its antiparticles (see e.g., reviews [1, 2]). The basic idea behind the asymmetric dark matter scenario is that the same source of $\mathcal{CP}$ violation that leads to the baryogenesis also feeds into the dark sector, and hence similar abundances are achieved in both. Typically, in such models the dark matter candidate has a mass not so far from the tens of GeV to a few GeV unless there is a huge suppression or enhancement factor for the transfer of the asymmetry. In that sense it is a quite predictive top down approach.

On the cosmological side, it is still not clear what the source of baryon asymmetry of the Universe (BAU) is and at which epoch it occurred. There are vast ways of generating the BAU, but there are only a few testable models (see e.g., νMSM [3, 4]) due to having too many parameters and/or not being in reach for accelerator experiments or cosmological observations.

It has recently been pointed out that $\mathcal{CP}$ violation that occurs during inflation via a coupling of an inflaton to the hypercharge gauge fields via a dimension 5 operator of the form $(\alpha/f)\Phi F_{\mu\nu}\tilde{F}^{\mu\nu}$ leads to a successful baryogenesis[1] [6]. The basic idea is that during inflation there is a non-perturbative production of gauge fields with high occupation numbers leading to coherent maximally helical hypermagnetic fields [7], which in turn sources the well known chiral anomaly in the Standard Model (SM) producing an asymmetry in the SM particle species. The model only depends on two parameters, namely the scale of inflation, $H_{\rm inf}$ and the coupling of the inflaton to the hypercharge gauge fields α. With these basic ingredients, all that is needed to produce the required asymmetries is the SM physics, namely the chiral anomaly. In this work, we generalize this framework to include the generation of asymmetric dark matter and report on a relation between the $\mathcal{CP}$ violation that occurs

[1] Ref. [5] also considered a somewhat similar mechanism using the coupling of inflaton to gravity and by making use of gravitational anomaly.

during pseudoscalar inflation and the observed baryon and dark matter abundances in the Universe. Hence, we propose a mechanism that solves all the initial condition problems including the baryon and dark matter abundances.

This paper is organized as follows. In Sec. 2, we introduce our minimal ADM field content and interactions. We review the chiral anomaly in the SM in Sec. 3.1. We discuss the generation and evolution of maximally helical hypermagnetic fields during pseudoscalar inflation in Sec. 3.2 and Sec. 3.3, respectively, and calculate the rate of change of hypermagnetic helicity that feeds into the chiral anomaly in Sec. 3.4. We introduce the asymmetry parameters and the associated kinetic equations governing their evolution in Sec. 3.5. Our results appear in Sec. 3.6. We discuss various mechanisms for the annihilation of the symmetric part of the ADM in Sec. 4. We conclude with a summary of our results and a discussion in Sec. 5.

We use natural units $c = 1$, $\hbar = 1$ and set the Boltzmann constant $k_B = 1$. We parametrize the flat Friedman-Robertson-Walker (FRW) metric as $\mathrm{d}s^2 = a(\tau)^2(\mathrm{d}\tau^2 - \mathrm{d}\boldsymbol{x}^2)$, where a is the scale factor, τ is the conformal time, which is related to the cosmic time via $\mathrm{d}t = a\mathrm{d}\tau$.

2 A Minimal Model of Asymmetric Dark Matter

Before we discuss the details of the asymmetry generation mechanism, which will follow in Sec. 3, we first introduce the matter content and interactions of the messenger and dark sectors. We consider a minimal asymmetric dark matter model, adopted from Ref. [8], that is suitable for cogenerating an asymmetry in both the SM and ADM sectors from the same source of $\mathcal{CP}$ violation produced during pseudoscalar inflation.

We introduce a messenger sector that includes two left handed fermions, L_1, L_2, which are $\mathrm{SU(2)_L}$ doublets, and two right handed singlets, R_1, R_2, where all of them carry dark lepton global charges, D_{L_1}, D_{L_2}, respectively. The dark sector has two Dirac fermions, X_1, X_2 that are charged under the dark gauge group $\mathrm{U(1)_D}$ and also carry global dark lepton charges D_{L_1}, D_{L_2}, respectively. The fermion content is chosen such that it is minimal to cancel all the gauge anomalies of both the SM and dark gauge sector $\mathrm{U(1)_D}$ as well as the global Witten anomaly [9]. The fermionic field content of this minimal ADM model is summarized in Table 1, and its Lagrangian is given by

$$\mathcal{L}_{\mathrm{ADM}} = iL_i^\dagger \bar{\sigma}^\mu D_\mu^L L_i + iR_i^\dagger \sigma^\mu D_\mu^R R_i + i\bar{X}_i \gamma^\mu D_\mu^X X_i - \frac{1}{4} C_{\mu\nu} C^{\mu\nu} + \mathcal{L}_{\mathrm{Yuk}}\,, \tag{2.1}$$

where $\bar{\sigma}^\mu = (1, -\boldsymbol{\sigma})$, $\sigma^\mu = (1, \boldsymbol{\sigma})$, $\{\sigma^i\}$ are Pauli matrices, $\{\gamma^\mu\}$ are Dirac matrices,

$$D_\mu^L = \partial_\mu + ig_{\mathrm{y}} Y_{L_i} A_\mu + ig_{\mathrm{w}} \frac{\sigma^a}{2} W_\mu^a + ig_D C_\mu\,, \tag{2.2a}$$

$$D_\mu^R = \partial_\mu + ig_{\mathrm{y}} Y_{R_i} A_\mu + ig_D C_\mu\,, \tag{2.2b}$$

$$D_\mu^X = \partial_\mu + ig_D C_\mu\,, \tag{2.2c}$$

$A_\mu, {W_\mu}^a, C_\mu$ are the $\mathrm{U(1)_Y}$ hypercharge, $\mathrm{SU(2)_L}$ weak and $\mathrm{U(1)_D}$ dark gauge fields, respectively, and $g_{\mathrm{y}}, g_{\mathrm{w}}, g_D$ are the corresponding gauge couplings. The Yukawa Lagrangian is given by

$$\mathcal{L}_{\mathrm{Yuk}} = y_{L_1} L_1^\dagger H^c R_1 + y_{L_2} L_2^\dagger H R_2 + y_{XL_1} L_1^\dagger H X_1^R + y_{XL_2} L_2^\dagger H^c X_2^R + \mathrm{h.c.}\,, \tag{2.3}$$

the Higgs doublet, H, and its conjugate

$$H = \begin{pmatrix} H^+ \\ H^0 \end{pmatrix}\,, \qquad H^c = i\sigma_2 H^* = \begin{pmatrix} {H^0}^\dagger \\ -H^- \end{pmatrix}\,. \tag{2.4}$$

Fermions			Gauge charges				Global charges	
	field	handedness	I_3	Y	Q	Q_D	D_{L_1}	D_{L_2}
Messenger	L_1^u	left	1/2	1	1	1	1	0
	L_1^d	left	-1/2	1	0	1	1	0
	R_1	right	0	2	1	1	1	0
	L_2^u	left	1/2	-1	0	-1	0	1
	L_2^d	left	-1/2	-1	-1	-1	0	1
	R_2	right	0	-2	-1	-1	0	1
DM	X_1	both	0	0	0	1	1	0
	X_2	both	0	0	0	-1	0	1

Table 1. Messenger and dark sector fermion content, their chiralities and local and global charges. Weak isospin, I_3, hypercharge, Y, and electromagnetic charge, Q, are the SM electroweak $\mathrm{SU(2)_L} \times \mathrm{U(1)_Y}$ charges, whereas Q_D is the gauged dark $\mathrm{U(1)_D}$ charge. All the fermions have dark lepton-like charges given by D_{L_1} and D_{L_2}. We use the convention $Q = I_3 + Y/2$.

have hypercharges $Y_H = 1$ and $Y_{H^c} = -1$, respectively,

The messenger states

$$L_i = \begin{pmatrix} L_i^u \\ L_i^d \end{pmatrix} \tag{2.5}$$

are much more massive than the DM states, X_i, hence, they can decay via the following channels:

$$L_1 \longrightarrow X_1^R + H\,, \qquad L_2 \longrightarrow X_2^R + H^c\,. \tag{2.6}$$

These are the only decays that conserve all the charges in Table 1. As we will show in Sec. 3, an asymmetry is first generated in the messenger sector, and then gets transferred to the dark sector via the decays given in Eq. (2.6). Once the asymmetry is generated for the right-handed component of X_i, the dark gauge interaction $\mathrm{U(1)_D}$ equilibrates the left and right handed dark fermions. Since the decay rate

$$\Gamma_{L_i \to X_i^R + H} \sim \frac{1}{8\pi} y_{X L_i} m_L\,, \tag{2.7}$$

is much larger than the Hubble rate $H \sim T^2/M_{\rm pl}$ for messenger masses of $m_L \sim 1$ TeV, for instance, we will consider that the asymmetry generated in the messenger sector gets quickly converted into the dark matter states. Hence, we assume that the number densities are related as $n_{X_i} = n_{L_i}$ in what follows.

In addition to the asymmetric component of the ADM, there will be a symmetric part that is thermally produced. In order to annihilate the symmetric component efficiently, we will consider two scenarios, where the $\mathrm{U(1)_D}$ dark photons can be massless or massive. We will discuss both cases in detail in Sec. 4. We will now present our proposed co-generation mechanism in detail in the following section.

3 Pseudoscalar Inflation and Asymmetry Generation

The asymmetry in both the SM and the messenger sector is generated via the coupling of the hypercharge gauge field to a pseudoscalar inflaton as was studied in Ref. [6] for baryogenesis. The

Lagrangian that we will consider has the form

$$\mathcal{L} = \frac{1}{2}(\partial_\mu \Phi)^2 - V(\Phi) - \frac{1}{4} Y_{\mu\nu} Y^{\mu\nu} - \frac{\alpha}{4f} \Phi Y_{\mu\nu} \tilde{Y}^{\mu\nu} \,, \tag{3.1}$$

where Φ is a pseudoscalar inflaton field, $V(\Phi)$ is a flat potential satisfying the slow-roll conditions, $Y_{\mu\nu}$ is the hypercharge field strength, α is a dimensionless coupling, and f is the axion constant of dimension mass.

As the inflaton slow-rolls, it provides a time dependent background to populate the modes of the hypercharge gauge fields due to the dimension-5 coupling given in Eq. (3.1). Besides, since the inflaton under consideration is a pseudoscalar, it will only lead to over abundance in a given helicity mode of the gauge fields. Hence, as a result, hypermagnetic fields that are coherent over the horizon scale at the given epoch are produced with net Chern-Simons density (or magnetic helicity) that breaks $\mathcal{CP}$ macroscopically [7] (see also Refs. [10–14]). It has been recently noted in Ref. [6] that such hypermagnetic fields can source the baryon asymmetry of the Universe through the chiral anomaly in the Standard Model as all the Sakharov criteria [15] are satisfied in this process (see also Refs. [16–45] for the evolution of hypermagnetic fields and their effect on particle asymmetries). It was found that the observed baryon asymmetry can be easily achieved in a generic set of inflaton parameters, i.e., the Hubble rate during inflation $H_{\rm inf}$ and the coupling of the inflaton to the hypercharge field, α. In this work, we extend this mechanism to include a messenger sector that carries both dark and SM charges so that we can relate the observed dark matter and baryon abundances in the Universe to a single source of $\mathcal{CP}$ violation generated during inflation.

As the messenger sector fermions carry the SM charges, hence the hypercharge, there will be an accompanying asymmetry in L_i and R_i fermions. Subsequently, the decay of L_i leads to the transfer of this asymmetry into the dark fermions X_i. To set our notation, we will briefly go over the chiral anomaly in the SM, review how the helical hypermagnetic fields are generated during inflation, discuss how they evolve in the primordial plasma and finally derive the the kinetic equations governing the evolution of asymmetries in particle species in the SM, messenger and dark sectors. We present our main results at the end of this section.

3.1 Chiral Anomaly

Since the SM has chiral fermions, there is a chiral anomaly associated with each species, both gauge and global [46]. The gauge anomaly is terminal, but it is cancelled in the SM [46]. However, there remains a global anomaly, namely the baryon, B, and lepton, L, numbers are separately anomalous in the SM so do the additional global dark charges D_{L_1}, D_{L_2} for the messenger sector that we have introduced. To put it in a compact form, each species that are charged under the SM gauge groups exhibit the chiral anomaly given as (see e.g., Ref. [6] or appendix of Ref. [18] for the full set of anomaly equations)

$$\partial_\mu j^\mu_f = C^f_{\rm y} \frac{\alpha_{\rm y}}{16\pi} Y_{\mu\nu} \tilde{Y}^{\mu\nu} + C^f_{\rm w} \frac{\alpha_{\rm w}}{8\pi} W^a_{\mu\nu} \tilde{W}^{a\,\mu\nu} + C^f_{\rm s} \frac{\alpha_{\rm s}}{8\pi} G^a_{\mu\nu} \tilde{G}^{a\,\mu\nu}, \tag{3.2}$$

where the coefficients C^f_j are given in Table 2 for all the chiral fermions in the SM and the messenger sector for the corresponding SM gauge groups. α_j's are the fine structure constants of the corresponding SM gauge groups, $\alpha_j = g_j^2/(4\pi)$.

The currents associated with the baryon and lepton numbers in terms of the individual fermionic

f	$C_{\rm y}^f$	$C_{\rm w}^f$	$C_{\rm s}^f$
q	$N_{\rm c}N_{\rm w}y_q^2$	$N_{\rm c}$	$N_{\rm w}$
ℓ	$N_{\rm w}y_\ell^2$	1	0
u_R	$-N_{\rm c}y_{u_R}^2$	0	-1
d_R	$-N_{\rm c}y_{d_R}^2$	0	-1
e_R	$-y_{e_R}^2$	0	0
L_i	$N_{\rm w}y_{L_i}^2$	1	0
R_i	$-y_{R_i}^2$	0	0

Table 2. Coefficients C_j^f in Eq. (3.2). The multiplicities $N_{\rm c}=3$ and $N_{\rm w}=2$ take into account the color and weak isospin states of a given family of leptons and quarks, and the SM hypercharges are $y_q=1/3$, $y_\ell=-1$, $y_{u_R}=4/3$, $y_{d_R}=-2/3$, $y_{e_R}=-2$. The charge conjugates q^c, ℓ^c, u_R^c, d_R^c, e_R^c, L_i^c and R_i^c have the same coefficients, C_j^f, with all the signs flipped.

currents are

$$j_B^\mu = \frac{1}{3}\sum_{i=1}^{3}\left(j_{q^i}^\mu + j_{u_R^i}^\mu + j_{d_R^i}^\mu\right), \tag{3.3a}$$

$$j_L^\mu = \sum_{i=1}^{3}\left(j_{\ell^i}^\mu + j_{e_R^i}^\mu\right), \tag{3.3b}$$

and for the both dark lepton like numbers

$$j_{L_D^i}^\mu = j_{L_i}^\mu + j_{R_i}^\mu + j_{X_i}^\mu . \tag{3.4}$$

We note that all these currents are anomalous, and thus not conserved:

$$\frac{1}{N_g}\partial_\mu j_B^\mu = \frac{1}{N_g}\partial_\mu j_L^\mu = \partial_\mu j_{L_D^i}^\mu = \frac{\alpha_{\rm w}}{8\pi}W_{\mu\nu}^a\tilde{W}^{\mu\nu\,a} - \frac{\alpha_{\rm y}}{8\pi}Y_{\mu\nu}\tilde{Y}^{\mu\nu}, \tag{3.5}$$

where $N_g=3$ is the number of generations in the SM. There is an accidental conserved current, $\partial_\mu j_{B-L}^\mu = 0$ in the SM, which has important consequences for the baryon asymmetry of the Universe, namely, baryons can be converted into leptons and vice versa with the selection rule $3\,\Delta N_L = \Delta N_B$ since any baryon number violation is compensated by a lepton number violation [46]. Similarly, $\partial_\mu j_{L_D^1-L_D^2}^\mu = 0$ in our setup due to the similarity of the fermionic field content, hence,

$$3\,\Delta N_{L_D^i} = 3\,\Delta N_L = \Delta N_B. \tag{3.6}$$

Moreover it trivially follows that all the gauge currents [47]

$$j_{\rm y}^\mu = \sum_{\text{particles}} Y_\psi\bar{\psi}\gamma^\mu\psi\,, \tag{3.7a}$$

$$j_{\rm w}^{\mu\,a} = \sum_{\text{left particles}} \bar{\psi}_i\tau_{ij}^a\gamma^\mu\psi_j\,, \tag{3.7b}$$

$$j_{\rm s}^{\mu\,a} = \sum_{\text{quarks}} \bar{\psi}_i\eta_{ij}^a\gamma^\mu\psi_j\,, \tag{3.7c}$$

$$j_{Q_D}^\mu = \sum_{\text{dark particles}} Q_\psi^D\bar{\psi}\gamma^\mu\psi\,, \tag{3.7d}$$

with τ_{ij}^a, η_{ij}^a the generators of $\mathrm{SU}(2)_{\rm L}$, $\mathrm{SU}(3)_{\rm c}$ respectively, are not anomalous, i.e., $\partial_\mu j_{\rm y}^\mu = \partial_\mu j_{\rm w}^{\mu\,a} = \partial_\mu j_{\rm s}^{\mu\,a} = \partial_\mu j_{Q_D}^\mu = 0$, which ensure that unitarity is not violated. It is well known that the non-Abelian gauge theories have topologically distinct degenerate vacua, transition between which leads

to the change of baryon, lepton and dark lepton numbers. However, we stress that $\mathrm{U}(1)_{\mathrm{Y}}$ sector can also source the chiral anomaly provided that there is a net $Y_{\mu\nu}\tilde{Y}^{\mu\nu}$, e.g., hypermagnetic fields with net helicity. In other words, in the Abelian case, the magnetic helicity is the Abelian Chern-Simon number. We will explain next how such field configurations are produced during inflation.

3.2 Hypermagnetic Fields from Pseudoscalar Inflation

In this section, we summarize the generation of helical hypermagnetic fields during pseudoscalar inflation to set the notation and to make the paper self contained, see Ref. [7] for details.

The equation of motion for the hypercharge field strength $Y_{\mu\nu}$ derived from Eq. (3.1) is

$$g_{\mu\nu}\nabla^{\mu}Y^{\nu\rho} = -\frac{\alpha}{f}g_{\mu\nu}(\nabla^{\mu}\Phi)\tilde{Y}^{\nu\rho}\,, \tag{3.8}$$

where $g_{\mu\nu}$ is the flat FRW metric and ∇^{μ} is the corresponding covariant derivative. Using the radiation gauge $A_0 = 0$, $\boldsymbol{\nabla}\cdot\boldsymbol{A} = 0$, we obtain the equation of motion for the gauge field as

$$\left(\frac{\partial^2}{\partial\tau^2} - \nabla^2 - \frac{\alpha}{f}\frac{\partial\Phi}{\partial\tau}\,\boldsymbol{\nabla}\times\right)\boldsymbol{A} = 0\,, \tag{3.9}$$

where the terms involving $\boldsymbol{\nabla}\Phi$ drop out due to the homogeneity of the inflaton field. In this gauge, the hyperelectric and hypermagnetic fields are respectively given by $\boldsymbol{E} = -\partial_{\tau}\boldsymbol{A}/a^2$ and $\boldsymbol{B} = \boldsymbol{\nabla}\times\boldsymbol{A}/a^2$, where a is the scale factor in the FRW universe. We promote the vector potential to a quantum operator in the Heisenberg picture

$$\hat{\boldsymbol{A}}(\tau,\boldsymbol{x}) = \sum_{\lambda=\pm}\int\frac{\mathrm{d}^3k}{(2\pi)^{3/2}}\left[\boldsymbol{\epsilon}_{\lambda}\hat{a}_{\lambda}(\boldsymbol{k})A_{\lambda}(\tau,\boldsymbol{k})\mathrm{e}^{i\boldsymbol{k}\cdot\boldsymbol{x}} + \boldsymbol{\epsilon}^{*}_{\lambda}\hat{a}^{\dagger}_{\lambda}(\boldsymbol{k})A^{*}_{\lambda}(\tau,\boldsymbol{k})\mathrm{e}^{-i\boldsymbol{k}\cdot\boldsymbol{x}}\right], \tag{3.10}$$

where we used the circular polarization basis $\boldsymbol{\epsilon}_{\pm}$ that obey to the properties $\boldsymbol{k}\cdot\boldsymbol{\epsilon}_{\pm} = 0$, and $\boldsymbol{k}\times\boldsymbol{\epsilon}_{\pm} = \mp i|\boldsymbol{k}|\boldsymbol{\epsilon}_{\pm}$, such that $|\boldsymbol{\epsilon}_{\pm}|^2 = 1$. Defining a parameter

$$\xi = \frac{\alpha\dot{\phi}_0}{2fH_{\mathrm{inf}}}\,, \tag{3.11}$$

and using the fact that $a(t) = \mathrm{e}^{H_{\mathrm{inf}}t}$ during inflation we obtain

$$\frac{\partial^2 A_{\pm}}{\partial\tau^2} + k\left(k \mp \frac{2\xi}{\tau}\right)A_{\pm} = 0\,. \tag{3.12}$$

We distinguish three cases that lead to solutions with different asymptotic behaviors. At early times, when $|k\tau| \gg |2\xi|$, the solution is a vacuum mode, hence a free wave $A_{\pm} = \mathrm{e}^{-ik_0\tau}/\sqrt{2}$. When $|k\tau| \sim |2\xi|$ the field develops an instability. Depending on the sign of ξ, either A_+ or A_- modes will be amplified ($\xi \gtrless 0 \Leftrightarrow A_{\pm}$ amplified). In the limit $|k\tau| \ll |2\xi|$ the solution for the growing mode is given by [7]

$$A_{\pm} \cong \frac{1}{\sqrt{2k}}\left(\frac{k}{2\xi\; a(\tau)H_{\mathrm{inf}}}\right)^{1/4}\mathrm{e}^{\pi\xi - 2\sqrt{2\xi k/[a(\tau)H_{\mathrm{inf}}]}}\,. \tag{3.13}$$

whereas the other mode is exponentially suppressed. Note that due to the $\mathrm{e}^{\pi\xi}$ factor, the gauge potential grows tremendously for moderate values of $\xi \geqslant 1$.

3.3 Evolution of Hypermagnetic Fields in Plasma

We assume instant reheating so that immediately after inflation the Universe becomes filled with a plasma of relativistic particles. Therefore, the evolution of hypermagnetic and hyperelectric fields are governed by the relevant magnetohydrodynamics (MHD) equations [20]

$$\frac{\partial \boldsymbol{B}}{\partial t} = -\boldsymbol{\nabla} \times \boldsymbol{E}\,, \tag{3.14a}$$

$$\frac{\partial \boldsymbol{E}}{\partial t} + \boldsymbol{J} = \boldsymbol{\nabla} \times \boldsymbol{B}\,, \tag{3.14b}$$

$$\boldsymbol{\nabla} \cdot \boldsymbol{B} = 0\,, \tag{3.14c}$$

$$\boldsymbol{\nabla} \cdot \boldsymbol{E} = \rho\,, \tag{3.14d}$$

$$\boldsymbol{\nabla} \cdot \boldsymbol{J} = 0\,, \tag{3.14e}$$

$$\boldsymbol{J} = \sigma(\boldsymbol{E} + \boldsymbol{v} \times \boldsymbol{B})\,, \tag{3.14f}$$

where $\boldsymbol{v}$ is the plasma fluid velocity and $\sigma \simeq 100T$ is the hypercharge conductivity [48]. Assuming a neutral plasma, $\rho = 0$, with sufficiently slowly varying hyperelectric field such that $\partial_t \boldsymbol{E} = 0$, and combining equations (3.14a), (3.14b) and (3.14f), we obtain the evolution equations for the hypermagnetic fields

$$\frac{\partial \boldsymbol{B}}{\partial t} = \boldsymbol{\nabla} \times (\boldsymbol{v} \times \boldsymbol{B}) + \frac{1}{\sigma}\nabla^2 \boldsymbol{B}\,, \tag{3.15a}$$

$$\boldsymbol{E} = \frac{1}{\sigma}(\boldsymbol{\nabla} \times \boldsymbol{B}) - \boldsymbol{v} \times \boldsymbol{B}\,. \tag{3.15b}$$

The former equation states that the time evolution of the hypermagnetic field depends on an advection term and a dissipation term when the hyperconductivity is finite. The Reynolds number $\mathcal{R}$ is defined as the ratio of these two terms in the Fourier space

$$\mathcal{R} = \frac{v\sigma}{k_p}\,, \tag{3.16}$$

where k_p is the last mode that exits the horizon after inflation

$$k_p \simeq \frac{H_{\rm inf}}{\xi}\frac{T}{T_{\rm rh}}\,. \tag{3.17}$$

For $\mathcal{R} < 1$ the hypermagnetic field will quickly dissipate as the dissipation term dominates whereas for $\mathcal{R} > 1$ a turbulent flow will be generated, and hence, the magnetic field will be sustained. Assuming instant reheating, the reheating temperature can be estimated as

$$T_{\rm rh} \simeq \frac{1}{4}\sqrt{M_{\rm pl} H_{\rm inf}}\,, \tag{3.18}$$

and thus,

$$\mathcal{R} = 25 v \xi \sqrt{\frac{M_{\rm pl}}{H_{\rm inf}}}, \tag{3.19}$$

which is much bigger than unity for velocities [6]

$$v > \frac{10^{-5}}{\xi}\sqrt{\frac{H_{\rm inf}}{10^{14}\ {\rm GeV}}}\,. \tag{3.20}$$

We therefore consider the plasma as turbulent in what follows. In the next section, we show that this condition leads to conservation of helicity of the maximally helical hypermagnetic fields generated during inflation.

3.4 Hypermagnetic Helicity

Hypermagnetic helicity feeds into the chiral anomaly and eventually sources the baryon and dark matter asymmetries. We can deduce the useful relation from Eq. (3.15b)

$$\boldsymbol{E}\cdot\boldsymbol{B}=\frac{1}{\sigma}\boldsymbol{B}\cdot\boldsymbol{\nabla}\times\boldsymbol{B}\,, \tag{3.21}$$

where we used $\boldsymbol{B}\cdot\boldsymbol{v}\times\boldsymbol{B}=0$.

The magnetic helicity is defined as

$$\mathcal{H}=\int \mathrm{d}^3x\ \boldsymbol{A}\cdot\boldsymbol{B}\,. \tag{3.22}$$

Using the MDH equations and relation (3.21), we obtain the rate of change of the spatially averaged helicity density as

$$\frac{\partial h}{\partial t}=-\lim_{V\to\infty}\frac{2}{\sigma V}\int_V \mathrm{d}^3x\ \boldsymbol{B}\cdot\boldsymbol{\nabla}\times\boldsymbol{B}\,. \tag{3.23}$$

Using Eq. (3.10), we obtain the spatially averaged quantity of interest

$$\langle\boldsymbol{B}\cdot\boldsymbol{\nabla}\times\boldsymbol{B}\rangle_{\rm inf}=\frac{1}{a^5}\int\frac{\mathrm{d}^3k|\boldsymbol{k}|^3}{(2\pi)^3}\left(|A_+|^2-|A_-|^2\right)\,, \tag{3.24}$$

where the integral is over the comoving momenta $\boldsymbol{k}$. Note that only one of the modes $A_\pm$ is amplified as shown in the previous section. Thus, the produced field has maximal helicity. After setting one of the modes to zero and using Eq. (3.13), we obtain[2] [6]

$$\langle\boldsymbol{B}\cdot\boldsymbol{\nabla}\times\boldsymbol{B}\rangle=\ \pm I\frac{H^5\mathrm{e}^{2\pi\xi}}{\xi^6}\,, \tag{3.25}$$

where $I=6.848\cdot10^{-4}$ and the overall sign depends on the choice of the mode $A_\pm$, respectively. Here, we cut off the integral at $k_c\simeq2\xi Ha(\tau)$ in order to be in the range of validity of the expression for $A_\pm$. When performing the integral, we ignored residual terms that are proportional to $\xi^{-1}\mathrm{e}^{-8\xi}$ as they are exponentially suppressed since $\xi\gg|k\tau|$. Therefore, at the end of inflation, the change of helicity finally reads [6]

$$\frac{\partial h}{\partial t}=\mp2I\frac{\mathrm{e}^{2\pi\xi}}{\sigma\xi^6}\left(\frac{H_{\rm inf}}{a}\right)^5\,, \tag{3.26}$$

Here, cosmological redshift has been taking into account and the scale factor has been normalized such that it is one at the end of inflation. We note that to generate baryons rather than antibaryons, the negative sign has to be chosen, corresponding to the mode A_+ as we will see in the next section.

3.5 Kinetic Equations

The set of kinetic equations is found by integrating the anomaly equations (3.2) over spacetime. The number density of a given particle species in terms of a current reads

$$n_i=\lim_{V\to\infty}\frac{1}{V}\int_V \mathrm{d}^3x\ j_i^0\,, \tag{3.27}$$

and defining the asymmetry parameter of a given species as

$$\eta_f=\frac{n_f-n_{\bar f}}{s}\,, \tag{3.28}$$

[2]We note that the the produced hypermagnetic fields are maximally helical saturating the realizability condition $h_{\rm M}(k)\leqslant 2e_{\rm M}(k)/k$ (see e.g., Ref. [49]). Here, for instance for a given helicity mode, say A_+, the following relations are always satisfied: $\int\mathrm{d}k\ h_{\rm M}(k)\equiv\frac{1}{V}\int_V\mathrm{d}^3x\ \langle\boldsymbol{A}\cdot\boldsymbol{B}\rangle=\int\mathrm{d}k\ k^3\ |A_+|^2$ whereas $\int\mathrm{d}k\ e_{\rm M}(k)\equiv\frac{1}{V}\int_V\mathrm{d}^3x\ \frac{1}{2}\ \langle\boldsymbol{B}^2\rangle=\frac{1}{2}\int\mathrm{d}k\ k^4\ |A_+|^2$.

where, s is the entropy density. The relevant asymmetry parameters for the SM and messenger sector fermions are

$$\eta_q = \frac{1}{6s} N_{\rm g}^{\rm SM} N_{\rm w} N_{\rm c} \mu_q T^2 \,, \tag{3.29a}$$

$$\eta_\ell = \frac{1}{6s} N_{\rm g}^{\rm SM} N_{\rm w} \mu_\ell T^2 \,, \tag{3.29b}$$

$$\eta_{u_R} = \frac{1}{6s} N_{\rm g}^{\rm SM} N_{\rm c} \mu_{u_R} T^2 \,, \tag{3.29c}$$

$$\eta_{d_R} = \frac{1}{6s} N_{\rm g}^{\rm SM} N_{\rm c} \mu_{d_R} T^2 \,, \tag{3.29d}$$

$$\eta_{e_R} = \frac{1}{6s} N_{\rm g}^{\rm SM} \mu_{e_R} T^2 \,, \tag{3.29e}$$

$$\eta_L = \frac{1}{6s} N_{\rm g}^{\rm DM} N_{\rm w} \mu_L T^2 \,, \tag{3.29f}$$

$$\eta_R = \frac{1}{6s} N_{\rm g}^{\rm DM} \mu_R T^2 \,, \tag{3.29g}$$

where $N_{\rm g}^{\rm SM} = 3$ and $N_{\rm g}^{\rm DM} = 2$ are the multiplicity factors for the SM and messenger sector families, respectively.

Upon integrating and thermally averaging the right hand side of the anomaly equations (3.2), we obtain three contributions. The first contribution comes from the hypercharge sector through the term $Y_{\mu\nu}\tilde{Y}^{\mu\nu} = -4\,\boldsymbol{E}\cdot\boldsymbol{B}$ which brings the rate of change of helicity density as we derived in Eqs. (3.21), (3.23) and (3.26). The other two contributions come from the $\mathrm{SU(2)_L}$ and $\mathrm{SU(3)_c}$ sphalerons, i.e., the weak and the strong sphalerons, respectively. The weak sphalerons relax the baryon+lepton number charge of the fermions charged under $\mathrm{SU(2)_L}$ whereas the strong sphalerons relax the chiral charge of the quarks charged under $\mathrm{SU(3)_c}$ [50–52]. We note that since sphalerons act on a global level, relaxing global charges, we defined the asymmetry parameters as a sum over all internal degrees of freedom (spin, color, isopsin and family). Finally, the kinetic equation[3] corresponding to the seven asymmetry parameters given in Eqs. (3.29a)-(3.29g) is (see Ref. [6])

$$\frac{\partial \eta_f}{\partial t} = C_{\rm y}^f \frac{\alpha_{\rm y}}{4\pi s}\frac{\partial h}{\partial t} - C_{\rm w}^f \Gamma_{\rm w}(\eta_q + \eta_\ell + \eta_L) - C_{\rm s}^f \Gamma_{\rm s}(\eta_q - \eta_{u_R} - \eta_{d_R})\,. \tag{3.30}$$

The coefficients C_j^f are given by the Table 2. In Eq. (3.30), $\Gamma_{\rm w} = 25\alpha_{\rm w}^5 T$ [53] and $\Gamma_{\rm s} = 100\alpha_{\rm s}^5 T$ [54] are the weak and strong sphaleron rates per unit time, respectively. Notice that this set of equations respect the Sakharov conditions [15] since: 1) the anomalous $B/L/L_D^i$ currents provide a $B/L/L_D^i$ number violation; 2) the term containing $\dot{h}$ has different sign for different chiralities hence breaks $\mathcal{C}/\mathcal{CP}$; 3) the $\dot{h}$ term is a source term (external field produced during inflation) and hence describes an out of equilibrium process.

Since we add new species to the Standard Model, the number of relativistic degrees of freedom increases:

$$g_* = g_*^{\rm SM} + g_*^{\rm M} + g_*^{\rm DM} = 106.75 + \frac{7}{8}\cdot 12 + \frac{7}{8}\cdot 8 + 2 = 126.25\,, \tag{3.31}$$

where we also considered a massless dark photon corresponding to the dark $\mathrm{U(1)_D}$ gauge field.

It is more convenient to express Eq. (3.30) in terms of a dimensionless variable x defined as

$$x = D\frac{M_{\rm pl}}{T}\,, \tag{3.32a}$$

$$D = \sqrt{\frac{45}{4\pi^3 g_*}}\,. \tag{3.32b}$$

[3]Here we neglect both the Yukawa terms and the chiral magnetic effect, which can change the final values of the asymmetry parameters slightly. See, e.g., Ref. [43] and Ref. [44], where the Yukawa terms and the chiral magnetic effect are taken into account for baryogenesis, respectively.

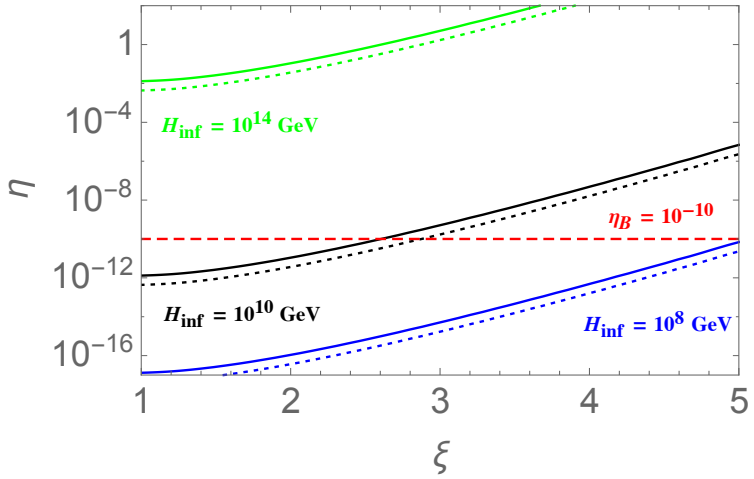

Figure 1. Numerical solutions of the kinetic equations given by Eq. (3.30). The lines show the result for the baryon asymmetry and the dotted one corresponds to the asymmetry in one family of DM. The red dashed line shows the observed value of the baryon asymmetry $\eta_B \simeq 10^{-10}$ which can be achieved for instance with $\xi = 1$ and $H_{\rm inf} = 5.6 \cdot 10^{10}$ GeV. The messenger sector asymmetry is $\eta_L = \eta_B/3$ for all values of $H_{\rm inf}$ and ξ as also can be obtained from the relation Eq. (3.6).

As soon as inflation ends, the radiation dominated era begins, and thus, we have the relation $H = 1/(2t) = T^2/(M_{pl}D)$. Performing this change of variable in Eq. (3.30) yields our final master equation

$$\frac{\partial \eta_f}{\partial x} = -C^f_{\rm y}\gamma_{\rm y} - C^f_{\rm w}\gamma_{\rm w}(\eta_q + \eta_\ell + \eta_L) - C^f_{\rm s}\gamma_{\rm s}(\eta_q - \eta_{u_R} - \eta_{d_R})\,, \tag{3.33}$$

with $\gamma_{\rm y} = \frac{\mathcal{I}e^{2\pi\xi}\alpha_{\rm y}}{\xi^6\sqrt{D}}\frac{T}{\sigma}\left(\frac{H_{\rm inf}}{M_{\rm pl}}\right)^{5/2}$ and $\gamma_{\rm w/s} = \frac{\Gamma_{\rm w/s}}{T}$. This equation is much more convenient to solve since the system of equations becomes just a set of first order differential equations with constant coefficients.

This set of kinetic equations is valid from the end of inflation until the weak sphalerons shut off, at temperature $T = \frac{8\pi v}{\sqrt{4\pi\alpha_{\rm w}}} \simeq 10$ TeV, where $v = 246$ GeV is the Higgs vacuum expectation value. For simplicity we assumed that the $\gamma_{\rm y}$ source shuts off at the same temperature even if it contributes to the evolution of η_f until electroweak phase transition, $T_{\rm EW} \simeq 160$ GeV.

3.6 Results

The solution of the system of equations (3.30) allows us to obtain the parameter space for the inflation parameters, namely, $H_{\rm inf}$ and ξ, in order to produce the observed value of the baryon asymmetry $\eta_B = 1\times10^{-10}$ [55]. We assume that initially all the asymmetry parameters given by Eqs. (3.29a)-(3.29g) are zero. We show the parameter space in Figures 1 and 2 for $1 \leqslant \xi \leqslant 5$ and 10^8 GeV $\leqslant H_{\rm inf} \leqslant 10^{14}$ GeV. Recall that only for $\xi > 1$ the analytic solution of the mode is given by Eq. (3.13) that we have used in our calculation[4].

The solution also provides a relation for any inflation parameters between the asymmetry parameters of the SM and messenger sectors: $\eta_B = 3\eta_L$ [see Eq. (3.6)]. Not surprisingly, because the equations for dark lepton number 1 and 2 are identical, their asymmetry parameters are equal: $\eta_{L_1} = \eta_{L_2}$. Since we take $n_L = n_X$ it is possible to compute the typical mass of the DM candidates as follows.

[4]Note that there is a constraint on the parameter $\xi \lesssim 4$ from non-Gaussianities caused by the hypermagnetic fields, see, e.g., Refs.[56, 57].

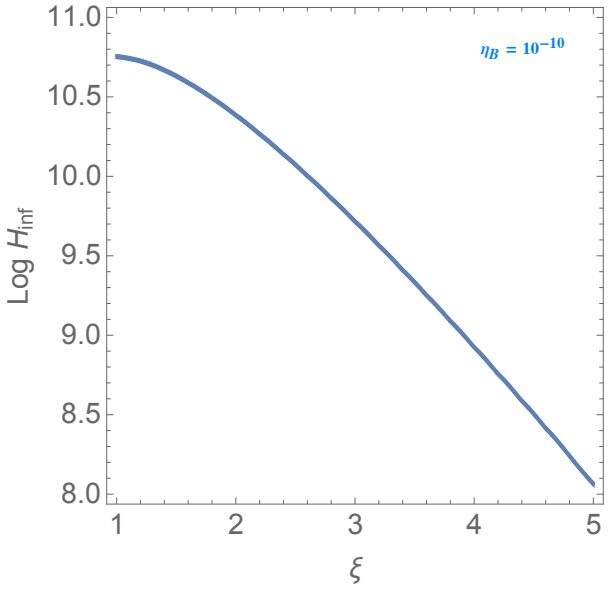

Figure 2. Numerical solutions of the kinetic equations given by Eq. (3.30). This plot shows the values of the parameters $H_{\rm inf}$ and ξ in order to have the observed baryon asymmetry $\eta_B \simeq 10^{-10}$ with $\eta_L = \eta_B/3$.

Today neither the dark matter nor the baryonic matter is relativistic: $\rho_i = m_i n_i = m_i \eta_i s_0 = \Omega_i \rho_c$, where s_0 is the actual entropy density. This yields the relation

$$\frac{\Omega_{X_i}}{\Omega_b} = \frac{m_{X_i}}{m_p} \frac{\eta_{X_i}}{\eta_B}\,, \tag{3.34}$$

for each dark matter particle X_i, where $m_p = 938.73$ MeV is the proton mass. Since observation cannot distinguish Ω_{X_1} and Ω_{X_2} which sum up to Ω_{DM}, we compute the equivalent DM mass by performing a sum on both dark species contribution $m_{DM} = \sum m_{X_i}$ and we get:

$$m_{DM} = m_p \frac{\eta_B}{\Omega_b} \sum_i \frac{\Omega_{X_i}}{\eta_{L_i}} = m_p \frac{\Omega_{DM}}{\Omega_b} \frac{\eta_B}{\eta_{L_{1,2}}} \simeq 15 \text{ GeV}, \tag{3.35}$$

which is in the range of the allowed values [1]. This is the total mass of the DM particles and depending on whether one of them is lighter than the other leads to the dominant component mass in the range of $7 - 15$ GeV. In other words, if $m_{X_1} \sim m_{X_2}$, we predict the DM mass to be around 7 GeV whereas for $m_{X_1} \gg m_{X_2}$ (or the other way around), the DM mass is predicted to be around 15 GeV.

Now that we have successfully generated an asymmetry in the both the SM and the dark matter sectors, we will turn our attention into getting rid of the possible thermal symmetric component of dark matter.

4 Annihilating the Symmetric Component of Dark Matter

There are three possibilities in order to annihilate the symmetric part of the DM: 1) the DM annihilates into SM states, 2) it annihilates into messenger states that eventually decay to SM states, 3) it annihilates into dark radiation. The two first possibilities are forbidden by our model since the DM candidates cannot annihilate into the SM because they do not carry any of the SM charges. Besides their annihilation into the other dark sector species (the messengers of our model) is not efficient

enough since they are the lightest. Therefore the only remaining possibility is direct annihilation into dark radiation, that is why we added a gauge interaction between DM states in the first place when we introduced our model in Section 2.

We consider a $\mathrm{U}(1)_{\mathrm{D}}$ gauge group whose mediator is the dark photon γ_D. There are now two cases: either γ_D is massless, and we have an unbroken $\mathrm{U}(1)_{\mathrm{D}}$ or $\mathrm{U}(1)_{\mathrm{D}}$ is broken, and thus, γ_D is massive. In the first case the γ_D production increases the radiation component in the primordial plasma which affects the big bang nucleosynthesis (BBN) and the cosmic microwave background (CMB). Alternatively, we can take a massive $\mathrm{U}(1)_{\mathrm{D}}$, in which case the $\mathrm{U}(1)_{\mathrm{D}}$ group is spontaneously broken and γ_D can mix kinematically with $\mathrm{U}(1)_{\mathrm{Y}}$ photon and decay into SM states. This case is safer from cosmological constraints as we will see next. We shall explore these two cases in detail in the next subsections.

As we argued briefly, aside from the asymmetry generation that leads to the observed DM abundance, we have a thermal production of messenger particles with

$$n_L = \frac{3\zeta(3)}{4\pi^2} g_L T^3 \,. \tag{4.1}$$

The symmetric part of the messengers then decay very efficiently to X_i according to Eq. (2.6). DM annihilates into dark photons with cross-section (see e.g., section 4.2 of [2])

$$\langle \sigma v \rangle \simeq \frac{\pi \alpha_D^2}{m_{X_i}^2} \simeq 2 \cdot 10^{-8} \left(\frac{g_D}{0.1}\right)^4 \left(\frac{10\ \mathrm{GeV}}{m_{X_i}}\right)^2 \ \mathrm{GeV}^{-2} \,. \tag{4.2}$$

The annihilation rate is then simply $\Gamma_{X\bar{X}\to\gamma_D\gamma_D} = n\langle\sigma v\rangle \gg H$. Hence the symmetric part of the messenger and dark sectors annihilate quickly into dark photons within a Hubble time. Next, we will discuss the massive and massless γ_D cases separately.

4.1 Massless γ_D

It is possible to find out the actual temperature and density of the relic γ_D as it is done usually for neutrinos. Using entropy conservation we obtain a relation between the visible and dark sectors after their decoupling that occur at $T \sim m_X \sim 10$ GeV

$$\frac{g_V T_V^3}{g_D T_D^3} = \frac{g_V^{dec}}{g_D^{dec}} \,, \tag{4.3}$$

where V (respectively D) denote the visible (dark) photon. Referring to Table 1, we find that

$$g_D^{dec} = 2 \cdot 2 \cdot 2 \cdot \frac{7}{8} + 2 = 9 \,, \tag{4.4a}$$

$$g_D = 0 \cdot \frac{7}{8} + 2 = 2 \,, \tag{4.4b}$$

since at V-D decoupling there are both X_1, X_2 and their antiparticles and one massless γ_D. X_1 and X_2 are not relativistic in the current epoch so we do not count them here, and there is still one massless γ_D. At $T \sim 10$ GeV, the SM plasma contains every particle except the top quark, the three W bosons, all the Higgs and all the messenger particles. Thus, the corresponding effective number of relativistic degrees of freedom is $g_V^{dec} = 86.25$. We find the temperature of dark photons in the current epoch as

$$T_{\gamma_D} = \left(\frac{g_D^{dec}}{g_V^{dec}} \frac{g_V}{g_D}\right)^{1/3} T_\gamma = \left(\frac{9}{86.25} \frac{2}{2}\right)^{1/3} T_\gamma \,. \tag{4.5}$$

A good measure of extra relativistic degrees of freedom is the effective number of relativistic neutrino species defined as the ratio of energy density of one neutrino species (1 left handed neutrino + 1 right handed antineutrino so there is a factor 2)

$$N_{\rm eff}^{\rho} = \frac{\rho}{\rho_\nu}\,, \tag{4.6}$$

where we have

$$\rho_\nu \;=\; 2\cdot\frac{7\pi^2}{240}T_\nu^4\,, \tag{4.7a}$$

$$\rho_{\gamma_D} \;=\; 2\cdot\frac{\pi^2}{30}T_{\gamma_D}^4\,, \tag{4.7b}$$

and

$$T_\nu = \left(\frac{4}{11}\right)^{1/3} T_\gamma\,. \tag{4.8}$$

Therefore,

$$\Delta N_{\rm eff}^{\gamma_D} = \frac{\rho_{\gamma_D}}{\rho_\nu} = \frac{8}{7}\left(\frac{11}{4}\right)^{4/3}\left(\frac{g_D^{dec}}{g_V^{dec}}\frac{g_V}{g_D}\right)^{4/3} = 0.22\,. \tag{4.9}$$

This is smaller than the maximum allowed value $\Delta N_{\rm eff} = 0.334$ by the Planck collaboration [55] so the massless case is marginally allowed by the cosmological observations. The value can be lowered by two mechanisms: increasing the degrees of freedom in the dark sector or increase the V-D decoupling temperature, which will increase g_V^{dec}.

4.2 Massive γ_D

In order to give γ_D a mass we must add a dark Higgs field in the model to break $\mathrm{U(1)_D}$, that is a complex scalar field φ_D with a dark charge q_D. The Lagrangian is [58]

$$\mathcal{L}_{\varphi_D} = D_\mu\varphi_D^* D^\mu\varphi_D - \lambda\left(|\varphi_D|^2 - v_D^2\right)^2\,, \tag{4.10}$$

with $D_\mu = \partial_\mu + ig_D C_\mu$ and where v_D is the vacuum expectation value of φ_D. The physical mass of a particle is roughly given by the product of the Higgs VEV and the coupling constant. Since the dark photon mass is

$$M_{\gamma_D} = \sqrt{2}q_D g v_D\,, \tag{4.11}$$

which we take to be around 100 MeV as an example, it implies a smaller Higgs VEV and a smaller dark Higgs mass, $m_{\varphi_D} = 2\sqrt{\lambda}v_D$. The dark Higgs mass is much smaller than the visible Higgs mass, allowing the latter to decay in the former via the term

$$\mathcal{L}_{\varphi_D H} = \lambda_{\varphi_D H}|\varphi_D|^2|H|^2\,, \tag{4.12}$$

which turns out to yield a negligibly small contribution.

The kinetic mixing is given by the effective Lagrangian

$$\mathcal{L}_{\rm mix} = \frac{\varepsilon}{2}Y_{\mu\nu}C^{\mu\nu}, \tag{4.13}$$

where $C^{\mu\nu}$ is the field strength associated to $\mathrm{U(1)_D}$. The kinetic mixing of $\mathrm{U(1)_Y}$ and $\mathrm{U(1)_D}$ is given by the parameter ϵ and reads [59]

$$\epsilon \sim \frac{g_Y g_D}{16\pi^2}\ln\frac{M_L^+}{M_L^-}\,, \tag{4.14}$$

where M_L^+ and M_L^- are respectively the higher and lower mass of the different L messenger states. This simply comes from a 1-loop diagram with messenger fermions in the loop. The logarithmic factor is typically of the order one, hence

$$\epsilon \sim 6 \cdot 10^{-3} \left(\frac{g_Y}{0.1}\right) \left(\frac{g_D}{0.1}\right) . \tag{4.15}$$

Then, the γ_D decay rate is [58, 60]

$$\Gamma_{\gamma_D \to l\bar{l}} = \frac{\epsilon^2 \alpha_Y}{3} M_{\gamma_D} \sqrt{1 - \frac{4m_l^2}{M_{\gamma_D}^2}} \left(1 + \frac{2m_l^2}{M_{\gamma_D}^2}\right) , \tag{4.16}$$

for the SM leptons and

$$\Gamma_{\gamma_D \to q\bar{q}} = \left. \frac{\sigma_{e^+e^- \to q\bar{q}}}{\sigma_{e^+e^- \to \mu^+\mu^-}} \right|_{s=M_{\gamma_D}^2} \Gamma_{\gamma_D \to l\bar{l}} , \tag{4.17}$$

for hadrons. Of course, these decay channels are allowed only if $M_{\gamma_D} > 2m_f$. The decay rate for an electron-positron channel is

$$\Gamma_{\gamma_D \to e^+e^-} \simeq 1.2 \cdot 10^{-7} \left(\frac{\epsilon}{6 \cdot 10^{-3}}\right)^2 \left(\frac{M_{\gamma_D}}{100 \text{ MeV}}\right) \text{ GeV}. \tag{4.18}$$

or $\Gamma = 1.82 \cdot 10^{17}$ s^{-1}, exceeding the Hubble rate by several orders of magnitude. Thus, the massive dark photon can efficiently be converted into the SM species, and hence, the symmetric component of the DM is removed successfully. For $M_{\gamma_D} < 210$ MeV, this is the only allowed channel. When M_{γ_D} increases and it allows more channels (say n), hence quicker decay, the total decay rate can be parametrized as

$$\Gamma_d = n \cdot \Gamma_{\gamma_D \to f\bar{f}} , \tag{4.19}$$

unless we are at a threshold of pair production.

5 Summary and Discussion

We proposed a new mechanism to generate asymmetric dark matter and the baryon asymmetry of the Universe via the same source of $\mathcal{CP}$ violation that occurs during inflation. The coupling of the inflaton to the SM hypercharge gauge fields via the dimension five operator $(\alpha/f)\Phi F_{\mu\nu}\tilde{F}^{\mu\nu}$ leads to generation of coherent hypermagnetic fields with maximal helicity, which in turn source the chiral anomaly in the SM and yield the desired asymmetries in both the SM and DM sectors. We showed that for a wide range of inflationary parameters, $H_{\rm inf}$ and ξ, the observed BAU and DM abundances can be achieved. In the minimal ADM model we considered, we found that the DM mass is in the range of $m_X \sim 7 - 15$ GeV, depending on whether they have comparable masses or one of the two DM species is relatively lighter, respectively. The DM mass can take a different range of values if the minimal ADM field content is extended as this will affect the ratio between the BAU and the DM asymmetry parameters.

We also gave two scenarios for annihilating the symmetric part of the ADM. By coupling the DM fermions to a $\mathrm{U(1)_D}$ gauge field, the symmetric part can be efficiently annihilated into the dark photons, γ_D. In the first scenario we considered, $\mathrm{U(1)_D}$ is unbroken, and hence γ_D is massless and contributes to the relativistic degree of freedom today. We found that the contribution of γ_D, $\Delta N_{\rm eff} = 0.22$, is within the allowed range of $N_{\rm eff} = 3.15 \pm 0.23$ provided by the Planck collaboration [55]. However, we note that as the constraint on $\Delta N_{\rm eff}$ continues to improve, this scenario might become problematic. One way out is to increase the field content in the ADM sector to dilute the dark radiation component.

In the second scenario that we have considered for annihilating the symmetric part of the ADM, the $\mathrm{U(1)_D}$ is broken, hence the dark photons are massive. These photons decay into the SM species via a gauge kinetic mixing efficiently. Hence, this is a safer route to annihilate the symmetric component of ADM and is free from the constraints.

Since in the minimal ADM model we considered there are two DM candidates carrying two different quantum numbers, there is a possibility for them to combine and form dark Hydrogen-like atoms. For the massless γ_D case, dark atoms can form provided that [61]

$$\frac{\alpha_D^6}{\mathcal{R}}\left(\frac{\Omega_{DM}h^2}{0.11}\right)\left(\frac{1\text{ GeV}}{m_{DM}-B_D}\right)\left(\frac{1\text{ keV}}{B_D}\right)\geqslant 1.5\cdot 10^{-16}\,, \tag{5.1}$$

with

$$\mathcal{R}=\left.\frac{T_{\gamma_D}}{T_\gamma}\right|_{z=0}\,, \tag{5.2}$$

and B_D the binding energy of the dark Hydrogen-like atom. Taking $\Omega_{DM}h^2=0.11$, $B_D=1$ keV, $g_D=0.1$ and our value of $\mathcal{R}=0.47$ [see Eq. (4.5)], we conclude that this condition is not reached for our value of $m_{DM}=7-15$ GeV. For the massive γ_D case, dark atoms can form provided that [58]

$$m_{\gamma_D}<\alpha_D\frac{m_{X_1}m_{X_2}}{m_{DM}}\,, \tag{5.3}$$

For $m_{\gamma_D}=100$ MeV and $g_D=0.1$ this condition cannot be respected either for the range of m_{DM} that we have. Therefore, in our setup the dark atoms cannot form.

We would also like to point out that the model of ADM that we considered with the dark $\mathrm{U(1)_D}$ interaction is compatible with the observation of haloes and subhaloes in the galaxies, namely, addressing the the so-called "missing-satellite problem" as was discussed extensively in Ref. [61]. In a nutshell, this can be understood as follows. The interaction between the DM mediated by a massless or light force carrier reproduces the large-scale structure of the universe while suppressing the formation of structure at smaller scales [58].

Finally, we note that in the simplest version of the natural inflation model [62] that we considered as an example to study the asymmetry generation in ADM and baryons, either a curvaton field [63] is needed to explain the observed density perturbations or some other dynamical mechanism is needed to be implemented (see e.g., string theory inspired models [64, 65]). To achieve the observed BAU and hence the DM abundance, we require $H_{\rm inf}$ to be not so large as can be read off from our Figures 1 and 2. A model of inflation that has $H_{\rm inf}\leqslant 5.6\cdot 10^{10}$ GeV, $\xi\gtrsim 1$ and that also explains observed amplitude of the density perturbations leads to a complete picture of the early Universe, namely, solving all the initial conditions problems including the BAU and DM abundances in a single framework. The interrelations between our proposed mechanism and various models of inflation that satisfy these criteria remain to be studied.

Acknowledgments

We would like to thank Mohamed Anber, Kohei Kamada and Mikhail Shaposhnikov for discussions. ES is supported by the Swiss National Science Foundation and Alexander von Humboldt Foundation. YC is supported by the Institute of Physics at Ecole Polytechnique Fédérale de Lausanne.

References

[1] K. Petraki and R. R. Volkas, *Review of asymmetric dark matter*, *Int. J. Mod. Phys.* **A28** (2013) 1330028, [1305.4939].

[2] K. M. Zurek, *Asymmetric Dark Matter: Theories, Signatures, and Constraints*, *Phys. Rept.* **537** (2014) 91–121, [1308.0338].

[3] T. Asaka, S. Blanchet and M. Shaposhnikov, *The nuMSM, dark matter and neutrino masses*, *Phys. Lett.* **B631** (2005) 151–156, [hep-ph/0503065].

[4] T. Asaka and M. Shaposhnikov, *The nuMSM, dark matter and baryon asymmetry of the universe*, *Phys. Lett.* **B620** (2005) 17–26, [hep-ph/0505013].

[5] S. H.-S. Alexander, M. E. Peskin and M. M. Sheikh-Jabbari, *Leptogenesis from gravity waves in models of inflation*, *Phys. Rev. Lett.* **96** (2006) 081301, [hep-th/0403069].

[6] M. M. Anber and E. Sabancilar, *Hypermagnetic Fields and Baryon Asymmetry from Pseudoscalar Inflation*, *Phys. Rev.* **D92** (2015) 101501, [1507.00744].

[7] M. M. Anber and L. Sorbo, *N-flationary magnetic fields*, *JCAP* **0610** (2006) 018, [astro-ph/0606534].

[8] J. Shelton and K. M. Zurek, *Darkogenesis: A baryon asymmetry from the dark matter sector*, *Phys. Rev.* **D82** (2010) 123512, [1008.1997].

[9] E. Witten, *An SU(2) Anomaly*, *Phys. Lett.* **B117** (1982) 324–328.

[10] M. S. Turner and L. M. Widrow, *Inflation Produced, Large Scale Magnetic Fields*, *Phys.Rev.* **D37** (1988) 2743.

[11] B. Ratra, *Cosmological 'seed' magnetic field from inflation*, *Astrophys.J.* **391** (1992) L1–L4.

[12] A. Dolgov, *Breaking of conformal invariance and electromagnetic field generation in the universe*, *Phys.Rev.* **D48** (1993) 2499–2501, [hep-ph/9301280].

[13] M. Gasperini, M. Giovannini and G. Veneziano, *Primordial magnetic fields from string cosmology*, *Phys.Rev.Lett.* **75** (1995) 3796–3799, [hep-th/9504083].

[14] P. Adshead, J. T. Giblin, T. R. Scully and E. I. Sfakianakis, *Magnetogenesis from axion inflation*, *JCAP* **1610** (2016) 039, [1606.08474].

[15] A. Sakharov, *Violation of CP Invariance, C Asymmetry, and Baryon Asymmetry of the Universe*, *Pisma Zh.Eksp.Teor.Fiz.* **5** (1967) 32–35.

[16] M. Joyce and M. E. Shaposhnikov, *Primordial magnetic fields, right-handed electrons, and the Abelian anomaly*, *Phys. Rev. Lett.* **79** (1997) 1193–1196, [astro-ph/9703005].

[17] B. A. Campbell, S. Davidson, J. R. Ellis and K. A. Olive, *On the baryon, lepton flavor and right-handed electron asymmetries of the universe*, *Phys. Lett.* **B297** (1992) 118–124, [hep-ph/9302221].

[18] A. J. Long, E. Sabancilar and T. Vachaspati, *Leptogenesis and Primordial Magnetic Fields*, *JCAP* **1402** (2014) 036, [1309.2315].

[19] A. J. Long and E. Sabancilar, *Chiral Charge Erasure via Thermal Fluctuations of Magnetic Helicity*, *JCAP* **1605** (2016) 029, [1601.03777].

[20] M. Giovannini and M. E. Shaposhnikov, *Primordial hypermagnetic fields and triangle anomaly*, *Phys. Rev.* **D57** (1998) 2186–2206, [hep-ph/9710234].

[21] M. Giovannini and M. E. Shaposhnikov, *Primordial magnetic fields, anomalous isocurvature fluctuations and big bang nucleosynthesis*, *Phys. Rev. Lett.* **80** (1998) 22–25, [hep-ph/9708303].

[22] M. Giovannini, *Hypermagnetic knots, Chern-Simons waves and the baryon asymmetry*, *Phys. Rev.* **D61** (2000) 063502, [hep-ph/9906241].

[23] M. Giovannini, *Primordial hypermagnetic knots*, *Phys. Rev.* **D61** (2000) 063004, [hep-ph/9905358].

[24] K. Bamba, *Baryon asymmetry from hypermagnetic helicity in dilaton hypercharge electromagnetism*, *Phys. Rev.* **D74** (2006) 123504, [hep-ph/0611152].

[25] K. Bamba, C. Q. Geng and S. H. Ho, *Hypermagnetic Baryogenesis*, *Phys. Lett.* **B664** (2008) 154–156, [0712.1523].

[26] A. Boyarsky, J. Frohlich and O. Ruchayskiy, *Self-consistent evolution of magnetic fields and chiral asymmetry in the early Universe*, *Phys. Rev. Lett.* **108** (2012) 031301, [1109.3350].

[27] A. Boyarsky, O. Ruchayskiy and M. Shaposhnikov, *Long-range magnetic fields in the ground state of the Standard Model plasma*, *Phys. Rev. Lett.* **109** (2012) 111602, [1204.3604].

[28] S. Rostam Zadeh and S. S. Gousheh, *Contributions to the $U_Y(1)$ Chern-Simons term and the evolution of fermionic asymmetries and hypermagnetic fields*, *Phys. Rev.* **D94** (2016) 056013, [1512.01942].

[29] A. Boyarsky, J. Frohlich and O. Ruchayskiy, *Magnetohydrodynamics of Chiral Relativistic Fluids*, *Phys. Rev.* **D92** (2015) 043004, [1504.04854].

[30] E. V. Gorbar, I. A. Shovkovy, S. Vilchinskii, I. Rudenok, A. Boyarsky and O. Ruchayskiy, *Anomalous Maxwell equations for inhomogeneous chiral plasma*, *Phys. Rev.* **D93** (2016) 105028, [1603.03442].

[31] V. B. Semikoz and D. D. Sokoloff, *Large - scale magnetic field generation by alpha-effect driven by collective neutrino - plasma interaction*, *Phys. Rev. Lett.* **92** (2004) 131301, [astro-ph/0312567].

[32] V. B. Semikoz and D. D. Sokoloff, *Magnetic helicity and cosmological magnetic field*, *Astron. Astrophys.* **433** (2005) L53, [astro-ph/0411496].

[33] V. B. Semikoz and D. D. Sokoloff, *Large-scale cosmological magnetic fields and magnetic helicity*, *Int. J. Mod. Phys.* **D14** (2005) 1839–1854.

[34] V. B. Semikoz, D. D. Sokoloff and J. W. F. Valle, *Is the baryon asymmetry of the Universe related to galactic magnetic fields?*, *Phys. Rev.* **D80** (2009) 083510, [0905.3365].

[35] P. M. Akhmet'ev, V. B. Semikoz and D. D. Sokoloff, *Flow of hypermagnetic helicity in the embryo of a new phase in the electroweak phase transition*, *Pisma Zh. Eksp. Teor. Fiz.* **91** (2010) 233, [1002.4969].

[36] M. Dvornikov and V. B. Semikoz, *Leptogenesis via hypermagnetic fields and baryon asymmetry*, *JCAP* **1202** (2012) 040, [1111.6876].

[37] V. B. Semikoz, D. D. Sokoloff and J. W. F. Valle, *Lepton asymmetries and primordial hypermagnetic helicity evolution*, *JCAP* **1206** (2012) 008, [1205.3607].

[38] M. Dvornikov and V. B. Semikoz, *Lepton asymmetry growth in the symmetric phase of an electroweak plasma with hypermagnetic fields versus its washing out by sphalerons*, *Phys. Rev.* **D87** (2013) 025023, [1212.1416].

[39] V. B. Semikoz, A. Yu. Smirnov and D. D. Sokoloff, *Hypermagnetic helicity evolution in early universe: leptogenesis and hypermagnetic diffusion*, *JCAP* **1310** (2013) 014, [1309.4302].

[40] V. B. Semikoz and A. Yu. Smirnov, *Leptogenesis in the Symmetric Phase of the Early Universe: Baryon Asymmetry and Hypermagnetic Helicity Evolution*, *J. Exp. Theor. Phys.* **120** (2015) 217–225, [1503.06758].

[41] V. B. Semikoz, A. Yu. Smirnov and D. D. Sokoloff, *Generation of hypermagnetic helicity and leptogenesis in the early Universe*, *Phys. Rev.* **D93** (2016) 103003, [1604.02273].

[42] E. Sabancilar, *Electromagnetic Currents from Electroweak Fermion Level Crossing*, 1310.8632.

[43] T. Fujita and K. Kamada, *Large-scale magnetic fields can explain the baryon asymmetry of the Universe*, *Phys. Rev.* **D93** (2016) 083520, [1602.02109].

[44] K. Kamada and A. J. Long, *Baryogenesis from decaying magnetic helicity*, *Phys. Rev.* **D94** (2016) 063501, [1606.08891].

[45] K. Kamada and A. J. Long, *Evolution of the Baryon Asymmetry through the Electroweak Crossover in the Presence of a Helical Magnetic Field*, 1610.03074.

[46] G. 't Hooft, *Symmetry Breaking Through Bell-Jackiw Anomalies*, *Phys.Rev.Lett.* **37** (1976) 8–11.

[47] M. D. Schwartz, *Quantum Field Theory and the Standard Model*. Cambridge University Press, 2014.

[48] P. B. Arnold, G. D. Moore and L. G. Yaffe, *Transport coefficients in high temperature gauge theories. 1. Leading log results*, *JHEP* **0011** (2000) 001, [hep-ph/0010177].

[49] G. B. Field and S. M. Carroll, *Cosmological magnetic fields from primordial helicity*, *Phys. Rev.* **D62** (2000) 103008, [astro-ph/9811206].

[50] V. Kuzmin, V. Rubakov and M. Shaposhnikov, *On the Anomalous Electroweak Baryon Number Nonconservation in the Early Universe*, *Phys.Lett.* **B155** (1985) 36.

[51] S. Y. Khlebnikov and M. Shaposhnikov, *The Statistical Theory of Anomalous Fermion Number Nonconservation*, *Nucl.Phys.* **B308** (1988) 885–912.

[52] V. A. Rubakov and M. E. Shaposhnikov, *Electroweak baryon number nonconservation in the early universe and in high-energy collisions*, *Usp. Fiz. Nauk* **166** (1996) 493–537, [hep-ph/9603208].

[53] G. D. Moore, C.-r. Hu and B. Muller, *Chern-Simons number diffusion with hard thermal loops*, *Phys.Rev.* **D58** (1998) 045001, [hep-ph/9710436].

[54] G. D. Moore, *Computing the strong sphaleron rate*, *Phys.Lett.* **B412** (1997) 359–370, [hep-ph/9705248].

[55] Planck collaboration, P. A. R. Ade et al., *Planck 2015 results. XIII. Cosmological parameters*, *Astron. Astrophys.* **594** (2016) A13, [1502.01589].

[56] R. Z. Ferreira and M. S. Sloth, *Universal Constraints on Axions from Inflation*, *JHEP* **12** (2014) 139, [1409.5799].

[57] R. Z. Ferreira, J. Ganc, J. Norea and M. S. Sloth, *On the validity of the perturbative description of axions during inflation*, *JCAP* **1604** (2016) 039, [1512.06116].

[58] K. Petraki, L. Pearce and A. Kusenko, *Self-interacting asymmetric dark matter coupled to a light massive dark photon*, *JCAP* **1407** (2014) 039, [1403.1077].

[59] B. Holdom, *Two U(1)'s and Epsilon Charge Shifts*, *Phys. Lett.* **B166** (1986) 196–198.

[60] B. Batell, M. Pospelov and A. Ritz, *Probing a Secluded U(1) at B-factories*, *Phys. Rev.* **D79** (2009) 115008, [0903.0363].

[61] F.-Y. Cyr-Racine and K. Sigurdson, *Cosmology of atomic dark matter*, *Phys. Rev.* **D87** (2013) 103515, [1209.5752].

[62] K. Freese, J. A. Frieman and A. V. Olinto, *Natural inflation with pseudo - Nambu-Goldstone bosons*, *Phys.Rev.Lett.* **65** (1990) 3233–3236.

[63] D. H. Lyth and D. Wands, *Generating the curvature perturbation without an inflaton*, *Phys.Lett.* **B524** (2002) 5–14, [hep-ph/0110002].

[64] K. Enqvist and M. S. Sloth, *Adiabatic CMB perturbations in pre - big bang string cosmology*, *Nucl.Phys.* **B626** (2002) 395–409, [hep-ph/0109214].

[65] S. Dimopoulos, S. Kachru, J. McGreevy and J. G. Wacker, *N-flation*, *JCAP* **0808** (2008) 003, [hep-th/0507205].

Baryogenesis from combined Higgs – scalar field inflation

Yann Cado, Mariano Quirós

Institut de Física d'Altes Energies (IFAE) and
The Barcelona Institute of Science and Technology (BIST),
Campus UAB, 08193 Bellaterra, Barcelona, Spain

Abstract

We study a modification of the Higgs inflation scenario where we introduce an extra scalar ϕ, with mass m, coupled to the Ricci scalar as $g\phi^2 R$, and mixed with the Higgs field h via the Lagrangian term $\mu\phi h^2$. Both fields participate in the inflation process in a unitary theory that predicts values of the cosmological observables in agreement with the results from the Planck/BICEP/Keck collaborations. In addition, by means of a $\mathcal{CP}$-odd effective operator that couples ϕ to the Chern-Simons term of the hypercharge gauge group as $f_\phi^{-1}\phi\, Y_{\mu\nu}\tilde{Y}^{\mu\nu}$, maximally helical magnetic fields are produced during the last e-folds of inflation. We found a window in the coupling f_ϕ where these fields survive all constraints until the electroweak phase transition, and source the baryon asymmetry of the Universe through the Standard Model chiral anomaly. From a phenomenological perspective, the model can solve the Standard Model instability problem at the scale $\mathcal{Q}_I \simeq 10^{11}$ GeV, provided that $\mu \lesssim m \lesssim \mathcal{Q}_I$, and for $m \lesssim \mathcal{O}$(few) TeV, the ϕ-h mixing becomes sizable while the theory turns natural. The latter thus predicts modifications of the trilinear and quartic couplings that could be explored at the HE-LHC, as well as at future colliders, and allows for direct ϕ production at the LHC followed by decay into hh. Present results from ATLAS and CMS already put (mild) bounds on the mass of the heavy scalar as $m \gtrsim 0.55$ TeV at 95% C.L.

Contents

1 Introduction **3**

2 The model **6**
- 2.1 Jordan frame 7
- 2.2 Stability of the potential 10
- 2.3 Einstein frame 10

3 Inflation **13**

4 Gauge field production **17**
- 4.1 Helical magnetic fields 18
- 4.2 Schwinger effect 23
  - 4.2.1 Maximal estimate 24
  - 4.2.2 Equilibrium estimate 25
  - 4.2.3 Final comments 26
- 4.3 Self-consistency condition 26

5 Reheating **28**

6 Baryogenesis **31**

7 Constraints **32**
- 7.1 Helicity evolution: Magnetohydrodynamics and Reynolds numbers 32
- 7.2 The chiral plasma instability 35
- 7.3 Primordial non-Gaussianity 36
- 7.4 The baryon isocurvature perturbation 37
- 7.5 Summary of constraints 37

8 Some phenomenological considerations **39**

9 Conclusion **44**

A UV completion for $\mathcal{CP}$-violation **47**

B Baryon isocurvature perturbations **50**

1 Introduction

Electroweak (EW) baryogenesis is an appealing mechanism to understand the baryon asymmetry of the Universe (BAU) [1] (for reviews see Refs. [2–7]), which is testable at EW energies. Although the Standard Model (SM) contains all necessary ingredients required by the three Sakharov conditions, it quantitatively fails as the amount of $\mathcal{CP}$-violation in the CKM phase is too small and moreover, given the experimental value of the Higgs mass, the electroweak phase transition (EWPT) is not strong enough first order, but a continuous crossover [8, 9]. This mechanism should then require beyond the SM physics.

It was more recently realized, Refs. [10–16], that maximally helical hypermagnetic fields can be produced at the end of (axial) inflation, and can generate the observed BAU, via the $B+L$ anomaly, during the EWPT. In this kind of theories, $\mathcal{CP}$ is spontaneously violated by the effective dimension-five operator $aY^{\mu\nu}\widetilde{Y}_{\mu\nu}$, where a is the axial field, $Y^{\mu\nu}$ the strength of the hypercharge gauge field Y^{μ}, and $\widetilde{Y}^{\mu\nu}$ its dual, whose generation requires an ultraviolet (UV) completion of the model. The generation of the observed BAU was further elaborated in a number of papers, see e.g. Refs. [17–20].

In a recent paper [21], we proposed a mechanism where the helical hypermagnetic fields were produced after inflation by the Higgs doublet field $\mathcal{H}$ with a $\mathcal{CP}$-violating $|\mathcal{H}|^2 Y^{\mu\nu}\widetilde{Y}_{\mu\nu}$ dimension-six operator, thus entirely relying the nonperturbative production of gauge fields on SM physics. Of course generating the $\mathcal{CP}$-odd operator $|\mathcal{H}|^2 Y^{\mu\nu}\widetilde{Y}_{\mu\nu}$ requires a UV completion, which can be similar to that giving rise to the $\mathcal{CP}$-even operator $aY^{\mu\nu}\widetilde{Y}_{\mu\nu}$, for which $\mathcal{CP}$ is (spontaneously) violated for background values of the axial field a.

Moreover there are theories, dubbed as Higgs inflation (HI) models [22–24] (for a review see [25]), where the inflaton is identified with the SM Higgs boson, thus linking the cosmological observables during the inflationary period of inflation with SM quantities. These models are based on assuming, in the Jordan frame, a coupling between the Higgs doublet $\mathcal{H}$ and the Ricci scalar R as $\mathcal{L} = -(M_{\rm Pl}^2/2)R - \xi_{\mathcal{H}}|\mathcal{H}|^2 R + \cdots$, where the ellipses refers to the SM Lagrangian. This model has been shown to have a (dynamical) cutoff $M_{\rm Pl}/\xi_{\mathcal{H}}$, for values of the Higgs at the electroweak scale, i.e. $h \sim v$ [26–31], while at values of the Higgs where inflation happens, i.e. $h \sim M_{\rm Pl}/\sqrt{\xi_{\mathcal{H}}}$, the cutoff has been proven to be $\sim M_{\rm Pl}/\sqrt{\xi_{\mathcal{H}}}$, at least for two-by-two tree level scattering amplitudes, avoiding thus unitarity violation [32–34]. Moreover, HI models have to face another challenge: for actual values of the Higgs boson and top-quark masses the SM potential becomes unstable at values of the Higgs field $h \sim \mathcal{Q}_I \sim 10^{11}$ GeV. This question has been tackled in Ref. [35], where the case of an unstable potential was considered, taking into account radiative corrections. Because of the Higgs-Ricci coupling the theory becomes nonrenormalizable in the Einstein frame and requires the addition of an infinite number of counterterms. By assuming a scale invariant UV completion it is found that there are threshold effects at scales $\sim M_{\rm Pl}/\xi_{\mathcal{H}}$ which generate jumps of the SM quartic coupling to positive values (although one cannot determine their amplitude from the theory) and therefore HI can proceed in the usual way. Still the potential has two minima: the EW minimum and a much deeper (unphysical) minimum associated to the instability of the original SM potential. The evolution of the Higgs field after inflation will depend on the reheating process, and in particular on the reheating temperature. If the reheating temperature is high enough such that the unphysical minimum is dominated by the thermal corrections, then the Higgs will relax to the symmetric phase, otherwise the Higgs would go to the unphysical vacuum and it would stay there forever.

Motivated by HI, we will propose a model where the SM potential is simply stabilized by a scalar field ϕ coupled to the Higgs (this coupling was already pursued in Refs. [36, 37]) and with a mass $m \lesssim \mathcal{Q}_I$, opening up the possibility of direct or indirect detection at present (LHC) and future

accelerators. Moreover if the stabilizing field has a weak enough self-coupling ϕ^4 and is coupled to the Ricci tensor as $\sim g\phi^2 R$, it can trigger cosmological inflation, as the potential becomes flat in the Einstein frame, while the COBE normalization does not impose strong constraints on the g coupling. In this theory the inflaton can couple to the Chern-Simons component of the SM hypercharge and trigger baryogenesis via the production of helical magnetic fields. Finally through the coupling of the inflaton and the Higgs field, the latter will also be a component of the inflaton sector, although we will work out a model where the parameters are such that cosmological inflation will be mainly driven by the stabilizing field ϕ. The model thus combine HI, baryogenesis via production of helical magnetic fields and stabilization of the SM potential by modifying the renormalization group running, to provide a successful history of the Universe.

In the present paper we will follow the above guideline in order to build such a model of inflation, which consists in a modification of the HI model by the introduction of a scalar field ϕ, with a two-field potential $V(h,\phi)$ in which analytical relations between both fields are enforced by its shape. One major difference with respect to a previous attempt, Ref. [37], is that ϕ is coupled to the Ricci scalar as $(g/2)\phi^2 R$, with $\phi \lesssim \Lambda_\phi \equiv M_{\rm Pl}/g$ [1], where Λ_ϕ is the theory cutoff, while $\xi_{\mathcal{H}} \ll 1$, thus satisfying the most naive unitarity requirement. Therefore, in our model the Higgs field is not the only inflaton, but a component of the inflaton system, as inflation is really driven along a particular path in the two-field space, while its orthogonal direction has a strong curvature around its minimum, where the field system is anchored.

This paper is organized as follows. In Sec. 2 we introduce the potential in the Jordan frame, as a function of the fields ϕ and h, which (for Planckian values of the field ϕ) can be approximated by the most general renormalizable polynomial satisfying the $\mathbb{Z}_2$ symmetry $\phi \to -\phi$. As the Ricci term is quadratic in ϕ, $g\phi^2 R$, the beginning of inflation will be controlled by the quartic term $\lambda_\phi \phi^4$, and the size of the amplitude of density perturbations is provided by the smallness of λ_ϕ, for values of $\phi \leq \Lambda_\phi$, consistent with the naive unitarity of the theory. The smallness of the coupling λ_ϕ is stable under radiative corrections, and so is technically natural, but the Higgs potential is unstable for values of the renormalization scale $\mathcal{Q}_I \simeq 10^{11}$ GeV. If the mass m of the ϕ field is $m < \mathcal{Q}_I$, the field ϕ decouples for values of $\mathcal{Q} < \mathcal{Q}_I$. Then, in the presence of a potential term softly breaking the $\mathbb{Z}_2$ symmetry, $-\mu\phi|\mathcal{H}|^2$, there is a threshold correction in the one-loop β function of the Higgs quartic coupling that can stabilize the EW vacuum. This mechanism was introduced in Ref. [37] and we will use it to constrain our parameter space.[2]

[1] It has been proved, in Refs. [29, 31], that there is no tree-level unitarity problem for the amplitude $\mathcal{A}(\phi\phi \to \phi\phi)$ as, in the Einstein frame, see Eq. (2.30), there appears the effective operator $\phi^2(\partial_\mu\phi)^2/\Lambda_\phi^2$ that—upon integration by parts gives, on-shell, the correction $m^2\phi^4/\Lambda_\phi^2$—leads to a four-point function that does not grow with the energy, and thus does not violate unitarity. A similar result is obtained in the Jordan frame, where the amplitude $\mathcal{A}(\phi\phi \to \phi\phi)$ grows, in the s-channel, with the energy, and behaves as s/Λ_ϕ^2. However, considering the cross channels, there is a cancellation, and the four-point amplitude behaves as $(s+t+u)/\Lambda_\phi^2 \propto m^2/\Lambda_\phi^2$. However, the quick conclusion that unitarity is not violated at the scale Λ_ϕ has been challenged in Refs. [30, 31], where it was pointed out that, in the Jordan frame, the above cancellation is very unlikely to appear in loop-induced corrections to the same process $\phi\phi \to \phi\phi$, leading to a cutoff at the value $\sim 4\pi\Lambda_\phi$, where a loop factor has been included. The observation is similar for higher order processes, since e.g. $\phi\phi \to \phi\phi + n\phi$ has a cross section that scales as $\lambda_\phi^2 s^{n/2-1} g^n/M_{\rm Pl}^n$, where λ_ϕ is the ϕ quartic coupling. This indicates that the perturbative description breaks down for energies $\sqrt{s} \gtrsim \lambda_\phi^{-2/n}\Lambda_\phi$, which goes to Λ_ϕ for large values of n. Similarly, in the Einstein frame, on top of the nonproblematic effective operator $\phi^2(\partial_\mu\phi)^2$, other higher order operators, as e.g. $\phi^2(\partial_\mu\phi)^4$, are expected to be generated by loop effects, and so are expected to trigger violations of unitarity beyond the scale Λ_ϕ. In view of these arguments we will conservatively consider in this paper Λ_ϕ as the scale at which unitarity is violated.

[2] Should we have, instead, considered a linear Ricci term, $g\phi R$, and a quadratic, $m^2\phi^2$, inflationary potential, one could also have achieved the amount of flatness required by the slow roll conditions during the inflationary period, but

The properties of the inflationary model are presented in Sec. 3. There, we will prove that all observational constraints from the Planck and BICEP/Keck collaborations on the slow roll parameters, or equivalently on the spectral index, the spectral index running and the tensor-to-scalar ratio, can be satisfied for a range of the parameter g such that $g \ll 1$, thus easily satisfying the unitarity condition for the model.

The nonperturbative production of gauge fields at the end of inflation is presented in Sec. 4. In particular we will consider the $\mathcal{CP}$-violating dimension-five operator $1/(4f_\phi)\phi Y_{\mu\nu}\widetilde{Y}^{\mu\nu}$, provided by some UV completion, to trigger baryogenesis at the EWPT. We postpone to App. A the details of a particularly simple UV completion giving rise to such an operator. Similar UV completions were proposed in Ref. [38], and recently in Refs. [39, 40], to generate the BAU using various mechanisms, so we can be agnostic about its origin. We have found a critical value of the parameter f_ϕ, such that for $f_\phi \gtrsim f_\phi^c$ the backreaction of the produced gauge fields on the inflationary dynamics can be neglected, and so we have explicitly considered this region in the numerical analysis. Moreover, in the presence of magnetic fields, as those produced in this work, there appear fermionic currents, a phenomenon called the Schwinger effect, and, for sufficiently strong magnetic fields, their backreaction on the gauge fields cannot be neglected. As exactly solving the equations of motion of gauge fields, in the presence of the Schwinger fermionic currents, is beyond the scope of the present paper, we have followed recent proposals in the literature for gauge field estimates [20, 41], and have worked out two simple approximations: the *maximal estimate*, obtained upon maximizing the value of the helicity, and the *equilibrium estimate*. A detailed recent analysis [42] shows that the exact solutions lie in between both estimates, so we can reliably corner the final allowed region in the relevant parameter space.

The reheating mechanism has been studied in Sec. 5, and we have consistently considered the region $f_\phi > f_\phi^c$, where the reheating takes place perturbatively by the leaading inflaton decay process $\Gamma(\phi \to hh)$. The inflaton width, as well as the reheating temperature $T_{\rm rh}$, are then functions of the inflaton mass parameter m. In order to stabilize the EW vacuum, the latter must lie in the interval $m \in [1\,\text{TeV}, \mathcal{Q}_I]$ which implies, for reheating temperatures, the interval $T_{\rm rh}/T_{\rm rh}^{\rm ins} \in [10^{-2}\,, 10^{-6}]$, where $T_{\rm rh}^{\rm ins} \simeq 2\cdot 10^{15}$ GeV would be the instant reheating temperature, i.e. the reheating temperature in the hypothetical case where $\Gamma(\phi \to hh)$ equals the Hubble parameter at the end of inflation.

We show in Sec. 6 how the baryon asymmetry is generated when helicity transforms into baryon number at the EW crossover. In particular we show that this mechanism works for $f_\phi > f_\phi^c$, and provides an upper bound on f_ϕ which depends on the value of the reheating temperature.

In Sec. 7 we consider all relevant conditions for the helical magnetic fields to survive from the end of inflation, when they are generated, to the EWPT, when they convert into the baryon asymmetry. In particular we have considered the constraints from magnetohydrodynamics (MHD) and Reynolds numbers, from chiral plasma instability, from the non-Gaussianity of the inflaton primordial fluctuations and from the baryon isocurvature perturbations. Some technical details about the latter are postponed to App. B. Globally they constrain the region where the baryogenesis mechanism works, leaving an allowed range for the values of the parameter f_ϕ, which depends on the ratio $T_{\rm rh}/T_{\rm rh}^{\rm ins}$. Readers not interested in the technical details of the analysis can straightforwardly go to Sec. 7.5, and in particular to Fig. 9, which summarizes the combined results.

In Sec. 8 some phenomenological considerations, from the point of view of particle physics, are presented. First of all we study the naturalness problem generated by the mass hierarchy $m \gg m_h$, where m_h is the Higgs mass, which leads either to a fine-tuning or considering $m = \mathcal{O}(\text{TeV})$. The

the size of the amplitude of density perturbations, now controlled by m, would have yielded a value $m > \mathcal{Q}_I$, which is too large to stabilize the EW vacuum.

latter case is phenomenologically appealing as the $\mathbb{Z}_2$-breaking term in the potential generates a mixing between the singlet ϕ and the Higgs field h. This mixing, which is negligible in the case of very large values of the parameter m, can be sizable, and with relevant phenomenological applications, for the case of $m = \mathcal{O}(\text{TeV})$ and, furthermore, is already bounded by the present LHC measurements of Higgs signal strengths. As the mixing angle is inversely proportional to m, the latter already provide mild lower bounds on m, as $m \gtrsim 0.4$ TeV, a region where electroweak observables are shown to be in agreement with their experimental values. Moreover, the mixing introduces modifications on the SM parameters λ_3 and λ_4, which could lead to constraints at the HE-LHC at $\sqrt{s} = 27$ TeV, or even in future colliders with center of mass energies of 100 TeV. Finally the singlet state can be produced at LHC by means of its mixing with the Higgs field. Present upper bounds, from the ATLAS and CMS collaborations, on the production cross section lead to upper bounds on the mixing parameter and, consequently, to lower bounds on m as $m \gtrsim 0.7$ TeV at 95% C.L., while future runs are expected to provide stronger bounds on it.

Finally we summarize the results and present our conclusions in Sec. 9.

2 The model

As stated in the previous section we consider, on top of the Higgs field h, the scalar field ϕ with the Lagrangian $\mathcal{L}_J$ as [3]

$$\mathcal{L}_J = -\frac{M_{\rm Pl}^2}{2}R - \frac{g}{2}\phi^2 R + \frac{1}{2}(\partial_\mu h)^2 + \frac{1}{2}(\partial_\mu \phi)^2 - U(\phi, h), \tag{2.1}$$

which contains a coupling of the field ϕ to the Ricci scalar [4], and the potential is given by

$$\begin{aligned} U(\phi, h) &= U_{\rm SM}(h) + \frac{1}{2}m^2\phi^2 + \frac{1}{2}\lambda_{\phi h}\phi^2 h^2 + \frac{1}{4}\lambda_\phi \phi^4 - \frac{1}{2}\mu \phi h^2 \\ U_{\rm SM}(h) &= -\frac{1}{2}\mu_h^2 h^2 + \frac{1}{4}\lambda_0 h^4. \end{aligned} \tag{2.2}$$

The first four terms of the potential $U(\phi, h)$ in Eq. (2.2) constitute the most general renormalizable potential invariant under the $\mathbb{Z}_2$ symmetry, $\phi \to -\phi$, while the last term is a soft breaking of such symmetry. Besides, for large Higgs field configurations we will be neglecting the mass term μ_h^2, as compared to the λ_0 term, in $U_{\rm SM}(h)$.

The parameters $\lambda_{\phi h}$ and λ_ϕ should be constrained by the slow roll conditions during inflation to very small values $\lambda_{\phi h}, \lambda_\phi \ll 1$, as we will see later on. Their smallness is radiatively stable, as can easily be deduced from their one-loop β functions [5]

$$\beta_{\lambda_{\phi h}} = \frac{\lambda_{\phi h}}{16\pi^2}\left[12\lambda_0 + 8\lambda_{\phi h} + 6\lambda_\phi - \left(\frac{9}{2}g_2^2 + \frac{9}{10}g_1^2 - 6y_t^2\right)\right]\theta(t - t_0), \tag{2.3a}$$

$$\beta_{\lambda_\phi} = \frac{1}{16\pi^2}(8\lambda_{\phi h}^2 + 18\lambda_\phi^2)\theta(t - t_0), \tag{2.3b}$$

where $t - t_0 = \log(\mathcal{Q}/m)$, and $\mathcal{Q}$ is the renormalization scale. In particular the choice $\lambda_{\phi h} = 0$ is technically natural at one loop, as can be seen from Eq. (2.3a). For simplicity we will adopt hereafter the value $\lambda_{\phi h} = 0$. Moreover, from the amplitude of density perturbations, we will see that typically $\lambda_\phi \simeq 10^{-12}$, a value that is very mildly changed by radiative corrections.

[3] In our notation the Lagrangian $\mathcal{L}$ will not contain the factor $\sqrt{-g}$, so that the action S is given by $S = \int d^4x\sqrt{-g}\mathcal{L}$.

[4] Notice that in our model we do not need to primarily introduce any $\xi_{\mathcal{H}}|\mathcal{H}|^2 R$ term. Although a small value of the parameter $\xi_{\mathcal{H}}$ will be generated anyway by radiative corrections [43], its effects on the inflation mechanism will always be negligible, even for values of $\xi_{\mathcal{H}} \simeq \mathcal{O}(1)$; so for simplicity we are assuming that $\xi_{\mathcal{H}} = 0$.

[5] We are defining conventionally here $\beta_X \equiv dX/dt$.

2.1 Jordan frame

The previous Lagrangian is defined in the so-called Jordan frame, and it is a valid framework provided that the field ϕ satisfies the condition $\phi \ll M_{\rm Pl}/\sqrt{g}$. This region, as we will see, encompasses part of the inflationary period, and in particular the end of inflation. The trajectory of fields ϕ and h will proceed along the submanifold given by the minimum of the two-dimensional potential surface, providing a relationship between both fields, as anticipated in the introduction of this paper.

To find the relationship between both fields ϕ and h, along the potential minimum direction, we will follow a general procedure summarized here. Given a potential $V(x, y)$ of two fields x and y, the contour lines corresponding to constant values of the function $V(x, y) =$ constant, satisfy the relation $dV = 0$, which reads

$$\frac{\partial V}{\partial x}\, dx + \frac{\partial V}{\partial y}\, dy = 0 \quad \Rightarrow F(x, y) \equiv \frac{dy}{dx} = -\frac{\partial V/\partial x}{\partial V/\partial y}, \tag{2.4}$$

where, by definition, the function $F[x, y]$ is the slope along the contour lines at the point (x, y). We wish to find the direction $y = f(x)$ that intersects orthogonally every contour line. The slope of this line is obviously $f'(x)$ and the slope of the orthogonal line is $-1/f'(x)$, so the condition for the orthogonal intersection is

$$F(x, f(x)) = -1/f'(x). \tag{2.5}$$

The idea behind the regions is to divide the potential valley into segments such that $\phi = ah^n$. The regions are separated according to which term dominates in the potential. Hence, we will find it useful to work with logarithmic variables

$$y = \log \phi, \qquad x = \log h, \tag{2.6}$$

where the ϕ and h fields are considered in some arbitrary mass units, such that the relation between fields translate into straight lines $y = nx + \log a$. Given the shape of our potential we find a unique solution to (2.5) in each region.

The direction $\phi = f(h)$ that intersects orthogonally every contour line in the plane (h, ϕ) is given by the solution to the equation

$$\frac{\partial V/\partial h}{\partial V/\partial \phi} \cdot \frac{h}{\phi}\bigg|_{\phi = f(h)} = \frac{1}{f'(h)} \tag{2.7}$$

where Eqs. (2.4) and (2.5) have been used.

Therefore, the trajectory in the (ϕ, h) plane is given by relation (2.7), which changes according to the different regions of the potential that we will now introduce. This is validated by the plot of the total potential exhibited in Fig. 1. In all cases, the valley acts as an attractor for the fields, as shown in Ref. [37].

Region A

In this region both fields take their maximum allowed values in the Jordan Frame, and the potential can be approximated by the quartic coupling terms

$$U_{\rm A} \simeq \frac{1}{4}\lambda_0 h^4 + \frac{1}{4}\lambda_\phi \phi^4\,. \tag{2.8}$$

The direction along the minimum can be found, after applying Eq. (2.7) to the potential (2.8), with the function $f(h) = (\lambda_0/\lambda_\phi)^{-1/4} h$, i.e.

$$h = \left(\frac{\lambda_\phi}{\lambda_0}\right)^{\frac{1}{4}} \phi\,. \tag{2.9}$$

We plot in Fig. 1 the complete inflationary potential in the Einstein frame (see Sec. 2.3) and show the direction from Eq. (2.9) with a solid (green) line as specified in the figure caption.

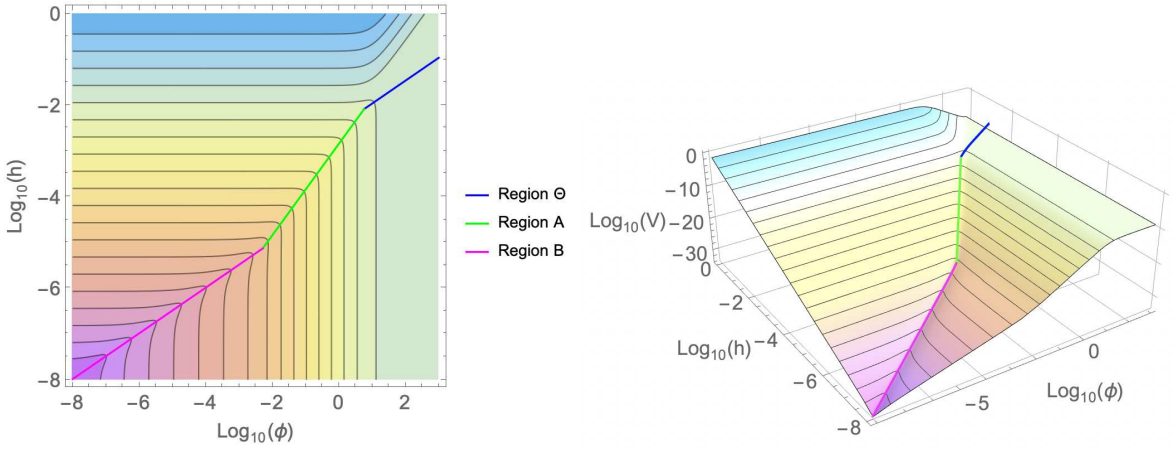

Figure 1: *Left panel: Contour plot of the potential $V(\phi, h)$ in units where $M_{\rm Pl} = 1$ with Regions Θ, A and B and the corresponding minimum submanifolds. Right panel: 3D plot of the potential with the same color code. We use the following numerical values: $g = 0.01$, $m = 10^{10}$ GeV, $\lambda_0 = 0.23$, $\delta_\lambda = 0.15$, $\lambda_\phi = 10^{-12}$.*

Its region of validity is then given by

$$\frac{M_{\rm Pl}}{\sqrt{g}} \gtrsim \phi \gtrsim \frac{2\sqrt{2}m}{\sqrt{\lambda_\phi}} \left(\frac{\delta_\lambda}{\lambda_0}\right)^{\frac{1}{2}}, \qquad h \gtrsim \frac{2\sqrt{2}m}{(\lambda_\phi \lambda_0)^{\frac{1}{4}}} \left(\frac{\delta_\lambda}{\lambda_0}\right)^{\frac{1}{2}}, \tag{2.10}$$

where we have defined the constant δ_λ as

$$\delta_\lambda \equiv \frac{\mu^2}{2m^2}\,. \tag{2.11}$$

Along the minimum direction (2.9) the potential can be written, as a function of ϕ, as

$$U_{\rm A}(\phi) \simeq \frac{1}{2}\lambda_\phi \phi^4\,, \tag{2.12}$$

which will be used in the next section to describe the end of inflation.

To make contact with HI results, in this region we can also use the Higgs field as the explicit variable using the relation between the fields h and ϕ given by Eq. (2.9). This implies that the Ricci term in Eq. (2.1) can be equivalently written as $-\xi_{\rm A}/2\; h^2 R$, with $\xi_{\rm A} = g\sqrt{\lambda_0/\lambda_\phi}$. For typical values of the parameters (e.g. $g \simeq 0.01$, $\lambda_0 \simeq 0.2$, $\lambda_\phi \simeq 10^{-12}$, see Secs. 2.2 and 3), we get $\xi_{\rm A} \approx 4 \cdot 10^4$, which is the value required by HI. Moreover the potential (2.12) can be written, using again (2.9) as

$$U_{\rm A}(h) \simeq \frac{1}{2}\lambda_0 h^4\,. \tag{2.13}$$

This result shows how, in region A, the results of HI could be interpreted in our model with $g \ll 1$, being perfectly consistent with the unitarity condition $\phi \lesssim \Lambda_\phi$.

Region B

In this region, where

$$\phi \lesssim \frac{2\sqrt{2}m}{\sqrt{\lambda_\phi}} \left(\frac{\delta_\lambda}{\lambda_0}\right)^{\frac{1}{2}}, \qquad\qquad m \lesssim h \lesssim \frac{2\sqrt{2}m}{(\lambda_\phi \lambda_0)^{\frac{1}{4}}} \left(\frac{\delta_\lambda}{\lambda_0}\right)^{\frac{1}{2}} \tag{2.14}$$

the potential can be approximated by

$$U_{\rm B} \simeq -\frac{1}{2}\mu\phi h^2 + \frac{1}{2}m^2\phi^2 + \frac{1}{4}\lambda_0 h^4, \tag{2.15}$$

which, using Eq. (2.7), has its minimum along the direction

$$\phi = f(h) \equiv \left(-\frac{3\mu}{4m^2} + \sqrt{\frac{9\mu^2}{16m^4} + \frac{2\lambda_0}{m^2}}\right) h^2 \,. \tag{2.16}$$

Direction (2.16) is shown in the potential plot, Fig. 1, with a solid (magenta) line. If we define the coupling λ as

$$\lambda \equiv \lambda_0 - \delta_\lambda \,, \tag{2.17}$$

in the limit $\lambda \ll 1$ we can write the minimum condition as

$$\phi \simeq \sqrt{\frac{\delta_\lambda}{2}}\, \frac{h^2}{m}\, [1 + \mathcal{O}(\lambda)] \tag{2.18}$$

and the potential (2.15) becomes

$$U_{\rm B} \simeq \frac{1}{4}\lambda h^4 + \mathcal{O}(\lambda^2), \tag{2.19}$$

which shows that the effective quartic coupling in this region is given by λ, instead of λ_0 as in the original potential (2.2).

Region C

In this region $v < \mathcal{Q} \equiv h < m$, where v is the Higgs vacuum expectation value (VEV) and $\mathcal{Q}$, the renormalization scale, is here identified with the classical value of the Higgs field h. The field ϕ hence decouples and is integrated out as

$$\phi = \frac{\mu}{2m^2} h^2 + \mathcal{O}(h^6) \simeq \sqrt{\frac{\delta_\lambda}{2}}\, \frac{h^2}{m}, \tag{2.20}$$

which yields a potential

$$U_{\rm C} \simeq \frac{1}{4}\lambda h^4 + \mathcal{O}(h^8). \tag{2.21}$$

Notice that, to leading order, the solution to the equation of motion of ϕ, Eq. (2.20), agrees with the minimum condition in Region B, Eq. (2.18), which guarantees the continuity between both regions. Moreover the stability of the potential in both Regions B and C is provided by the same condition, $\lambda > 0$.

2.2 Stability of the potential

In Region C, $h < m$, the inflaton field ϕ is integrated out and the potential, as a function of the Higgs h, is given by Eq. (2.21), so that the parameter λ runs as the quartic coupling in the SM potential, according to the SM β function, $\beta_\lambda^{\rm SM}$. In Regions B and A, $h > m$, the inflaton ϕ propagates and thus there is an extra contribution to the running of the parameter λ as [37]

$$\beta_\lambda = \beta_\lambda^{\rm SM} + \frac{1}{2\pi^2}\delta_\lambda(3\lambda + \delta_\lambda)\,\theta(t - t_0), \tag{2.22}$$

where $\theta(x)$ is the Heaviside function, equal to 1 (0) for $x \geq 0$ ($x < 0$), and $t - t_0 = \log(h/m)$. The parameter δ_λ also runs with the renormalization scale as

$$\beta_{\delta_\lambda} = \frac{1}{2\pi^2}\delta_\lambda(3\lambda + 2\delta_\lambda)\,\theta(t - t_0). \tag{2.23}$$

The extra contribution to the running of λ in Eq. (2.22) can solve the Higgs vacuum instability problem provided that:

- The inflaton mass m is smaller than the SM instability scale, $\mathcal{Q}_I \sim 10^{11}$ GeV.
- The value of δ_λ at the scale $\mathcal{Q} = m$, $\delta_\lambda(m)$, is large enough in order to significantly change the value of $\beta_\lambda^{\rm SM}$.

Of course, smaller values of m (i.e. wider regions where ϕ propagates) allow smaller values of $\delta_\lambda(m)$ to satisfy the second criterion. Conversely, for values of m close to $\mathcal{Q}_I$ the minimum value of $\delta_\lambda(m)$ that solves the instability is a largish one.

As we have seen, the condition for the stability of the potential is that the coupling λ defined in Eq. (2.17) is positive definite, $\lambda \geq 0$. We have solved at two-loop the RGE's of the theory for the following set of values of the input parameters [44] at the pole top mass $M_t = 172.76$ GeV,

$$\begin{aligned} g_Y(M_t) = 0.358545, \quad g_2(M_t) = 0.64765, \quad g_3(M_t) = 1.1618, \\ \lambda(M_t) = 0.12607, \qquad h_t(M_t) = 0.9312. \end{aligned} \tag{2.24}$$

In Fig. 2 we show the two-loop running of the parameters λ and λ_0 for two extreme cases, with a light ($m = 1$ TeV, upper panels) and a heavy ($m = 10^{10}$ GeV, lower panels) inflaton. As we can see typical values of δ_λ are smaller for smaller values of m. We have chosen $\delta_\lambda = 0.05$ for $m = 1$ TeV, and $\delta_\lambda = 0.15$ for $m = 10^{10}$ GeV. In both cases the value of $\delta_\lambda(m)$ can be tuned to smaller values, such that the corresponding values of λ at high scales are smaller. On the other hand, larger values of δ_λ are bound by imposing that the theory remains in the perturbative regime up to the high scale. In particular we find, for large values of m, $m \simeq \mathcal{Q}_I$, $\delta_\lambda(m) \lesssim 0.35$, while for m in the TeV region, $\delta_\lambda(m) \lesssim 0.2$. The dashed lines in the left panels are the SM running, shown for comparison. On both left panels, we can see that the condition $0 < \lambda \ll 1$ is satisfied while $\delta_\lambda \gg \lambda$ at $\mathcal{Q} \sim M_{\rm Pl}$.

2.3 Einstein frame

For values of the ϕ field such that $\phi > M_{\rm Pl}/\sqrt{g}$ we must redefine the metric and go to the so-called Einstein frame to recover the Einstein-Hilbert action for the Ricci scalar. To do so, we perform a Weyl redefinition of the metric:

$$g_{\mu\nu} \to \Theta\, g_{\mu\nu}, \qquad\qquad \sqrt{-g} \to \Theta^2\sqrt{-g}. \tag{2.25}$$

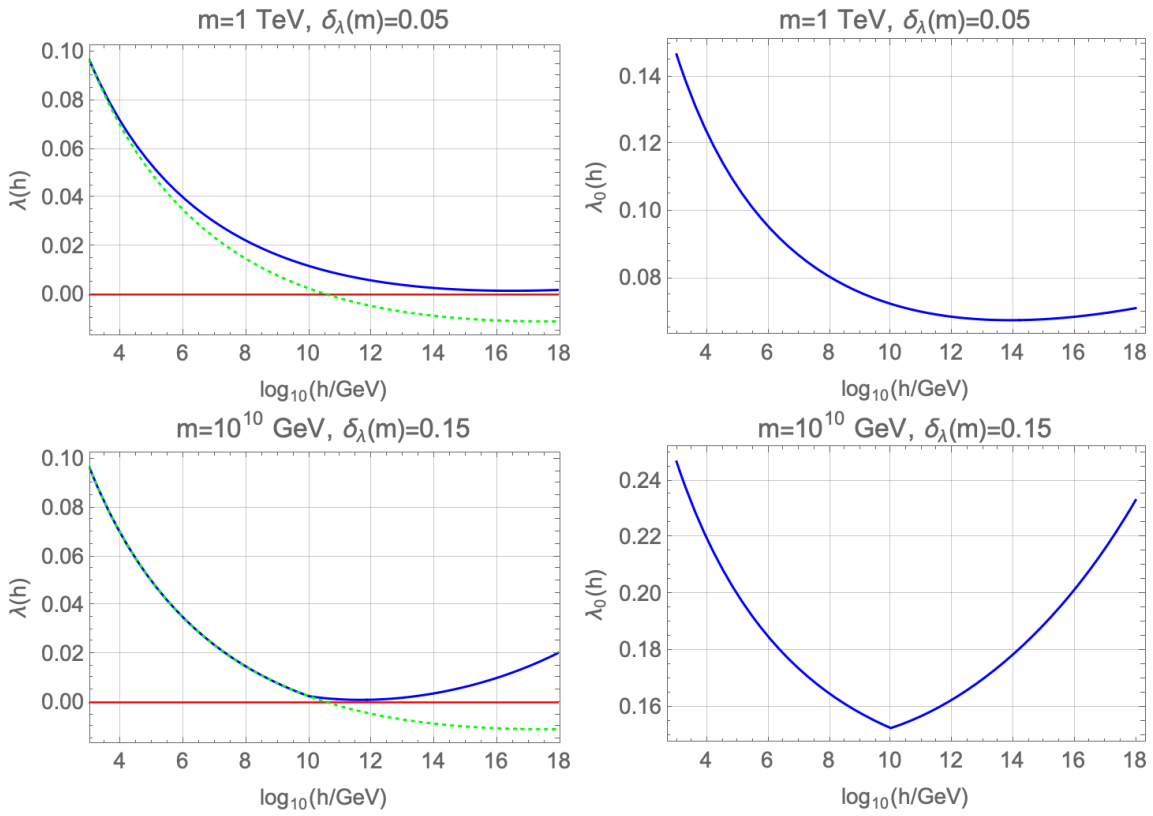

Figure 2: *In blue, two-loop running of λ (left panels) and λ_0 (right panels) for two cases. Top panels: with $m = 1$ TeV, $\delta_\lambda(m) = 0.05$. Bottom panels: with $m = 10^{10}$ GeV, $\delta_\lambda(m) = 0.15$. The green dashed line is the SM running. In both cases one has $\lambda_0 \simeq \delta_\lambda$ for $\mathcal{Q} \sim M_{\rm Pl}$.*

For the Ricci scalar this implies

$$R \to \frac{R}{\Theta} - \bar{R}, \quad \bar{R} = \frac{6}{\Theta^{3/2}} \frac{\partial_\mu \left(g^{\mu\nu} \sqrt{-g}\, \partial_\nu \sqrt{\Theta} \right)}{\sqrt{-g}}. \tag{2.26}$$

Note that R is absent in the correction term $\bar{R}$, hence we will define Θ by demanding that the explicit coupling between ϕ and R disappears from the Lagrangian in the Einstein frame. The Ricci part of the action transforms then as

$$S_R \to S_R^E = -\int d^4x \sqrt{-g} \left(\frac{M_{\rm Pl}^2}{2} + \frac{g\phi^2}{2} \right) \left(R\Theta - \bar{R}\Theta^2 \right) \tag{2.27}$$

and so the definition

$$\Theta(\phi) = \left(1 + \frac{g\phi^2}{M_{\rm Pl}^2} \right)^{-1} \tag{2.28}$$

leads to

$$S_R^E = \int d^4x \sqrt{-g} \left[-\frac{M_{\rm Pl}^2}{2} R + 3\Theta^2 \frac{g^2\phi^2}{M_{\rm Pl}^2} \partial_\mu\phi\partial^\mu\phi \right]. \tag{2.29}$$

We can see from the second (dimension-six effective operator) term in Eq. (2.29) that the cutoff of the theory Λ_ϕ is identified as $\Lambda_\phi \equiv M_{\rm Pl}/g$ (see however comments in footnote 1).

In the meantime the kinetic terms of ϕ and h get transformed to $\frac{\Theta}{2}(\partial_\mu\phi\partial^\mu\phi + \partial_\mu h\partial^\mu h)$ so that the (noncanonical) kinetic terms are given by

$$\mathcal{L}^E_{\rm kin} = \frac{\Theta}{2}\left(1 + \frac{6g^2\phi^2}{M^2_{\rm Pl}}\,\Theta\right)\,\partial_\mu\phi\partial^\mu\phi + \frac{\Theta}{2}\partial_\mu h\partial^\mu h \tag{2.30}$$

leading to the action in the Einstein frame

$$S_E = \int d^4x\sqrt{-g}\left(-\frac{M^2_{\rm Pl}}{2}R + \mathcal{L}^{\rm E}_{\rm kin} - V(\Theta, h)\right), \tag{2.31}$$

where the Einstein frame potential $V(\phi, h)$ is given by

$$V(\phi, h) = \Theta^2(\phi)\, U(\phi, h), \tag{2.32}$$

and $U(\phi, h)$ is given by Eq. (2.2). The potential region where the values of the field ϕ satisfy the condition $\phi > M_{\rm Pl}/\sqrt{g}$ is denoted as Region Θ and is explored hereafter.

Region Θ

As just stated, the Region Θ is characterized by the potential $V(\phi, h)$ in the Einstein frame, i.e. Eq. (2.32) for $g\phi^2 > M^2_{\rm Pl}$, and a straightforward application of Eq. (2.5) shows that, using Eq. (2.7), the direction along the minimum in the two-dimensional potential is given by

$$h^2 = M_{\rm Pl}\left(\frac{\lambda_\phi}{3g\lambda_0}\right)^{\frac{1}{2}}\phi, \tag{2.33}$$

from where the function $f(h)$ in Eq. (2.7) can easily be read out. Along this direction the potential is

$$V_\Theta(\phi) = \Theta^2(\phi)\,\frac{\lambda_\phi}{4}\,\phi^2\left(\frac{M^2_{\rm Pl}}{3g} + \phi^2\right) \simeq \Theta^2(\phi)\,\frac{\lambda_\phi}{4}\,\phi^4, \tag{2.34}$$

where again the last equality comes from the very definition of the Θ region. Notice that the values of the field ϕ at the beginning of inflation, and in particular its value ϕ_* at horizon crossing of the present Universe, belong to Region Θ.

In Fig. 1 we plot the potential in the Einstein frame $V(\phi, h)$ for a chosen set of the parameters values, and we superimpose the lines of minimum submanifolds given by Eqs. (2.33), (2.10) and (2.16), for Regions Θ, A and B, respectively. As we can see they intersect orthogonally, by construction, the contour lines of the potential. In the left panel we plot the contour lines of the potential and in the right panel the three-dimensional plot with the same color codes.

We can try to make contact with HI in Region Θ, as we did in Region A, using the Higgs field h as the explicit variable, by means of the relation between the fields ϕ and h given in Eq. (2.33), which we can write as

$$g\phi^2 = \xi_\Theta\frac{h^4}{M^2_{\rm Pl}}, \qquad\qquad \text{with} \quad \xi_\Theta \equiv \frac{3g^2\lambda_0}{\lambda_\phi}\,. \tag{2.35}$$

The Ricci coupling can then be written as $-\xi_\Theta h^4 R/M^2_{\rm Pl}$, where $\xi_\Theta \simeq 3\cdot 10^7$ by using the typical values of the parameters, $g \simeq 0.01$, $\lambda_0 \simeq 0.2$, $\lambda_\phi \simeq 10^{-12}$ (see Secs. 2.2 and 3). Similarly, we can also write the potential as

$$V_\Theta(h) \simeq \left(1 + \xi_\Theta\frac{h^4}{M^4_{\rm Pl}}\right)^{-2}\,\frac{\lambda_\phi}{4g^2}\,\xi^2_\Theta\,\frac{h^8}{M^4_{\rm Pl}}\,. \tag{2.36}$$

These two expressions show that our model, written in terms of the Higgs field, departs from the conventional HI as it requires an effective dimension-eight operator for the potential which could only appear when the Standard Model is completed by some UV theory, giving rise, after decoupling, to higher dimensional operators.

3 Inflation

Inflation takes place only in Regions Θ (for $\sqrt{g}\phi > M_{\rm Pl}$), and A (for $\sqrt{g}\phi < M_{\rm Pl}$), thus we will choose conditions (2.33) and (2.9), respectively, to relate h and ϕ. In this case the kinetic term (2.30) along the minimum direction can be written in both Regions Θ and A, as

$$\mathcal{L}^{\rm R}_{\rm kin} = \frac{\Theta}{2}\left[1 + 6\frac{g^2\phi^2}{M_{\rm Pl}^2}\Theta + \Delta_{\rm R}\right]\partial_\mu\phi\partial^\mu\phi, \quad ({\rm R} = \Theta, {\rm A}) \tag{3.1}$$

where $\Delta_{\rm R}$ corresponds to the (tiny) contribution of the Higgs kinetic term

$$\Delta_{\rm A} = \left(\frac{\lambda_\phi}{\lambda_0}\right)^{\frac{1}{2}}, \qquad \Delta_\Theta = \frac{M_{\rm Pl}}{4\phi}\left(\frac{\lambda_\phi}{3g\lambda_0}\right)^{\frac{1}{2}} < \left(\frac{\lambda_\phi}{48\lambda_0}\right)^{\frac{1}{2}} \tag{3.2}$$

and the last inequality comes from the condition $\sqrt{g}\phi > M_{\rm Pl}$. Putting numbers we obtain that $\Delta_{\rm A} \sim 10^{-6}$ and $\Delta_\Theta \lesssim 10^{-7}$, so that $\Delta_{\rm R}$ can be safely neglected for numerical calculations in Eq. (3.1).

As for the potential in both inflationary regions, Θ and A, using the previous results we can write it as

$$V_{\rm R}(\phi) \simeq c_{\rm R}\, V(\phi), \quad V(\phi) = \Theta^2(\phi)\,\frac{1}{4}\,\lambda_\phi\,\phi^4\,, \quad c_{\rm A} = 2, \quad c_\Theta = 1\,, \tag{3.3}$$

so that, in both regions, they only differ by a global factor. As the slow roll parameters do depend on ratios of the potential and its derivatives, they will not depend on the global factor $c_{\rm R}$ and can thus be given a universal expression. So for the computation of the slow roll parameters we will just remove the global factor $c_{\rm R}$ and use $V(\phi)$ as the inflationary potential.

We can now define the inflaton χ as a field with canonical kinetic term as

$$\mathcal{L}_{\rm kin} = \frac{1}{2}\partial_\mu\chi\partial^\mu\chi, \tag{3.4}$$

where the change of variable $\phi \to \chi$ is done by

$$\frac{d\chi}{d\phi} \simeq \left[\Theta(\phi)\left(1 + \frac{6g^2\phi^2}{M_{\rm Pl}^2}\,\Theta(\phi)\right)\right]^{\frac{1}{2}} \equiv f(\phi), \tag{3.5}$$

the last equality simply being the definition of the function $f(\phi)$ for later use. Solving the above differential equation gives the approximation

$$\chi \simeq M_{\rm Pl}\sqrt{\frac{1+6g}{g}}\,{\rm arcsinh}\sqrt{g(1+6g)}\,\frac{\phi}{M_{\rm Pl}}, \tag{3.6}$$

which, for $\sqrt{g}\phi \gtrsim M_{\rm Pl}$, can be inverted to get

$$\phi \simeq \frac{M_{\rm Pl}}{2\sqrt{g(1+6g)}}\exp\left(\sqrt{\frac{g}{1+6g}}\,\frac{\chi}{M_{\rm Pl}}\right), \tag{3.7}$$

while $\phi \simeq \chi$, for $\sqrt{g}\phi \lesssim M_{\rm Pl}$, as in this limit the Jordan and Einstein frames should coincide.

However, although the slow roll parameters must be computed from the inflaton potential $V(\chi)$, we will not need to use this explicit solution to obtain the inflationary parameters. Instead, we can keep ϕ as the explicit variable, since performing the change of variables (3.5) in the slow roll parameters definition allows us to avoid making inevitable approximations stemming from the relationship between

the fields ϕ and χ. Hence, we can keep the description of the model in terms of the ϕ field and the potential $V(\phi)$ given in Eq. (3.3).[6] In this framework the slow roll parameters can be written as [45]

$$\epsilon(\phi) = \frac{M_{\rm Pl}^2}{2}\left(\frac{V'(\chi)}{V(\chi)}\right)^2 = \frac{M_{\rm Pl}^2}{2}\left(\frac{V'(\phi)}{V(\phi)}\right)^2 f^{-2}(\phi), \tag{3.8a}$$

$$\eta(\phi) = M_{\rm Pl}^2\,\frac{V''(\chi)}{V(\chi)} = M_{\rm Pl}^2\left[\frac{V''(\phi)}{V(\phi)}f^{-2}(\phi) - \frac{V'(\phi)}{V(\phi)}\,f'(\phi)f^{-3}(\phi)\right], \tag{3.8b}$$

$$\begin{aligned}\xi^2(\phi) &= M_{\rm Pl}^4\,\frac{V'(\chi)V'''(\chi)}{V^2(\chi)} = M_{\rm Pl}^4\,\frac{V'(\phi)}{V(\phi)}f^{-4}(\phi) \\ &\cdot\left[\frac{V'''(\phi)}{V(\phi)} - 3\frac{V''(\phi)}{V(\phi)}f'(\phi)f^{-1}(\phi) + \frac{V'(\phi)}{V(\phi)}\left(3f'^{\,2}(\phi)f^{-2}(\phi) - f''(\phi)f^{-1}(\phi)\right)\right],\end{aligned} \tag{3.8c}$$

where the function $f(\phi)$ was defined in (3.5). Their current observational bounds are, from Ref. [46]:

$$\begin{aligned}&\epsilon < 0.0044 && (95\%\text{C.L.}),\\ &\eta = -0.015 \pm 0.006 && (68\%\text{C.L.}),\\ &\xi^2 = 0.0029^{+0.0073}_{-0.0069} && (95\%\text{C.L.}).\end{aligned} \tag{3.9}$$

We should evaluate the slow-roll parameters at the field value $\phi_* = \phi(N_*)$ with

$$N_* = \frac{1}{M_{\rm Pl}^2}\int_{\chi_E}^{\chi_*}\frac{V(\chi)}{V'(\chi)}\,d\chi = \frac{1}{M_{\rm Pl}^2}\int_{\phi_E}^{\phi_*}\frac{V(\phi)}{V'(\phi)}\,f^2(\phi)\,d\phi, \tag{3.10}$$

being N_* the number of e-folds at which the reference scale exits the horizon. Here ϕ_E, the value of ϕ at the end of inflation, is defined by the condition $\epsilon(\phi_E) = 1$ and can be computed analytically. A plot of its dependence on g is shown on the left panel of Fig. 3. One can evaluate the integral (3.10) to find

$$N_* = \frac{1}{4}\left[\frac{(1+6g)(\phi_*^2 - \phi_E^2)}{2M_{\rm Pl}^2} - 3\log\frac{M_{\rm Pl}^2 + g\phi_*^2}{M_{\rm Pl}^2 + g\phi_E^2}\right] \tag{3.11}$$

and then solve for $\phi_* \equiv \phi(N_*)$.[7] A plot of ϕ_*, for $N_* = 60$, and its dependence on g is shown in the left panel of Fig. 3. The dark shading region is excluded as there $\phi_* > \Lambda_\phi \equiv M_{\rm Pl}/g$ and so there is a unitarity violation (see however footnote 1). This constraint provides an upper bound on the value of the parameter g as $g \lesssim 0.0508$.[8]

We display, in the right panel of Fig. 3, the functions $\epsilon(\phi_*)$ and $\eta(\phi_*)$ as functions of g. The observational constraints (3.9) provide a lower bound on the Ricci coupling as $g \gtrsim 0.0096$. When combined with the upper bound from unitarity, the allowed region in the g parameter is given in the

[6] From here on we will use primes to denote derivatives of a function with respect to its functional dependence, e.g., $V'(\chi) = dV(\chi)/d\chi$ and $V'(\phi) = dV(\phi)/d\phi$.

[7] We can solve Eq. (3.11) for $\phi(N_*)$ recursively, first ignoring the logarithm for the first iteration and then inserting each solution into the next iteration (which this time contains all terms). The sequence converges quickly to the exact solution. After 3–4 iterations the relative error is already $\sim 10^{-3}$ at most.

[8] For $g < 1$ the cutoff Λ_ϕ is trans-Planckian, and from Fig. 3 we can see that during inflation $\Delta\phi \simeq 20\,M_{\rm Pl}$, which satisfies the so-called Lyth bound [47]. Such behavior induces nonnegligible quantum gravity corrections to the potential. However, the terms induced by quantum gravity effects are suppressed, not by factors $\phi^n/M_{\rm Pl}^n$, but by factors $V/M_{\rm Pl}^4$ and $m^2/M_{\rm Pl}^2$, see Sec. 2.4 of Ref. [48]. Hence, as long as the inflationary potential takes sub-Planckian values and $m \ll M_{\rm Pl}$ (like in our model), quantum gravity effects are insignificant, regardless of the values of g or Λ_ϕ.

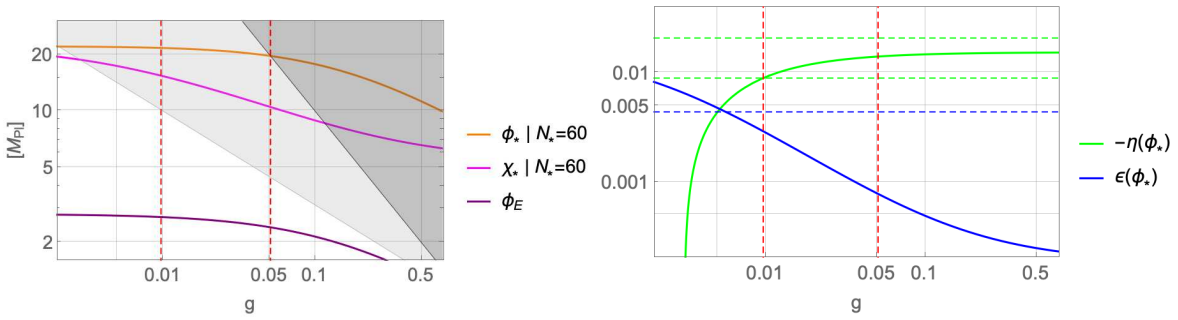

Figure 3: *Left panel: ϕ_E, ϕ_* and χ_* in unit of $M_{\rm Pl}$, as functions of g. The dark shading region violates the unitarity bound $\phi < M_{\rm Pl}/g$. The white area corresponds to Region A and the light shading one to Region Θ. Right panel: slow roll parameters evaluated at the beginning of inflation and their corresponding observational bounds (dashed, matching color). The bound for $\epsilon(\phi_*)$ is an upper bound.*

range [9]

$$0.0096 \lesssim g \lesssim 0.0508. \tag{3.12}$$

Finally we have found that, in the relevant region of the g parameter, the parameter ξ^2 is $|\xi^2| \sim 10^{-4}$, well in agreement with the experimental range in Eq. (3.9).

For the allowed region of the slow roll parameters in Fig. 3, the cosmological observables, the scalar spectral index $n_s \simeq 1 - 6\epsilon(\phi_*) + 2\eta(\phi_*)$, the spectral index running $n_s' \simeq 16\epsilon(\phi_*)\eta(\phi_*) - 24\epsilon^2(\phi_*) - 2\xi^2(\phi_*)$, and the tensor to scalar ratio $r = 16\,\epsilon(\phi_*)$, fall inside the experimental range given by [46, 50],

$$n_s = 0.9649 \pm 0.0042, \qquad n_s' = -0.0045 \pm 0.0067, \qquad r = 0.014^{+0.010}_{-0.011} \tag{3.13}$$

where we have included, in the last r determination, the most recent combined result from the BICEP/Keck collaboration [50]. In particular, for the allowed range in the coupling g (3.12) the theory predicts

$$0.96448 \lesssim n_s \lesssim 0.96695 \qquad (0.96783) \tag{3.14a}$$

$$-0.00063 \lesssim n_s' \lesssim -0.00019 \qquad (-0.00005) \tag{3.14b}$$

$$0.0467 \gtrsim r \gtrsim 0.0124 \qquad (0.00296) \tag{3.14c}$$

where the unbracketed right-hand side (RHS) bounds come from the unitarity bound, while the bracketed ones come from disregarding the latter in view of the comments in footnote 1 [10]. As we can see both predicted ranges (with/without considering the unitarity bound) in (3.14) nicely fit inside the allowed range in Eq. (3.13). These results also agree with those of model $(n, p) = (2, 4)$ in the recent work of Ref. [51], where general inflationary models with nonminimal inflaton couplings to gravity have been analyzed.

[9] One should worry about the stability, under radiative corrections, of such small values of the g parameter. Contributions to the one-loop $\beta_{\xi_{\mathcal{H}}}$ function, in the Ricci coupling $(\xi_{\mathcal{H}}/2)\, h^2 R$, from the contribution of the SM fields (top quark, gauge and Higgs bosons), have been computed in Refs. [43, 49] where it is shown that the renormalization from the weak to the high scale of $\xi_{\mathcal{H}}$ is $\lesssim 20\%$. In the case of our coupling $(g/2)\,\phi^2 R$, as ϕ is not directly coupled to the SM fields, the g running between m and the high scales is suppressed by the mixing angle α between the fields ϕ and h (see Sec. 8), so that $\beta_g \simeq 2\delta_\lambda (v^2/m^2)\beta_{\xi_{\mathcal{H}}} \ll \beta_{\xi_{\mathcal{H}}}$. In this way the running of the g parameter can be safely neglected.

[10] If we disregard the unitarity bound, see the comments in footnote 1, there is no upper bound on g from observational constraints and the cosmological observables for larger values of g asymptotically go to the RHS values in parenthesis.

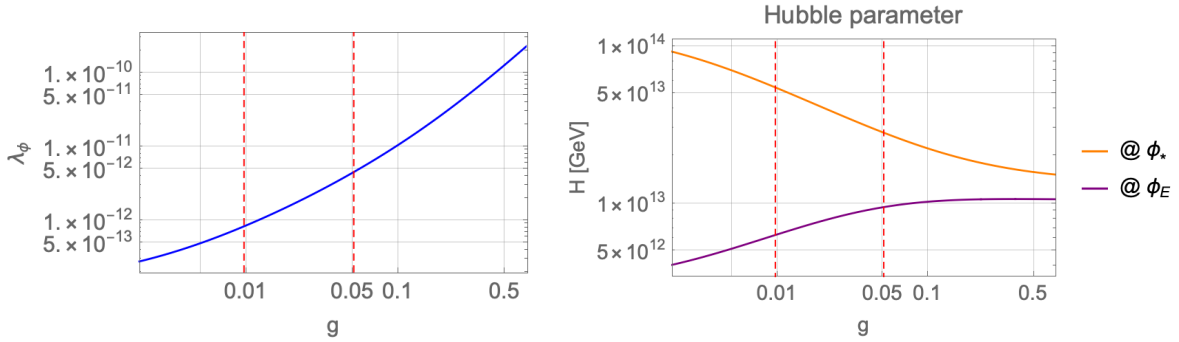

Figure 4: *Left panel: The inflaton self-coupling λ_ϕ as a function of g. Right panel: The Hubble parameter H at the end of inflation $H(\phi_E)$ and for the number of e-folds N_*, $H(\phi_*)$ as functions of g. In both plots the vertical red lines show the range for g where the slow roll cosmological observables and unitarity constraints are met.*

We now use the constraint on the amplitude of scalar fluctuations to find an analytical relation for the inflaton self-coupling λ_ϕ, since this quantity is obtained from the potential as

$$A_s = \frac{1}{24\pi^2 M_{\rm Pl}^4}\frac{V_\Theta(\phi_*)}{\epsilon(\phi_*)}, \tag{3.15}$$

where we are using as inflaton potential V_Θ, as the ϕ_* line in the left panel of Fig. 3 is inside the light shading region, where the inflaton potential corresponds to that in Region Θ, Eq. (3.3). We can then compute λ_ϕ as

$$\lambda_\phi = 96\,\pi^2\,g^2\,A_s\,\epsilon(\phi_*)\left(1+\frac{M_{\rm Pl}^2}{g\phi_*^2}\right)^2. \tag{3.16}$$

Using the observed value of A_s from Ref. [46], $A_s^{\rm obs} = 2.2\cdot 10^{-9}$, as well as the values of $\epsilon(\phi_*)$ and ϕ_* from Fig. 3, we plot, in the left panel of Fig. 4 the parameter λ_ϕ as a function of the Ricci coupling g. Notice that, inside the allowed region in Eq. (3.12), we obtain $\lambda_\phi \sim 10^{-12}$ as postulated earlier.

Finally we can compute the Hubble parameter during inflation $H(\phi)$. From the Friedmann equation we have that the energy density of the inflaton reads as $\rho(\phi) = 3M_{\rm Pl}^2 H^2(\phi)$. Since we are assuming a slow roll evolution of the inflaton, we can neglect the kinetic part in the energy density and consider $\rho(\phi) \simeq V_{\rm R}(\phi)$. Therefore in Region A, i.e. around the end of inflation and, in particular, at ϕ_E, $H_E \equiv H(\phi_E)$,

$$H(\phi) = \frac{M_{\rm Pl}}{g}\sqrt{\frac{\lambda_\phi}{6}}\left(1+\frac{M_{\rm Pl}^2}{g\phi^2}\right)^{-1}. \tag{3.17}$$

For the value $\phi = \phi_*$, in Region Θ, this further simplifies to

$$H_* \equiv H(\phi_*) = 2^{3/2}\pi M_{\rm Pl}\sqrt{\epsilon(\phi_*)A_s^{\rm obs}}. \tag{3.18}$$

We plot in the right panel of Fig. 4 the Hubble parameters at the end of inflation, i.e. for $\phi = \phi_E$, H_E, and at the beginning of inflation, for a number of e-folds $N_* = 60$, H_*. As we can see from the right panel of Fig. 4, for the lower bound of g, $g \simeq 0.01$, the Hubble parameter changes, between ϕ_E and ϕ_*, by one order of magnitude, from $H_* \simeq 5.5\cdot 10^{13}$ GeV, to $H_E \simeq 6.4\cdot 10^{12}$ GeV. On the other hand, for the upper bound of g, $g \simeq 0.05$, the Hubble parameter changes by a few, from $H_* \simeq 2.8\cdot 10^{13}$ GeV

to $H_E \simeq 10^{13}$ GeV. As we can see the absolute upper bound on the Hubble parameter in our model is $H_* \lesssim 5.5 \cdot 10^{13}$ GeV, or equivalently an inflation scale $V_\Theta^{1/4}(\phi_*) \lesssim 1.5 \cdot 10^{16}$ GeV, in agreement with the observational upper bounds from the Planck collaboration, Ref. [46], given by

$$H_*^{\rm obs} < 6 \cdot 10^{13} \ \ {\rm GeV}, \qquad\qquad (V_*^{\rm obs})^{1/4} < 1.6 \cdot 10^{16} \ {\rm GeV} \quad (95\% \ {\rm C.L.}). \tag{3.19}$$

Consequently our model, independently of the value of m, is a high scale inflation model, where the Hubble parameter does depend on the value of g and is maximized for its lower bound.

4 Gauge field production

In this section we will consider the generation of fully helical hypermagnetic fields that will be transformed into baryon asymmetry at the EWPT. Of course all modes produced during inflation, except the last modes that exit the horizon at the end of inflation reentering the horizon at the onset of reheating, get diluted [14]. For that reason we will be concerned by the last e-folds of inflation, corresponding to the inflaton value $\phi \simeq \phi_E$, well inside Region A with a potential given by Eq. (3.3).

We need a source of $\mathcal{CP}$-violation and we will assume the $\mathcal{CP}$-odd dimension-five operator given by

$$\sqrt{-g}\,\mathcal{L}_{\not{\mathcal{CP}}} = -\frac{1}{4}\frac{\phi}{\tilde{f}_\phi} Y_{\mu\nu}\widetilde{Y}^{\mu\nu}, \tag{4.1}$$

where $Y^{\mu\nu}$ is the field strength of the hypercharge gauge field Y^μ, and $\widetilde{Y}^{\mu\nu} = \frac{1}{2}\epsilon^{\mu\nu\rho\sigma}Y_{\rho\sigma}$ its dual tensor. This Lagrangian term is scale invariant (it does not change when going from the Jordan to the Einstein frame), and should appear in the effective theory after integrating out some UV physics, heavier than the inflaton field. A possible and simple UV completion, with a heavy vectorlike fermion coupled to the field ϕ by a $\mathcal{CP}$-violating Yukawa coupling, and giving rise to Eq. (4.1) is presented in App. A. However, in the rest of this paper, we will be agnostic about the origin of such a term as it may arise from a great variety of models.

In addition to this, by virtue of the minimum condition in Region A, Eq. (2.9), the Higgs background value is nonzero (it is anchored to the value of the field ϕ), and so the electroweak symmetry is broken, meaning we are producing ordinary $U(1)_{\rm EM}$ magnetic fields, as the Z fields are very massive for those values of the background field h, and hence much harder to produce. In this way the $\mathcal{CP}$-violating term in the broken phase, at the end of inflation, will look like

$$\sqrt{-g}\,\mathcal{L}_{\not{\mathcal{CP}}} = -\frac{1}{4}\frac{\phi}{f_\phi} F_{\mu\nu}\widetilde{F}^{\mu\nu}, \tag{4.2}$$

where $F_{\mu\nu}$ is the electromagnetic field strength, corresponding to the photon field A_μ, and we have rescaled the constant f_ϕ as

$$f_\phi = \frac{\tilde{f}_\phi}{\cos^2\theta_W}, \tag{4.3}$$

where θ_W is the EW angle.

At reheating, h will drop at its potential minimum at zero, because of the sudden dominance of the thermal correction terms, and we will recover the symmetric phase. This is a necessary requirement for a successful baryogenesis as the helical fields participating in the chiral anomaly must belong to the unbroken electroweak sector. This is because, in the symmetric phase of the electroweak plasma, the chiral anomaly induces the phenomenon where variations in baryon, N_B, and lepton, N_L, number

can be induced by changes in the $SU(2)_L$ Chern-Simons number $N_{\rm cs}$ and/or $U(1)_Y$ hypermagnetic helicity $\mathscr{H}_Y$ as

$$\Delta N_B = \Delta N_L = N_g \left(\Delta N_{\rm cs} - \frac{g_Y^2}{16\pi^2}\, \Delta \mathscr{H}_Y \right), \tag{4.4}$$

where $N_g = 3$ is the number of fermion generations and g_Y the $U(1)_Y$ coupling. This equation tells us that any change in the $U(1)_Y$ helicity leads to a fermion asymmetry, in particular when projecting ordinary magnetic fields into hypermagnetic fields at the end of inflation. However, as long as $T \gtrsim 160$ GeV, the electroweak sphalerons are in equilibrium in the plasma, hence any fermion asymmetry gets washed out in less than a Hubble time, and only the $U(1)_Y$ helical fields remain.

As the $U(1)_Y$ helical magnetic fields participate in the baryogenesis process [18], while $U(1)_{\rm EM}$ helical magnetic fields are produced at the end of inflation, the projection of the latter on the former must be taken into account with a factor [11]

$$\boldsymbol{A}_Y = \cos\theta_W\, \boldsymbol{A}, \qquad \mathscr{H}_Y = \cos^2\theta_W\, \mathscr{H}\,. \tag{4.5}$$

The Z fields can also project onto $U(1)_{\rm Y}$ fields but, as stated before, we will ignore this contribution as they were too heavy to be produced.

Moreover after inflation, in Region B, the Higgs will start relaxing to its minimum and, if some conditions are satisfied, the Higgs could source extra helical magnetic fields, as was studied in Ref. [21], and eventually overproduce the BAU from the induced coupling

$$\sqrt{-g}\,\mathcal{L}_{\not{CP}} = -\frac{1}{4}\sqrt{2\delta_\lambda}\frac{|\mathcal{H}|^2}{m f_\phi}\cos^2\theta_W Y_{\mu\nu}\widetilde{Y}^{\mu\nu} \equiv -\frac{1}{4}\frac{|\mathcal{H}|^2}{\Lambda_{\mathcal{H}}^2} Y_{\mu\nu}\widetilde{Y}^{\mu\nu}\,, \tag{4.6a}$$

$$\Lambda_{\mathcal{H}} \simeq 8.7\cdot 10^{13}\ \text{GeV}\left(\frac{m}{10^{10}\ \text{GeV}}\right)^{\frac{1}{2}}\left(\frac{\delta_\lambda}{0.15}\right)^{-\frac{1}{4}}\left(\frac{f_\phi}{0.1\, M_{\rm Pl}}\right)^{\frac{1}{2}}, \tag{4.6b}$$

where we have used the minimum condition in Eq. (2.18). Nevertheless the required relaxation mechanism found in Ref. [21] should not work under the present conditions, because one necessary condition for the Higgs relaxing into the hypermagnetic fields is not fulfilled here, namely that $h \gtrsim 3\cdot 10^{15}$ GeV at the end of inflation. In fact in our model, as a consequence of the definition (2.16) of Region B,

$$h \lesssim \frac{2\sqrt{2}m}{(\lambda_\phi\lambda_0)^{\frac{1}{4}}}\left(\frac{\delta_\lambda}{\lambda_0}\right)^{\frac{1}{2}} \lesssim 4\cdot 10^{13}\ \text{GeV},$$

where we chose the parameters configuration that maximizes the RHS bound. Therefore a significant production of helical magnetic fields from the Higgs decay after inflation is unlikely, and we can consider $\mathcal{L}_{\not{CP}}$ as inactive in Region B.

4.1 Helical magnetic fields

As stated earlier, we will mainly be interested in values of the inflaton field near the end of inflation, i.e. $\phi \simeq \phi_E$, which means that ϕ and h evolve in Region A of the potential, given by (3.3). For such values of ϕ, the differential equation (3.5) admits the simple solution $\phi \simeq \chi + \mathcal{O}(g)$. We recall that χ is the true inflaton field with canonical kinetic term and action

$$\begin{aligned} S \simeq \int d^4x \left[\sqrt{-g}\left(-\frac{M_{\rm Pl}^2}{2}R + \frac{1}{2}\partial_\mu\chi\partial^\mu\chi - \frac{1}{4}F_{\mu\nu}F^{\mu\nu} - V(\chi)\right) - \frac{\chi}{4f_\phi}\, F_{\mu\nu}\tilde{F}^{\mu\nu}\right] \\ + \int d^4x\, \sqrt{-g}\, i\,\bar{\psi}\not{\mathcal{D}}\psi, \end{aligned} \tag{4.7}$$

[11] Bold characters stands for 3D vectors in space.

where we have included the interaction of fermionic currents, corresponding to charge Q fermions, with the electromagnetic fields (encoded in the covariant derivative $\mathcal{D}_\mu \equiv \partial_\mu - eQA_\mu$), the $\mathcal{CP}$-violation term and the inflaton potential

$$V(\chi) = \frac{\lambda_\phi}{2}\left(1 + \frac{g\chi^2}{M_{\rm Pl}^2}\right)^{-2}\chi^4. \tag{4.8}$$

Varying the action (4.7) with respect to $A_\mu = (A_0, \boldsymbol{A})$ leads to the gauge equations of motion in the radiation gauge, $A_0 = 0$ and $\boldsymbol{\nabla}\cdot\boldsymbol{A} = 0$,

$$\left(\frac{\partial^2}{\partial\tau^2} - \nabla^2 - \frac{\chi'}{f_\phi}\,\boldsymbol{\nabla}\times\right)\boldsymbol{A} = 0, \tag{4.9}$$

where τ is the conformal time, defined by $g_{\mu\nu} = a^2(\tau)\,\eta_{\mu\nu}$, and we assume a homogeneous inflaton with only zero mode, $\chi(\tau, \boldsymbol{x}) = \chi(\tau)$. Unless otherwise specified, all quantities and fields are *comoving*.

During the inflationary period one has [12]

$$\chi' = \dot\chi a \simeq -\frac{\dot\chi}{\tau H(\chi)}\,, \tag{4.10}$$

and the field velocity $\dot\chi$ is computed from the equation of motion for the inflaton obtained from the action (4.7)

$$\ddot\chi + 3H(\chi)\,\dot\chi + V'(\chi) = \frac{\boldsymbol{E}\cdot\boldsymbol{B}}{a^4 f_\phi}, \tag{4.11}$$

where we have used that $F_{\mu\nu}\tilde F^{\mu\nu} = -4\,\boldsymbol{E}\cdot\boldsymbol{B}$. From the slow roll conditions, we can neglect $\ddot\chi$, since

$$\frac{\ddot\chi}{3H\dot\chi} = \frac{\epsilon - \eta}{3}, \tag{4.12}$$

where we are already neglecting the backreaction of the generated magnetic field on the inflaton (i.e. we are neglecting the term $\boldsymbol{E}\cdot\boldsymbol{B}/a^4 f_\phi$ in Eq. (4.11)), a hypothesis that will be self-consistently checked a posteriori (see Sec. 4.3). During the last e-folds of inflation, our model provides $|\epsilon - \eta|\,/\,3 < 0.1$. Hence, we obtain

$$\chi' = \frac{M_{\rm Pl}^2}{\tau}\,\frac{V'(\chi)}{V(\chi)}, \tag{4.13}$$

where we have made use of Eq. (4.10).

We now quantize the gauge field $\boldsymbol{A}$ in momentum space

$$\boldsymbol{A}(\tau, \boldsymbol{x}) \,=\, \sum_{\lambda=\pm}\int \frac{d^3k}{(2\pi)^3}\,\left[\boldsymbol{\epsilon}_\lambda(\boldsymbol{k})\,a_\lambda(\boldsymbol{k})\,A_\lambda(\tau,\boldsymbol{k})\,e^{i\boldsymbol{k}\cdot\boldsymbol{x}} + \text{h.c.}\right], \tag{4.14}$$

where $\lambda = \pm$ is the photon polarization and $a_\lambda(\boldsymbol{k})$ ($a^\dagger_\lambda(\boldsymbol{k})$) are annihilation (creation) operators that fulfill the canonical commutation relations

$$[a_\lambda(\boldsymbol{k}), a^\dagger_{\lambda'}(\boldsymbol{k'})] = (2\pi)^3\delta_{\lambda\lambda'}\delta^{(3)}(\boldsymbol{k} - \boldsymbol{k'})\,. \tag{4.15}$$

[12] As for fields, we denote the derivative with respect to τ with a prime and the derivative with respect to the cosmic time t with a dot, e.g. $\chi' = d\chi/d\tau$ and $\dot\chi = d\chi/dt$.

The polarization vectors $\boldsymbol{\epsilon}_\lambda(\boldsymbol{k})$ satisfy the conditions [13]

$$\begin{aligned} \boldsymbol{k}\cdot\boldsymbol{\epsilon}_\lambda(\boldsymbol{k}) &= 0\,, & \boldsymbol{k}\times\boldsymbol{\epsilon}_\lambda(\boldsymbol{k}) &= -i\lambda k\,\boldsymbol{\epsilon}_\lambda(\boldsymbol{k})\,, \\ \boldsymbol{\epsilon}^*_{\lambda'}(\boldsymbol{k})\cdot\boldsymbol{\epsilon}_\lambda(\boldsymbol{k}) &= \delta_{\lambda\lambda'}\,, & \boldsymbol{\epsilon}^*_\lambda(\boldsymbol{k}) &= \boldsymbol{\epsilon}_\lambda(-\boldsymbol{k})\,, \end{aligned} \tag{4.16}$$

where $k\equiv|\boldsymbol{k}|$. The equation of motion for the modes yields

$$\frac{\partial^2 A_\lambda}{\partial\tau^2} + k\left(k+\lambda\,\frac{2\xi}{\tau}\right)A_\lambda = 0, \tag{4.17}$$

which is the Coulomb wave equation, with

$$\xi = \frac{M_{\rm Pl}^2}{2f_\phi}\,\frac{V'(\chi)}{V(\chi)} = \frac{M_{\rm Pl}}{f_\phi}\sqrt{\frac{\epsilon(\chi)}{2}} > 0, \tag{4.18}$$

where Eq. (4.13) has been used and $\epsilon(\chi)$ is the slow-roll parameter. Let us mention that, even if the first equality in Eq. (4.18) looks model dependent, as it depends on the potential and its derivative, in fact it is very model independent because the last relation only relies on the slow roll regime of the inflationary potential, and $\epsilon(\chi)\simeq 1$ at the end of inflation. We have done a self-consistency check by comparing the numerical results of both expressions and found no significative difference, see below.

As already emphasized, all modes produced during inflation will get diluted, except the last mode that exits the horizon right before the end of inflation. This mode reenters the horizon at the onset of reheating and is the source for the BAU. Hence, it is only necessary to consider the mode produced at $\phi_E\simeq\chi_E$, for which $\epsilon(\chi_E)\simeq 1$, and hence, using the last equality in Eq. (4.18) we obtain for ξ the constant value

$$\xi \simeq \frac{M_{\rm Pl}}{\sqrt{2}f_\phi}\,. \tag{4.19}$$

We numerically checked that this approximation coincides with the exact solution:

$$\xi = \left[\frac{M_{\rm Pl}^2}{2f_\phi}\,\frac{V'(\phi)}{V(\phi)}\,\frac{d\phi}{d\chi}\right]_{\phi=\phi_E}, \tag{4.20}$$

where equations (3.5) and (4.8) should be used. A plot of ξ as a function of g is shown in the top left panel of Fig. 5 (solid lines) where we compute the exact solution in Eq. (4.20). As we can see the values of ξ are nearly constant with respect to g, a behavior that is well approximated by the expression of ξ in Eq. (4.19). A plot of ξ as a function of f_ϕ is displayed in the bottom left panel of Fig. 5 (solid lines) for the range of values of g allowed by the final inflationary analysis. As all results of the following sections are very sensitive to the precise value of the parameter ξ we will use next the exact expression for ξ in all numerical calculations.

Notice that in this section we are neglecting, in the RHS of Eq. (4.17), the possible effect of the fermion currents $eQ\,\boldsymbol{J}_\psi$, appearing in the action Eq. (4.7), and in particular their backreaction on the produced helical magnetic fields. This phenomenon, known as the Schwinger effect, will appear for sufficiently strong magnetic fields, hence for large (small) enough values of the ξ (f_ϕ) parameter. In this section we will consider the case of backreactionless fermion currents (i.e. small values of ξ) and will devote Sec. 4.2 (where those values will be quantified) to the analysis of the Schwinger effect and its backreaction on the helical magnetic fields.

[13] A simple realization can be given in terms of a real basis with the orthonormal vectors $(\boldsymbol{k}/|\boldsymbol{k}|,\boldsymbol{e}_i)$, $(i=1,2)$, such that $\boldsymbol{k}\cdot\boldsymbol{e}_i=\boldsymbol{e}_1\cdot\boldsymbol{e}_2=0$ and $\boldsymbol{e}_i\cdot\boldsymbol{e}_i=1$, with $\boldsymbol{\epsilon}_\lambda\equiv(\boldsymbol{e}_1+i\lambda\boldsymbol{e}_2)/\sqrt{2}$, from where identities (4.16) follow.

The general solution of (4.17) is

$$A_\lambda = \frac{iF_0(\lambda\xi,-k\tau)+G_0(\lambda\xi,-k\tau)}{\sqrt{2k}} \tag{4.21}$$

where F_0 and G_0 are, respectively, the regular and irregular Coulomb wave functions with index 0 [10].[14] At early times, the above solution has the asymptotic behavior that corresponds to the Bunch-Davies vacuum of the modes. In fact during inflation, where $\epsilon(\chi) \ll 1$, we obtain, using Eq. (4.18), that $\xi \ll 1$ and therefore $|k\tau| \gg 2\xi$, so we can write $A_\lambda \propto e^{-ik\tau}$. However, at the end of inflation $\epsilon(\chi_E) \simeq 1$ and so we can have $\xi \gtrsim 1$. Then, only one mode develops both parametric and tachyonic instabilities for $k \simeq k_c$ where

$$k_c = 2\xi a_E H_E, \qquad a_E = a(\tau_E), \tag{4.22}$$

while the other one stays close to its vacuum. As in our model $\xi > 0$, and during inflation $\tau < 0$, the mode exhibiting the instability is the one with the $\lambda = +$ polarization. For late times, $k \ll k_c$ (i.e. $|k\tau| \ll 2\xi$), F_0 can be neglected and the growing mode solution can be approximated by [10, 14, 52]

$$A_\lambda \simeq \frac{G_0}{\sqrt{2k}} \simeq \frac{1}{\sqrt{2k}}\left(\frac{k}{2\xi a_E H_E}\right)^{\frac{1}{4}} \exp\left\{\pi\xi - 2\sqrt{\frac{2\xi k}{a_E H_E}}\right\}. \tag{4.23}$$

Another assumption in this solution is that $H(\chi) \simeq H_E$ during the last e-folds of inflation. As we have seen that the g dependence of ξ is mild, the main g dependence of all our predictions from here on, will arise only from the g dependence of the Hubble parameter H_E, see the right panel of Fig. 4. Moreover, from the approximated value of the ξ parameter in Eq. (4.19) we can see that ξ can be traded for the value of the parameter f_ϕ such that $\xi \gg 1$ corresponds to $f_\phi \ll M_{\rm Pl}$. Moreover, as we see from the explicit solution in Eq. (4.23), there is an exponential magnification for large values of ξ. However, as shown later on in Sec. 4.3, for very large values of ξ, the backreaction on the inflation dynamics from magnetic fields cannot be neglected, which will lead to upper bounds on the values of ξ, or correspondingly to lower bounds on the values of f_ϕ.

Assuming homogeneity in momentum space, the comoving $U(1)_{\rm EM}$ helicity is by definition

$$\mathscr{H} = \lim_{V\to\infty}\frac{1}{V}\int_V d^3x\,\langle \boldsymbol{A}\cdot\boldsymbol{B}\rangle = \int_0^{k_c} dk\,\frac{k^3}{2\pi^2}\left(|A_+|^2-|A_-|^2\right), \tag{4.24}$$

where $\langle\cdot\rangle$ is the expectation value of quantum fields and the integral $V^{-1}\int_V d^3x$ is the spatial average, which is trivial for space independent quantities. Since the magnetic fields are maximally helical, we can neglect one mode and set the other one to (4.23). We cut off the integral at the last mode to exit the horizon given by (4.22). The resulting computation gives the amount of comoving helicity at the time of the end of inflation, as

$$\mathscr{H} \simeq \frac{45}{2^{15}}\,\frac{a_E^3 H_E^3}{\pi^2\xi^4}\,e^{2\pi\xi}, \tag{4.25}$$

where we have used the approximation for $\xi \gg 1$.[15]

On the right panels of Fig. 5, we display the magnetic helicity in function of g (top panel) and f_ϕ (bottom panel). The exponential regime given by Eq. (4.25) is shown by solid lines for values $f_\phi \gtrsim 0.15\,M_{\rm Pl}$ ($\xi \lesssim 4.7$). For solid lines with $f_\phi \lesssim 0.15\,M_{\rm Pl}$, and dotted lines, the backreaction of fermion currents on the magnetic fields (Schwinger effect) cannot be neglected, as we will see in the next section where we will continue our comments on these plots.

[14] See also Sec. 14 of Ref. [52].

[15] In fact, we have found that the approximation is valid up to $\mathcal{O}(e^{-8\xi})$ terms, so that it is good enough for $\xi \gtrsim$ 2-3.

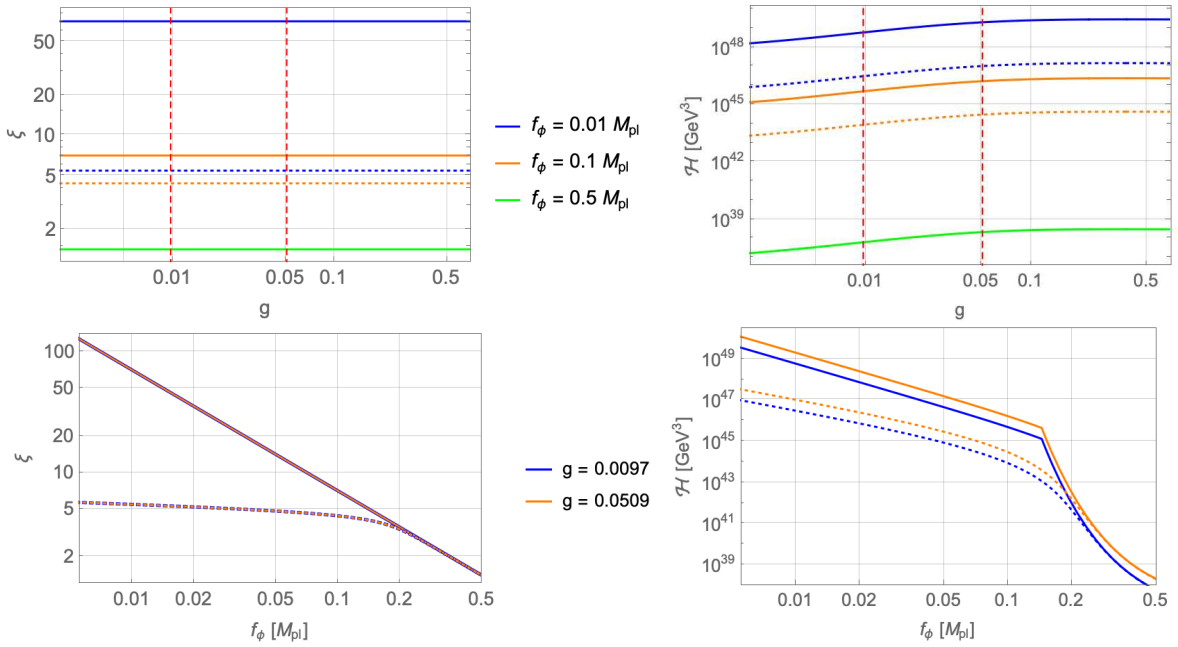

Figure 5: *Top panels: the ξ parameter (left panel) and produced helicity at the end of inflation (right panel) as a function of g for various values of f_ϕ. The vertical red lines display the range for g where the inflation model is valid. Bottom panels: the same as top panels but as functions of f_ϕ in the same interval of values of g. In all panels solid lines correspond to the Schwinger effect maximal estimate while dashed lines are the equilibrium estimate. In the bottom left panel, blue and orange lines overlap since the result is insensitive to g.*

The comoving $U(1)_{\rm EM}$ energy density in the magnetic and electric fields are similarly computed as

$$\rho_B \equiv \lim_{V\to\infty} \frac{1}{2\,V} \int_V d^3x \, \langle \boldsymbol{B}^2 \rangle = \int_0^{k_c} dk \, \frac{k^4}{4\pi^2} \left(|A_+|^2 + |A_-|^2 \right), \tag{4.26a}$$

$$\rho_E \equiv \lim_{V\to\infty} \frac{1}{2\,V} \int_V d^3x \, \langle \boldsymbol{E}^2 \rangle = \int_0^{k_c} dk \, \frac{k^2}{4\pi^2} \left(|\partial_\tau A_+|^2 + |\partial_\tau A_-|^2 \right). \tag{4.26b}$$

Using the (backreactionless) value (4.23) for A_+, and neglecting the other mode, we similarly obtain the analytical solutions at the end of inflation, for $\xi \gg 1$ (see footnote 15)

$$\rho_B \simeq \frac{315}{2^{18}} \, \frac{a_E^4 H_E^4}{\pi^2 \xi^5} \, e^{2\pi\xi}, \tag{4.27a}$$

$$\rho_E \simeq \frac{63}{2^{16}} \, \frac{a_E^4 H_E^4}{\pi^2 \xi^3} \, e^{2\pi\xi} = \frac{4\xi^2}{5} \, \rho_B. \tag{4.27b}$$

Hence the total comoving electromagnetic energy density is

$$\rho_{\rm EM} = \rho_E + \rho_B \simeq \rho_B \left(1 + \frac{4\xi^2}{5} \right). \tag{4.28}$$

Finally, we will also need the correlation length of the magnetic field which can be estimated as [53]

$$\ell_B = \frac{2\pi}{\rho_B}\int_0^{k_c} dk\,\frac{k^3}{4\pi^2}\left(|A_+|^2+|A_-|^2\right). \tag{4.29}$$

Likewise its analytical solution at the end of inflation is given by

$$\ell_B \simeq \frac{8}{7}\frac{\pi\,\xi}{a_E H_E}, \tag{4.30}$$

Note that the above three quantities are comoving and apply to ordinary electromagnetic field, while we will denote in subsequent sections their equivalents for the hypercharge $U(1)_Y$ in the symmetric phase with the index Y. The corresponding physical quantities are given by $\mathscr{H}^{\rm ph} = \mathscr{H}/a^3$, $\rho^{\rm ph} = \rho/a^4$, $\ell_B^{\rm ph} = a\ell_B$. Finally, we will conventionally set $a_E = 1$.

To close this section, we would like to underline that maximally helical fields, $\boldsymbol{E}(\boldsymbol{k})$ and $\boldsymbol{B}(\boldsymbol{k})$, in (Fourier transformed) momentum space are collinear as, using the identities (4.16), one can easily check that both are proportional to $\boldsymbol{\epsilon}_\lambda(\boldsymbol{k})$. Besides, these fields in configuration space are, using the approximation (4.23), (almost) collinear. In fact, one can compute, using our approximated solution for the backreactionless solution, the angle θ measuring the collinearity of the electric and magnetic fields, as

$$\cos\theta = \frac{\langle \boldsymbol{E}\cdot\boldsymbol{B}\rangle}{|E|\cdot|B|}, \tag{4.31}$$

where we define [16]

$$|E| \equiv \sqrt{\langle \boldsymbol{E}^2\rangle}\,, \qquad\qquad |B| \equiv \sqrt{\langle \boldsymbol{B}^2\rangle}\,. \tag{4.32}$$

Using Eqs. (4.27) and (4.45) we obtain, for $\xi \gg 1$

$$\cos\theta \simeq \frac{3\sqrt{5}}{7} \simeq 0.958, \tag{4.33}$$

which corresponds to the angle $\theta \simeq 0.0016\pi$. As a result we have proved that the fields $\boldsymbol{E}$ and $\boldsymbol{B}$ are (almost) collinear, a property that will be used when applying the Schwinger effect in the next section.

4.2 Schwinger effect

In the presence of strong gauge fields, i.e. for $\xi \gg 1$, fermions charged under the gauge group are produced by the backreaction of gauge fields which source the fermion equations of motion. The corresponding currents can then, in turn, backreact on the produced gauge fields and change their (so-called backreactionless) solutions. This phenomenon is called the Schwinger effect and we will consider it in this section. Moreover, the fermions produced by this effect are at the origin of another phenomenon, called the *chiral plasma instability*, that we will study in Sec. 7.2.

As the Higgs VEV is different from zero at the end of inflation, as we have already explained, the EW gauge bosons are massive and the system is in the broken phase. Massless gauge bosons are the photons, and we can consider the theory of electrically charged fermions in the presence of the $U(1)_{\rm EM}$ gauge group. In the case of a Dirac fermion with mass m and electric charge Q, the produced current satisfies the Ohm's law $\mathbf{J} = \sigma\mathbf{E}$, where σ is the Schwinger conductivity given, for collinear $\boldsymbol{E}$ and $\boldsymbol{B}$ fields, by [42]

$$\sigma = \mathrm{tr}\,\frac{|eQ|^3}{6\pi^2}\frac{|B|}{a^2 H}\,\coth\left(\frac{\pi|B|}{|E|}\right)\exp\left(-\frac{\pi m^2 a^2}{|eQ|\,|E|}\right), \tag{4.34}$$

[16] Hereafter in this paper we are skipping the space average, as all background quantities are homogenous and so $\lim_{V\to\infty}\frac{1}{V}\int_V d^3x = 1$.

where the trace runs over all charged fermions ψ_i, with mass m_i and charge Q_i, such that $\pi m_i^2 \ll |eQ_i||E|$, and $e(\mathcal{Q}) = \sqrt{4\pi\alpha(\mathcal{Q})} \simeq 0.33$ is the electromagnetic gauge coupling at the characteristic scale of Schwinger pair production $\mathcal{Q} \simeq \rho_{\rm EM}^{1/4}$ [42]. However, as the Higgs VEV is suppressed with respect to the classical value of ϕ, see Eq. (2.9), while Yukawa couplings for first and second generation fermions, are small, their corresponding square masses are much smaller than typical values of the produced electric field, and so we can make the simple reasonable approximation that only the first and second generation fermions are massless and contribute to the conductivity (4.34).

We have to stress here that, in spite of the fact that the Higgs VEV is large after inflation $h_E \simeq 10^{15}$ GeV, which yields large masses m_f for fermions, as the typical values of the produced electric fields are also large, typically $|E| \simeq h_E^2$, the small values of the Yukawa couplings for light fermions make that their pair production is not effectively blocked. Moreover, as their contribution to the conductivity is exponential in m_f^2 we can consider fermions that contribute to the conductivity as effectively massless. Here we have considered for simplicity that the two first generations of quarks and leptons contribute to the conductivity. Had we considered also the third generation would have amounted to a global factor in σ of 3/2, which would not change at all the qualitative results in this paper.

The backreaction of fermionic currents, the Schwinger effect, has been proven to roughly be encoded into a redefinition of the ξ parameter, $\xi \to \xi_{\rm eff}$, as [41]

$$\xi_{\rm eff} = \xi - \Delta\xi, \qquad \Delta\xi = \frac{e^3}{3\pi^2} \coth\left(\frac{\pi|B|}{|E|}\right) \frac{|E|}{H_E^2}\,, \tag{4.35}$$

where only first and second generation fermions have been considered. The correction becomes significant, $\Delta\xi/\xi \gtrsim 0.1$, for $\xi \gtrsim 3.7$, which corresponds to $f_\phi \lesssim 0.19\, M_{\rm Pl}$. Hence for $\xi \gtrsim 3.7$ the Schwinger effect must be taken into account, and the amplitudes of the gauge fields in equilibrium must satisfy the equation [41]

$$2\xi_{\rm eff} H|E|\,|B| - 2H(|E|^2 + |B|^2) = \dot\rho_{\rm EM} = 0 \tag{4.36}$$

Previous studies [20, 41, 42] have considered two regimes: (i) Maximal estimate and (ii) Equilibrium estimate. We will use them to compute the MHD quantities yielding the BAU, i.e., the helicity, its derivative, the electric and magnetic energies, as well as the magnetic correlation length. Both regimes follow different strategies: in the maximal estimate all quantities are capped by other relations that still depend on the parameter ξ, whereas in the equilibrium case the exponential relations from the previous section stay with the counterpart of the substitution (4.35) on ξ.

4.2.1 Maximal estimate

In this case we assume the exponential behaviors of the backreactionless solutions to be valid until they saturate the maximal value that we will display hereafter. We numerically determine the value of crossing, which happens for $\xi \simeq 4.4$–4.7 depending on each quantity, corresponding to $f_\phi \simeq 0.15\, M_{\rm Pl}$. However, as we just saw, for such value the Schwinger effect can no longer be neglected, so there remains in this process a gray area of uncertainty as to the exact transition between the two regimes.

The maximum electric and magnetic energy density can be estimated as the solution of Eq. (4.36) [41], i.e.

$$|E|^2 + |B|^2 = \xi_{\rm eff}|E|\,|B|. \tag{4.37}$$

This replacement yields an equation relating the $|E|$ and $|B|$ fields that can be solved analytically. We then choose, as definition of our maximal estimate, the solution $(|E|, |B|)$ of (4.37) that maximizes the

product $|E|\cdot|B|$.[17] For $\xi \gg 1$, the result approximates to:

$$|E|_{\rm max} \simeq \frac{2\pi^2}{e^3}\,\xi H_E^2, \tag{4.38a}$$

$$|B|_{\rm max} \simeq \frac{2\pi^2}{3e^3}\,\xi^2 H_E^2, \tag{4.38b}$$

although, in the numerical calculations, we of course use the exact solutions. Hence we obtain our maximal helicity estimate

$$\mathscr{H}_{\rm max} \simeq \frac{8\pi^4}{9e^6}\,\xi^3 H_E^3 \tag{4.39}$$

as well as our maximal energy density estimate

$$\rho_{\rm EM}^{\rm max} \simeq \frac{2\pi^4}{9e^6}\,\xi^4 H_E^4. \tag{4.40}$$

Finally, combining (4.24) and (4.29), and assuming maximally helical magnetic field, we get for the correlation length (still for large ξ)

$$\ell_B^{\rm max} = \pi\,\frac{\mathscr{H}_{\rm max}}{\rho_B^{\rm max}} \simeq \frac{4\,\pi}{\xi H_E}\,. \tag{4.41}$$

In this case the upper labels "max" on $\rho_{\rm EM}^{\rm max}$ and $\ell_B^{\rm max}$ mean that they are computed from maximal quantities, but do not necessarily mean upper bounds. In fact the estimate for $\ell_B^{\rm max}$ is a conservative one, as it matches the corresponding backreactionless quantity at a small value, $\xi \simeq 1.4$, so in principle we would expect higher values for $\ell_B^{\rm max}$, giving rise to bigger Reynolds numbers (see Sec. 7.1). Still we will use the estimate in Eq. (4.41) for our numerical calculations.

We finally recall that in this case the parameter ξ remains as given by (4.19), hence it corresponds to the solid lines displayed in the left panels of Fig. 5. For the solid lines of the right panels, however, the helicity has two regimes: it first obeys the exponential relation (4.25) until it reaches its maximal value, then follows (4.39).

4.2.2 Equilibrium estimate

In this case, we take into account the backreaction of the chiral fermions on the gauge fields by just replacing the parameter ξ with the effective one given by (4.35) in the backreactionless solutions. Using (4.27) and (4.32) the latter becomes

$$\frac{63}{2^{15}\pi^2}\,\frac{e^{2\pi\xi_{\rm eq}}}{\xi_{\rm eq}^3} = \left(\frac{3\pi^2}{e^3}\right)^2 (\xi-\xi_{\rm eq})^2\,\tanh^2\left(\sqrt{\frac{5}{4}}\,\frac{\pi}{\xi_{\rm eq}}\right). \tag{4.42}$$

When the backreactionless solutions are used, and to make it explicit which case we are handling, we chose to label the effective parameter as $\xi_{\rm eq}$. The solution of Eq. (4.42) provides the function $\xi_{\rm eq} = \xi_{\rm eq}(\xi)$ and, using (4.19), we can obtain $\xi_{\rm eq}$ as a function of f_ϕ (and g) that we plot on the left panels of Fig. 5 in dotted lines.

[17] Notice that our definition of maximal estimate departs from that used in Ref. [41], where separate maximal conditions to the configurations for the fields E and B (corresponding to absolute maximal values independently reached by the configurations E and B) are imposed, so that their corresponding partners do not satisfy Eq. (4.37). Conversely, our criterium of maximizing the helicity guarantees that our solution satisfies Eq. (4.37).

Next, the MHD quantities are calculated in the same way as in the case without considering the Schwinger effect, but with the replacement $\xi \to \xi_{\rm eq}$, hence

$$\mathscr{H}_{\rm eq} = \mathscr{H}(\xi_{\rm eq}), \qquad \rho^{\rm eq}_{B/E} = \rho_{B/E}\,(\xi_{\rm eq}), \qquad \ell^{\rm eq}_{B} = \ell_{B}\,(\xi_{\rm eq}), \tag{4.43}$$

where (4.25), (4.27) and (4.30) should be used. On the right panels of Fig. 5, we plot the equilibrium estimate for the helicity as a function of f_ϕ and g in dotted lines.

4.2.3 Final comments

Needless to say, neither the maximal nor the equilibrium estimates are true solutions to the gauge equations of motion in the presence of the Schwinger effect, which introduces highly nonlinear effects into them. However, numerical solutions taking into account the backreaction from fermion currents have been recently considered in Refs. [42, 54] which show that, for values of the ξ parameter for which the Schwinger effect becomes relevant, the numerical solution for the different quantities, in particular for the helicity, lies between the maximal and equilibrium estimates. This feature remains if the Bunch-Davies vacuum is damped by the conducting medium, even for extreme cases of very large damping, leading to very suppressed vacua. Therefore, we expect that the solution to the complicated problem of taking into account all the backreaction from Schwinger fermions currents will be somewhere between the two considered estimates, and thus the allowed region by the BAU will be in between the allowed regions that we will exhibit in Secs. 6 and 7 for both estimates.

4.3 Self-consistency condition

In previous subsections, we have computed the helical gauge fields generated in the presence of the inflationary background, after estimating the backreaction of fermion currents on gauge fields, but we have neglected the backreaction of gauge fields on the inflaton dynamics. We will now compute the conditions to have negligible backreaction of the generated gauge fields on the inflaton equations of motion, such that we can reliably trust the inflationary predictions, and therefore the actual generation of helical magnetic fields. Needless to say this condition is mainly a simplifying one, and allows to work out the inflationary model independently on the generated gauge fields. As we will see in Sec. 5, this condition is also related to the possibility of reheating the Universe after the inflationary period by the preheating mechanism, although this scenario deserves further studies.

Once we have obtained the helicity, we can compute the RHS of the inflaton equation of motion (4.11), as in the radiation gauge they are simply related by

$$\langle \boldsymbol{E}\cdot\boldsymbol{B}\rangle = -\frac{1}{2}\frac{d}{d\tau}\langle \boldsymbol{A}\cdot\boldsymbol{B}\rangle. \tag{4.44}$$

Ignoring for the moment the Schwinger effect on the produced gauge fields, using (4.24), (4.25) and the relation in the de Sitter universe $aH = -\tau^{-1}$, one gets at the end of inflation, for $\xi \gg 1$

$$|\langle \boldsymbol{E}\cdot\boldsymbol{B}\rangle| \simeq \frac{135}{2^{16}}\frac{a_E^4 H_E^4}{\pi^2\xi^4}\, e^{2\pi\xi}. \tag{4.45}$$

In the absence of backreaction of the gauge field on the inflaton equation of motion, the inflationary equation (4.11) with slow roll conditions reduces to $3H\dot{\chi} \simeq -V'(\chi)$. Thus, in order to consistently neglect the backreaction on the inflaton, we must simply enforce that, in the inflaton equation of motion (4.11), the RHS term is negligible compared to the potential term, i.e.

$$\frac{\sqrt{2}\,\xi}{M_{\rm Pl}}\left|\frac{\langle \boldsymbol{E}\cdot\boldsymbol{B}\rangle}{V'(\chi)}\right| \ll 1, \tag{4.46}$$

where we used (4.19). This condition is independent of the reheating temperature and should hold during the full magnetogenesis process, hence during the last few e-folds of inflation, so we can evaluate it using the above solutions for $\langle \boldsymbol{E}\cdot\boldsymbol{B}\rangle$ at the end of inflation. Then, using the definition of the slow roll parameter $\epsilon(\chi)$, we can write $V' \simeq \sqrt{2}V/M_{\rm Pl}$ at the end of inflation, and hence, for $\chi \simeq \chi_E$, Eq. (4.46) becomes

$$\xi\,|\langle \boldsymbol{E}\cdot\boldsymbol{B}\rangle| \ll V(\chi_E). \tag{4.47}$$

Moreover it is interesting to note that, if we ignore the Schwinger effect, combining $\rho_{\rm EM} \simeq \rho_E$ given by (4.27b), together with (4.45), we get

$$2\,\rho_{\rm EM} \simeq \xi\,|\langle \boldsymbol{E}\cdot\boldsymbol{B}\rangle|\,. \tag{4.48}$$

Notice that, for collinear $\boldsymbol{E}$ and $\boldsymbol{B}$ with the substitution $\xi \to \xi_{\rm eff}$, this equation yields the starting point of the Schwinger maximal estimate, i.e. Eq. (4.37).

Hence, the condition (4.46) evaluated at the end of inflation is equivalent to imposing

$$2\,\rho_{\rm EM} \ll V(\chi_E). \tag{4.49}$$

Notice that the condition (4.49) is stronger than the condition for neglecting $\rho_{\rm EM}$ in the Friedman equation, i.e., $\rho_{\rm EM} \ll 3H^2M_{\rm Pl}^2 \simeq V(\chi_E)$, so that the latter does not need to be imposed.

Now taking into account the Schwinger effect, the equilibrium estimate is obtained by the replacement $\xi \to \xi_{\rm eq}$ in the expression (4.45), as described in Sec. 4.2.2. Hence, the consistency condition in the Schwinger equilibrium estimate is given by Eq. (4.49) where $\xi \to \xi_{\rm eq}$, i.e.

$$2\,\rho_{\rm EM}^{\rm eq} \ll V(\chi_E), \tag{4.50}$$

a stronger condition than the one coming from the Friedman equation $\rho_{\rm EM}^{\rm eq} \ll V(\chi_E)$, but much weaker than Eq. (4.49) where we were ignoring the Schwinger effect, since $\rho_{\rm EM}^{\rm eq} \ll \rho_{\rm EM}$.

On the other hand, for the maximal estimate, using the results from Sec. 4.2.1, we can write

$$|\langle \boldsymbol{E}\cdot\boldsymbol{B}\rangle|_{\rm max} \simeq |E|_{\rm max}\,|B|_{\rm max} \simeq \frac{1}{3}\left(\frac{2\pi^2}{e^3}\right)^2 \xi^3 H_E^4\,, \tag{4.51}$$

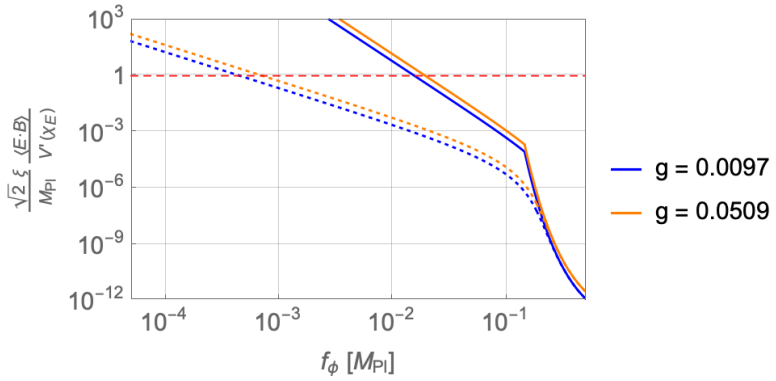

Figure 6: *Ratio between the potential term and the backreaction term in the inflaton equation of motion, see Eq. (4.46), for the range of values of g allowed by inflation. Solid lines are the maximal estimate while dashed lines are the equilibrium estimate, after taking into account the Schwinger effect.*

where in the first step we maximize the product by assuming a collinear configuration of $\boldsymbol{E}$ and $\boldsymbol{B}$ [41], while the second step is justified for large values of ξ. A similar reasoning for the consistency condition does apply to this case, for which the total density is dominated by the energy stored in the magnetic field, $\rho_{\rm EM} \simeq \rho_B$, and such that the explicit maximal estimate found implies that, for large ξ,

$$6\,\rho_{\rm EM}^{\rm max} \simeq \xi\ |\langle \boldsymbol{E}\cdot\boldsymbol{B}\rangle|_{\rm max}\,. \tag{4.52}$$

Hence, in the maximal estimate, imposing condition (4.46) is equivalent to requiring

$$6\,\rho_{\rm EM}^{\rm max} \ll V(\chi_E), \tag{4.53}$$

which is again stronger than the condition for neglecting the total gauge energy density in the Friedman equation, $\rho_{\rm EM}^{\rm max} \ll V(\chi_E)$.

We display in Fig. 6 the left-hand side of Eq. (4.46) as a function of f_ϕ for the range allowed on the parameter g by the inflationary observables, using for the $|E|$ and $|B|$ fields both the maximal and the equilibrium estimates. In conclusion, condition (4.46) is satisfied for:

$$\begin{aligned} f_\phi &\gtrsim 1.9\cdot 10^{-2}\,M_{\rm Pl} \qquad \text{(Maximal estimate)},\\ f_\phi &\gtrsim 7.2\cdot 10^{-4}\,M_{\rm Pl} \qquad \text{(Equilibrium estimate)}. \end{aligned} \tag{4.54}$$

5 Reheating

At the stage of inflation all the energy is concentrated in the slowly rolling inflaton field. Soon after, it begins to oscillate near the minimum of its effective potential and eventually perturbatively decays into SM particles that interact with each other, and come to a state of thermal equilibrium in a process called *reheating*. However, the Universe can also be reheated nonperturbatively in a much quicker timescale through coherent fields effects while it oscillates in its potential, in a process known as *preheating* [55].

In inflationary models where the inflaton is coupled to the Chern-Simons term with coupling $1/f_\phi$, as in Eq. (4.2), recent lattice simulations [56, 57], in the absence of fermionic currents, have shown that even for a negligible electromagnetic energy density at the end of inflation, the Universe can efficiently preheat provided that the coupling $1/f_\phi$ in Eq. (4.2) is large enough. In particular preheating occurs when $f_\phi \lesssim f_\phi^c$, with $f_\phi^c \simeq 0.11 M_{\rm Pl}$, i.e. for $\xi \gtrsim \xi_c$ with $\xi_c \simeq 6.7$. However, in this region the backreaction of the fermion currents on the helical gauge fields cannot be neglected, and we should adapt the previous results to our different estimates in the presence of the Schwinger effect.

For the equilibrium estimate, we have seen in Sec. 4.2.2 that the effect of the backreaction can be encoded into the redefinition of the parameter $\xi \to \xi_{\rm eq}$ while using the backreactionless solutions but as functions of $\xi_{\rm eq}$. Therefore a straightforward application of the results from Refs. [56, 57] should provide the condition for efficient preheating as $\xi_{\rm eq} \gtrsim \xi_{\rm eq}^c$ with $\xi_{\rm eq}^c \simeq 6.7$ which translates, using Eq. (4.42), to

$$f_\phi \lesssim 2.4\cdot 10^{-4} M_{\rm Pl}. \qquad \text{(Equilibrium estimate)} \tag{5.1}$$

This bound is outside the region where we can neglect the backreaction of the helical fields on the inflaton, Eq. (4.54).

In the case of the Schwinger maximal estimate of the electromagnetic fields, see Sec. 4.2.1, we can easily perform a similar translation on the same requirement. To this end, we define a new effective parameter $\xi_{\rm max}$ that mimics the effect of the maximal estimate once plugged into the backreactionless solutions as

$$|\langle \boldsymbol{E}\cdot\boldsymbol{B}\rangle|_{\xi_{\rm max}} = |E_{\rm max}(\xi)|\ |B_{\rm max}(\xi)|, \tag{5.2}$$

where $|E_{\rm max}(\xi)|$ and $|B_{\rm max}(\xi)|$ are the maximal estimates of the electromagnetic fields from Eqs. (4.38), and $\langle \boldsymbol{E}\cdot\boldsymbol{B}\rangle_{\xi_{\rm max}}$ is the corresponding backreactionless product given by (4.45) evaluated at $\xi=\xi_{\rm max}$. From there, the condition for efficient preheating $\xi_{\rm max}\gtrsim\xi^c_{\rm max}$, with $\xi^c_{\rm max}\simeq 6.7$, translates into

$$f_\phi \lesssim 5.6\cdot 10^{-3} M_{\rm Pl}, \qquad \text{(Maximal estimate)} \tag{5.3}$$

which again is inconsistent with the condition (4.54) on no backreaction of helical fields on the inflaton dynamics.

The previous results can be easily understood by considering that, in the presence of the backreaction of the Schwinger currents on the helical fields, the required coupling, between ϕ and the Chern-Simons term, for preheating must be much stronger than in the backreactionless case. This is because the produced helical gauge fields are much weaker, in the presence of backreaction, for a fixed value of the coupling $M_{\rm Pl}/f_\phi$.

We thus conclude that, after considering the backreaction of fermion currents on the helical fields in both estimates, the preheating mechanism is not consistent with the self-consistency condition obtained in Sec. 4.3. Hence, in our model preheating does not occur and reheating should take place by perturbative decays of the inflaton into the SM matter only.

Reheating then takes place after inflation, during the inflaton oscillations around its minimum, by perturbative inflaton decays. In this period, between the end of inflation $t_E\sim 1/H_E$ and the reheating time $t_{\rm rh}\sim 1/\Gamma_\chi$, where Γ_χ is the inflaton decay width, the Universe temperature first grows from zero to a maximum temperature T_0 given by [58, 59]

$$T_0 \simeq 0.61\sqrt{T_{\rm rh}T^{\rm ins}_{\rm rh}}, \tag{5.4}$$

where, assuming thermalization,

$$T_{\rm rh}=\left(\frac{90}{\pi^2 g_*}\right)^{\frac{1}{4}}\sqrt{\Gamma_\chi M_{\rm Pl}} \tag{5.5}$$

is the reheating temperature and $g_*=106.75$ is the number of relativistic degrees of freedom. Also, in this work we define $T^{\rm ins}_{\rm rh}$ as a reference temperature given by the above equation with $\Gamma_\chi\simeq H_E$. It would correspond to the reheating temperature for instant reheating, and takes the value $T^{\rm ins}_{\rm rh}\simeq 2.13\ (2.61)\cdot 10^{15}$ GeV for $g\simeq 0.01\ (0.05)$ in our model.

The temperature T_0 is attained at a time t_0 when the scale factor a grows by an $\mathcal{O}(1)$ factor, i.e. $a_0\simeq 1.5\, a_E$, and, after that [18], the Universe evolves toward the reheating temperature following the law $T\sim a^{-3/8}$ [43], with a scale factor $a_{\rm rh}$ given by

$$a_{\rm rh}\simeq 0.4\ a_E\left(\frac{T^{\rm ins}_{\rm rh}}{T_{\rm rh}}\right)^{\frac{4}{3}}. \tag{5.6}$$

At the reheating temperature, the inflaton energy density has completely decayed and the Universe is fully dominated by radiation, giving rise to a radiation dominated era where the temperature evolves as $T\sim 1/a$. Of course, the value of the inflaton decay width Γ_χ, and the reheating temperature $T_{\rm rh}$, depend on the particular interactions between the inflaton and the Standard Model particles that we will now explore.

[18] The energy density is dominated, after the end of inflation, by the inflaton energy density $\rho_\chi(t)$, which decays as $e^{-\Gamma_\chi t}$, so that at the reheating temperature the energy density is dominated by the radiation energy density $\rho_R(t)$.

In the present model, the Lagrangian from Eq. (2.2) contains the interaction term $\sqrt{\delta_\lambda/2}\, m\, \chi h^2$ which gives rise to the leading inflaton decay channel $\chi \to hh$, with a decay width given by [60]

$$\Gamma(\chi \to hh) = \frac{\delta_\lambda\, m}{16\pi}\sqrt{1-\frac{4m_h^2}{m^2}}, \tag{5.7}$$

where $m_h = 125.25$ GeV is the Higgs mass. As the inflaton is stabilizing the EW vacuum (see Sec. 2.2), which has an instability around $\mathcal{Q}_I \simeq 10^{11}$ GeV, we can reliably put the upper bound on m as $m \lesssim \mathcal{Q}_I$, and fix $m \simeq 5\cdot 10^{10}$ GeV while $\delta_\lambda \lesssim 0.35$ on perturbative grounds (see Sec. 2.2). This gives for the decay width $\Gamma(\chi \to hh) \simeq 3.5\cdot 10^8$ GeV leading, using Eq. (5.5), to a reheating temperature given by $T_{\rm rh} \simeq 1.6\cdot 10^{13}$ GeV, which corresponds to $T_{\rm rh}/T_{\rm rh}^{\rm ins} \sim 10^{-2}$. On the other hand, the lowest bound on m, fixed by phenomenological considerations (see Sec. 8) to $m \simeq 10^3$ GeV, together with $\delta_\lambda \lesssim 0.2$ (see Sec. 2.2) provide $\Gamma(\chi \to hh)$ of a few GeV and correspondingly $T_{\rm rh} \simeq 10^9$ GeV, which corresponds to $T_{\rm rh}/T_{\rm rh}^{\rm ins} \sim 10^{-6}$. Hence from now on, we will consider the temperature ratio $T_{\rm rh}/T_{\rm rh}^{\rm ins}$ as a parameter of the model, which will become handy for the baryogenesis and constraints calculations. We also stress that this ratio mainly reflects the dependence of coming results on m, as just sketched above.

There are of course other channels that can contribute to Γ_χ but, as we will demonstrate hereafter, they are all subdominant. For instance, the coupling (4.1) gives rise to the decay channel $\chi \to AA$ into two gauge bosons with a decay width given by [56]

$$\Gamma(\chi \to AA) \simeq \frac{m^3}{64\pi f_\phi^2}, \tag{5.8}$$

which is subleading with respect to the channel $\chi \to hh$ for the relevant values of m and f_ϕ. In particular $\Gamma(\chi \to AA) \simeq 10^{-5}$ GeV for $m = 5\cdot 10^{10}$ GeV, while $\Gamma(\chi \to AA) \simeq 10^{-28}$ GeV for $m = 10^3$ GeV. Moreover, there is a mixing angle α between ϕ and h (see Sec. 8), which is sizable for $m \sim \mathcal{O}$(few) TeV, while of course is negligible for $m \gg 1$ TeV, given by $\sin\alpha \simeq \sqrt{2\delta_\lambda}v/m$. This mixing opens up the χ decays into the SM channels, with a total decay width into all SM channels given by $\Gamma(\chi \to \text{SM}) = \sin^2\alpha \cdot \Gamma(h \to \text{SM}) \simeq 4\sin^2\alpha$ MeV, in all cases subleading with respect to the decay width $\Gamma(\chi \to hh)$.

Note added: after this paper appeared on the arXivs, the possibility that the Lagrangian in Eq. (2.2) could induce preheating by the explosive production of scalar fields after inflation was considered in Ref. [61]. In this case, we can identify the scalar fields of Ref. [61] with the Higgs field [19] and this mechanism, if implemented, would be more efficient than the perturbative production that has been considered so far in this section. First of all, as we wanted the inflaton to stabilize the Higgs potential we have imposed the condition on its mass $m < 10^{-7}M_{\rm Pl}$. This means that during preheating the inflaton potential term $\frac{1}{4}\lambda_\phi\phi^4$ will dominate the mass term $\frac{1}{2}m^2\phi^2$, as $\lambda_\phi \simeq 10^{-12}$ and $\phi_E \simeq M_{\rm Pl}$. In Ref. [61] it was proven that there is no runaway solutions provided that $\delta_\lambda < \lambda_0/4$, and preheating imposes the mild condition $2\delta_\lambda > (100\, m/\phi_E)^2$, always satisfied as $100\, m/\phi_E < 10^{-5}$. Still in the rest of the paper we will be agnostic about the (p)reheating mechanism and will consider the reheating temperature $T_{\rm rh}$ as a free parameter.

[19] The relation between the parameters q_3 and q_χ in Ref. [61] and our parameters can be written as

$$q_3 = \sqrt{2\delta_\lambda}\frac{\phi_E}{m}, \quad q_\chi = \frac{\lambda_0\phi_E^2}{m^2}.$$

6 Baryogenesis

Using the helical gauge fields produced at the end of inflation, and assuming that their corresponding helicity remains after reheating (a hypothesis that will be self-consistently checked a posteriori, see Sec. 7.1), until the EWPT (which we assume to be the SM crossover), we can compute the conversion of the helicity into the $(B+L)$ asymmetry, and therefore the baryon asymmetry of the Universe (BAU).

At a temperature around the electroweak scale, $T_{\rm EW} \approx 160$ GeV, the Higgs VEV departs from zero and smoothly transitions to the SM VEV at $T = 0$, $v = 246$ GeV, making the off-diagonal elements of the gauge bosons mass matrix gradually compete with the thermal mass for W^3_μ on the diagonal, that decreases with decreasing temperature. This results in a phase transition controlled by the EW angle θ_W whose temperature dependence is subject to significant uncertainties [8, 9]. Following Refs. [20, 21] we define the parameter f_{θ_W}, which encodes all the details of the EW transition and its uncertainties, as

$$f_{\theta_W} = -\sin(2\theta_W)\,\frac{d\theta_W}{d\ln T}\bigg|_{T=135\ \rm GeV}, \quad 5.6\cdot 10^{-4} \lesssim f_{\theta_W} \lesssim 0.32. \tag{6.1}$$

This gives rise to a source term for the $(B+L)$ asymmetry, while the electroweak sphalerons are still in equilibrium for $T \gtrsim 130$ GeV. In Ref. [18], it was shown in detail how the source and washout terms balance each other around an equilibrium value of the baryon asymmetry around $T = 135$ GeV, which is finally given by

$$\eta_B \simeq 4\cdot 10^{-12}\, f_{\theta_W}\,\frac{\mathscr{H}_Y}{H_E^3}\left(\frac{H_E}{10^{13}\,\rm GeV}\right)^{\frac{3}{2}}\left(\frac{T_{\rm rh}}{T_{\rm rh}^{\rm ins}}\right) \simeq 9\cdot 10^{-11}, \tag{6.2}$$

where we have imposed the observed value [62] in the right-hand side.

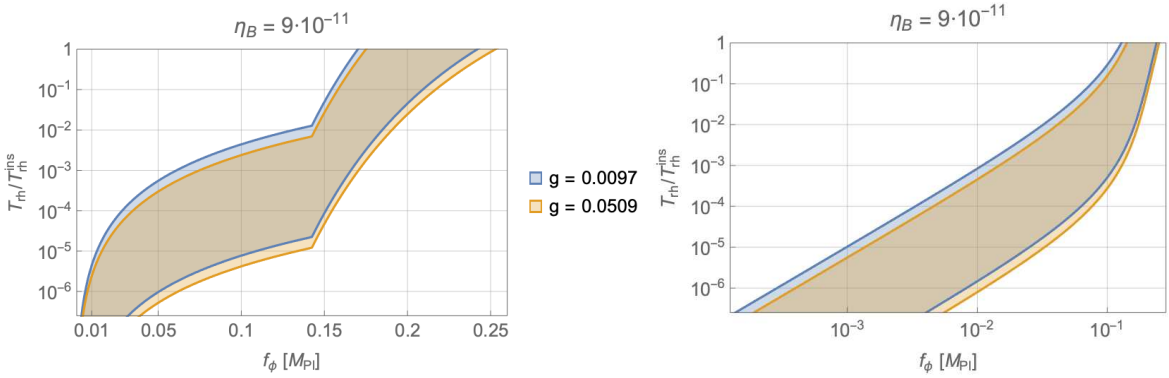

Figure 7: *The baryogenesis region. In the shading region the value of η_B satisfies Eq. (6.2). Left panel: Schwinger maximal estimate. Right panel: Schwinger equilibrium estimate.*

.

In Fig. 7 we show—in the plane $(f_\phi, T_{\rm rh}/T_{\rm rh}^{\rm ins})$, for both bounds on the allowed g range, Eq. (3.12), and for both Schwinger estimates for the magnetic fields, i.e., maximal (left panel) and equilibrium (right panel) estimates—the region where the value of η_B satisfies Eq. (6.2) taking into account the range in Eq. (6.1) for the quantity f_{θ_W}. As we can see from both panels, together with the range (3.12) on the g parameter where inflationary conditions in Ref. [46] are satisfied, there is an absolute

upper bound on the parameter f_ϕ as $f_\phi \lesssim 0.25\, M_{\rm Pl}$ for both Schwinger estimates, corresponding to the reference (instant) reheating temperature, where the baryogenesis conditions are met. Moreover, for the highest reheating temperature we can get from our model of inflation, $T_{\rm rh} \simeq 10^{-2}\, T_{\rm rh}^{\rm ins}$, the bound lowers to $f_\phi \lesssim 0.19\ (0.17)\, M_{\rm Pl}$ for the maximal (equilibrium) Schwinger estimate. Putting together the lower bounds from (4.54), and the requirement that $T_{\rm rh}/T_{\rm rh}^{\rm ins} \gtrsim 10^{-6}$, one gets the global ranges

$$\begin{aligned} 1.9\cdot 10^{-2} \;\lesssim\; f_\phi\,/\,M_{\rm Pl} \;\lesssim\; 0.19 \qquad & \text{(Maximal estimate)}, \\ 7.2\cdot 10^{-4} \;\lesssim\; f_\phi\,/\,M_{\rm Pl} \;\lesssim\; 0.17 \qquad & \text{(Equilibrium estimate)}, \end{aligned} \tag{6.3}$$

where baryon asymmetry can be generated consistently with the condition of no backreaction of the helical gauge fields on the inflationary dynamics.

However, as we will see next, the helical magnetic fields, produced at the end of inflation, interact after reheating with the thermal plasma and there are a number of constraints that have to be satisfied for the helicity to reach the temperatures where the EWPT takes place. As we will see, these constraints may reduce the allowed region in the parameters space.

7 Constraints

We have computed, up to now, the baryon asymmetry generated by helical magnetic fields produced after inflation when their helicity decays into $(B+L)$ asymmetry at the electroweak crossover, and identified the region of the parameter space $(g, f_\phi, T_{\rm rh})$ where the observed value of the baryon asymmetry is reproduced. However, there are a number of constraints that can further narrow the region of the parameter space where the BAU can really be reproduced by our theory and will be analyzed in this section.

7.1 Helicity evolution: Magnetohydrodynamics and Reynolds numbers

Helical magnetic fields are produced at the end of inflation, and we assume their comoving quantities stay constant until reheating, at temperature $T_{\rm rh}$. However, at reheating a thermal plasma is generated by the decay of the inflaton into the SM particles and consequently the electroweak symmetry is restored—by the appearance of thermal masses—until the EWPT. Hence the helicity in photons $\mathscr{H}$ gets transformed into helicity in hypercharge gauge fields $\mathscr{H}_Y$, as sketched at the beginning of Sec. 4, see Eq. (4.5). The latter then interacts with the thermal plasma which, in turn, backreacts on the gauge fields.

This system can be described by the so-called MHD equations [53, 63, 64], and has been studied for the case at hand in Ref. [21]. In a nutshell, the physical quantities of interest (amplitudes, energy densities, correlation length and helicity) do not scale adiabatically in such an environment, or equivalently their comoving quantities are not constant. Therefore there can be a magnetic *diffusion* effect leading to the decay of the helicity. If, on the other hand, the magnetic *induction* is the leading effect, then the helicity can be conserved until the EWPT and the baryogenesis mechanism can take place. This effect is measured by the magnetic Reynolds number $\mathcal{R}_m$, and we will see that it is enough to require $\mathcal{R}_m > 1$ at reheating for the helicity to be conserved until the EW crossover. Hence, in this section we will study how this constraint affects the region of the parameter space that yields the BAU.

The magnetic Reynolds number is defined as the ratio of the magnetic induction term over the magnetic diffusion term of the corresponding MHD equation. It can be written as

$$\mathcal{R}_m \equiv \sigma v \ell_{B_Y}, \tag{7.1}$$

where $\sigma = c_\sigma T_{\rm pl}^c/(\alpha_Y \log(\alpha_Y^{-1}))$ is the conductivity of the thermal plasma, with $c_\sigma \simeq 4.5$, and

$$T_{\rm pl}^c \simeq 0.8\, T_{\rm rh}^{\rm ins} \left(\frac{T_{\rm rh}^{\rm ins}}{T_{\rm rh}}\right)^{\frac{1}{3}} \tag{7.2}$$

is the typical (comoving) temperature of the plasma, where we have used Eq. (5.6) with $a_E = 1$.

In addition, the typical bulk velocity of the plasma v can be estimated from the MHD Navier-Stokes equation for the velocity field. The general solution should be computed numerically, but for asymptotic cases, when one term clearly dominates over the others in the equation, we can sketch some approximations. To do so, like in the magnetic case, we can compute the electric Reynolds number $\mathcal{R}_e$, given by

$$\mathcal{R}_e \equiv \frac{v \ell_{B_Y}}{\nu}, \tag{7.3}$$

where $\nu = c_\nu/(\alpha_Y^2 \log(\alpha_Y^{-1}) T_{\rm pl}^c)$ is the kinematic viscosity, with $c_\nu \simeq 0.01$. If $\mathcal{R}_e > 1$, then there is an equipartition between the kinetic energy in the plasma and the magnetic energy. In the opposite case, where $\mathcal{R}_e < 1$, the kinetic energy and velocity are smaller than the magnetic energy. Relying, in this way, on the value of $\mathcal{R}_e$, we can compute all quantities in these two separate cases:

- *Viscous* regime: $\mathcal{R}_e < 1 < \mathcal{R}_m$,
- *Turbulent* regime: $1 < \mathcal{R}_e < \mathcal{R}_m$.

We omit the other cases, where $\mathcal{R}_m < 1$, since we will not be interested in them.

In summary, the evolution of these two scaling regimes with respect to conformal time τ behave as [20, 65]

$$\mathcal{R}_e < 1: \qquad B_Y \propto \tau^{-\frac{1}{2}}, \qquad \ell_{B_Y} \propto \tau, \qquad v \sim \ell_{B_Y} B_Y^2/(\nu\rho) \propto \tau^0, \tag{7.4a}$$

$$\mathcal{R}_e > 1: \qquad B_Y \propto \tau^{-\frac{1}{3}}, \qquad \ell_{B_Y} \propto \tau^{\frac{2}{3}}, \qquad v \sim B_Y/\sqrt{\rho} \propto \tau^{-\frac{1}{3}}, \tag{7.4b}$$

where

$$\rho \simeq 0.4\, \rho_\chi \left(\frac{T_{\rm rh}^{\rm ins}}{T_{\rm rh}}\right)^{\frac{4}{3}}, \qquad \rho_\chi \simeq 3 M_{\rm Pl}^2 H_E^2, \tag{7.5}$$

is the plasma energy density. Inserting the latter relations for v in (7.1) for both cases, we can estimate the magnetic Reynolds number at reheating as [21]

$$\text{For} \quad \mathcal{R}_e^{\rm rh} < 1 \quad \Rightarrow \quad \mathcal{R}_m^{\rm rh} \approx 5.9 \cdot 10^{-6}\, \frac{\rho_{B_Y} \ell_{B_Y}^2}{H_E^2} \left(\frac{H_E}{10^{13}\,\text{GeV}}\right) \left(\frac{T_{\rm rh}}{T_{\rm rh}^{\rm ins}}\right)^{\frac{2}{3}}, \tag{7.6a}$$

$$\text{For} \quad \mathcal{R}_e^{\rm rh} > 1 \quad \Rightarrow \quad \mathcal{R}_m^{\rm rh} \approx 1.1 \cdot 10^{-1}\, \frac{\sqrt{\rho_{B_Y}} \ell_{B_Y}}{H_E} \left(\frac{H_E}{10^{13}\,\text{GeV}}\right)^{\frac{1}{2}} \left(\frac{T_{\rm rh}}{T_{\rm rh}^{\rm ins}}\right)^{\frac{1}{3}} \tag{7.6b}$$

where the magnetic energy density is roughly given by $\rho_{B_Y} \approx B_Y^2/2$. From (7.4), using (7.1) and (7.3), we see that in both regimes both Reynolds numbers grow with time according to the same scaling relations:

$$\mathcal{R}_e < 1: \qquad \mathcal{R}_m \propto \tau, \qquad \mathcal{R}_e \propto \tau, \tag{7.7a}$$

$$\mathcal{R}_e > 1: \qquad \mathcal{R}_m \propto \tau^{\frac{1}{3}}, \qquad \mathcal{R}_e \propto \tau^{\frac{1}{3}}. \tag{7.7b}$$

Hence, once the requirement $\mathcal{R}_m^{\rm rh} > 1$ is reached, the magnetic Reynolds number remains greater than one, as long as there is a plasma filling the Universe. The conservation of helicity is due to an

inverse cascade in which the helicity is transferred from smaller to larger scales, reflected in the growth of ℓ_{B_Y}. Therefore, to guarantee the survival of the comoving helicity at the EWPT, it is enough to compute both Reynolds numbers at the end of inflation, allowing us to ignore the evolution of the plasma at later times.

Now, all we have to know is which regime (viscous or turbulent) does apply at the reheating temperature. This is given by the value of $\mathcal{R}_e$ at that time. Inserting the above expressions for v, Eqs. (7.4a) and (7.4b), in the definition of $\mathcal{R}_e$, Eq. (7.3), we obtain at reheating [21]

$$\text{For} \quad \mathcal{R}_e^{\rm rh} < 1 \quad \Rightarrow \quad \mathcal{R}_e^{\rm rh} \approx 2.5 \cdot 10^{-9} \, \frac{\rho_{B_Y} \, \ell_{B_Y}^2}{H_E^2} \left(\frac{H_E}{10^{13}\,\text{GeV}} \right) \left(\frac{T_{\rm rh}}{T_{\rm rh}^{\rm ins}} \right)^{\frac{2}{3}}, \tag{7.8a}$$

$$\text{For} \quad \mathcal{R}_e^{\rm rh} > 1 \quad \Rightarrow \quad \mathcal{R}_e^{\rm rh} \approx 5.4 \cdot 10^{-5} \, \frac{\sqrt{\rho_{B_Y}} \, \ell_{B_Y}}{H_E} \left(\frac{H_E}{10^{13}\,\text{GeV}} \right)^{\frac{1}{2}} \left(\frac{T_{\rm rh}}{T_{\rm rh}^{\rm ins}} \right)^{\frac{1}{3}}. \tag{7.8b}$$

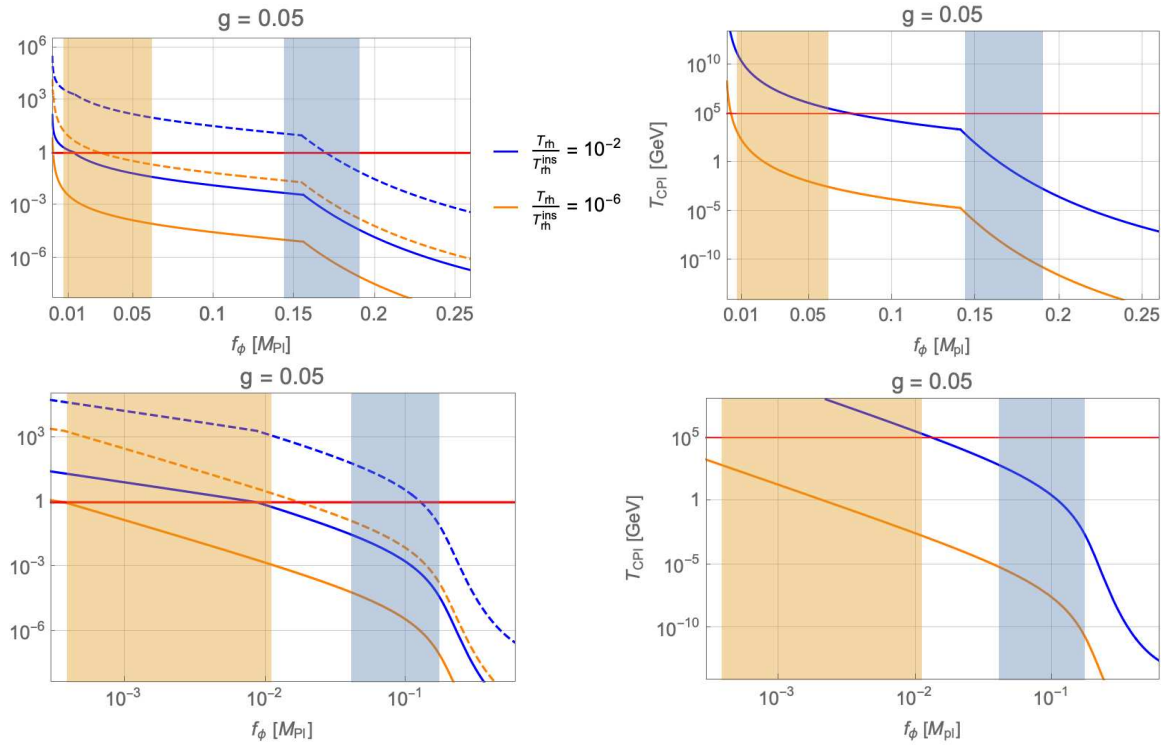

Figure 8: *Left panels: Plot of the electric (solid lines) and magnetic (dashed lines) Reynolds number at reheating as a function of f_ϕ for different values of $T_{\rm rh}/T_{\rm rh}^{\rm ins} = 10^{-2}$ (blue color) and 10^{-6} (orange color). The ranges of successful baryogenesis for the different values of $T_{\rm rh}/T_{\rm rh}^{\rm ins}$ are displayed here by the vertical bands, whose colors match the corresponding lines color. We see that the production of the helical magnetic fields at reheating always occurs for $\mathcal{R}_e < 1$ but not necessarily for $\mathcal{R}_m > 1$, in the correct baryogenesis region. The latter condition must nevertheless be met for successful baryogenesis, which reduces the parameter window mainly (but not only) for high reheating temperatures. Right panels: Plot of the $T_{\rm CPI}$ temperature. In the baryogenesis regions we always have $T_{\rm CPI} < 10^5$ GeV. Top panels correspond to the Schwinger maximal estimate, and bottom panels to the equilibrium estimate.*

In our scenario it turns out that $\mathcal{R}_e^{\rm rh} < 1$ for the range of parameters that provides a successful baryogenesis, as displayed in the left panels of Fig. 8 (solid lines) for the two extreme values of the parameter $T_{\rm rh}/T_{\rm rh}^{\rm ins} = 10^{-2}$ (blue color) and 10^{-6} (orange color). Thus, the plasma starts in the viscous regime and the magnetic Reynolds number should be computed using Eq. (7.6a). Plots of $\mathcal{R}_m^{\rm rh}$, as a function of f_ϕ, are shown in the left panels of Fig. 8 (dashed lines) for the same values of the parameter $T_{\rm rh}/T_{\rm rh}^{\rm ins}$ and the same color codes. We consider the Schwinger maximal (top left panel) and equilibrium (bottom left panel) estimates for the gauge fields. In all cases we exhibit the regions allowed by the baryogenesis constraint, which depend on the corresponding values of the parameter $T_{\rm rh}/T_{\rm rh}^{\rm ins}$, using the same color code than for the different lines (both for $\mathcal{R}_e^{\rm rh}$ and $\mathcal{R}_m^{\rm rh}$) in the plot. Then even if $\mathcal{R}_e^{\rm rh} < 1$, at some later time τ the plasma will eventually fall into the turbulent regime where $\mathcal{R}_e > 1$, with evolution given by Eq. (7.6b).

As we can see from the dashed lines in the left panel plots of Fig. 8 the condition $\mathcal{R}_m^{\rm rh} > 1$ is not satisfied everywhere in the region allowed by baryogenesis. Therefore, as summarized in Fig. 9, the condition for magnetic induction dominance, $\mathcal{R}_m > 1$, constrains the available region (6.3) from the baryogenesis window. Of course, once the condition $\mathcal{R}_m^{\rm rh} > 1$ is satisfied (at the reheating temperature), its value increases with time, see Eq. (7.7b), which guarantees that the condition will be fulfilled until the EWPT.

7.2 The chiral plasma instability

When the symmetric phachiral plasma instabilityse is restored during reheating both, the asymmetries in the particle/antiparticle number densities, and the hypercharge helicity, are generated via the Schwinger effect, as described in Sec. 4.2, and via the chiral anomaly, as stated at the beginning of Sec. 4, see Eq. (4.4). In the absence of any other process, the newly generated asymmetry will relax into the same amount of the newly generated helicity but with opposite sign, as the gauge fields configuration has lower energy density than the fermion states configuration, resulting in a cancellation of the total helicity and hence no baryogenesis at the EWPT. This phenomenon is called the chiral plasma instability (CPI) [66–72], and has to be avoided for a successful baryogenesis.

CPI can be avoided if we require that the CPI timescale is long enough to allow all fermionic states to come into chemical equilibrium (so that sphalerons can erase their corresponding asymmetries in particle number densities) before CPI can happen. The estimated temperature at which CPI takes place is [21]

$$T_{\rm CPI}/{\rm GeV} \approx 4 \cdot 10^{-7}\ \frac{\mathscr{H}_Y^2}{H_E^6}\left(\frac{H_E}{10^{13}\,{\rm GeV}}\right)^3\left(\frac{T_{\rm rh}}{T_{\rm rh}^{\rm ins}}\right)^2 . \tag{7.9}$$

The last fermion species to enter chemical equilibrium, through its Yukawa coupling with the left-handed electron e_L, is the right-handed electron, e_R, and it happens at the temperature $T \sim 10^5$ GeV. Indeed, when the fermionic states are in chemical equilibrium, their asymmetry is washed out through weak sphalerons and Yukawa couplings. Therefore the constraint $T_{\rm CPI} \lesssim 10^5$ GeV guarantees that the CPI cannot occur before the smallest Yukawa coupling reaches equilibrium and all particle number density asymmetries are erased, preventing thus the cancellation of the helicity generated at the reheat temperature.

In the right panels of Fig. 8 we show the plot of $T_{\rm CPI}$ as a function of f_ϕ for both, Schwinger maximal (top panel) and equilibrium (bottom panel), estimates and values of $T_{\rm rh}/T_{\rm rh}^{\rm ins} = 10^{-2}$ (blue color) and 10^{-6} (orange color). In each plot, the region between the vertical bands is that selected by the baryogenesis mechanism for the corresponding value of $T_{\rm rh}/T_{\rm rh}^{\rm ins}$ with the same color code. As we

can see from Fig. 8, the range of values for $T_{\rm CPI}$ in the corresponding baryogenesis region is

$$10^2 \text{ GeV} \gtrsim T_{\rm CPI} \gtrsim 10^{-3} \text{ GeV} \tag{7.10}$$

which then prevents the cancellation of any previously generated helicity. So, as we will explicitly exhibit in Fig. 9, this constraint is satisfied in all the region provided by the baryogenesis condition.

7.3 Primordial non-Gaussianity

Inflation predicts that the statistical distribution of primordial fluctuations is nearly Gaussian. Measuring deviations from a Gaussian distribution, i.e., non-Gaussian correlations in primordial fluctuations, is a powerful test of inflation. While the two-point function for $\delta\chi$ defines the power spectrum, the three-point correlation function encodes departures from Gaussianity [73, 74]. Helical gauge fields yield a new source of cosmological perturbations for the inflaton field $\delta\chi$ as

$$\left(\frac{\partial^2}{\partial t^2} + 3H\frac{\partial}{\partial t} - \frac{\nabla^2}{a^2}\right)\delta\chi = -\frac{4}{a^4 f_\phi}\,\boldsymbol{E}\cdot\boldsymbol{B}. \tag{7.11}$$

The magnitude of the three-point function is conventionally quantified using the parameters $f_{\rm NL}$. non-Gaussian effects from helical gauge fields are maximal when the three modes have comparable wavelength, the so-called equilateral form, which in the backreactionless case where gauge fields are given by Eq. (4.23) is given by [75, 76]

$$f_{\rm NL}^{\rm equil} \simeq 4.7\cdot 10^{-16}\,\frac{e^{6\pi\xi_{\rm CMB}}}{\xi_{\rm CMB}^9}, \tag{7.12}$$

where $\xi_{\rm CMB} \equiv \xi(\chi_*)$. However, we have seen that the Schwinger effect significantly reduces the magnitude of the RHS of Eq. (7.11), for a fixed value of f_ϕ, and that we can mimic its effect by the replacement of the effective parameters $\xi_{\rm eq}$ and $\xi_{\rm max}$, for the equilibrium and maximal estimates respectively, in the backreactionless expression for $\langle \boldsymbol{E}\cdot\boldsymbol{B}\rangle$, Eq. (4.45). Hence, in the same way as we did at the beginning of Sec. 5, we identify the primordial non-Gaussianity constraint with $\xi_{\rm eq}$ and $\xi_{\rm max}$ before translating them back to f_ϕ by the use of Eqs. (4.42) and (5.2).

Current observational bounds on non-Gaussianity of the cosmic microwave background (CMB) anisotropies lead to [77]

$$f_{\rm NL}^{\rm equil} = -26 \pm 47 \tag{7.13}$$

which translate, from Eq. (7.12) into $\xi_{\rm CMB} \lesssim 2.54$ (95% C.L.). Using now the scaling relation

$$\frac{\xi_{\rm eq/max}}{\xi_{\rm CMB}} = \sqrt{\frac{\epsilon(\chi_E)}{\epsilon(\chi_*)}} = \sqrt{\frac{1}{\epsilon(\chi_*)}} \tag{7.14}$$

where $\xi_{\rm eq/max} \equiv \xi_{\rm eq/max}(\chi_E)$ is the value of the effective ξ parameter at the end of inflation in the equilibrium/maximal Schwinger estimate, one can compute corresponding upper bounds on $\xi_{\rm eq/max}$, at the end of inflation. In fact, for the lower value of g allowed by the cosmological observables in our inflation model, $g \simeq 0.01$, one gets $\xi_{\rm eq/max} \lesssim 47$ while for the upper bound, $g \simeq 0.05$, one gets $\xi_{\rm eq/max} \lesssim 91$. However those values of $\xi_{\rm eq/max}$ are never reached in our model, as they would correspond to negligibly small values of f_ϕ which are never met.

In conclusion, in the presence of the Schwinger effect the produced gauge fields are never strong enough to trigger non-Gaussianity in the distribution of the primordial inflaton fluctuations, in good agreement with present observations. In other words the model prediction in the presence of the fermionic Schwinger currents is $f_{\rm NL}^{\rm equil} \simeq 0$, and so we will not consider further this constraint.

7.4 The baryon isocurvature perturbation

Many models of baryogenesis using (hyper)magnetic fields try to simultaneously explain the origin of the large scale, intergalactic magnetic fields (IMF) measured today by the Fermi satellite [78–80]. They all face a balance problem when addressing this issue.

While maximally helical fields can indeed generate the BAU without explaining the observed IMF, they would suffer from baryon overproduction should they try to accommodate IMF. In the case of a mixture of helical and nonhelical fields, the baryogenesis is less effective so that stronger hypermagnetic fields are needed to explain the present BAU, and hence they could meet the lower bound from the IMF observations.

However, it has been recently shown that such models are inconsistent with the baryon isocurvature perturbations, that are constrained by the observations of cosmic microwave background on large scales [81]. In particular, it was pointed out that the baryon isocurvature perturbations at a scale larger than the neutron diffusion scale at the Big Bang Nucleosynthesis (BBN) epoch is constrained by the deuterium overproduction due to the second-order effect [82]. This translates into an upper bound on the volume average of the baryon isocurvature perturbation, as

$$\overline{\mathcal{S}^2}_{\rm B,BBN} < 0.016 \quad (2\sigma). \tag{7.15}$$

It was shown that, regardless of their helicity properties, hypermagnetic fields with too large strength and coherence length are not allowed before the EWPT [81]. Still baryogenesis from the hypermagnetic helicity decay can be responsible for the present BAU, but additional magnetogenesis, or an unknown mechanism of the magnetic field amplification after the EWPT, is needed to fit the IMF observations. However the constraint becomes more severe for less helical hypermagnetic fields. In our model the magnetic field produced at the end of inflation is maximally helical and we do not cope with the IMF observations. Hence we should be safe from this constraint. Nevertheless, we will deserve to App. B the detailed calculation where it is proven that the bound (7.15) is indeed widely satisfied in our model, so that this constraint does not need to be taken into account any further.

7.5 Summary of constraints

To close this section, we would like to compile all our results about baryogenesis into a single plot, see Fig. 9. Here, we have displayed in the plane $(f_\phi, T_{\rm rh}/T_{\rm rh}^{\rm ins})$ all the relevant constraints described in this section. In particular:

- The generated baryon asymmetry at the EW crossover, given by Eq. (6.2), should be given by the observational value
$$\eta_B \simeq 9 \cdot 10^{-11}, \tag{7.16}$$
where the broadness of the prediction band is associated to the uncertainty in the determination of the parameter f_{θ_W}.

- The magnetic diffusion given by MHD, leading to the helicity decay should be smaller than the magnetic induction, to allow helicity to be conserved until the electroweak phase transition. This happens when the magnetic Reynolds number at reheating given by Eq. (7.6a) is
$$\mathcal{R}_m^{\rm rh} \gtrsim 1. \tag{7.17}$$

- As the symmetric phase is restored during reheating, an asymmetry via chiral anomaly is generated and decays into a helicity with opposite sign, resulting into a cancellation of the total

helicity with no baryogenesis at the EWPT. This phenomenon, called chiral plasma instability, can be avoided if the temperature at which it is produced $T_{\rm CPI}$, given by Eq. (7.9), is smaller than the temperature at which all fermion species enter chemical equilibrium through their Yukawa couplings, and in particular the last species to reach chemical equilibrium, e_R. This condition is satisfied provided that

$$T_{\rm CPI} \lesssim 10^5 \text{ GeV}. \tag{7.18}$$

We shall choose the overlapping region as that meeting all the constraints. We removed the dependence on g as the results are not sensitive to it, preferring to choose the value $g = 0.05$ in the

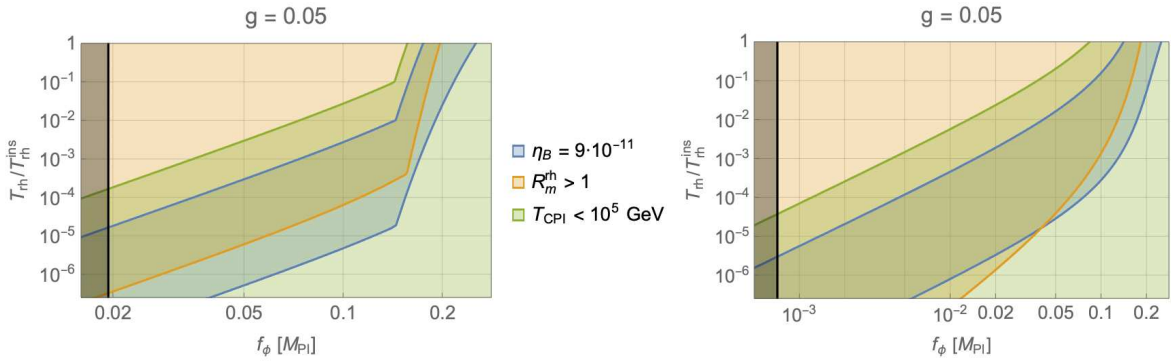

Figure 9: *Summary of constraints on baryogenesis for* $g = 0.05$ *(the dependence on* g *is tiny) in the plane* $(f_\phi/M_{\rm Pl}, T_{\rm rh}/T_{\rm rh}^{\rm ins})$. *The considered constraints are on* η_B *(blue area), on the magnetic Reynolds number (orange area) and on chiral plasma instability (green area). We seek for the overlapping region. On the left side of each plot, the black band displays the region where the backreaction of gauge fields on the inflaton can no longer be neglected. Left panel: Schwinger maximal estimate. Right panel: Schwinger equilibrium estimate.*

allowed range from the inflation model.

From Fig. 9 we can conclude that the CPI constraint is satisfied in all the region where the constraint of having enough baryon asymmetry η_B holds. On the other hand the constraint from the magnetic Reynolds number is effective for the case of the Schwinger maximal estimate, by cutting off the larger available values of the parameter f_ϕ for every value of $T_{\rm rh}$. However, for the Schwinger equilibrium estimate the magnetic Reynolds number constraint is effective for the larger values of $T_{\rm rh}/T_{\rm rh}^{\rm ins}$, by cutting off the larger values of the parameter f_ϕ, while for the smaller values of $T_{\rm rh}$, in particular for $T_{\rm rh} \lesssim 5{\cdot}10^{-4}\, T_{\rm rh}^{\rm ins}$, it entirely covers the region satisfied by the constraint on η_B. Finally, given the range $m \in [10^3\,, 5\cdot 10^{10}]$ GeV, for the corresponding range on $T_{\rm rh}/T_{\rm rh}^{\rm ins} \in [10^{-2}\,, 10^{-6}]$, we get the available (approximated) regions, for $g \in [0.01\,, 0.05]$,

$$\begin{aligned} &f_\phi/M_{\rm Pl} \in [0.14\,, 0.17] && \text{for} \quad T_{\rm rh}/T_{\rm rh}^{\rm ins} = 10^{-2} \\ &f_\phi/M_{\rm Pl} \in [1.9\cdot 10^{-2}\,, 2.8\cdot 10^{-2}] && \text{for} \quad T_{\rm rh}/T_{\rm rh}^{\rm ins} = 10^{-6} \end{aligned} \qquad \text{(Maximal estimate)},$$

$$\begin{aligned} &f_\phi/M_{\rm Pl} \in [4.1\cdot 10^{-2}\,, 0.13] && \text{for} \quad T_{\rm rh}/T_{\rm rh}^{\rm ins} = 10^{-2} \\ &f_\phi/M_{\rm Pl} \in [7.2\cdot 10^{-4}\,, 1.1\cdot 10^{-2}] && \text{for} \quad T_{\rm rh}/T_{\rm rh}^{\rm ins} = 10^{-6} \end{aligned} \qquad \text{(Equilibrium estimate)}.$$

Let us also mention that the condition (4.46) on the nonbackreaction of the gauge fields on the inflaton, displayed by the black bands, becomes a constraint only at low temperature, $T_{\rm rh}/T_{\rm rh}^{\rm ins} \lesssim$

$2 \cdot 10^{-5}$ $(3 \cdot 10^{-6})$ for the Schwinger maximal (equilibrium) estimate. Finally, the condition for the nonbackreaction of fermion currents on the gauge fields, which corresponds to $f_\phi \gtrsim 0.19\, M_{\rm Pl}$, is outside the region of validity of the baryogenesis region, which shows that the Schwinger effect can never be neglected in the baryogenesis analysis.

8 Some phenomenological considerations

In some chaotic inflation models, the mass of the inflaton is constrainted to a high value because of the observational constraint on the scalar perturbations amplitude. In our model, though, we have two terms in the inflaton potential: while inflation is controlled by the quartic term, dominant at Planckian scales, the quadratic one controls reheating and low energy physics. Thus the value of the inflaton mass is decoupled from the inflationary dynamics.

In previous sections, we have considered on the one hand the upper value of the inflaton mass as $m \lesssim \mathcal{Q}_I$, small enough to solve the instability problem of the Higgs potential, and on the other hand we have roughly imposed $m \gtrsim 1$ TeV on phenomenological grounds for the theory to not being excluded by present experimental data. In fact, an inflaton mass at the TeV scale could have implications for low energy physics. Therefore, in this section we will make some considerations from the point of view of collider physics and the Standard Model in the presence of the inflaton field with the interactions appearing in the Lagrangian (2.2).

The naturalness problem

First of all, our theory has two hierarchically separated scales, the inflaton mass m and the Higgs mass $m_h = 125.25$ GeV, with $m \gg m_h$. As such, the theory should exhibit a hierarchy problem, which in general implies an unnatural fine-tuning of the parameters. In the absence of any symmetry protecting the EW scale from the high-scale UV physics, one has either to accept the fine-tuning (as it is customary done in the Standard Model) or to lower the value of the mass m as much as possible. More quantitatively, the coupling in the Lagrangian $\mu\phi|\mathcal{H}|^2 = \sqrt{2\delta_\lambda} m|\mathcal{H}|^2$ generates a contribution to the Higgs mass term μ_h^2 through the one-loop radiative corrections. In the limit $\mu \to 0$ (i.e. $\delta_\lambda \to 0$), there is an enhanced $\mathbb{Z}_2$ symmetry $\phi \to -\phi$ indicating that any value of μ, as small as it can be, is natural in the sense of 't Hooft, since in this limit the symmetry is recovered. Moreover, this coupling induces a correction to the parameter μ_h^2 in the Lagrangian as [83]

$$\Delta\mu_h^2 \simeq -\frac{\delta_\lambda}{8\pi^2}\, m^2\, \log\frac{m^2}{m_h^2}\,. \tag{8.1}$$

Naturalness would then require $|\Delta\mu_h^2| \lesssim \mu_h^2 = m_h^2/2$, which translates into the bound

$$m \lesssim 1.2 \text{ TeV}\,, \tag{8.2}$$

where we have considered the typical value of the coupling $\delta_\lambda \simeq 0.1$. This leads to the exciting possibility of having an inflaton with an $\mathcal{O}$(TeV) mass, which does not spoil naturalness, solve the problem of the instability of the EW minimum, and has phenomenological implications for present and future colliders.

The Higgs-inflaton mixing

Near the vacuum, the potential for the Higgs and ϕ fields is given by

$$V(\phi,\mathcal{H}) = -\sqrt{2\delta_\lambda}\, m\, \phi|\mathcal{H}|^2 + \frac{1}{2}m^2\phi^2 - \mu_h^2|\mathcal{H}|^2 + \lambda_0|\mathcal{H}|^4\,. \tag{8.3}$$

The vacuum is defined as the solution to the minimum equations $\partial V/\partial\phi = \partial V/\partial h = 0$, which provides $\langle h\rangle = v = 246$ GeV and $\langle\phi\rangle = v_\phi$, with

$$\mu_h^2 = \lambda v^2, \qquad\qquad v_\phi = \sqrt{\frac{\delta_\lambda}{2}}\,\frac{v^2}{m}, \tag{8.4}$$

where the parameters δ_λ and λ were defined in Eqs. (2.11) and (2.17), respectively.

In the presence of the parameter δ_λ, there is a mixing between the Higgs h and ϕ fields given by the squared mass matrix at the minimum

$$\mathcal{M}^2 = \begin{pmatrix} 2(\lambda+\delta_\lambda)v^2 & -\sqrt{2\delta_\lambda}\,mv \\ -\sqrt{2\delta_\lambda}\,mv & m^2 \end{pmatrix}. \tag{8.5}$$

This matrix is diagonalized by an orthogonal rotation with angle α [20] as

$$\begin{pmatrix} c_\alpha & s_\alpha \\ -s_\alpha & c_\alpha \end{pmatrix} \mathcal{M}^2 \begin{pmatrix} c_\alpha & -s_\alpha \\ s_\alpha & c_\alpha \end{pmatrix} = \begin{pmatrix} m_{\tilde h}^2 & 0 \\ 0 & m_{\tilde\phi}^2 \end{pmatrix}, \tag{8.6}$$

such that the mass eigenstates are

$$\tilde h = c_\alpha\, h + s_\alpha\,\phi, \qquad\qquad \tilde\phi = c_\alpha\,\phi - s_\alpha\, h\,, \tag{8.7}$$

and the mass eigenvalues are

$$\frac{m_{\tilde h,\,\tilde\phi}^2}{m^2} = \frac{1}{2} + (\lambda+\delta_\lambda)\,\frac{v^2}{m^2} \mp \sqrt{\frac{1}{4} - (\lambda-\delta_\lambda)\,\frac{v^2}{m^2} + (\lambda+\delta_\lambda)^2\,\frac{v^4}{m^4}}. \tag{8.8}$$

In this way the physical mass eigenstate $\tilde h$ is associated with the Standard Model Higgs, with a mass $m_{\tilde h} = 125.25$ GeV, while $\tilde\phi$ is the physical singlet, and both of them are coupled to the SM fields through the mixing angle α.

Hence this theory predicts then the existence of a scalar $\tilde\phi$ that decays mainly into the channel $\tilde\phi \to \tilde h\tilde h$ with a decay rate

$$\Gamma(\tilde\phi\to\tilde h\tilde h) = \frac{\kappa^2\, m}{32\pi}\sqrt{1-\frac{4m_{\tilde h}^2}{m_{\tilde\phi}^2}}, \quad \kappa = \sqrt{2\delta_\lambda}c_\alpha(1-3s_\alpha^2) + 6s_\alpha c_\alpha^2(\lambda+\delta_\lambda)\frac{v}{m}. \tag{8.9}$$

which was responsible for the reheating in Sec. 5. Contour lines of $\Gamma(\tilde\phi\to\tilde h\tilde h)$ are exhibited in the upper left panel of Fig. 10 in the parameter space (m,δ_λ). As we can see, typically the width of the resonance $\tilde\phi$ is around a few GeV. As was already stated in Sec. 5, there are also subleading decay channels into SM particles ($X\in$ SM), as $\tilde\phi\to X\bar X$, induced by the mixing with the Higgs, with very suppressed branching fractions

$$\mathcal{B}(\tilde\phi\to X\bar X) = \mathcal{B}(\tilde h\to X\bar X)\cdot s_\alpha^2\,\frac{\Gamma_{\tilde h}}{\Gamma_{\tilde\phi}} \tag{8.10}$$

as $\Gamma_{\tilde h}\simeq 4c_\alpha^2$ MeV in the SM, $\Gamma_{\tilde\phi}\simeq\Gamma(\tilde\phi\to\tilde h\tilde h)\simeq$ few GeV, so that $s_\alpha^2\Gamma_{\tilde h}/\Gamma_{\tilde\phi}\ll 1$.

[20] We are using the notation $c_\alpha\equiv\cos\alpha$, $s_\alpha\equiv\sin\alpha$, $t_\alpha\equiv\tan\alpha$.

Electroweak precision constraints

The doublet-singlet mixing can affect the electroweak precision observables (EWPO) through changes in the gauge boson propagators. Explicit expressions for the modified scalar contributions to the W and Z propagators are given in Refs. [84, 85]. In particular the contribution to the S and T oblique parameters from the new physics, $\Delta S \equiv S^{\rm NP} - S^{\rm SM}$ and $\Delta T \equiv T^{\rm NP} - T^{\rm SM}$, are found to be given by

$$\Delta T \simeq \frac{3}{16\pi}\frac{s_\alpha^2}{s_W^2}\left[\left(\frac{1}{c_W^2}\frac{m_{\tilde h}^2}{m_{\tilde h}^2-m_Z^2}\log\frac{m_{\tilde h}^2}{m_Z^2} - \frac{m_{\tilde h}^2}{m_{\tilde h}^2-m_W^2}\log\frac{m_{\tilde h}^2}{m_W^2}\right) - \left(m_{\tilde h}\to m_{\tilde\phi}\right)\right] \tag{8.11}$$

and

$$\Delta S = \frac{s_\alpha^2}{12\pi}\left[\frac{\hat m_{\tilde h}^6 - 9\hat m_{\tilde h}^4 + 3\hat m_{\tilde h}^2 + 5 + 12\hat m_{\tilde h}^2\log(\hat m_{\tilde h}^2)}{(\hat m_{\tilde h}^2-1)^3} - \left(\hat m_{\tilde h}\to \hat m_{\tilde\phi}\right)\right] \tag{8.12}$$

where we are defining masses in units of m_Z, i.e. $\hat m_X \equiv m_X/m_Z$.

The model predictions, Eqs. (8.11) and (8.12), must be compared with the experimental values, given by [62]

$$\Delta T = 0.05 \pm 0.06, \quad \Delta S = 0.0 \pm 0.07 \tag{8.13}$$

and 92% correlation between the S and T parameters. This gives rise to a $\Delta\chi^2(m,\delta_\lambda)$ distribution, which defines the allowed region in the parameter space (m,δ_λ), exhibited in all panels of Fig. 10. In particular we display, in orange shading, the region in the parameter space (m,δ_λ) for which $\Delta\chi^2(m,\delta_\lambda) < 5.99$, that corresponds to the bound at 95% C.L. As we can see, for large values of the parameter δ_λ the lower bound on m can be near the TeV scale.

LHC constraints

In this section we will consider several constraints arising from LHC physics where we are led to the exciting possibility to explore the inflaton sector at present and future high energy colliders and, in particular, at the LHC.

- The Higgs signal strength

From Eq. (8.7) we see that the coupling of the mass eigenstate $\tilde h$ to the SM particles, is suppressed, with respect to the coupling of the SM Higgs h, by the factor c_α. Given that, the signal strength modifier r_i^f for a specific process $i \to \tilde h \to f$, is given by

$$r_i^f = \frac{\sigma_i\,\mathcal{B}^f}{(\sigma_i)_{\rm SM}\,\mathcal{B}^f_{\rm SM}} \simeq c_\alpha^2 \tag{8.14}$$

where σ_i is the production cross section for the initial state into $\tilde h$, and $\mathcal{B}^f$ its branching fraction on the final state. For the last equality we have considered that the production cross section is suppressed by c_α^2 while the branching fraction is approximately equal to the SM one. Experimental data from ATLAS [86] and CMS [87] provide the global values

$$r = 1.11^{+0.09}_{-0.08} \quad \text{(ATLAS)}, \qquad\qquad r = 1.17 \pm 0.1 \quad \text{(CMS)} \tag{8.15}$$

which are consistent with a value of $r = 1$ (the SM prediction) with $\sim 10\%$ error, thus providing a lower bound on c_α as

$$c_\alpha^2 \gtrsim 0.9. \tag{8.16}$$

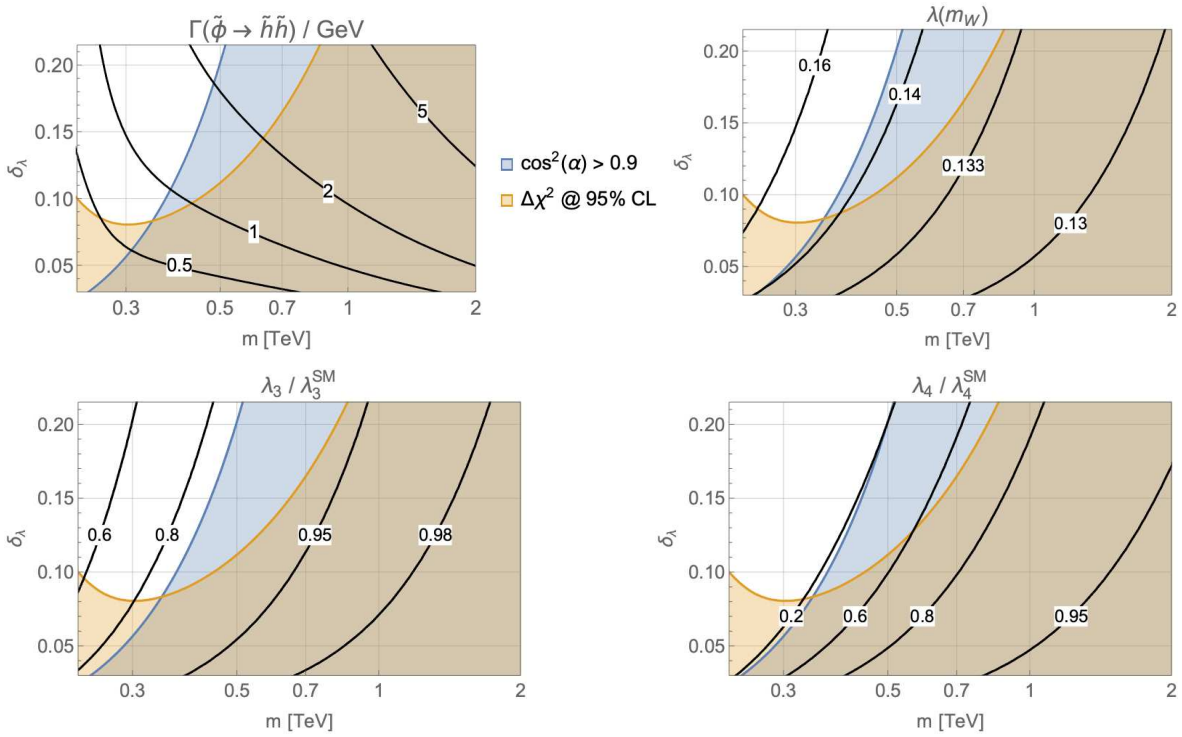

Figure 10: *Contour lines in the plane* $(m/TeV, \delta_\lambda)$ *of the decay rate* $\Gamma(\tilde{\phi} \to \tilde{h}\tilde{h})/GeV$ *(top left panel), the quartic parameter at the weak scale* $\lambda(m_W)$ *(top right panel) as well as the Higgs trilinear (bottom left panel) and quartic (bottom right panel) couplings normalized to the SM values with the regions of validity defined by the signal strength modifier (8.16) (blue) and the constraints from the electroweak parameters (8.13) (orange) superimposed. One should read the contour lines in black that pass through the overlapping region, and hence that satisfy both constraints. As discussed in Sec. 2.2, for* $m \sim \mathcal{O}(TeV)$*, to solve the stability problem and after imposing that the theory remains in the perturbative regime up to the high scale, the parameter* δ_λ *is constrained to be in the region* $0.05 \lesssim \delta_\lambda \lesssim 0.2$.

For $m \gg v$ the mixing angle is $s_\alpha \simeq \sqrt{2\delta_\lambda}(v/m) \ll 1$ so that the bound (8.16) is easily satisfied. However for TeV values of m the bound (8.16) translates into a lower bound on the value of m. We shade in blue, in all panels of Fig. 10, the region in the parameter space (m, δ_λ), where this constraint is satisfied. In particular we see that, for $\delta_\lambda = 0.1$, the bound (8.16) is satisfied for $m \gtrsim 0.4$ TeV. For $m \simeq 1$ TeV and $\delta_\lambda = 0.1$, the mixing is given by $c_\alpha^2 \simeq 0.988$, which is not excluded by the actual LHC data.

- Trilinear and quartic Higgs couplings

As the light state $\tilde{h}$ is to be identified with the SM Higgs, with mass $m_{\tilde{h}} = 125.25$ GeV, for any fixed value of the parameter δ_λ the experimental value of the Higgs mass fixes the value of the quartic parameter at the weak scale, $\lambda(m_W)$, at a different value than in the SM case. In the upper right panel of Fig. 10 we plot contour lines of $\lambda(m_W)$ in the parameter space (m, δ_λ). As we can see $\lambda(m_W) > \lambda_{\rm SM}(m_W)$, and only for values of $m \to \infty$ one recovers the SM value.

Moreover, the mixing of the Higgs with the singlet ϕ modifies, in the broken phase, the trilinear

λ_3 and quartic λ_4 SM couplings. Recent experiments on di-Higgs searches are putting bounds on these two parameters by looking for possible departures with respect to the SM values $\lambda_3^{\rm SM} \equiv v\lambda_{\rm SM}$ and $\lambda_4^{\rm SM} \equiv \lambda_{\rm SM}$. In our theory the h-ϕ mixing angle α generates such a departure. After going to the broken phase by means of the shifts $\tilde{\phi} \to \tilde{\phi} + \tilde{v}_\phi$, $\tilde{h} \to \tilde{h} + \tilde{v}$ (where $\tilde{v} \equiv c_\alpha\, v + s_\alpha\, v_\phi$ and $\tilde{v}_\phi \equiv c_\alpha\, v_\phi - s_\alpha\, v$), and integrating out the field $\tilde{\phi}$, which yields the value

$$\tilde{\phi} = c_\alpha \left[\sqrt{\frac{\delta_\lambda}{2}}(1 - 3s_\alpha^2) + 3(\lambda + \delta_\lambda) s_\alpha c_\alpha \frac{v}{m} \right] \frac{\tilde{h}^2}{m} + \cdots , \tag{8.17}$$

one gets the Higgs potential, in the broken phase,

$$V(\tilde{h}) = \frac{1}{2} m_{\tilde{h}}^2 \tilde{h}^2 + \lambda_3 \tilde{h}^3 + \frac{1}{4}\lambda_4 \tilde{h}^4 + \cdots \tag{8.18}$$

where the ellipses are higher order terms, giving rise to powers $\tilde{h}^n$ $(n > 4)$ in the potential, and

$$\begin{aligned} \lambda_3 &= c_\alpha^3\, v \left[\lambda + \delta_\lambda - t_\alpha \sqrt{\frac{\delta_\lambda}{2}} \frac{m}{v} \right], \\ \lambda_4 &= c_\alpha^4 \lambda + c_\alpha^2(-c_\alpha^4 - 4s_\alpha^4 + 4c_\alpha^2 s_\alpha^2 + c_\alpha^2)\delta_\lambda \\ &\quad -6\sqrt{2\delta_\lambda}\, c_\alpha^3 s_\alpha (c_\alpha^2 - 2s_\alpha^2)(\lambda + \delta_\lambda)\frac{v}{m} - 18 s_\alpha^2 c_\alpha^4 (\lambda + \delta_\lambda)^2 \frac{v^2}{m^2}. \end{aligned} \tag{8.19}$$

The model can then, in the future, be excluded or confirmed by experimental data on trilinear (and quartic) Higgs couplings data. Notice that in the limit $m \gg m_h$ the mixing angle behaves as $s_\alpha \simeq \sqrt{2\delta_\lambda}\, v/m$ so that $\lambda_3 \simeq \lambda_3^{\rm SM}$ and $\lambda_4 \simeq \lambda_4^{\rm SM}$ [21], and the decoupling is automatic. We plot in the bottom panels of Fig. 10 contour lines of the trilinear and quartic couplings, normalized to the corresponding SM values, as functions of the parameters m and δ_λ. At present, with 89 fb^{-1} of LHC data, the triple Higgs coupling has been constrained by the ATLAS collaboration to be $\lambda_3/\lambda_3^{\rm SM} = 4.0^{+4.3}_{-4.1}$, excluding it outside the interval $[-3.2\,, 11.9]$ at 95% C.L. [88], while the CMS collaboration finds $\lambda_3/\lambda_3^{\rm SM} = 0.6^{+6.3}_{-1.8}$, excluding it outside the interval $[-3.3\,, 8.5]$ at 95% C.L. [89]. Theoretical studies based on the HE-LHC at $\sqrt{s} = 27$ TeV and 15 ab^{-1} luminosity foresee exploring the interval range $\lambda_3/\lambda_3^{\rm SM} \in [0.6\,, 1.46]$ at 68% C.L. [90], while a future 100 TeV hadron collider could achieve the trilinear coupling measurement within better than 5% accuracy [91], thus potentially imposing strong constraints on m from the plots in Fig. 10.

- Heavy Higgs production

Finally the state $\tilde{\phi}$ can be produced at the LHC by the same mechanisms of Higgs production with a cross section given by

$$\sigma(pp \to \tilde{\phi} + X) = s_\alpha^2\, \sigma(pp \to H + X) \tag{8.20}$$

where H is a heavy SM-like Higgs with a mass equal to m. Using the results of inclusive cross sections for $\sigma(pp \to H)$ for the leading mechanism of gluon-gluon fusion (ggf) [92] we plot, in Fig. 11, the cross section $\sigma_{ggf}(pp \to \tilde{\phi})$ as a function of m for two relevant values of the parameter δ_λ for $m \lesssim 1$ TeV and a center of mass energy $\sqrt{s} = 13$ TeV. Given that, as we have explained earlier in this section $\mathcal{B}(\tilde{\phi} \to \tilde{h}\tilde{h}) \simeq 1$, we can compare these cross sections with the SM cross sections for di-Higgs production $\sigma(pp \to hh)$ given by $\sigma_{ggf}^{\rm SM}(hh) \simeq 33.5$ fb [93].

[21] Of course, in the limit $m \gg v$, $\lambda \simeq \lambda_{\rm SM}$ as exhibited in the top right panel of Fig. 10.

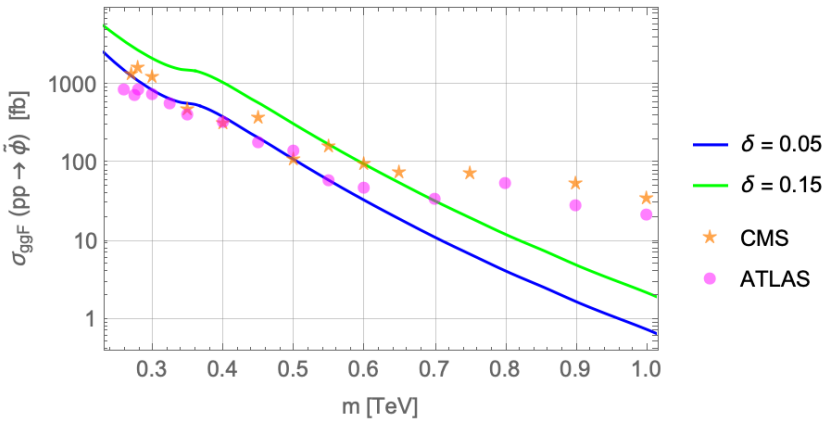

Figure 11: *Plots of cross section $\sigma(pp \to \tilde{\phi})$ in fb for relevant values of $\delta_\lambda = 0.05,\ 0.15$. The dots (stars) are the 95% C.L. upper bound from ATLAS [94] (CMS [95]), that bring the approximate constraint $m \gtrsim 0.55$-0.7 TeV, depending on the value of δ_λ.*

The predicted cross sections in Fig. 11 are compared with the present experimental upper bounds at 95% C.L. on the production of a scalar field ($\tilde{\phi}$) which decays into two Higgs bosons, from ATLAS with luminosities 27.5-36.1 fb^{-1} [94] and CMS with luminosity 35.9 fb^{-1} [95], at present LHC center of mass energies, $\sqrt{s} = 13$ TeV (see Fig. 11). We conclude from here that the present lower bounds on the value of m are

$$m \gtrsim 0.55\ (0.7)\ \text{TeV}\ @\ 95\%\ \text{C.L.}, \quad \text{for}\ \delta_\lambda = 0.05\ (0.15), \tag{8.21}$$

while in the future much stronger bounds could be achieved.

9 Conclusion

In this paper, we have explored the possibility of modifying the Higgs inflation theory by means of the introduction of an extra scalar field ϕ, with the Ricci coupling $(g/2)\phi^2 R$, and an interaction term $\mu\,\phi h^2$ to solve the stability problem of the electroweak vacuum. Both fields, ϕ and h, participate in the dynamics of inflation through the two-field potential $V(\phi, h)$, which has the shape of a valley in which they are related by simple analytical expressions so that we can express one field in term of the other. This allows us to define the true inflaton field χ as the one following the valley with canonical kinetic term although we kept the description in terms of ϕ for mathematical convenience.

A key point is that we have considered for the ϕ field a quartic coupling λ_ϕ and a mass m, such that inflation is driven by the quartic coupling term, while reheating is driven by the mass term. The Lagrangian coupling $\delta_\lambda = \mu^2/2m^2$ triggers a positive contribution to the β function of the Higgs quartic coupling such that, if the mass scale m is in the range 1 TeV $\lesssim m \lesssim \mathcal{Q}_I$, where $\mathcal{Q}_I \simeq 10^{11}$ GeV is the instability scale of the electroweak potential, the instability problem of the electroweak vacuum can be solved just by roughly imposing the mild constraint $\delta_\lambda \lesssim \mathcal{O}(1)$.

We find that the beginning of inflation $\phi = \phi_*$ ($N_* = 60$) is mainly driven by the scalar field ϕ, and since the amplitude of density perturbations is fixed by the ϕ quartic coupling (and not by the Higgs quartic coupling), the main problem of Higgs inflation is easily solved with $g \lesssim 1$. On the other hand, the end of inflation ($N \simeq 0$), where the hypermagnetic helicity will be produced, is equally

driven by both the scalar ϕ and the Higgs h quartic terms, so that the role played by the Higgs field is relevant. Both regimes are separated, for $g \simeq 0.01$ (0.05), by a critical value of the field $\phi_c/M_{\rm Pl} \simeq 10$ (4), which corresponds to the critical number of e-folds $N_c \simeq 12$ (2). After imposing the Planck and BICEP/Keck conditions on the slow roll parameters and the unitarity condition $\phi_* \lesssim M_{\rm Pl}/g$ (see however footnote 1 for a nuance) we obtain the allowed interval on the parameter g, $0.01 \lesssim g \lesssim 0.05$, which translates into the prediction for the cosmological observables in agreement with observations, and with a Hubble parameter almost saturating the Planck upper bound $H_*^{\rm obs} < 6 \cdot 10^{13}$ GeV:

$$0.965 \lesssim n_s \lesssim 0.967, \qquad 0.047 \gtrsim r \gtrsim 0.012, \qquad 5.5 \cdot 10^{13}\ \text{GeV} \gtrsim H(\phi_*) \gtrsim 2.8 \cdot 10^{13}\ \text{GeV}$$

During the last e-folds of inflation we generate maximally helical magnetic fields that will source the BAU via the $(B+L)$ anomaly of the SM during the EWPT [10–21]. This results from the introduction of a coupling of the Chern-Simons term of the hypercharge gauge group with the inflaton, as $\phi Y_{\mu\nu}\widetilde{Y}^{\mu\nu}$, with coupling strength $M_{\rm Pl}/f_\phi$, that breaks the $\mathcal{CP}$ symmetry. This effective $\mathcal{CP}$ breaking operator can be easily obtained from a UV completion with a $\mathcal{CP}$-violating Yukawa coupling of ϕ to a hypercharged vector like heavy fermion, as it is shown in App. A. This source of $\mathcal{CP}$-violation is needed by the Sakharov conditions [1], the two other conditions being provided by the chiral anomaly of the SM, which violates the baryon number, and the helical magnetic fields conversion to baryon asymmetry at the EWPT, which happens during EW sphalerons freeze out, when they go out of thermal equilibrium.

We have undertaken both backreation processes, namely the one of the gauge fields on the inflaton, and the one of the thermally produced chiral fermions on the gauge fields, known as the Schwinger effect. The latter significantly reduces the amount of electromagnetic energy and helicity generated at the end of inflation as, for $f_\phi/M_{\rm Pl} \lesssim 0.19$, we have to trade their exponential behavior with two polynomial cases: the maximal and the equilibrium estimates. This raises the effective coupling of the $\mathcal{CP}$-violating term $M_{\rm Pl}/f_\phi$, thus compensating its lowest overall value since electromagnetic fields are simultaneously weakened.

As for the former issue, we have found a critical value of the coupling strength of ϕ to gauge bosons in the $\mathcal{CP}$-violating operator, f_ϕ^c, such that for $f_\phi \gtrsim f_\phi^c$, the backreaction of the gauge field on the inflaton can be neglected. In particular we find $f_\phi^c/M_{\rm Pl} \simeq 0.02$ $(7 \cdot 10^{-4})$ for the Schwinger maximal (equilibrium) estimate. On the contrary, for $f_\phi \lesssim f_\phi^c$, the field ϕ is *strongly* coupled to the gauge fields, the backreaction of the latter on the inflaton equations of motion cannot be neglected, and the preheating of the Universe proceeds by the nonperturbative production of gauge fields. In this paper we have concentrated in the case $f_\phi \gtrsim f_\phi^c$, where the field ϕ is *weakly* coupled to the gauge fields, the backreaction of gauge fields on the inflaton dynamics can be neglected and the Universe reheating proceeds by the perturbative decay of the inflaton into SM particles. Besides, we have considered the constraints from non-Gaussianity of primordial fluctuations, and baryon isocurvature perturbations, and find that they have no influence on our model.

Concerning the value of the baryon asymmetry of the Universe generated at the EW crossover, η_B depends on the value of the reheat temperature $T_{\rm rh}$, and in particular on its ratio with respect to the reference instant reheat temperature $T_{\rm rh}/T_{\rm rh}^{\rm ins}$ (in our model $T_{\rm rh}^{\rm ins} \simeq 2 \cdot 10^{15}$ GeV). As we are imposing no backreaction of gauge fields on the inflaton dynamics, and reheating should proceed by perturbative inflaton decays, the value of $T_{\rm rh}/T_{\rm rh}^{\rm ins}$ depends on the inflaton decay width Γ_χ. In our model the inflaton mainly decays through the channel $\chi \to hh$, with a width which increases with the value of the inflaton mass m and ranges in the interval 1 GeV $\lesssim \Gamma_\chi \lesssim 10^9$ GeV, which corresponds to $10^{-6} \lesssim T_{\rm rh}/T_{\rm rh}^{\rm ins} \lesssim 10^{-2}$, for 1 TeV $\lesssim m \lesssim 5 \cdot 10^{10}$ GeV.

Moreover, as helicity is converted into baryon asymmetry at the EWPT, while it was produced at the end of inflation, it has to survive MHD processes between these two times. By imposing that the magnetic Reynolds number is bigger than unity, and that the chiral plasma instability effect does not washout the produced gauge fields, the available parameter window is reduced by an amount which depends on the value of the reheating temperature. We have shown that all these constraints are satisfied for a large range of the parameters f_ϕ and $T_{\rm rh}$, very insensitive to the value of the parameter g, inside its allowed range from cosmological observables:

$f_\phi/M_{\rm Pl} \in [0.14\,, 0.17]$	for	$T_{\rm rh}/T_{\rm rh}^{\rm ins} = 10^{-2}$	(Maximal estimate)
$f_\phi/M_{\rm Pl} \in [1.9\cdot 10^{-2}\,, 2.8\cdot 10^{-2}]$	for	$T_{\rm rh}/T_{\rm rh}^{\rm ins} = 10^{-6}$	
$f_\phi/M_{\rm Pl} \in [4.1\cdot 10^{-2}\,, 0.13]$	for	$T_{\rm rh}/T_{\rm rh}^{\rm ins} = 10^{-2}$	(Equilibrium estimate)
$f_\phi/M_{\rm Pl} \in [7.2\cdot 10^{-4}\,, 1.1\cdot 10^{-2}]$	for	$T_{\rm rh}/T_{\rm rh}^{\rm ins} = 10^{-6}$	

The complete available parameter region is summarized in Fig. 9.

Notice that the fact that the inflaton potential has both quadratic and quartic terms allows to decouple the mass m from the actual value of the amplitude of density perturbations, which in the absence of a quartic term would fix its value to $m \simeq 10^{12}$ GeV (or smaller at the price of the introduction of a curvaton scalar), allowing any value $m < \mathcal{Q}_I$ in order to stabilize the electroweak vacuum. This is achieved by the contribution, to the Higgs quartic coupling β function, provided by the coupling δ_λ in the Lagrangian term, $\sqrt{2\delta_\lambda}\, m\, \phi\, |\mathcal{H}|^2$. We have found for the parameter δ_λ the absolute bounds, $\delta_\lambda \gtrsim 0.05$ in order to solve the stability problem, and $\delta_\lambda \lesssim 0.35$ to not spoil the perturbativity of the theory, although its particular range depends on the actual value of m. Nevertheless, values $m \gg m_h$ create a naturalness/fine-tuning problem, essentially given by the fact that there appears a loop correction to the Higgs squared mass term μ_h^2. It translates into a fine-tuning of the order of $4\pi^2/(\delta_\lambda \rho^2 \log \rho^2)$ where $\rho \equiv m/m_h$. While for $\delta_\lambda \simeq 0.1$ and $m = 10^{10}$ GeV the fine tuning is $\sim 10^{-14}$ (similar to the SM fine-tuning), and for $m = 10$ TeV it is ~ 0.01, there is essentially no fine-tuning for values $m \lesssim 1$ TeV. This leads to the exciting possibility of a light inflaton which could possibly be detected by direct measurements at LHC and/or future colliders.

The key point here was that the Lagrangian term $\sqrt{2\delta_\lambda}\, m\, \phi\, |\mathcal{H}|^2$ creates a ϕ-h mixing, sizable for low values of the mass m, leading to an interesting phenomenology for high energy colliders. In fact all the collider phenomenology is triggered by the mixing angle α. The mass eigenstates $(\tilde\phi, \tilde h)$, where $\tilde h$ should be identified with the experimentally detected Higgs with a mass equal to 125.25 GeV, are related to the weak states (ϕ, h) by a rotation with angle α. This fact triggers that $\lambda(m_W)$ be different from $\lambda_{\rm SM}(m_W) \simeq 0.13$, which leads to predictions on the ratios $\lambda_3/\lambda_3^{\rm SM}$ and $\lambda_4/\lambda_4^{\rm SM}$ which could be probed by future experiments, as HE-LHC and/or a 100 TeV collider. The mixing is already bounded by present ATLAS and CMS results on the SM Higgs signal strengths, which provides the bound $m \gtrsim 0.3$ (0.45) TeV for $\delta_\lambda = 0.05$ (0.15). It also generates a contribution to the oblique electroweak observables, and yields for e.g. $\delta_\lambda = 0.15$ the lower bound $m \gtrsim 0.5$ TeV. Finally, the mixing is responsible for the inflaton production and decay. In particular $\tilde\phi \to \tilde h \tilde h$, triggered by the coupling δ_λ, is the main decay channel, while other decay channels into the SM particles, via the mixing s_α, are subleading. The inflaton $\tilde\phi$ can also be produced mainly by the gluon-gluon fusion mechanism through its Higgs mixing. Present data from ATLAS and CMS translate into lower bounds $m \gtrsim 0.55$ (0.7) TeV at 95% C.L. for $\delta_\lambda = 0.05$ (0.15).

There are a number of research lines which could be safely explored in the future. First of all, we have considered models of inflation based on the Ricci coupling $\phi^2 R$, and a ϕ dependent potential dominated, for large values of ϕ, by the quartic coupling. This kind of theories, when considered in the Einstein frame, give naturally rise, for large values of ϕ, to flat potentials, appropriate for inflation, without invoking any particular symmetry. It is clear that similar results could be obtained for theories with a Ricci coupling as $F(\phi)R$, and a Jordan frame potential behaving, for large values of ϕ, as $U(\phi) \simeq F^2(\phi)$. In particular it would be interesting to see what kind of theories would produce enough baryon asymmetry in the presence of a period of preheating, by the nonperturbative production of gauge fields. A very recent work [51] has already explored a general class of inflationary potentials and shown consistency with cosmological observables. In particular our model, labeled therein by $(n, p) = (2, 4)$, give results for the cosmological observables, which are in good agreement with this paper. These general theories are therefore good candidates to generate also the observed value of the BAU, provided they contain the inflaton coupling to the Chern-Simons term. In addition, as far as we are aware of, there are no in-depth studies in the literature of preheating mechanisms taking into account the Schwinger effect, which has led us to make some shortcuts in this article. Therefore we leave for future work a more rigorous study of nonperturbative production of gauge fields at preheating, leading to the BAU, that takes this effect into account. Lastly, at the level of particle physics it remains as an exciting playground the possibility of detecting the inflaton at present or future colliders, or that future experimental results on the production of heavy scalars, coupled to the SM fields, or on the measurements of the trilinear and quartic Higgs couplings, by di-Higgs production, could start cornering the present theory and put stronger bounds on the mass of the inflaton and its mixing with the SM Higgs.

Acknowledgments

This work is supported by the Departament d'Empresa i Coneixement, Generalitat de Catalunya Grant No. 2017SGR1069, by the Ministerio de Economía y Competitividad Grant No. FPA2017-88915-P. IFAE is partially funded by Centres de Recerca de Catalunya. Y. C. is supported by the European Union's Horizon 2020 research and innovation programme under the Marie Skłodowska-Curie Actions No. 754558.

A UV completion for $\mathcal{CP}$-violation

$\mathcal{CP}$-violation in our model is driven by the effective dimension-five operator

$$S_{\not{\mathcal{CP}}} = -\int d^4x \, \frac{\phi}{4\tilde{f}_\phi} Y_{\mu\nu}\tilde{Y}^{\mu\nu} \tag{A.1}$$

where $Y^{\mu\nu}$ is the hypercharge field strength.

A simple UV completion generating such effective operator can be a massive (with mass M) hypercharged vectorlike fermion ψ with a $\mathcal{CP}$-violating Yukawa coupling to ϕ as

$$\mathcal{L} = -\bar{\psi}_L(M + |\lambda_\psi| e^{i\theta_\lambda}\phi)\psi_R + \text{h.c.} = -|\lambda_\psi|\phi\left[\cos\theta_\lambda \bar{\psi}\psi + \sin\theta_\lambda \bar{\psi} i\gamma_5 \psi\right] \tag{A.2}$$

where $\mathcal{CP}$-violation is induced by the angle θ_λ. The $\mathcal{CP}$-even $\phi Y_{\mu\nu}Y^{\mu\nu}$, and $\mathcal{CP}$-odd $\phi Y_{\mu\nu}\tilde{Y}^{\mu\nu}$, couplings are generated by loop diagrams where the fermion ψ propagates in the loop and emits two gauge

bosons Y_μ, via the $\cos\theta_\lambda$ and $\sin\theta_\lambda$ couplings in Eq. (A.2), respectively. The corresponding Feynman diagrams are finite and thus one gets $\tilde{f}_\phi \propto M$. For maximal $\mathcal{CP}$-violation, i.e. $\theta_\lambda = \pm\pi/2$, only the coupling $\phi Y_{\mu\nu}\tilde{Y}^{\mu\nu}$ is generated such that

$$M \simeq \frac{|\lambda_\psi| g_Y^2}{4\pi^2}\tilde{f}_\phi \simeq 8\cdot 10^{15}\ \text{GeV}\,|\lambda_\psi|\,(\tilde{f}_\phi/M_{\rm Pl})\,. \tag{A.3}$$

- Stability of the inflationary potential

The UV completion here proposed could affect the stability of the inflationary potential through radiative corrections in the high energy theory. In fact, the coupling in Eq. (A.2) provides a correction to the β function of the coupling λ_ϕ, similar to the correction to the β function of the Higgs quartic coupling coupling β_λ from the top quark Yukawa coupling. This contribution comes from the box diagram with four ϕ external legs, where the fermion ψ is exchanged, and the resulting contribution to β_{λ_ϕ} is given by

$$\Delta\beta_{\lambda_\phi} = -\frac{2|\lambda_\psi|^4}{16\pi^2}\,\theta(t-t_M), \quad t - t_M = \log(Q/M). \tag{A.4}$$

Notice that the correction given by Eq. (A.4) is negative, as it arises from a fermion loop, which can lead the coupling λ_ϕ to negative values and thus destabilize the whole inflationary scenario, a process similar to the destabilization of the EW vacuum by the loop corrections induced by the top quark. It is then required to prevent such destabilization. A sufficient condition to not destabilize the quartic inflaton coupling, without any tuning of parameters, is to impose $|\lambda_\psi| \lesssim \lambda_\phi^{1/4}$ which translates, using the typical value, from Fig. 4, $\lambda_\phi \simeq 10^{-12}$, into $|\lambda_\psi| \lesssim 10^{-3}$, and so into an upper value of the ψ-mass as

$$M \lesssim 10^{13}\ \text{GeV}(\tilde{f}_\phi/M_{\rm Pl}). \tag{A.5}$$

Notice that in the limit $\lambda_\psi \to 0$ the UV Lagrangian has the enhanced $\mathbb{Z}_2$ symmetry, $\phi \to -\phi$, and thus any small value of λ_ψ is natural in the sense of 't Hooft. For instance, values of $\lambda_\psi \sim 10^{-12}$ would lead to values of $M \simeq \mathcal{O}(\text{TeV})$.

- Naturalness problem

The UV completion brings a new naturalness problem as there is the hierarchy of masses $M \gg m_h$. In fact, the presence of the vectorlike fermion ψ coupled to the field ϕ through the coupling (A.2), along with the ϕ-h mixing generates the Lagrangian

$$\mathcal{L} = |\lambda_\psi| s_\alpha\,\tilde{h}\,\bar{\psi} i\gamma_5\psi + |\lambda_\psi| c_\alpha\,\tilde{\phi}\,\bar{\psi} i\gamma_5\psi \tag{A.6}$$

whose first term provides at one-loop (for scales $\mathcal{Q} \gtrsim M$) a contribution to the mass parameter μ_h^2 as

$$\Delta\mu_h^2 \simeq \frac{1}{4\pi^2}\,s_\alpha^2\,|\lambda_\psi|^2\,M^2\log\frac{M^2}{m_h^2} \tag{A.7}$$

which would require, for large values of M, a fine-tuning. In particular, the naturalness condition $\Delta\mu_h^2 \lesssim m_h^2/2$ implies, for $m \simeq 1$ TeV, the upper bounds on M and $|\lambda_\psi|$ given by

$$M \lesssim (7.6,\,2.5,\,0.8)\cdot 10^8\ \text{GeV}, \quad |\lambda_\psi| \lesssim (1,\,3,\,10)\cdot 10^{-6}\,, \tag{A.8}$$

where the values in parenthesis correspond to $\tilde{f}_\phi/M_{\rm Pl} = (0.1, 0.01, 0.001)$, respectively, and where we have used $\delta_\lambda = 0.15$.

Of course the second term of (A.6) can create a second naturalness problem, as $M \gg m$ by radiative corrections providing a one-loop contribution to $m^2_{\tilde{\phi}}$ as

$$\Delta m^2_{\tilde{\phi}} \simeq \frac{1}{4\pi^2}\, c^2_\alpha\, |\lambda_\psi|^2\, M^2 \log \frac{M^2}{m^2} \tag{A.9}$$

However, once we have solved the naturalness problem between M and m_h, as $m^2 \gg m^2_h$, the second naturalness problem between M and m is automatically solved as, for all values in Eq. (A.8), it turns out that $\Delta m^2_{\tilde{\phi}}/m^2 \simeq 0.4$.

- Cosmological problems

The Lagrangian (A.2) has the (ψ number) discrete $\mathbb{Z}_2$ symmetry $\psi \to -\psi$ making the fermion ψ cosmologically stable, inconsistent with direct Dark Matter detection, and possibly overclosing the Universe. A simple way out is explicitly breaking the $\mathbb{Z}_2$ symmetry. For instance we can identify $\psi \equiv E$ with a heavy vectorlike, $SU(2)$ singlet, lepton $E = (E_L, E_R)^T$, with hypercharge -1, as the SM right-handed leptons e_{R_i}. We can then generate a tiny mixing of e.g. the third generation leptons with E by means of the Yukawa coupling Y'_3

$$\mathcal{L}_E = -M \bar{E}_L E_R - Y_3 \bar{\ell}_{L_3} H \tau_R - Y'_3 \bar{\ell}_{L_3} H E_R + h.c. \tag{A.10}$$

The mixing in (A.10) generates a mass matrix as

$$\begin{pmatrix} \bar{\tau}_L & \bar{E}_L \end{pmatrix} \mathcal{M} \begin{pmatrix} \tau_R \\ E_R \end{pmatrix}, \quad \mathcal{M} = \begin{pmatrix} m_3 & m'_3 \\ 0 & M \end{pmatrix} \tag{A.11}$$

where $m_3 = Y_3 v/\sqrt{2}$ is the τ-lepton mass in the absence of the mixing with the heavy fermion, and $m'_3 \equiv Y'_3 v/\sqrt{2}$. One can diagonalize the mass matrix $\mathcal{M}$ with left and right unitary transformations, with angles θ_L and θ_R, respectively, as

$$\mathcal{M}_d = U_L^\dagger \mathcal{M} U_R, \qquad U_{L/R} = \begin{pmatrix} \sin\theta_{L/R} & \cos\theta_{L/R} \\ -\cos\theta_{L/R} & \sin\theta_L \end{pmatrix}. \tag{A.12}$$

In the limit $M \gg m_3, m'_3$ we get

$$\sin\theta_L \simeq \frac{m'_3}{M}\left[1 + \frac{m_3^2}{M^2} + \cdots\right], \quad \sin\theta_R \simeq \frac{m_3 m'_3}{M^2}\left[1 + \frac{m_3^2 - m_3'^2}{M^2} + \cdots\right]. \tag{A.13}$$

As a consequence of the mixing the mass eigenfunctions are shifted as

$$\tau_R \to \tau_R + \frac{m_3 m'_3}{M^2} E_R, \quad E_R \to E_R - \frac{m_3 m'_3}{M^2}\tau_R. \tag{A.14a}$$

$$\tau_L \to \tau_L + \frac{m'_3}{M} E_L, \quad E_L \to E_L - \frac{m'_3}{M}\tau_L. \tag{A.14b}$$

and the mass eigenvalues as

$$m_3 \to m_\tau = m_3\left[1 - \frac{m_3'^2}{2M^2} + \cdots\right], \quad M \to M\left[1 + \frac{m_3'^2}{2M^2} + \cdots\right] \tag{A.15}$$

by which the fermion E decays as $E \to H\tau$, as well as to leptons and gauge bosons through the mixing with τ_L and τ_R, as $E \to W\nu_\tau$ or $E \to \tau Z, \tau\gamma$. These decays prevent the heavy fermion from overclosing the Universe.

B Baryon isocurvature perturbations

Baryon isocurvature perturbations can be generated by the presence of strong gauge fields [81]. To be conservative, in this section we will consider the case where the generated gauge fields are as strong as possible: where one neglects the backreaction from the fermionic Schwinger currents (the backreactionless case). Borrowing the notation from [81], we have in our case for the symmetric and antisymmetric combinations, $S(k) = (|A_+(k)|^2 + |A_-(k)|^2)/2$ and $A(k) = (|A_+(k)|^2 - |A_-(k)|^2)/2$. For the case of maximally helical gauge fields one obtains

$$S(k) \simeq A(k) \simeq \frac{|A_+|^2}{2} \simeq \frac{1}{4k_\lambda}\left(\frac{k}{k_\lambda}\right)^{-\frac{1}{2}} \frac{e^{2\pi\xi}}{\xi} \exp\left(-4\sqrt{\frac{k}{k_\lambda}}\right), \tag{B.1}$$

where we are choosing e.g. $A_+(k)$ as the amplified mode, and (4.23) was used together with the definition $k_\lambda = a_{\rm E} H_E/2\xi \simeq 10^{12}$ GeV, which corresponds to the spectrum peak of A_+. Writing $B^2 \simeq 2\rho_B$ in term of k_λ, and using (4.27a), we obtain a relation for the spectrum given by [81]

$$A(k) \simeq \frac{1024\,\pi^2}{315}\frac{B^2}{k_\lambda^5}\left(\frac{k}{k_\lambda}\right)^{-\frac{1}{2}} \exp\left(-4\sqrt{\frac{k}{k_\lambda}}\right). \tag{B.2}$$

It may be interesting to note that in these terms, the magnetic field and the helicity are written as

$$B^2 \simeq \frac{1}{4\pi^2}\frac{315}{1024}\frac{e^{2\pi\xi}}{2\xi}\, k_\lambda^4, \qquad\qquad \mathscr{H} \simeq \frac{2}{7}\frac{B^2}{k_\lambda}. \tag{B.3}$$

From this we can estimate the baryon isocurvature perturbation at the BBN as

$$\overline{\mathcal{S}^2}_{\rm B,BBN} \simeq \frac{7\sqrt{\pi}}{20\sqrt{3}}\left(\frac{k_d}{k_\lambda}\right)^3 \left(\frac{k_\lambda}{k_\lambda^{\rm EWPT}}\right)^3 + \mathcal{O}\left(\frac{k_d}{k_\lambda}\right)^5, \tag{B.4}$$

where k_d is the comoving neutron diffusion scale at the BBN, $k_d^{-1} \simeq 0.0025$ pc. From the expansion ratio $k_d/k_\lambda \sim 10^{-42}$, we can see that Eq. (B.4) is suppressed provided that $k_\lambda/k_\lambda^{\rm EWPT}$ is not too big, which we will next demonstrate.

Eq. (B.4) should be evaluated at the time of baryon asymmetry production at $T_{\rm EWPT} \simeq 135$ GeV, hence the rescaling for the wave number k_λ. At first glance, this rescaling could appear to be exactly one since k_λ is comoving, but because of the peculiar dynamic of the plasma decribed by the MHD equations, comoving quantities do scale with the expansion of the Universe after reheating, as already stated in section 7.1.

We shall now study how the comoving coherence length scales until the EWPT. Every plasma quantity (field amplitude, correlation length, wave number) evolves adiabatically from reheating until the eddy turnover temperature $T_t \simeq v T_{\rm rh}$ where v is the typical bulk velocity of the plasma. For $T < T_t$ the scaling regime depends on the value of the electric Reynolds number at the end of inflation. The velocity of the plasma is

$$\mathcal{R}_e < 1 \quad \Rightarrow \quad v \approx 2.9\cdot 10^{-10}\,\frac{\ell_{B_Y}\rho_{B_Y}}{H_E^3}\left(\frac{H_E}{10^{13}\,{\rm GeV}}\right)^{\frac{3}{2}}\left(\frac{T_{\rm rh}}{T_{\rm rh}^{\rm ins}}\right) \tag{B.5a}$$

$$\mathcal{R}_e > 1 \quad \Rightarrow \quad v \approx 5.3\cdot 10^{-6}\,\frac{\sqrt{\rho_{B_Y}}}{H_E^2}\left(\frac{H_E}{10^{13}\,{\rm GeV}}\right)\left(\frac{T_{\rm rh}}{T_{\rm rh}^{\rm ins}}\right)^{\frac{2}{3}} \tag{B.5b}$$

For $\mathcal{R}_e^{\rm rh} < 1$, as $\mathcal{R}_e$ grows with time, we eventually reach the point where it becomes one, at temperature [20]

$$T_1 \equiv T(\mathcal{R}_e = 1) = \mathcal{R}_e^{\rm rh}\, T_t. \tag{B.6}$$

Once $\mathcal{R}_e > 1$, the scaling regimes for comoving quantities become (7.4b) until recombination.

In summary, the magnetic energy and correlation length scale adiabatically until the eddy turnover temperature T_t, then they scale according to (7.4a) until $\mathcal{R}_e = 1$, where the regime changes to (7.4b) until recombination. However we compute the scaling only until $T_{\rm EWPT} = 135$ GeV since the comparison with the neutron diffusion scale must be done at the EWPT temperature [81]. This yields a total dilution factor for comoving quantities as

$$\frac{B_Y^{\rm EWPT}}{B_Y^{\rm rh}} = \left(\frac{T_{\rm EWPT}}{T_1}\right)^{\frac{1}{3}} \left(\frac{T_1}{T_t}\right)^{\frac{1}{2}}, \tag{B.7a}$$

$$\frac{\ell_{B_Y}^{\rm EWPT}}{\ell_{B_Y}^{\rm rh}} = \left(\frac{T_{\rm EWPT}}{T_1}\right)^{-\frac{2}{3}} \left(\frac{T_1}{T_t}\right)^{-1}. \tag{B.7b}$$

We stress that T_t and T_1 depend on v, which in turn depends on ℓ_{B_Y} and ρ_B. For values of the parameters space yielding the correct BAU, e.g. for $g = 0.01$, $f_\phi = 0.15 M_{\rm Pl}$ and $T_{\rm rh} \simeq 10^{-2}\, T_{\rm rh}^{\rm ins}$ (blue region in Fig. 8) we find that $T_t \simeq 2 \cdot 10^8$ GeV and $T_1 \simeq 3 \cdot 10^7$ GeV. Then we get that the comoving quantities B_Y and ℓ_{B_Y} get scaled between the reheating and EWPT temperatures as

$$\frac{B_Y^{\rm EWPT}}{B_Y^{\rm rh}} \sim 10^{-2}, \quad \frac{\ell_{B_Y}^{\rm EWPT}}{\ell_{B_Y}^{\rm rh}} \sim 10^4. \tag{B.8}$$

Going back to the baryon isocurvature perturbation (B.4), we hence have

$$\left(\frac{k_\lambda}{k_\lambda^{\rm EWPT}}\right)^3 \propto \left(\frac{T_{\rm rh}}{T_{\rm rh}^{\rm ins}}\right)^{-4}, \quad \left(\frac{k_\lambda}{k_\lambda^{\rm EWPT}}\right)^3 \sim 10^{-13}, \tag{B.9}$$

which therefore get for the observable $\overline{\mathcal{S}^2}_{\rm B,BBN}$ an exceedingly small value. A similar result is obtained for all allowed values of the parameters $(g, f_\phi, T_{\rm rh})$, so for our model the prediction is $\overline{\mathcal{S}^2}_{\rm B,BBN} \simeq 0$. This result also holds for the case where the Schwinger effect is considered, as in this case gauge fields are much weaker than in the backreactionless case studied above, and so their contribution to $\overline{\mathcal{S}^2}_{\rm B,BBN}$ is expected to be much smaller.

References

[1] A. D. Sakharov, *Violation of $\mathcal{CP}$ Invariance, $\mathcal{C}$ asymmetry, and baryon asymmetry of the universe*, *Pisma Zh. Eksp. Teor. Fiz.* **5** (1967) 32–35.

[2] A. G. Cohen, D. B. Kaplan and A. E. Nelson, *Progress in electroweak baryogenesis*, *Ann. Rev. Nucl. Part. Sci.* **43** (1993) 27–70, [hep-ph/9302210].

[3] M. Quiros, *Field theory at finite temperature and phase transitions*, *Helv. Phys. Acta* **67** (1994) 451–583.

[4] V. A. Rubakov and M. E. Shaposhnikov, *Electroweak baryon number nonconservation in the early universe and in high-energy collisions*, *Usp. Fiz. Nauk* **166** (1996) 493–537, [hep-ph/9603208].

[5] M. Carena and C. E. M. Wagner, *Electroweak baryogenesis and Higgs physics*, *Adv. Ser. Direct. High Energy Phys.* **17** (1997) 320–358, [hep-ph/9704347].

[6] M. Quiros, *Finite temperature field theory and phase transitions*, in *ICTP Summer School in High-Energy Physics and Cosmology*, pp. 187–259, 1, 1999. hep-ph/9901312.

[7] D. E. Morrissey and M. J. Ramsey-Musolf, *Electroweak baryogenesis*, *New J. Phys.* **14** (2012) 125003, [1206.2942].

[8] M. D'Onofrio and K. Rummukainen, *Standard model cross-over on the lattice*, *Phys. Rev. D* **93** (2016) 025003, [1508.07161].

[9] K. Kajantie, M. Laine, K. Rummukainen and M. E. Shaposhnikov, *A Nonperturbative analysis of the finite T phase transition in SU(2) x U(1) electroweak theory*, *Nucl. Phys. B* **493** (1997) 413–438, [hep-lat/9612006].

[10] M. M. Anber and L. Sorbo, *N-flationary magnetic fields*, *JCAP* **10** (2006) 018, [astro-ph/0606534].

[11] K. Bamba, *Baryon asymmetry from hypermagnetic helicity in dilaton hypercharge electromagnetism*, *Phys. Rev. D* **74** (2006) 123504, [hep-ph/0611152].

[12] K. Bamba, C. Q. Geng and S. H. Ho, *Hypermagnetic Baryogenesis*, *Phys. Lett. B* **664** (2008) 154–156, [0712.1523].

[13] M. M. Anber and L. Sorbo, *Naturally inflating on steep potentials through electromagnetic dissipation*, *Phys. Rev. D* **81** (2010) 043534, [0908.4089].

[14] M. M. Anber and E. Sabancilar, *Hypermagnetic Fields and Baryon Asymmetry from Pseudoscalar Inflation*, *Phys. Rev. D* **92** (2015) 101501, [1507.00744].

[15] Y. Cado and E. Sabancilar, *Asymmetric Dark Matter and Baryogenesis from Pseudoscalar Inflation*, *JCAP* **04** (2017) 047, [1611.02293].

[16] E. I. Sfakianakis and J. van de Vis, *Preheating after Higgs Inflation: Self-Resonance and Gauge boson production*, *Phys. Rev. D* **99** (2019) 083519, [1810.01304].

[17] K. Kamada and A. J. Long, *Baryogenesis from decaying magnetic helicity*, *Phys. Rev. D* **94** (2016) 063501, [1606.08891].

[18] K. Kamada and A. J. Long, *Evolution of the Baryon Asymmetry through the Electroweak Crossover in the Presence of a Helical Magnetic Field*, *Phys. Rev. D* **94** (2016) 123509, [1610.03074].

[19] D. Jiménez, K. Kamada, K. Schmitz and X.-J. Xu, *Baryon asymmetry and gravitational waves from pseudoscalar inflation*, *JCAP* **12** (2017) 011, [1707.07943].

[20] V. Domcke, B. von Harling, E. Morgante and K. Mukaida, *Baryogenesis from axion inflation*, *JCAP* **10** (2019) 032, [1905.13318].

[21] Y. Cado, B. von Harling, E. Massó and M. Quirós, *Baryogenesis via gauge field production from a relaxing Higgs*, *JCAP* **07** (2021) 049, [2102.13650].

[22] F. L. Bezrukov and M. Shaposhnikov, *The Standard Model Higgs boson as the inflaton*, *Phys. Lett. B* **659** (2008) 703–706, [0710.3755].

[23] F. L. Bezrukov, A. Magnin and M. Shaposhnikov, *Standard Model Higgs boson mass from inflation*, *Phys. Lett. B* **675** (2009) 88–92, [0812.4950].

[24] F. Bezrukov, A. Magnin, M. Shaposhnikov and S. Sibiryakov, *Higgs inflation: consistency and generalisations*, *JHEP* **01** (2011) 016, [1008.5157].

[25] J. Rubio, *Higgs inflation*, *Front. Astron. Space Sci.* **5** (2019) 50, [1807.02376].

[26] T. Han and S. Willenbrock, *Scale of quantum gravity*, *Phys. Lett. B* **616** (2005) 215–220, [hep-ph/0404182].

[27] C. P. Burgess, H. M. Lee and M. Trott, *Power-counting and the Validity of the Classical Approximation During Inflation*, *JHEP* **09** (2009) 103, [0902.4465].

[28] J. L. F. Barbon and J. R. Espinosa, *On the Naturalness of Higgs Inflation*, *Phys. Rev. D* **79** (2009) 081302, [0903.0355].

[29] R. N. Lerner and J. McDonald, *Higgs Inflation and Naturalness*, *JCAP* **04** (2010) 015, [0912.5463].

[30] C. P. Burgess, H. M. Lee and M. Trott, *Comment on Higgs Inflation and Naturalness*, *JHEP* **07** (2010) 007, [1002.2730].

[31] M. P. Hertzberg, *On Inflation with Non-minimal Coupling*, *JHEP* **11** (2010) 023, [1002.2995].

[32] I. Antoniadis, A. Guillen and K. Tamvakis, *Ultraviolet behaviour of Higgs inflation models*, *JHEP* **08** (2021) 018, [2106.09390].

[33] A. Ito, W. Khater and S. Rasanen, *Tree-level unitarity in Higgs inflation in the metric and the Palatini formulation*, 2111.05621.

[34] G. K. Karananas, M. Shaposhnikov and S. Zell, *Field redefinitions, perturbative unitarity and Higgs inflation*, *JHEP* **06** (2022) 132, [2203.09534].

[35] F. Bezrukov, J. Rubio and M. Shaposhnikov, *Living beyond the edge: Higgs inflation and vacuum metastability*, *Phys. Rev. D* **92** (2015) 083512, [1412.3811].

[36] G. F. Giudice and H. M. Lee, *Unitarizing Higgs Inflation*, *Phys. Lett. B* **694** (2011) 294–300, [1010.1417].

[37] J. L. F. Barbon, J. A. Casas, J. Elias-Miro and J. R. Espinosa, *Higgs Inflation as a Mirage*, *JHEP* **09** (2015) 027, [1501.02231].

[38] M. Dine, P. Huet, R. L. Singleton, Jr and L. Susskind, *Creating the baryon asymmetry at the electroweak phase transition*, *Phys. Lett. B* **257** (1991) 351–356.

[39] M. Carena, M. Quirós and Y. Zhang, *Electroweak Baryogenesis from Dark-Sector CP Violation*, *Phys. Rev. Lett.* **122** (2019) 201802, [1811.09719].

[40] M. Carena, M. Quirós and Y. Zhang, *Dark CP violation and gauged lepton or baryon number for electroweak baryogenesis*, *Phys. Rev. D* **101** (2020) 055014, [1908.04818].

[41] V. Domcke and K. Mukaida, *Gauge Field and Fermion Production during Axion Inflation*, *JCAP* **11** (2018) 020, [1806.08769].

[42] E. V. Gorbar, K. Schmitz, O. O. Sobol and S. I. Vilchinskii, *Hypermagnetogenesis from axion inflation: Model-independent estimates*, *Phys. Rev. D* **105** (2022) 043530, [2111.04712].

[43] J. R. Espinosa, G. F. Giudice, E. Morgante, A. Riotto, L. Senatore, A. Strumia et al., *The cosmological Higgstory of the vacuum instability*, *JHEP* **09** (2015) 174, [1505.04825].

[44] J. Khoury and T. Steingasser, *Gauge hierarchy from electroweak vacuum metastability*, *Phys. Rev. D* **105** (2022) 055031, [2108.09315].

[45] A. De Simone, M. P. Hertzberg and F. Wilczek, *Running Inflation in the Standard Model*, *Phys. Lett. B* **678** (2009) 1–8, [0812.4946].

[46] Planck collaboration, Y. Akrami et al., *Planck 2018 results. X. Constraints on inflation*, *Astron. Astrophys.* **641** (2020) A10, [1807.06211].

[47] D. H. Lyth, *What would we learn by detecting a gravitational wave signal in the cosmic microwave background anisotropy?*, *Phys. Rev. Lett.* **78** (1997) 1861–1863, [hep-ph/9606387].

[48] A. D. Linde, *Particle physics and inflationary cosmology*, *Contemp. Concepts Phys.* **5** (1990) 1–362, [hep-th/0503203].

[49] M. Herranen, T. Markkanen, S. Nurmi and A. Rajantie, *Spacetime curvature and the Higgs stability during inflation*, *Phys. Rev. Lett.* **113** (2014) 211102, [1407.3141].

[50] BICEP/Keck collaboration, P. A. R. Ade et al., *Improved Constraints on Primordial Gravitational Waves using Planck, WMAP, and BICEP/Keck Observations through the 2018 Observing Season*, *Phys. Rev. Lett.* **127** (2021) 151301, [2110.00483].

[51] T. Kodama and T. Takahashi, *Relaxing inflation models with nonminimal coupling: A general study*, *Phys. Rev. D* **105** (2022) 063542, [2112.05283].

[52] M. Abramowitz and I. A. Stegun, *Handbook of Mathematical Functions: With Formulas, Graphs, and Mathematical Tables*. Dover Publications, 1965.

[53] R. Durrer and A. Neronov, *Cosmological Magnetic Fields: Their Generation, Evolution and Observation*, *Astron. Astrophys. Rev.* **21** (2013) 62, [1303.7121].

[54] E. V. Gorbar, K. Schmitz, O. O. Sobol and S. I. Vilchinskii, *Gauge-field production during axion inflation in the gradient expansion formalism*, *Phys. Rev. D* **104** (2021) 123504, [2109.01651].

[55] L. Kofman, A. D. Linde and A. A. Starobinsky, *Towards the theory of reheating after inflation*, *Phys. Rev. D* **56** (1997) 3258–3295, [hep-ph/9704452].

[56] P. Adshead, J. T. Giblin, T. R. Scully and E. I. Sfakianakis, *Gauge-preheating and the end of axion inflation*, *JCAP* **12** (2015) 034, [1502.06506].

[57] J. R. C. Cuissa and D. G. Figueroa, *Lattice formulation of axion inflation. Application to preheating*, *JCAP* **06** (2019) 002, [1812.03132].

[58] D. J. Chung, E. W. Kolb and A. Riotto, *Production of massive particles during reheating*, *Phys. Rev. D* **60** (1999) 063504, [hep-ph/9809453].

[59] G. F. Giudice, E. W. Kolb and A. Riotto, *Largest temperature of the radiation era and its cosmological implications*, *Phys. Rev. D* **64** (2001) 023508, [hep-ph/0005123].

[60] L. Kofman, A. D. Linde and A. A. Starobinsky, *Reheating after inflation*, *Phys. Rev. Lett.* **73** (1994) 3195–3198, [hep-th/9405187].

[61] C. Cosme, D. G. Figueroa and N. Loayza, *Gravitational wave production from preheating with trilinear interactions*, 2206.14721.

[62] Particle Data Group collaboration, P. Zyla et al., *Review of Particle Physics*, *PTEP* **2020** (2020) 083C01.

[63] M. Giovannini and M. E. Shaposhnikov, *Primordial hypermagnetic fields and triangle anomaly*, *Phys. Rev. D* **57** (1998) 2186–2206, [hep-ph/9710234].

[64] T. Vachaspati, *Progress on cosmological magnetic fields*, *Rept. Prog. Phys.* **84** (2021) 074901, [2010.10525].

[65] R. Banerjee and K. Jedamzik, *The Evolution of cosmic magnetic fields: From the very early universe, to recombination, to the present*, *Phys. Rev. D* **70** (2004) 123003, [astro-ph/0410032].

[66] K. Kamada, *Return of grand unified theory baryogenesis: Source of helical hypermagnetic fields for the baryon asymmetry of the universe*, *Phys. Rev. D* **97** (2018) 103506, [1802.03055].

[67] M. Joyce and M. E. Shaposhnikov, *Primordial magnetic fields, right-handed electrons, and the Abelian anomaly*, *Phys. Rev. Lett.* **79** (1997) 1193–1196, [astro-ph/9703005].

[68] A. Boyarsky, J. Frohlich and O. Ruchayskiy, *Self-consistent evolution of magnetic fields and chiral asymmetry in the early Universe*, *Phys. Rev. Lett.* **108** (2012) 031301, [1109.3350].

[69] Y. Akamatsu and N. Yamamoto, *Chiral Plasma Instabilities*, *Phys. Rev. Lett.* **111** (2013) 052002, [1302.2125].

[70] Y. Hirono, D. Kharzeev and Y. Yin, *Self-similar inverse cascade of magnetic helicity driven by the chiral anomaly*, *Phys. Rev. D* **92** (2015) 125031, [1509.07790].

[71] N. Yamamoto, *Scaling laws in chiral hydrodynamic turbulence*, *Phys. Rev. D* **93** (2016) 125016, [1603.08864].

[72] I. Rogachevskii, O. Ruchayskiy, A. Boyarsky, J. Fröhlich, N. Kleeorin, A. Brandenburg et al., *Laminar and turbulent dynamos in chiral magnetohydrodynamics-I: Theory*, *Astrophys. J.* **846** (2017) 153, [1705.00378].

[73] E. Komatsu, *The pursuit of non-gaussian fluctuations in the cosmic microwave background*. PhD thesis, Tohoku U., 2001. astro-ph/0206039.

[74] WMAP collaboration, E. Komatsu et al., *Seven-Year Wilkinson Microwave Anisotropy Probe (WMAP) Observations: Cosmological Interpretation*, *Astrophys. J. Suppl.* **192** (2011) 18, [1001.4538].

[75] N. Barnaby and M. Peloso, *Large Nongaussianity in Axion Inflation*, *Phys. Rev. Lett.* **106** (2011) 181301, [1011.1500].

[76] N. Barnaby, E. Pajer and M. Peloso, *Gauge Field Production in Axion Inflation: Consequences for Monodromy, non-Gaussianity in the CMB, and Gravitational Waves at Interferometers*, *Phys. Rev. D* **85** (2012) 023525, [1110.3327].

[77] Planck collaboration, Y. Akrami et al., *Planck 2018 results. IX. Constraints on primordial non-Gaussianity*, *Astron. Astrophys.* **641** (2020) A9, [1905.05697].

[78] A. Neronov and I. Vovk, *Evidence for strong extragalactic magnetic fields from Fermi observations of TeV blazars*, *Science* **328** (2010) 73–75, [1006.3504].

[79] F. Tavecchio, G. Ghisellini, L. Foschini, G. Bonnoli, G. Ghirlanda and P. Coppi, *The intergalactic magnetic field constrained by Fermi/LAT observations of the TeV blazar 1ES 0229+200*, *Mon. Not. Roy. Astron. Soc.* **406** (2010) L70–L74, [1004.1329].

[80] S. Ando and A. Kusenko, *Evidence for Gamma-Ray Halos Around Active Galactic Nuclei and the First Measurement of Intergalactic Magnetic Fields*, *Astrophys. J. Lett.* **722** (2010) L39, [1005.1924].

[81] K. Kamada, F. Uchida and J. Yokoyama, *Baryon isocurvature constraints on the primordial hypermagnetic fields*, *JCAP* **04** (2021) 034, [2012.14435].

[82] K. Inomata, M. Kawasaki, A. Kusenko and L. Yang, *Big Bang Nucleosynthesis Constraint on Baryonic Isocurvature Perturbations*, *JCAP* **12** (2018) 003, [1806.00123].

[83] A. de Gouvea, D. Hernandez and T. M. P. Tait, *Criteria for Natural Hierarchies*, *Phys. Rev. D* **89** (2014) 115005, [1402.2658].

[84] S. Profumo, M. J. Ramsey-Musolf and G. Shaughnessy, *Singlet Higgs phenomenology and the electroweak phase transition*, *JHEP* **08** (2007) 010, [0705.2425].

[85] V. Barger, P. Langacker, M. McCaskey, M. J. Ramsey-Musolf and G. Shaughnessy, *LHC Phenomenology of an Extended Standard Model with a Real Scalar Singlet*, *Phys. Rev. D* **77** (2008) 035005, [0706.4311].

[86] ATLAS collaboration, G. Aad et al., *Combined measurements of Higgs boson production and decay using up to 80 fb^{-1} of proton-proton collision data at $\sqrt{s} = 13$ TeV collected with the ATLAS experiment*, *Phys. Rev. D* **101** (2020) 012002, [1909.02845].

[87] CMS collaboration, A. M. Sirunyan et al., *Combined measurements of Higgs boson couplings in proton–proton collisions at* $\sqrt{s} = 13$ *TeV*, *Eur. Phys. J. C* **79** (2019) 421, [1809.10733].

[88] ATLAS collaboration, *Constraint of the Higgs boson self-coupling from Higgs boson differential production and decay measurements*, tech. rep., CERN, Geneva, Mar, 2019.

[89] CMS collaboration, A. M. Sirunyan et al., *Search for nonresonant Higgs boson pair production in final states with two bottom quarks and two photons in proton-proton collisions at* $\sqrt{s} = 13$ *TeV*, *JHEP* **03** (2021) 257, [2011.12373].

[90] S. Homiller and P. Meade, *Measurement of the Triple Higgs Coupling at a HE-LHC*, *JHEP* **03** (2019) 055, [1811.02572].

[91] D. Gonçalves, T. Han, F. Kling, T. Plehn and M. Takeuchi, *Higgs boson pair production at future hadron colliders: From kinematics to dynamics*, *Phys. Rev. D* **97** (2018) 113004, [1802.04319].

[92] LHC Higgs Cross Section Working Group collaboration, S. Dittmaier et al., *Handbook of LHC Higgs Cross Sections: 1. Inclusive Observables*, 1101.0593.

[93] LHC Higgs Cross Section Working Group collaboration, D. de Florian et al., *Handbook of LHC Higgs Cross Sections: 4. Deciphering the Nature of the Higgs Sector*, 1610.07922.

[94] ATLAS collaboration, G. Aad et al., *Combination of searches for Higgs boson pairs in pp collisions at* $\sqrt{s}$ *=13 TeV with the ATLAS detector*, *Phys. Lett. B* **800** (2020) 135103, [1906.02025].

[95] CMS collaboration, A. M. Sirunyan et al., *Combination of searches for Higgs boson pair production in proton-proton collisions at* $\sqrt{s} = 13$ *TeV*, *Phys. Rev. Lett.* **122** (2019) 121803, [1811.09689].

Numerical study of the Schwinger effect in axion inflation

Yann Cado, Mariano Quirós

Institut de Física d'Altes Energies (IFAE) and
The Barcelona Institute of Science and Technology (BIST),
Campus UAB, 08193 Bellaterra, Barcelona, Spain

Abstract

Previous studies demonstrate that the inflaton, when coupled to the hypercharge Chern-Simons density, can source an explosive production of helical hypermagnetic fields. Then, in the absence of fermion production, those fields have the capability of preheating the Universe after inflation and triggering a successful baryogenesis mechanism at the electroweak phase transition. In the presence of fermion production however, we expect a strong damping of the gauge fields production from the fermion backreaction, a phenomenon called Schwinger effect, thus jeopardizing their original capabilities. Using numerical methods we study the backreaction on the generated gauge fields and revisit the processes of gauge preheating and baryogenesis in the presence of the Schwinger effect. We have found that gauge preheating is very unlikely, while still having a sizable window in the parameter space to achieve the baryon asymmetry of the Universe at the electroweak phase transition.

Contents

1 Introduction **3**

2 The model **4**
- 2.1 Equations of motion 4
- 2.2 Observable quantities 5
- 2.3 The gauge vacuum 7

3 Slow Roll Analysis **8**
- 3.1 Absence of Schwinger effect 8
- 3.2 Presence of Schwinger effect 9
- 3.3 Numerical results at the end of inflation 11
  - 3.3.1 Constant Δ and ξ approximation 13
  - 3.3.2 Variable Δ and ξ 13

4 Full Analysis **14**
- 4.1 Full numerical results at the end of inflation 15
- 4.2 Inflationary models 16
  - 4.2.1 α-attractor models 16
  - 4.2.2 Hilltop quartic models 17
- 4.3 Numerical results beyond the end of inflation 18
- 4.4 End of reheating 20
- 4.5 Baryon asymmetry 22

5 Conclusions **24**

A Numerical method: the slow roll case **25**

B Numerical method: full analysis **28**

1 Introduction

Cosmological inflation [1–3] is nowadays a well-established paradigm to solve the classical (flatness, horizon, ...) problems of the Standard Cosmological Model, and to generate the primordial density perturbations giving rise to the present Universe structure. The achievements of cosmological inflation usually require the presence of one (or several) scalar field –the inflaton– giving rise to physics beyond the Standard Model (SM) of Particle Physics (BSM). In this way, along with the classical problems of the SM (hierarchy problem, baryogenesis, strong CP-problem, dark matter,...), cosmological inflation provides yet another motivation for BSM physics.

Although the existence of a period of cosmological inflation is pretty well stablished by observational cosmological data [4], there is no consensus on a detailed model. An interesting candidate for the inflaton is a pseudoscalar field ϕ, denoted in this paper as *axionlike particle*[1], which can then couple to the Chern-Simons density $F_{\mu\nu}\tilde{F}^{\mu\nu}$ of a $U(1)$ gauge field. In this case, and depending on the size of the coupling of the inflaton to the Chern-Simons term, there can be an explosive production of helical gauge fields at the end of inflation [7–9]. This exponential production can dominate the energy density of the Universe during the coherent oscillations of the inflaton around its minimum, a phenomenon dubbed as *gauge preheating* [10–12], and lead to a rapid production of inhomogeneities sourcing a significant gravitational wave background, leading to strong constraints on the inflaton Chern-Simons coupling from the Planck (and future CMB-S4) limits on the net energy density in gravitational waves [5, 6].

When the gauge field is identified with the SM hypercharge, Y_μ, with strength $Y_{\mu\nu}$, the inflaton coupling to the Chern-Simons density $Y_{\mu\nu}\tilde{Y}^{\mu\nu}$ gives rise to the production of helical hypermagnetic fields which can then survive until the electroweak phase transition (crossover), and trigger the baryon asymmetry of the Universe (BAU) [13–18]. However, in the presence of strong gauge fields, light fermions charged under the gauge group are produced by the backreaction of gauge fields that source the fermion equations of motion (EoM) [19, 20]. The corresponding currents can then, in turn, backreact on the produced gauge fields, a phenomenon called *Schwinger effect* (see e.g. Ref. [21]). The backreaction of fermion currents on the produced gauge fields acts as a damping force in the explosive production of helical gauge fields, and many of the conclusions from the gauge field production should be revised in the presence of the Schwinger effect[2], in particular those concerning the preheating capabilities and the baryogenesis mechanism.

In this paper, we will study the effect of the Schwinger particle production on the helical hypermagnetic fields produced at the end of inflation, and in particular its influence on the gauge preheating efficiency and baryogenesis capability. In order to consider the backreaction of the produced gauge fields on the inflationary equations of motion and that of the Schwinger effect on the gauge field production, we will use numerical methods, in particular, the fourth order Runge-Kutta (`RK4`) algorithm. Our numerical results are validated as they overlap with some recent semianalytical methods and the gradient expansion formalism of Refs. [22–25]. Our general finding is that the gauge field production is much less explosive than in the absence of the Schwinger effect, which will jeopardize the conclusions concerning the possibility of gauge preheating, although they leave an open window for baryogenesis.

The contents of this paper are as follows. In Sec. 2 we present the general lines of the model and the methods we will consider, including the relevant equations of motion in momentum space and

[1] With an (obvious) abuse of language, we are identifying in this paper axions with axionlike (or pseudoscalar) particles, which allow a wider choice for inflationary potentials [5, 6].

[2] One possible way out is if there are no light charged fields when gauge fields are produced, a condition that is not fulfilled here.

the observable quantities we will compute. In Sec. 3 we will present numerical results for the gauge sector assuming the slow roll conditions in the inflaton equations of motion. In order to check the validity of our approach, numerical results will be compared with some estimates from the literature, namely the backreactionless solution, the Schwinger equilibrium and maximal estimates as well as the gradient expansion formalism where dynamical results are obtained analytically and numerically in configuration space. Some details about the numerical methods will be explained in App. A. In Sec. 4 we will perform the full numerical calculation for two kinds of models that predict cosmological observables in agreement with the observed values: the α-attractor models and the quartic hilltop models. In all cases the gauge preheating efficiency does not seem good enough to ensure complete reheating, which has to be completed by other perturbative or nonperturbative mechanisms. Moreover we have reanalyzed the baryogenesis predictions in the presence of the Schwinger effect and found a sizable window where the BAU is correctly predicted. Again, some details about the numerical methods we used are described in App. B. Finally, our conclusions are presented in Sec. 5.

2 The model

The model action is given by

$$S = \int d^4x \left[\sqrt{-g}\left(\frac{1}{2}\partial_\mu\phi\partial^\mu\phi - \frac{1}{4}Y_{\mu\nu}Y^{\mu\nu} - V(\phi)\right) - \frac{\phi}{4f_\phi}\, Y_{\mu\nu}\tilde{Y}^{\mu\nu}\right] + \int d^4x\, \sqrt{-g}\, i\,\bar{\psi}\not{\mathcal{D}}\psi, \tag{2.1}$$

where ϕ is the pseudoscalar inflaton, V the inflaton potential, and f_ϕ provides the inverse coupling of the inflaton to the Chern-Simons term. $Y^{\mu\nu}$ is the field strength of the hypercharge gauge field Y^μ and $\widetilde{Y}^{\mu\nu} = \frac{1}{2}\epsilon^{\mu\nu\rho\sigma}Y_{\rho\sigma}$ its dual tensor. We also have included the interaction of fermionic currents, corresponding to hypercharge Q_Y fermions, with the hypercharge fields (encoded in the covariant derivative $\mathcal{D}_\mu \equiv \partial_\mu - g'Q_Y A_\mu$). All gauge field quantities are $U(1)$ hypercharge fields, i.e. $\boldsymbol{A}_Y$, $\boldsymbol{E}_Y$, $\boldsymbol{B}_Y$, etc. To make the notation lighter, we drop the index Y as there will be no ordinary electromagnetic fields in this work.

2.1 Equations of motion

Variation of the action with respect to ϕ and the hypercharge gauge field $A_\mu = (A_0, \boldsymbol{A})$ leads to the gauge equations of motion in the radiation gauge, $A_0 = 0$ and $\boldsymbol{\nabla}\cdot\boldsymbol{A} = 0$,

$$\ddot{\phi} + 3H\dot{\phi} + V'(\phi) = \frac{\boldsymbol{E}\cdot\boldsymbol{B}}{a^4 f_\phi}, \tag{2.2a}$$

$$\left(\frac{\partial^2}{\partial\tau^2} - \nabla^2 - \frac{a\,\dot{\phi}}{f_\phi}\,\boldsymbol{\nabla}\times\right)\boldsymbol{A} = \boldsymbol{J}, \tag{2.2b}$$

where we have used $Y_{\mu\nu}\tilde{Y}^{\mu\nu} = -4\,\boldsymbol{E}\cdot\boldsymbol{B}$ and $J^\mu = (\rho_c, \boldsymbol{J}) = ig'Q_Y\bar{\psi}\gamma^\mu\psi$. We assume that initially the Universe does not contain any asymmetry of charged particles and that these ones are produced only later in particle-antiparticle pairs. Therefore, we set the charge density to zero, $\rho_c = 0$. Finally, the current $\boldsymbol{J}$ is given by the Ohm's law

$$\boldsymbol{J} = \sigma\boldsymbol{E} = -\sigma\frac{\partial\boldsymbol{A}}{\partial\tau}, \tag{2.3}$$

where σ is the generalized conductivity, which will be defined later.

As it can be seen from the above system, we use cosmic time t for the inflaton dependence and the conformal time τ, defined by $g_{\mu\nu} = a^2(\tau)\,\eta_{\mu\nu}$, for the gauge field dependence. We denote the

derivative with respect to conformal time τ with a prime and the derivative with respect to the cosmic time t with a dot, e.g. $a' = da/d\tau$ and $\dot{a} = da/dt$. The Hubble parameter is defined as $H = \dot{a}(t)/a(t)$ where a is the scale factor. We assume a homogeneous inflaton with only zero mode, $\phi(t, \boldsymbol{x}) = \phi(t)$.

We now quantize the gauge field $\boldsymbol{A}$ in momentum space

$$\boldsymbol{A}(\tau, \boldsymbol{x}) = \sum_{\lambda=\pm} \int \frac{d^3k}{(2\pi)^3} \left[\boldsymbol{\epsilon}_\lambda(\boldsymbol{k})\, a_\lambda(\boldsymbol{k})\, A_\lambda(\tau, \boldsymbol{k})\, e^{i\boldsymbol{k}\cdot\boldsymbol{x}} + \text{h.c.}\right], \tag{2.4}$$

where λ is the photon polarization, and $a_\lambda(\boldsymbol{k})$ ($a^\dagger_\lambda(\boldsymbol{k})$) are annihilation (creation) operators that fulfill the canonical commutation relations

$$[a_\lambda(\boldsymbol{k}), a^\dagger_{\lambda'}(\boldsymbol{k'})] = (2\pi)^3 \delta_{\lambda\lambda'} \delta^{(3)}(\boldsymbol{k} - \boldsymbol{k'}). \tag{2.5}$$

The polarization vectors $\boldsymbol{\epsilon}_\lambda(\boldsymbol{k})$ satisfy the conditions[3]

$$\begin{aligned} \boldsymbol{k}\cdot\boldsymbol{\epsilon}_\lambda(\boldsymbol{k}) &= 0\,, & \boldsymbol{k}\times\boldsymbol{\epsilon}_\lambda(\boldsymbol{k}) &= -i\lambda k\, \boldsymbol{\epsilon}_\lambda(\boldsymbol{k})\,, \\ \boldsymbol{\epsilon}^*_{\lambda'}(\boldsymbol{k})\cdot\boldsymbol{\epsilon}_\lambda(\boldsymbol{k}) &= \delta_{\lambda\lambda'}\,, & \boldsymbol{\epsilon}^*_\lambda(\boldsymbol{k}) &= \boldsymbol{\epsilon}_\lambda(-\boldsymbol{k})\,, \end{aligned} \tag{2.6}$$

where $k \equiv |\boldsymbol{k}|$. Therefore, the equation of motion for the gauge modes yields

$$A''_\lambda + \sigma A'_\lambda + k\left(k - \lambda\frac{a\,\dot{\phi}}{f_\phi}\right) A_\lambda = 0\,. \tag{2.7}$$

In some special cases ($\sigma = 0$ and slow-roll inflation), this equation can be solved analytically, and we will do it in Sec. 3.1. In the general case, we will solve it using numerical methods.

2.2 Observable quantities

Once we obtain a solution to the modes A_λ, we can compute the (hyper)electromagnetic energy densities as

$$\rho_E \equiv \frac{1}{a^4}\int_{k_{\rm min}}^{k_c} dk\, \frac{k^2}{4\pi^2}\left(|A'_+|^2 + |A'_-|^2\right), \tag{2.8a}$$

$$\rho_B \equiv \frac{1}{a^4}\int_{k_{\rm min}}^{k_c} dk\, \frac{k^4}{4\pi^2}\left(|A_+|^2 + |A_-|^2\right). \tag{2.8b}$$

The upper integration limit comes because subhorizon modes have an oscillatory behavior and should be regarded as quantum fluctuations. Therefore, such modes do not contribute to the above classical observables and are excluded from the integration. More details and precise value of k_c will be given in Sec. 2.3. For the lower integration limit $k_{\rm min}$, see Eq. (A.5).

In this work, we will also make use of the (hyper)magnetic helicity and its derivative, defined as

$$\mathcal{H} \equiv \lim_{V\to\infty}\frac{1}{V}\int_V d^3x\, \frac{\langle \boldsymbol{A}\cdot\boldsymbol{B}\rangle}{a^3} = \frac{1}{a^3}\int_{k_{\rm min}}^{k_c} dk\, \frac{k^3}{2\pi^2}\left(|A_+|^2 - |A_-|^2\right), \tag{2.9a}$$

$$\mathcal{G} \equiv \frac{1}{2a}\frac{d\mathcal{H}}{d\tau} = -\lim_{V\to\infty}\frac{1}{V}\int_V d^3x\, \frac{\langle \boldsymbol{E}\cdot\boldsymbol{B}\rangle}{a^4}. \tag{2.9b}$$

[3] A simple realization can be given in terms of a real basis with the orthonormal vectors $(\boldsymbol{k}/|\boldsymbol{k}|, \boldsymbol{e}_i)$, $(i = 1, 2)$, such that $\boldsymbol{k}\cdot\boldsymbol{e}_i = \boldsymbol{e}_1\cdot\boldsymbol{e}_2 = 0$ and $\boldsymbol{e}_i\cdot\boldsymbol{e}_i = 1$, with $\boldsymbol{\epsilon}_\lambda \equiv (\boldsymbol{e}_1 + i\lambda\boldsymbol{e}_2)/\sqrt{2}$, from where identities (2.6) follow.

In the case of one Dirac fermion with mass m and hypercharge Q_Y, the conductivity can be written as[4] [19]

$$\sigma = \frac{|g' Q_Y|^3}{6\pi^2} \frac{a}{H} \sqrt{2\rho_B} \coth\left(\pi \sqrt{\frac{\rho_B}{\rho_E}}\right) \exp\left\{-\frac{\pi m^2}{\sqrt{2\rho_E}\,|g' Q_Y|}\right\}, \tag{2.10}$$

where $g' \simeq 0.4$ is computed at the characteristic scale $\mu \simeq (\langle \boldsymbol{E} \rangle^2 + \langle \boldsymbol{B} \rangle^2)^{1/4}$ where the Schwinger effect takes place [24]. This estimation is valid in the case of collinear electric and magnetic fields, an assumption that we have numerically checked by verifying that

$$\cos\theta \equiv \frac{|\mathcal{G}|}{2\sqrt{\rho_E \rho_B}} \simeq 1, \tag{2.11}$$

where θ is the spatial angle between $\boldsymbol{E}$ and $\boldsymbol{B}$.

Moreover, the massless hypercharged fermions that are continuously produced during inflation have an energy density given by

$$\rho_\psi = \lim_{V\to\infty} \frac{\sigma}{V} \int_V d^3x \, \frac{\langle \boldsymbol{A}\cdot\boldsymbol{E}\rangle}{a^4} = \frac{\sigma}{a^4} \int_{k_{\rm min}}^{k_c} dk \, \frac{k^2}{2\pi^2} \frac{d}{d\tau} \left(|A_+|^2 + |A_-|^2\right) \tag{2.12}$$

Notice that the observable quantities ρ_E, ρ_B, ρ_ψ, $\mathcal{H}$ and $\mathcal{G}$ are physical[5], while the fields $\boldsymbol{A}$, $\boldsymbol{E}$ and $\boldsymbol{B}$ as well as the conductivity σ and current $\boldsymbol{J}$ are comoving.

Concerning the Higgs vacuum expectation value, there are two possibilities during the inflationary period:

i) The first possibility, which we will consider throughout this paper, is that $\langle h \rangle = 0$, and so the electroweak symmetry is unbroken during the inflationary period. In order to ensure unbroken electroweak symmetry and hence massless SM fermions, which all contribute to the conductivity (2.10), we assume that the SM Higgs field h remains stabilized at the origin in field space by a large mass term throughout the inflationary period. Such a large mass can, e.g., be induced by a nonminimal coupling to the Ricci curvature scalar as $\mathcal{L} = \frac{1}{2}\xi h^2 R$ with $\xi > 3/16$ (see e.g. Ref. [26]). Hence, we get

$$\sigma \simeq \frac{41\, g'^3}{72\,\pi^2} \frac{a}{H} \sqrt{2\rho_B} \coth\left(\pi \sqrt{\frac{\rho_B}{\rho_E}}\right). \tag{2.13}$$

ii) The second possibility is that the electroweak symmetry is broken during the inflationary period. In this case after ΔN e-folds of inflation, there is a Gaussian distribution of values of the Higgs field with zero mean and variance $\langle h^2 \rangle = H^2 \Delta N/(4\pi^2)$ with probability $P(h, \Delta N) \propto \exp(-\frac{1}{2}\frac{h^2}{\langle h^2\rangle})$ dominated by the values $h \lesssim \sqrt{\langle h^2 \rangle}$, see Ref. [26][6]. In this case, the electroweak symmetry is broken and the hypercharge field strength $Y_{\mu\nu}$ in Eq. (2.1) is projected onto the electromagnetic field strength $F_{\mu\nu}$ with a coupling to the inflaton given by $f_\phi/\cos^2\theta_W$ where θ_W

[4] As the conductivity σ relates $\boldsymbol{J}$ and $\boldsymbol{E}$ in (2.3), it is a comoving quantity, i.e. it scales with the Universe expansion. Our definition differs from the one in [23, 24] where the authors used a physical conductivity that we will denote $\hat{\sigma}$ in this paper, their relation being $\sigma = a\,\hat{\sigma}$.

[5] They relate to the comoving ones ρ_E^c, ρ_B^c, $\mathcal{H}^c$, and $\mathcal{G}^c$ by the relations $\rho_{B,E}^c = a^4 \rho_{B,E}$, $\mathcal{H}^c = a^3\mathcal{H}$, $\mathcal{G}^c = a^4\mathcal{G}$.

[6] The SM Higgs potential is still unstable at a value of the Higgs field $h = h_I \simeq 10^{11}$ GeV and the condition for $P(h_I, \Delta N) < e^{-3\Delta N}$ (so that it is unlikely to find the Higgs away from its EW vacuum in any of the $e^{3\Delta N}$ causally disconnected regions formed during inflation) implies $H_E < \sqrt{2/3}\,\pi h_I/\Delta N$, a condition that is not fulfilled by any of the models of inflation we have considered. Therefore this possibility would require stabilization of the Higgs potential by some new physics.

is the electroweak angle. Now the conductivity for the hypermagnetic field in Eq. (2.10) should be replaced by a similar expression for the magnetic field, with the replacement $|g'Q_Y| \to |eQ|$, where $e = gg'/\sqrt{g^2+g'^2}$ and Q is the fermion electric charge. The condition for a fermion f to contribute to the magnetic conductivity $\pi m_f^2 < \sqrt{2\rho_E}\,|eQ_f|$ translates into the condition, for the fermion Yukawa coupling,

$$Y_f \lesssim 0.45 \left(\frac{\rho_E}{H^4}\right)^{1/4} \sqrt{|Q_f|}, \tag{2.14}$$

and we have computed all couplings at the characteristic scale $\mu \simeq (\langle \boldsymbol{E}\rangle^2 + \langle \boldsymbol{B}\rangle^2)^{1/4}$ where the Schwinger effect takes place. If the three generations of fermions satisfy the above condition then the conductivity for the magnetic field is given by Eq. (2.13) with the replacement $\frac{41g'^3}{72\pi^2} \to \frac{e^3}{\pi^2}$. We have checked that, in this case, the results for $f_\phi \lesssim 0.2\,M_{\rm pl}$ are consistent with all three generation fermions contributing to the magnetic conductivity. For $f_\phi \gtrsim 0.2\,M_{\rm pl}$ only the top quark does not contribute. Given that $41g'^3/72 \simeq 0.37$ while $e^3 \simeq 0.36$, at the scales where the Schwinger effect takes place, we have found that the results in this second case are qualitatively similar to those for the previous case, which will be worked out in detail in this paper.

Considering then the case *i)* above, the conductivity (2.13) yields a nontrivial integro-differential system as the damping term grows with the magnetic energy and hence backreacts on the amount of produced electric/magnetic fields. We aim to solve this setup of the Schwinger effect numerically. In the next sections we will consider specific cases where this system can be further simplified.

2.3 The gauge vacuum

At very early times, when $|a\dot{\phi}| \ll k f_\phi$, the modes are in their Bunch-Davies (BD) vacuum, hence

$$A_\lambda(\tau,k) = \frac{1}{\sqrt{2k}}\,\mathrm{e}^{-ik\tau} \qquad\qquad (\tau \to -\infty). \tag{2.15}$$

Initially, we can consider all the modes in the BD vacuum (which would be possible by initializing the numerical simulation such that $a_0 \ll k_0/H_0$). In that case, since $|A_+| = |A_-|$, the fields $\boldsymbol{E}$ and $\boldsymbol{B}$ are plane waves perpendicular to each other, as $\mathcal{G} = 0$ in (2.11) yields $\cos\theta = 0$. Therefore, there is no Schwinger effect and $\sigma = 0$.

It has recently been shown that in the presence of the conductivity σ, the BD vacuum amplitude of the modes that are still in the vacuum get damped by the ones that left it [23]. Indeed, consider we are at a time a_* where modes $k > k_*$ are still in the BD vacuum, while modes $k < k_*$ were amplified by both tachyonic and parametric instabilities from Eq. (2.7). Then, the equation of motion for modes such that $|a_*\dot{\phi}(\tau_*)| \ll k f_\phi$ does not reduce to a plane wave in the presence of a non-zero σ, but instead to $A_\lambda'' + \sigma A_\lambda' + k^2 A_\lambda = 0$, and Eq. (2.15) is not a solution anymore. To derive the generalized BD vacuum, we write the gauge equation of motion (2.7) in cosmic time:

$$\ddot{A}_\lambda + (\hat{\sigma} + H)\,\dot{A}_\lambda + \frac{k}{a}\left(\frac{k}{a} - \lambda\frac{\dot{\phi}}{f_\phi}\right) A_\lambda = 0, \tag{2.16}$$

where we used the identity $a^{-2}A_\lambda'' = \ddot{A}_\lambda + H\dot{A}_\lambda$, and perform the transformation $A_\lambda = \sqrt{\Delta}\,\mathcal{A}_\lambda$ with [23]

$$\Delta(t) = \exp\left\{-\int_{-\infty}^{t} \hat{\sigma}(t')\,dt'\right\}. \tag{2.17}$$

We recall that we have defined $\hat{\sigma} = \sigma/a$ as the physical conductivity in footnote 4. The above equation hence becomes

$$\mathcal{A}_\lambda'' + \left[\frac{k}{a}\left(\frac{k}{a} - \lambda\frac{\dot{\phi}}{f_\phi}\right) - \frac{\dot{\hat{\sigma}}}{2} - \frac{\hat{\sigma}^2}{4} - \frac{H\hat{\sigma}}{2}\right] a^2\mathcal{A} = 0, \tag{2.18}$$

where we used the fact that $\dot{\Delta}(t) = -\hat{\sigma}(t)\Delta(t)$. A mode crosses the horizon when the expression in the square brackets vanishes for the first time at least for one polarization, at $k = k_c$. The modes in the vacuum are then characterized by $k \gg k_c$. This yields the momentum of the mode that crosses the horizon at time t, namely the cutoff of the integrals:

$$k_c = \left|\frac{a\dot{\phi}}{2f_\phi}\right| + \sqrt{\left(\frac{a\dot{\phi}}{2f_\phi}\right)^2 + \frac{a^2}{2}\left[\dot{\hat{\sigma}} + \hat{\sigma}\left(\frac{\hat{\sigma}}{2} + H\right)\right]}. \tag{2.19}$$

Deep inside the horizon, when the first term in square brackets of (2.18) dominates, the solution must satisfy the BD condition (2.15). As we have seen, in the presence of finite conductivity, this equation does not fully describe the gauge-field mode function inside the horizon, as the damped BD condition includes an exponential damping factor

$$A_\lambda(\tau, k) = \sqrt{\frac{\Delta(t)}{2k}} e^{-ik\tau} \qquad (\tau \to -\infty). \tag{2.20}$$

The bottom line of this section is that the modes still in their BD vacuum see their amplitudes damped because of the effect of the modes that left their vacuum earlier and participate in the equations of motion (2.2a) and (2.7). The parameter Δ was first introduced in the context of the gradient expansion formalism in Ref. [23], where it was dynamically solved, while in Ref. [24] it was also considered as a free parameter and validated the corresponding procedure by numerical calculations. In order to compare with results from the gradient expansion formalism in configuration space, we will also both compute Δ numerically and consider it as a free parameter, although our final results will be based upon the dynamical calculation of Δ.

3 Slow Roll Analysis

The slow-roll inflation paradigm has been used by many authors to compute the amount of electromagnetic energy density [7, 27, 28], or baryogenesis through helicity [8, 9, 16, 18] at the end of inflation, with or without taking into account the Schwinger effect. Here we aim to validate our numerical results by comparison with the known analytical results at the end of inflation.

In this section we will take ϕ as a slowly rolling inflaton field such that $\ddot{\phi} \simeq 0$, $3H\dot{\phi} \simeq -V'(\phi)$, and so we can consider $\dot{\phi}$ and $H = H_E$ as constant. Doing so, we are neglecting the gauge field backreaction in the right-hand side of Eq. (2.2a), a hypothesis that we have consistently checked *a posteriori*. The results of this section will be model independent, within the hypothesis of the slow roll approximation.

3.1 Absence of Schwinger effect

Here we are assuming there is no Schwinger effect[7], i.e. $\sigma = 0$, hence we can rewrite (2.7) as

$$A_\lambda'' + k\left(k + \lambda\frac{2\xi}{\tau}\right) A_\lambda = 0, \tag{3.1}$$

[7]This condition should be considered as being fulfilled by some physical systems, as e.g. systems with no massless fermions, more than as an approximation to the full (more realistic) case.

where, following the slow roll equations,

$$\xi = -\frac{\dot{\phi}}{2H_E f_\phi} \tag{3.2}$$

is a constant. Since we are in de Sitter space, we can use the scale factor definition $a = -(H\tau)^{-1}$ and solve (3.1) asymptotically. At early time, when $|k\tau| \gg 2\xi$, the modes are in their BD vacuum given by (2.15), as here $\Delta = 1$. When $|k\tau| \sim 2\xi$, one of the modes develops both parametric and tachyonic instabilities leading to exponential growth while the other stays in the vacuum. During the last e-folds of inflation, i.e. $|k\tau| \ll 2\xi$, the growing mode has the solution [8, 27]

$$A_\lambda \simeq \frac{1}{\sqrt{2k}} \left(\frac{k}{2\xi a_E H_E}\right)^{\frac{1}{4}} \exp\left\{\pi\xi - 2\sqrt{\frac{2\xi k}{a_E H_E}}\right\}, \tag{3.3}$$

where a_E and H_E are, respectively, the scale factor and the Hubble parameter at the end of inflation. Here, as we assume a slow roll regime, we consider H_E constant and we take the convention $a_E = 1$.

Using (2.8) and (2.9) we can compute all electromagnetic quantities:

$$\rho_E \simeq \frac{63}{2^{16}} \frac{H_E^4}{\pi^2\xi^3} \mathrm{e}^{2\pi\xi}, \quad \rho_B \simeq \frac{315}{2^{18}} \frac{H_E^4}{\pi^2\xi^5} \mathrm{e}^{2\pi\xi}, \quad \mathcal{H} \simeq \frac{45}{2^{15}} \frac{H_E^3}{\pi^2\xi^4} \mathrm{e}^{2\pi\xi}, \quad \mathcal{G} \simeq \frac{135}{2^{16}} \frac{H_E^4}{\pi^2\xi^4} \mathrm{e}^{2\pi\xi}. \tag{3.4}$$

These results are only valid when the absence of backreaction on the inflaton equation of motion (2.2a) is guaranteed, hence when $|\mathcal{G}/V'(\phi)| \ll f_\phi$. This model-dependent condition puts a lower bound on the parameter f_ϕ or, equivalently, a higher bound on ξ. Using the slow roll equations and the definition of the slow roll parameters, this parameter can be written as

$$\xi = \frac{M_{\rm pl}}{f_\phi}\sqrt{\frac{\epsilon}{2}}, \tag{3.5}$$

where $\epsilon = (M_{\rm pl}^2/2)\,(V'/V)^2$. Therefore, at the end of inflation, where by definition $\epsilon = 1$, one has $\xi = M_{\rm pl}/\sqrt{2}f_\phi$, and the no backreaction condition in Eq. (2.2) provides the bound $\xi < 5.73$ (or equivalently $f_\phi > 0.12\,M_{\rm pl}$). In Fig. 1 we show, with orange lines, the quantities ρ_E, ρ_B, $\mathcal{H}$ and $\mathcal{G}$ evaluated at the end of inflation obtained from the analytical backreactionless solutions from Eqs. (3.4), while the blue dots are the numerical solutions, which correspond to the case $\sigma = 0$ (no Schwinger effect) and correspondingly $\Delta = 1$. We have used a Runge-Kutta method which is explained in App. A.

3.2 Presence of Schwinger effect

The Schwinger effect is taken into account by means of the conductivity σ in Eq. (2.7), as given by Eq. (2.10) [19]. The growth of σ with time then backreacts on the gauge field, as the damping term grows in its differential equation. We will compare our numerical calculations with three analytical (or semianalytical) results: the Schwinger maximal and equilibrium estimates [19, 24], as well as the gradient expansion formalism [22–24]. From the numerical point of view however, we aim to solve Eq. (2.7) with σ computed at each time step using (2.13). The details about the numerics will be displayed in Sec. 3.3.

Schwinger equilibrium estimate

In this case, the backreaction of the chiral fermions on the gauge fields is taken into account by just replacing the parameter ξ with the effective one [19]

$$\xi_{\rm eff} = \xi - \frac{41\,g'^3}{144\,\pi^2} \coth\left(\pi\sqrt{\frac{\rho_B}{\rho_E}}\right) \frac{\sqrt{2\rho_E}}{H_E^2}\,, \tag{3.6}$$

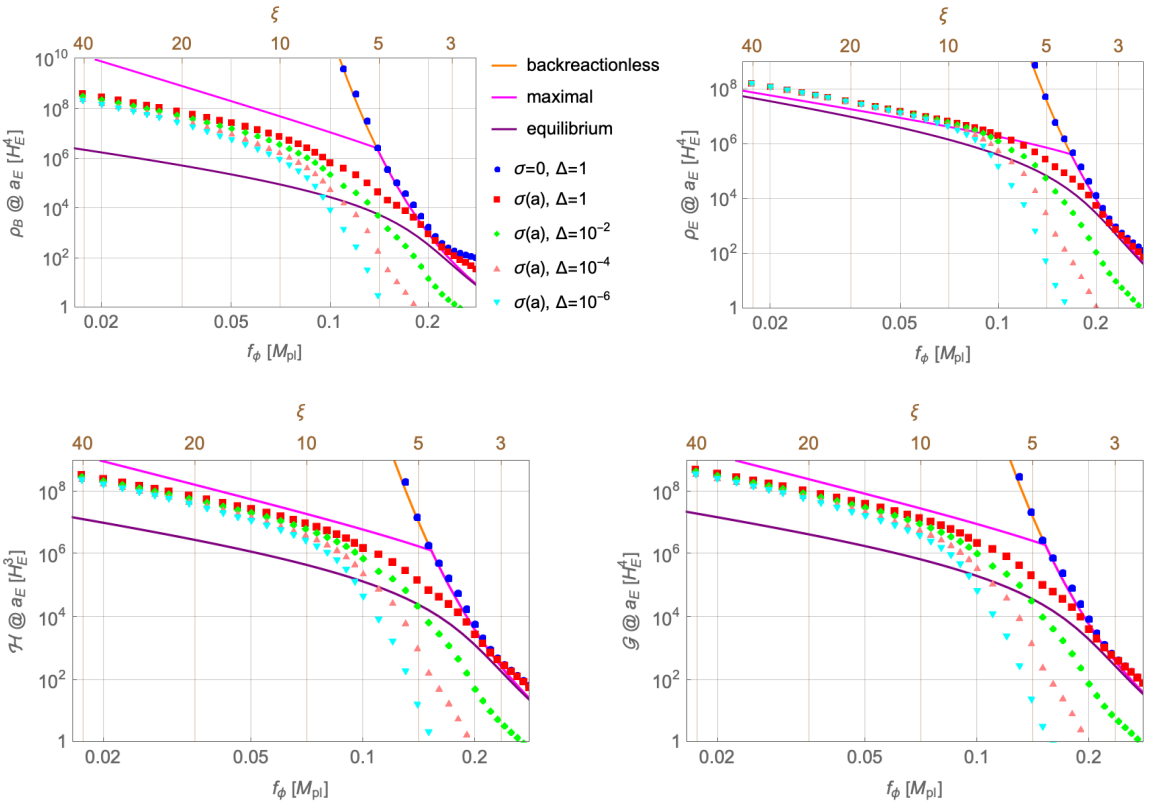

Figure 1: *Electric ρ_E and magnetic ρ_B energy densities, and the helicity $\mathcal{H}$ and its derivative $\mathcal{G}$, at the end of inflation (i.e. for $\epsilon(a_E) = 1$), in units of H_E, as functions of the coupling f_ϕ assuming Δ constant. We see the plots confirm the result from Fig. 1 of [24]. Here, we also assumed ξ constant.*

in the backreactionless solutions (3.4). This amounts to solving

$$\frac{63}{2^{15}\pi^2}\,\frac{\mathrm{e}^{2\pi\xi_{\rm eq}}}{\xi_{\rm eq}^3} = \left(\frac{144\,\pi^2}{41\,g'^3}\right)^2 (\xi-\xi_{\rm eq})^2\,\tanh^2\left(\sqrt{\frac{5}{4}}\,\frac{\pi}{\xi_{\rm eq}}\right), \tag{3.7}$$

which provides the function $\xi_{\rm eq} = \xi_{\rm eq}(\xi)$ that we plug in (3.4) instead of the bare ξ to obtain the quantities $\rho^E_{\rm eq}$, $\rho^B_{\rm eq}$, $\mathcal{H}_{\rm eq}$ and $\mathcal{G}_{\rm eq}$. These equilibrium estimates are shown with a purple line in the plots of Fig. 1.

Schwinger maximal estimate

In this case, we assume the exponential behaviors of the backreactionless solutions to be valid until they saturate the maximal value that we will display hereafter. We numerically determine the value of crossing, which happens for $\xi \simeq 4.4$-4.7 depending on each quantity.

The maximum helicity density can be estimated as the solution of [19]

$$|E|^2 + |B|^2 = \xi_{\rm eff}|E|\,|B|. \tag{3.8}$$

This replacement yields an equation relating the $|E|$ and $|B|$ fields that can be solved analytically. We then choose, as definition of our maximal estimate, the solution $(|E|, |B|)$ of (3.8) that maximizes the

product $|E|\cdot|B|$ [8]. This yields for $\xi \gg 1$

$$\rho^E_{\rm max} \simeq \frac{8}{9}\left(\frac{72\,\pi^2}{41\,g'^3}\right)^2 \xi^2 H_E^4, \tag{3.9a}$$

$$\rho^B_{\rm max} \simeq \frac{8}{81}\left(\frac{72\,\pi^2}{41\,g'^3}\right)^2 \xi^4 H_E^4, \tag{3.9b}$$

$$\mathcal{H}_{\rm max} = \frac{2\,\mathcal{G}_{\rm max}}{3H_E} \simeq \frac{32}{81}\left(\frac{72\,\pi^2}{41\,g'^3}\right)^2 \xi^3 H_E^3. \tag{3.9c}$$

The maximal estimates for the quantities $\rho^E_{\rm max}$, $\rho^B_{\rm max}$, $\mathcal{H}_{\rm max}$ and $\mathcal{G}_{\rm max}$ are shown with a pink line in the plots of Fig. 1.

Gradient expansion formalism

This method was introduced in Refs. [22–24] and transforms the EoM for the vector field $\boldsymbol{A}$ into EoM for observable quantities, in particular the electric $\boldsymbol{E}$ and magnetic $\boldsymbol{B}$ fields. As the spatial gradients in the EoM do always appear as $\mathrm{rot}\,\boldsymbol{E}$ and $\mathrm{rot}\,\boldsymbol{B}$, the EoM can be written as an infinite series in terms of the bilinears $\mathcal{E}^{(n)} = \langle \boldsymbol{E}\cdot\mathrm{rot}^n\boldsymbol{E}\rangle/a^n$, $\mathcal{G}^{(n)} = \langle \boldsymbol{E}\cdot\mathrm{rot}^n\boldsymbol{B}\rangle/a^n$ and $\mathcal{B}^{(n)} = \langle \boldsymbol{B}\cdot\mathrm{rot}^n\boldsymbol{B}\rangle/a^n$, with $n = 0, 1, \ldots$. In this way the coupled system of EoM for the fields $\boldsymbol{E}$ and $\boldsymbol{B}$ transforms into a system of coupled differential equations for the quantities $\mathcal{E}^{(n)}$, $\mathcal{B}^{(n)}$ and $\mathcal{G}^{(n)}$. This system is not block diagonal in the space of the n index so that the system has to be truncated to find solutions.

Moreover, the parameter $\Delta(t)$ in Eq. (2.17), which suppresses the gauge-field amplitude on small scales depends on the conductivity at all times $t' < t$. So, a precise determination of $\Delta(t)$ would require a complete analytical solution of the infinite-dimensional system of equations. While Δ was dynamically computed in Ref. [23], for the sake of simplicity and generality, it was considered as a free parameter in Ref. [24] and fixed to the values $\Delta = 1$, 10^{-2}, 10^{-4}, 10^{-6}. In our numerical approach we will consider Δ as a function of the conductivity σ, as the initial condition for $\boldsymbol{E}$ and $\boldsymbol{B}$ are plane waves, such that $\boldsymbol{E}\cdot\boldsymbol{B} = 0$ and therefore initially $\sigma = 0$ and so $\Delta = 1$. However, as time is evolving $\boldsymbol{E}$ and $\boldsymbol{B}$ will become collinear, and a nonvanishing conductivity will appear, as well as the function $\Delta(t) < 1$. In order to compare our numerical results with those from Ref. [24], we also will eventually enforce Δ to be a constant in our code. Upon considering a constant value of Δ, our results will agree pretty well with those obtained in the gradient expansion formalism, see Fig. 1. In the more realistic cases where we just compute the value of $\Delta(t)$, we will see that at the beginning $t = t_0$, just very deep inside the inflationary period, $\Delta(t_0) = 1$, while the value of Δ will decrease very fast and at the end of inflation $t = t_E$, $\Delta(t_E) \ll 1$.

3.3 Numerical results at the end of inflation

We will find it more convenient to change the variable from the time t to the scale factor a. The gauge field equation of motion (2.7) then becomes

$$\frac{\partial^2 A_\lambda}{\partial a^2} + \frac{1}{a}\left(2 + \frac{\sigma}{aH_E}\right)\frac{\partial A_\lambda}{\partial a} + \frac{k}{a^3 H_E}\left(\frac{k}{aH_E} - 2\lambda\xi\right)A_\lambda = 0. \tag{3.10}$$

We recall that, as we are considering the slow roll regime in this section, we do not need to solve the equation of motion for ϕ.

[8] Notice that our definition of maximal solution departs from that given in Refs. [19, 24], where the fields $|E|$ and $|B|$ are separately maximized, while we are maximizing the product $|E|\cdot|B|$, the relevant quantity for the baryon asymmetry generation.

The Bunch-Davis solutions can now be written as

$$A_\lambda(a,k) = \sqrt{\frac{\Delta(a)}{2k}}\, \mathrm{e}^{ik/aH_E}$$
$$\frac{\partial A_\lambda}{\partial a}(a,k) = \frac{\sqrt{\Delta(a)}}{a^2 H_E}\left(-i\sqrt{\frac{k}{2}} - \frac{\sigma}{2}\frac{1}{\sqrt{2k}}\right)\mathrm{e}^{ik/aH_E} \qquad (a \to 0), \tag{3.11}$$

with

$$\Delta(a) = \exp\left\{-\int_{a_0}^{a} \frac{\sigma(a')}{a'^2 H_E} da'\right\}. \tag{3.12}$$

The technical details of the numerical simulations for solving Eq. (3.10), subject to the boundary conditions (3.11), can be found in App. A. We display in Fig. 2 the spectra of all the observable quantities in order to see how the BD vacuum is dominating the spectra for large k and how the cutoff $k_c(a)$, given by (2.19), efficiently removes that part of the integration. The difference between the BD vacuum and the damped BD vacuum is also clear, as the first goes like k^3 whereas the second goes like $\Delta(a)k^3$ with Δ decreasing with time. Hence the asymptotic behaviors are not superimposed since Δ changes. Finally, we also see explicitly how the growth of ρ_E and ρ_B with the scale factor a is due to the increase in amplitude of the spectrum hump and its shift to larger values of k. For this illustrative purpose we used a constant value of ξ. Here we have fixed $f_\phi = 0.1\, M_{\rm pl}$, while for other values of this parameter the plots are similar.

Before moving to the full numerical results, we will compare our slow roll based inflaton numerical results with the recent literature on the subject.

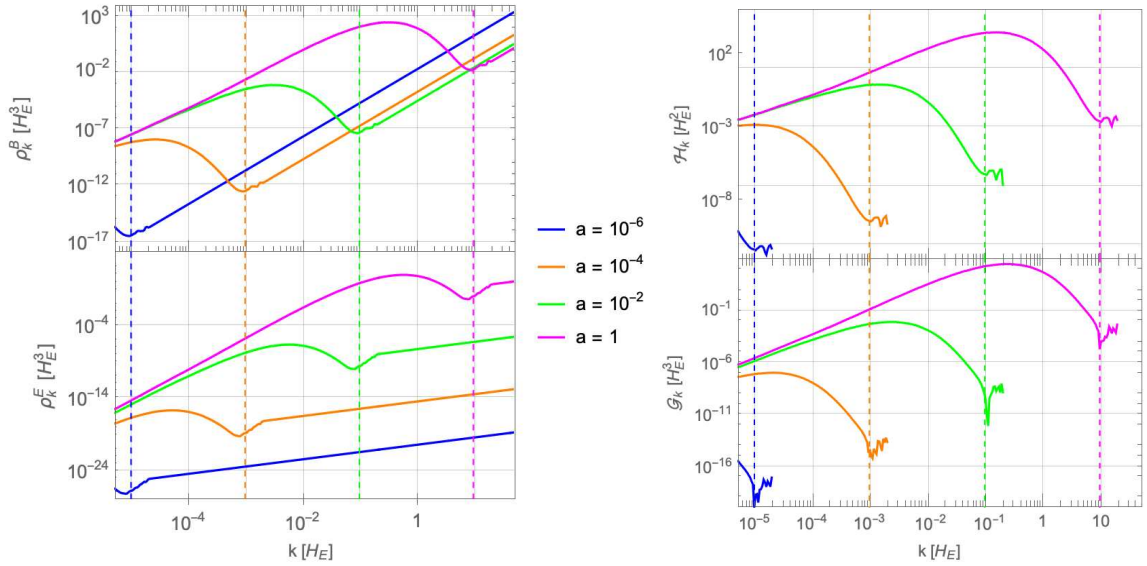

Figure 2: *Spectra of the magnetic energy (top left), electric energy (bottom left), helicity (top right) and its derivative (bottom right), i.e. the integrands of (2.8) and (2.9), for different values of a during inflation simulation. Here we used variable $\sigma(a)$ and $\Delta(a)$ with constant ξ. The color matching dashed vertical lines show the cutoff values $k_c(a)$ computed from (2.19).*

3.3.1 Constant Δ and ξ approximation

We will first assume that the parameters Δ and ξ are constants. As we already mentioned, the parameter Δ was fixed to constant values in Ref. [24] while ξ, as defined in Eq. (3.2), is often considered as a constant in the slow roll approximation. In Fig. 1, we displayed several results already present in the literature that we successfully reproduced with our numerical method. First the backreactionless case, where there is no conductivity, by simply enforcing $\sigma = 0$ (therefore $\Delta = 1$) in the code. The data set are displayed in blue and match the corresponding analytical value given by Eq. (3.4). Then, in order to reproduce results from [24], we considered a non-zero conductivity given by (2.13) while assuming Δ constant during inflation, thus making it a free parameter. In Fig. 1, we plot the quantities ρ_B, ρ_E, $\mathcal{H}$ and $\mathcal{G}$ at the end of inflation for chosen values of Δ. We can see that the results agree well with those using the gradient expansion formalism in Ref. [24].

3.3.2 Variable Δ and ξ

The benefit of the slow roll approximation is that the results look "model independent". However, the tradeoff comes with the need of having a constant parameter ξ as the slow roll regime implies an approximately constant $\dot{\phi}$. Besides, we know that this parameter can also be expressed in terms of the slow roll parameter ϵ (see Eq. (3.5)), which is indeed small and constant during inflation but then quickly becomes unity during the last e-folds. We also know that the modes produced during the last e-folds are the ones that contribute the most to the integrals (2.8) and (2.9), as all the modes previously generated get washed out by the Universe expansion.

All these observations lead us to conclude that the most important contribution to the quantities ρ_E, ρ_B, $\mathcal{H}$ and $\mathcal{G}$ is taking place during an epoch when the constant ξ approximation loses its relevance. Hence, in this section, we will instead specify an inflation model, namely the Starobinsky potential, and make its study in the slow roll regime with a function $\xi(a)$ that can be obtained from the model. We have chosen in this section the Starobinsky potential as it provides a realistic model of inflation, and will be a particular case of a more general class of models we will consider to make predictions using the full solution of the system. The purpose of this section will thus be to assess the goodness of the slow roll approximation when computing the full solution to the system (2.2).

The Starobinsky potential is given by

$$V = \Lambda^4 \left[1 - \exp\left\{-\sqrt{\frac{2}{3}}\frac{|\phi|}{M_{\rm pl}}\right\}\right]^2 . \tag{3.13}$$

Using the slow roll regime, the inflaton field ϕ is given by

$$\sqrt{\frac{2}{3}}\frac{\phi(a)}{M_{\rm pl}} = -\log\left(\frac{a_E}{a}\right)^{\frac{4}{3}} - \mathcal{W}_{-1}\left[-\beta e^{-\beta}\left(\frac{a_E}{a}\right)^{-\frac{4}{3}}\right] - \beta + \log\beta, \quad \beta = 1 + \frac{2}{\sqrt{3}} \tag{3.14}$$

where $\mathcal{W}_n$ is the nth branch of the Lambert function. The value of the function ξ is then given by

$$\xi(a) = \sqrt{\frac{2}{3}}\frac{M_{\rm pl}}{f_\phi}\frac{1}{\exp\left[\sqrt{\frac{2}{3}}\frac{\phi(a)}{M_{\rm pl}}\right] - 1} . \tag{3.15}$$

In Fig. 3, we display in blue results for the Starobinsky model, for various values of ϵ, when σ and Δ vary dynamically. Although the slow roll approximation loses its relevance for values of ϵ closer to 1 (an issue we address in the next section), we already see a difference with the plots in Fig. 1. This is because, no matter the value of the initial time, the function $\Delta(a)$ rapidly goes to extremely small

values, thus killing the BD modes that would have been amplified at the very end of inflation and that would have contributed the most to the integrals (2.8) and (2.9). With a constant Δ, this suppression is less effective and the tachyonic amplification yields higher energy densities and helicity.

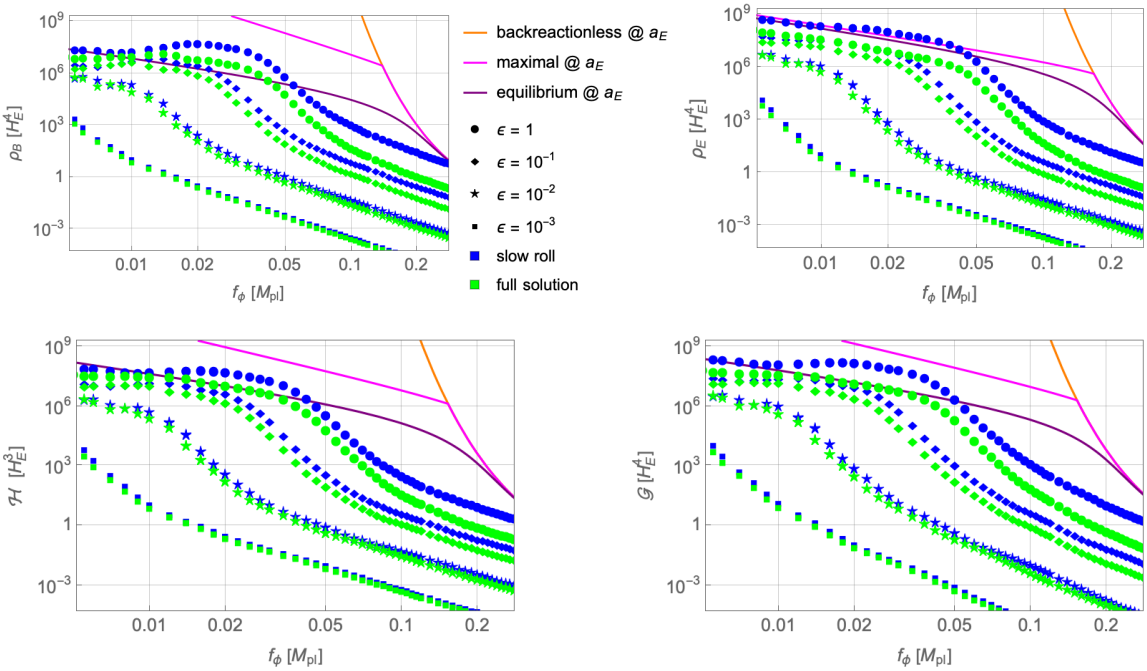

Figure 3: *Comparison between the slow roll approximation and the full solution for the Starobinsky model. The analytical estimates are given for $\epsilon = 1$. As expected, the slow roll computation diverges from the full solution as inflation is nearing the end, since the slow roll approximation is only valid in the regime $\epsilon \ll 1$. Hence the slow roll computation overshoots the value of all quantities, closer to the value given by the Schwinger equilibrium estimate for $f_\phi \lesssim 0.05\, M_{pl}$. As expected, we also have compared both analysis, slow roll and full solution, for values of a such that $\epsilon(a) \ll 1$ (in particular $\epsilon = 10^{-1}, 10^{-2}, 10^{-3}$) and found good agreement.*

4 Full Analysis

In this section, we are not using the slow roll hypothesis for the inflaton equation of motion and consider the full solution to the system (2.2) in specific models of inflation. We will choose a set of inflationary models that are well known to be in agreement with all cosmological constraints. Also, we do not assume any peculiar geometry of the Universe.

The equations to be solved during inflation are the system (2.2) written in terms of the variable a. Unlike in the previous section, the current change of variables must take into account that the Hubble parameter is not constant, but moreover we have $\frac{da}{dt} = \dot{a} = aH$, and we will define the auxiliary quantity $\mathcal{F}$ as

$$\mathcal{F} = -\frac{a}{H}\frac{dH}{da} = -\frac{a}{2H^2}\frac{dH^2}{da}. \tag{4.1}$$

We will relate it to the Friedmann equations

$$H^2 = \frac{\rho}{3M_{\rm pl}^2}, \tag{4.2a}$$

$$\frac{\ddot{a}}{a} = -\frac{3p+\rho}{6M_p^2}, \tag{4.2b}$$

which combine themselves into

$$\frac{a}{2}\frac{dH^2}{da} = \frac{dH}{dt} = \frac{\ddot{a}}{a} - H^2 = -\frac{p+\rho}{2M_p^2}, \tag{4.3}$$

where the total energy density and pressure are

$$\rho = \frac{1}{2}\dot{\phi}^2 + V + \rho_{\rm EM} + \rho_\psi, \tag{4.4a}$$

$$p = \frac{1}{2}\dot{\phi}^2 - V + \frac{\rho_{\rm EM}}{3} + \frac{\rho_\psi}{3}. \tag{4.4b}$$

Hence we have

$$H^2\mathcal{F} = -\frac{a}{2}\frac{dH^2}{da} = \frac{1}{M_{\rm pl}^2}\left(\frac{1}{2}\dot{\phi}^2 + \frac{2}{3}\rho_{\rm EM} + \frac{2}{3}\rho_\psi\right). \tag{4.5}$$

and the system (2.2) becomes

$$\frac{d^2\phi}{da^2} + \frac{4-\mathcal{F}}{a}\frac{d\phi}{da} + \frac{V'(\phi)}{a^2H^2} + \frac{\mathcal{G}}{a^2H^2 f_\phi} = 0 \tag{4.6a}$$

$$\frac{d^2A_\lambda}{da^2} + \frac{1}{a}\left(2-\mathcal{F}+\frac{\sigma}{aH}\right)\frac{dA_\lambda}{da} + \frac{k}{a^2H}\left(\frac{k}{a^2H} - \frac{\lambda}{f_\phi}\frac{d\phi}{da}\right)A_\lambda = 0. \tag{4.6b}$$

The Hubble parameter can be computed from the Friedmann equation (4.2a), where ρ is given by (4.4a). This way, we can compute the value of H and $\mathcal{F}$ at each time step recursively to feed the equations of motion, like we already do for σ and $\mathcal{G}$. The BD vacuum modes are identical to the previous case, see Eqs. (3.11). Finally, for comparison purposes, we can define a generalized time dependent instability parameter $\xi(a)$ as

$$\xi(a) = -\frac{a}{2f_\phi}\frac{d\phi}{da} \tag{4.7}$$

such that it corresponds to the definition (3.2). The simulations show that this parameter, obtained from full solution computation, significantly differs from the slow roll one at the very end of inflation.

4.1 Full numerical results at the end of inflation

In this subsection we will compare our results at the end of inflation, where we are making a full numerical analysis of the EoM, with those obtained using the slow roll approximation for the inflationary potential. For the sake of comparison we will concentrate on the Starobinsky model given by (3.13). In this current framework, we see in Fig. 3 that the four studied quantities, namely ρ_B, ρ_E, $\mathcal{H}$ and $\mathcal{G}$, are much closer to the Schwinger equilibrium estimate at the end of inflation.

We present in Fig. 3 the values of the physical observables evaluated at various stages of inflation, i.e. various values of the scale factor a, from $\epsilon(a) = 10^{-3}$ to $\epsilon(a) = 1$, as a function of the coupling f_ϕ for the Starobinsky model. We superimpose the analytical results from Secs. 3.1 and 3.2, and hence

the backreactionless solution as well as the Schwinger maximal and equilibrium estimates. From the plots we see that for $f_\phi \lesssim 0.05\, M_{\rm pl}$ the equilibrium estimate is a good approximation, especially for ρ_E where the predictions of maximal and equilibrium estimates merge. We also verify that $\cos\theta \simeq 1$ hence satisfying the assumption on parallel electric and magnetic fields leading to the conductivity definition (2.10).

In this setup, our numerical code is computing a value of the conductivity σ and Δ for each time step, hence we got the functions $\sigma(a)$ and $\Delta(a)$. The variation and presence of $\Delta(a)$ is not without effect on the final results. Indeed, the smallest ($k \gg H_E$) modes are the ones that most contribute to the integrals (2.8) and (2.9). Without the Schwinger effect, these modes are produced last, just at the end of inflation, and only briefly leave the horizon. They therefore should have a significant impact on preheating. When the Schwinger effect prevents their generation, by reducing them by a $\ll 1$ factor, while they are still in the BD vacuum, we can ask ourselves about the effectiveness of gauge preheating. It was shown in previous studies of gauge preheating [12] that its efficiency mainly depends on the electromagnetic energy fraction available at the end of inflation $\rho_{\rm EM}/\rho_{\rm tot}$. To shed light on the last point, we will extend, in the next section, our numerical results beyond the end of inflation when the inflaton is coherently oscillationg around its potential minimum. We will do that in a set of particularly interesting phenomenological models that we describe in the next section.

4.2 Inflationary models

We will here introduce two classes of models that all satisfy the cosmological constraints. They should be considered as a sample of possible models, and they are just chosen for illustrative purposes, as they do not exhaust by any means the allowed inflationary models.

4.2.1 α-attractor models

The α-attractor potential is given by [29]

$$V_\alpha(\phi) = \Lambda_\alpha^4 \left[1 - \exp\left\{-\sqrt{\frac{2}{3\alpha}}\frac{|\phi|}{M_{\rm pl}}\right\}\right]^2 . \tag{4.8}$$

Setting $\alpha = 1$ yields the R^2 model or Starobinsky potential (3.13). To make the comparison interesting, we choose to have $1 \leq \alpha \leq 100$, where cosmological observables are correctly reproduced. In the slow roll approximation, the field value at the end of inflation is

$$\phi_E = \sqrt{\frac{3\alpha}{2}}\, M_{\rm pl}\, \log\left(1 + \frac{2}{\sqrt{3\alpha}}\right). \tag{4.9}$$

We can readily compute ϕ_*, and evaluate the slow roll parameters $N_* = 60$ e-folds before the end of inflation. The slow roll parameters and the cosmic observables are in agreement with the cosmological contraints for the range

$$1 \leqslant \alpha \lesssim 100. \tag{4.10}$$

In particular, for $\alpha = 1\,(100)$ we get

$$\begin{aligned} &\epsilon_* \simeq 0.00019\ (0.00387), && \eta_* \simeq -0.0159\ (-0.00331) \\ &n_s \simeq 0.967\ (0.97), && r_* \simeq 0.003\ (0.062), \qquad H_E \simeq 0.82\ (1.13)\cdot 10^{13}\ \text{GeV}. \end{aligned} \tag{4.11}$$

in agreement with the observed values [4]

$$n_s^{\rm obs} \simeq 0.9649 \pm 0.0042, \quad r_*^{\rm obs} \lesssim 0.06, \quad H_*^{\rm obs} \lesssim 6\cdot 10^{13}\,\text{GeV}\ (95\%\,\text{CL}). \tag{4.12}$$

Using the observed value of A_s from Ref. [4], $A_s^{\rm obs} = 2.2 \cdot 10^{-9}$, we fix the vacuum energy. The result depends on α and is approximately given by $\Lambda_\alpha \simeq 3.4 \cdot 10^{-3}\, \alpha^{1/5}\, M_{\rm pl}$. We then obtain the values $\Lambda_1 = 3.152 \cdot 10^{-3}\, M_{\rm pl}$ and $\Lambda_{100} = 8.313 \cdot 10^{-3}\, M_{\rm pl}$.

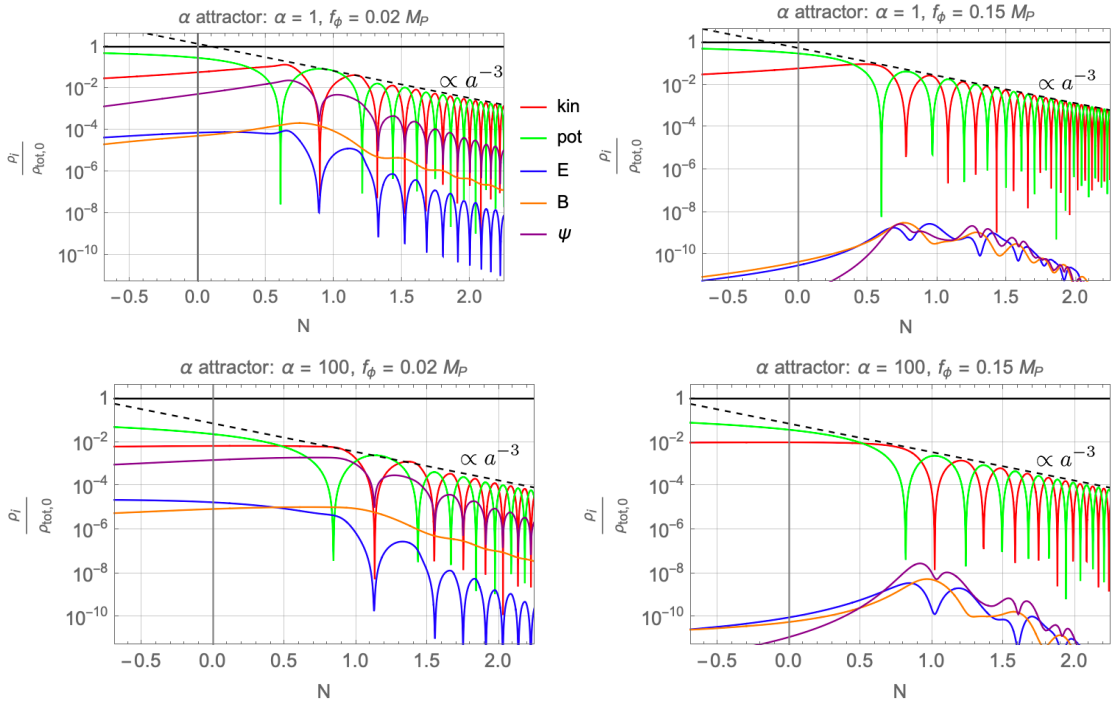

Figure 4: *Inflaton kinetic and potential energy density, as well as electric, magnetic and fermion energy density ratios to the initial total energy density of the Universe for the α-attractor models with $\alpha = 1$ (upper panels) and $\alpha = 100$ (lower panels). The vertical gray lines display the value a for which $\epsilon(a) = 1$ and the dashed line shows the expected scaling of the dominant sector.*

4.2.2 Hilltop quartic models

The hilltop model potential is given by [30]

$$V_{\rm h}(\phi) = \Lambda_{\rm h}^4 \left[1 - \left(\frac{\phi}{\mu}\right)^p\right]^2 . \tag{4.13}$$

The case $p = 4$ can be compatible with the Planck measurements. There are two ways for the field to relax to the minimum at $\phi = \mu$, with different initial conditions:

1. $\phi_* > \phi_E$: In this case the field $\phi > \mu$ is relaxing in a potential region that can be approximated by $V_{\rm h} \sim \phi^8$, and thus, the slow roll conditions are not met, as chaotic inflation is ruled out.

2. $\phi_* < \phi_E$: In this case the field $\phi < \mu$ is relaxing in a flat potential region and the model predicts correct inflationary observables for a large range of the parameter. In this work, we will study this option.

The slow roll parameters and the cosmic observables are in agreement with the contraints for the range

$$10M_{\rm pl} \lesssim \mu \lesssim 50M_{\rm pl}. \tag{4.14}$$

We fix the vacuum energy from the constraint on the amplitude of scalar fluctuations. The result depends on μ and is approximately $\Lambda_{\rm h} \simeq 6 \cdot 10^{-4}\, \mu^{2/3}\, M_{\rm pl}^{1/3}$. We then have the values $\Lambda_{\rm h} = 3.243 \cdot 10^{-3}\, M_{\rm pl}$ for $\mu = 10\, M_{\rm pl}$ and $\Lambda_{\rm h} = 8.081 \cdot 10^{-3}\, M_{\rm pl}$ for $\mu = 50\, M_{\rm pl}$.

In particular, for $\mu = 10\ (50)\, M_{\rm pl}$ we get

$$\begin{aligned} &\epsilon_* \simeq 0.00021\ (0.0041) && \eta_* \simeq -0.0207\ (-0.00328) \\ &n_s \simeq 0.957\ (0.97) && r_* \simeq 0.00335\ (0.0654), && H_E \simeq 0.64\ (1.1) \cdot 10^{13}\ \text{GeV}. \end{aligned} \tag{4.15}$$

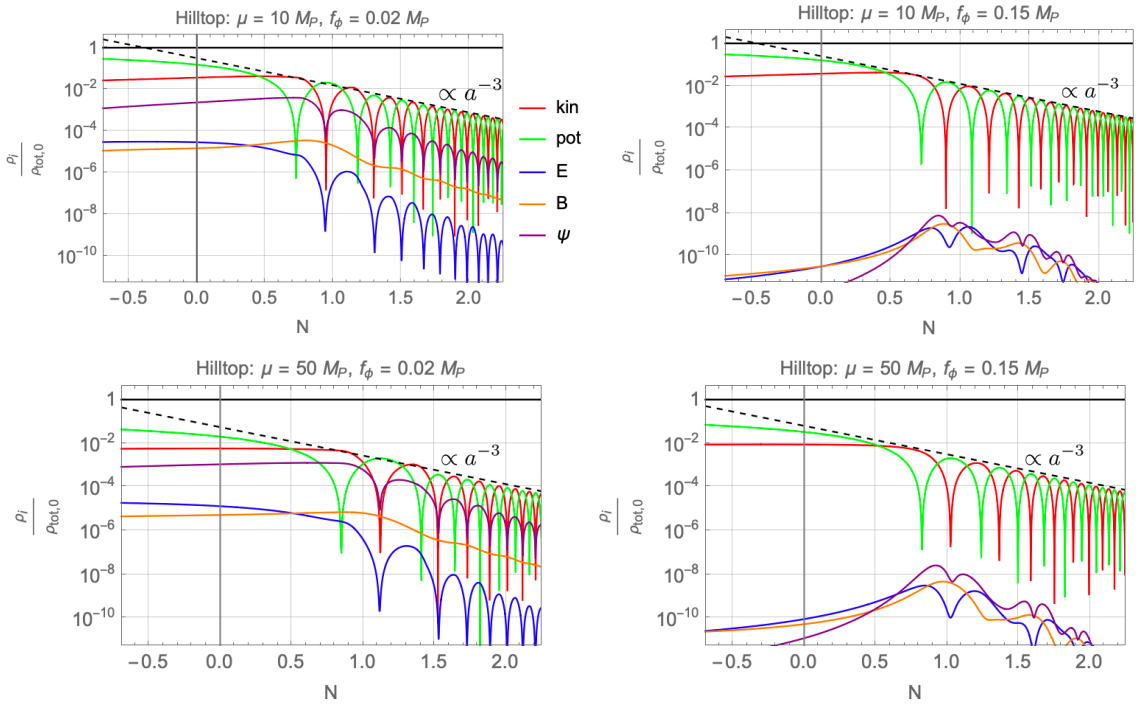

Figure 5: *Inflaton kinetic and potential energy density, as well as electric, magnetic and fermion energy density ratios to the initial total energy density of the Universe for the hilltop models with $\mu = 10\, M_{pl}$ (upper panels) and $\mu = 50\, M_{pl}$ (lower panels). The vertical gray lines display the value a for which $\epsilon(a) = 1$ and the dashed line shows the expected scaling of the dominant sector.*

4.3 Numerical results beyond the end of inflation

Now that we have established a method to numerically compute the quantities ρ_E, ρ_B, ρ_ψ, $\mathcal{H}$ and $\mathcal{G}$, we aim to study the system evolution past $\epsilon = 1$, and the onset of reheating. Indeed, the system (4.6) describes the most general interaction of the zero mode of both hypercharge gauge and inflaton fields. In particular, no assumption was made on the Universe geometry, hence there is no specific reason to stop its numerical computation at the end of inflation. We will also find it convenient to present some

numerical results using as the variable the number of e-folds before the end of inflation N, instead of the scale factor a, and related to it by

$$N = -\log \frac{a_E}{a} \tag{4.16}$$

such that $N = 0$ corresponds to the time a_E when $\epsilon(a_E) = 1$.

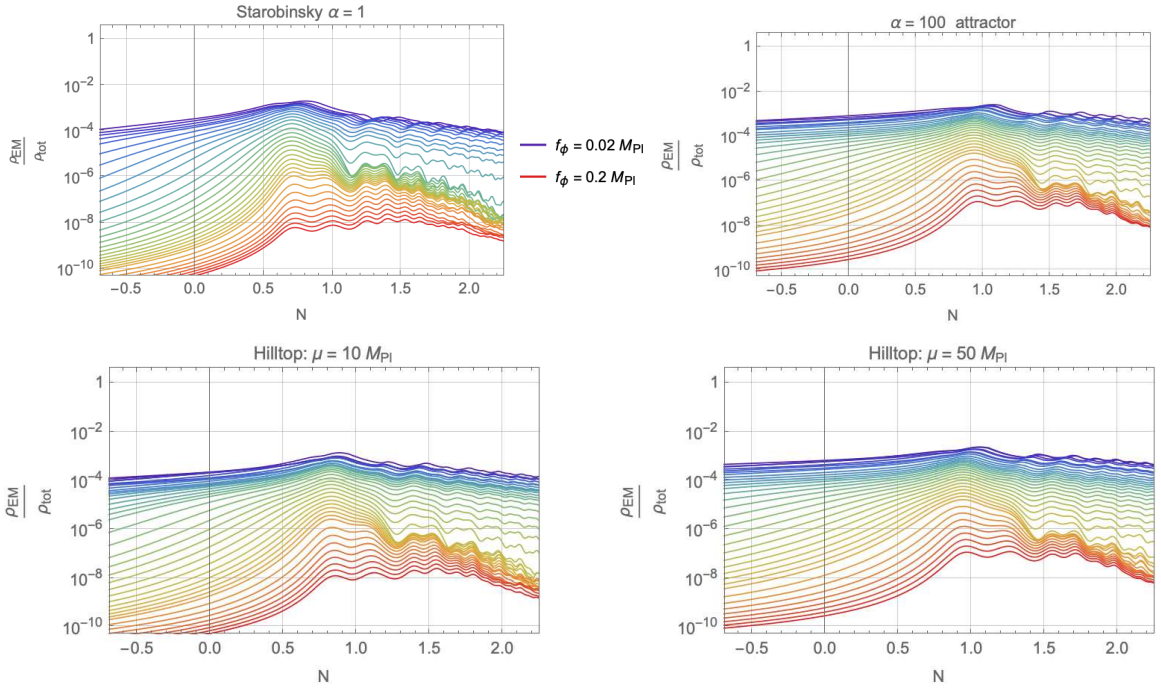

Figure 6: *Time evolution of the electromagnetic to total energy density fraction, during and after inflation for various values of the coupling f_ϕ. The upper panels correspond to the α-attractor model with $\alpha = 1$ (top left) and $\alpha = 100$ (top right) and the lower panels to the hilltop model with $\mu = 10\, M_{pl}$ (bottom left) and $\mu = 50\, M_{pl}$ (bottom right).*

We show the postinflationary energy breakdown for selected value of f_ϕ, for the α-attractor models in Fig. 4, $\alpha = 1$ (upper panels) and $\alpha = 100$ (lower panels), and the hilltop models of inflation in Fig. 5, with $\mu = 10\, M_{\rm pl}$ (upper panels) and $\mu = 50\, M_{\rm pl}$ (lower panels). From the inflaton behavior, we see that the Universe enters a matter domination era as $\rho_\phi \sim a^{-3}$. For high enough values of f_ϕ, i.e. $f_\phi \gtrsim 0.1\, M_{\rm pl}$, we reproduce the results shown in Ref. [12], whereas for $f_\phi \lesssim 0.1\, M_{\rm pl}$ the electric and magnetic fields exhibit a different behavior: the former decays faster than the latter while oscillating. This is due to the fact, already mentioned in Ref. [23], that the energy density for the electric component $\boldsymbol{E} = -\boldsymbol{A}'$ is much more sensitive to the Schwinger effect than the magnetic component $\boldsymbol{B}$, because it directly couples to the conductivity in the gauge field equation of motion (2.7). On the other hand, the magnetic component reflects spatial effects, as it is defined by $\boldsymbol{B} = \boldsymbol{\nabla} \wedge \boldsymbol{A}$. In this work, we do not consider the inflaton spatial effects, $\boldsymbol{\nabla}\phi$, because this would require one to implement real fermion interactions in a lattice simulation. Hence, for low values of f_ϕ, when the Schwinger effect is strongly affecting the system, the behavior of ρ_B is expected to be subject to changes when the spatial effects are enabled; namely we expect to see a faster decay, like that of ρ_E. As also observed in Ref. [23], the electric field, which is dominant during inflation, becomes

subdominant afterwards. Finally, we can see that for low values of f_ϕ the fermion energy density dominates the radiation energy density at the end of inflation as already highlighted in Ref. [23].

The authors of Ref. [12] quote a *sufficient criterion* for gauge preheating to happen, namely that at least an 80% fraction of the total energy density of the Universe is electromagnetic energy. In the absence of the Schwinger effect, they found that this criterion is satisfied for values $f_\phi \lesssim 0.1\, M_{\rm pl}$. However, as expected, the Schwinger effect significantly reduces the share of electromagnetic energy, as shown on Fig. 6 for the considered models, which displays the ratio $\rho_{\rm EM}/\rho_{\rm total}$ for the four previous considered cases. We can see that the maximum is attained with a value $\sim 10^{-3}$, which precludes any gauge preheating, at least for $f_\phi \gtrsim 0.01\, M_{\rm pl}$. Another conclusion from Ref. [12] is that the spatial effects of the inflaton become relevant for sufficiently low values of f_ϕ and contribute to preheating. Since we are neglecting them in our simplified calculation, any negative statement concerning the possibility of gauge preheating due to the lack of enough electromagnetic energy should be a conservative one.

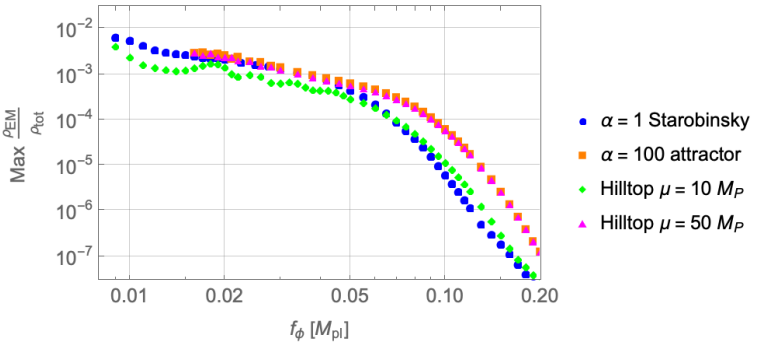

Figure 7: *Maximum value of the electromagnetic to total energy fraction as a function of f_ϕ for the four considered models: α-attractor models, with $\alpha = 1,\, 100$, and hilltop models, $\mu = 10,\, 50\, M_{pl}$. Preheating seems unlikely to occur.*

The final results from our analysis can be summarized in Fig. 7, where we plot the maximum value of the electromagnetic to total energy fraction as a function of f_ϕ (preheating efficiency) for the Starobinsky model, the α-attractor model with $\alpha = 100$ and the hilltop models with $\mu/M_{\rm pl} = 10, 50$. For $f_\phi \gtrsim 0.01\, M_{\rm pl}$, we obtain

$$\frac{\rho_{\rm EM}}{\rho_{\rm tot}} \lesssim 0.01, \tag{4.17}$$

which seems to prevent gauge preheating as its efficiency is far from the value of ~ 0.8 established in the numerical analysis of Ref. [12].

4.4 End of reheating

If gauge preheating does not occur, the inflaton will eventually decay by perturbative processes which depend on the inflaton total decay width Γ_ϕ. Therefore at the time $t_{\rm rh} \sim 1/\Gamma_\phi$, the inflaton has completely decayed and the radiation domination era starts.

Results from last sections have shown that shortly after inflation ends, the Universe is dominated by matter, hence we can approximate the Hubble parameter by

$$H \simeq \left(\frac{a_E}{a}\right)^{\frac{3}{2}} H_E, \qquad H \simeq \frac{2}{3t}, \tag{4.18}$$

where $H_E \equiv H(a_E)$, such that

$$a_{\rm rh} \simeq a_E \left(\frac{3H_E}{2\Gamma_\phi}\right)^{\frac{2}{3}} \tag{4.19}$$

is the end value after reheating by inflaton perturbative decays. Of course $a_{\rm rh}$ is a model-dependent quantity, which depends on the value of Γ_ϕ, which in turn, depends on the couplings of the inflaton to the matter.

In particular, the coupling $1/f_\phi$ of the inflaton to the hypercharge Chern-Simons density provides a channel for the perturbative decay of the inflaton into a pair of hyperphotons A, as $\phi \to AA$. This decay has a width given by [10]

$$\Gamma(\phi \to AA) \simeq \frac{m_\phi^3}{64\pi f_\phi^2}. \tag{4.20}$$

where m_ϕ is the inflaton mass given by

$$m_\phi^2 = \left.\frac{\partial^2 V}{\partial \phi^2}\right|_{\phi=\phi_{\rm min}}. \tag{4.21}$$

For the α-attractor (hilltop quartic) model, we have $\phi_{{\rm min},\alpha} = 0$ ($\phi_{{\rm min},\,h} = \mu$) and

$$m^2_{\phi,\,\alpha} = \frac{4\Lambda_\alpha^4}{3\alpha M_{\rm pl}^2}, \qquad\qquad m^2_{\phi,\,h} = \frac{32\Lambda_h^4}{\mu^2}. \tag{4.22}$$

In the simplest case where the inflaton is only coupled to the hypercharge gauge bosons through the Chern-Simons density, the total width is $\Gamma_\phi = \Gamma(\phi \to AA)$. Using the masses found above we have that

$$\Gamma_\phi \simeq 12\ (3.0) \cdot 10^{-18} \cdot \frac{M_{\rm pl}^3}{f_\phi^2}, \tag{4.23}$$

for $\alpha = 1$ (100) in the α-attractor models, and

$$\Gamma_\phi \simeq 4.2\ (21) \cdot 10^{-19} \cdot \frac{M_{\rm pl}^3}{f_\phi^2}, \tag{4.24}$$

for $\mu = 10$ (50) $M_{\rm pl}$ in the hilltop models.

The value of the scale factor and the temperature at reheating, $a_{\rm rh}$ and $T_{\rm rh}$, are given by

$$\frac{a_{\rm rh}}{a_E} \simeq 0.4 \left(\frac{T_{\rm rh}}{T_{\rm rh}^{\rm ins}}\right)^{-4/3}, \qquad\qquad \frac{T_{\rm rh}}{T_{\rm rh}^{\rm ins}} \simeq \sqrt{\frac{\Gamma_\phi}{H_E}}. \tag{4.25}$$

Consequently we can express $a_{\rm rh}$ and $T_{\rm rh}$ as functions of all the involved parameters, namely f_ϕ, and α (μ) for α-attractor (hilltop quartic) model. In particular, the relevant parameter for baryogenesis is the ratio $T_{\rm rh}/T_{\rm rh}^{\rm ins}$ given by

$$\frac{T_{\rm rh}}{T_{\rm rh}^{\rm ins}} \simeq 1.9\ (0.8) \cdot 10^{-4} \left(\frac{0.01}{f_\phi/M_{\rm pl}}\right), \tag{4.26}$$

for $\alpha = 1$ (100) in the α-attractor models, and

$$\frac{T_{\rm rh}}{T_{\rm rh}^{\rm ins}} \simeq 0.4\ (0.7) \cdot 10^{-4} \left(\frac{0.01}{f_\phi/M_{\rm pl}}\right), \tag{4.27}$$

for $\mu = 10$ (50) $M_{\rm pl}$ in the hilltop models. As we will see in the next section the obtained values of the ratio $T_{\rm rh}/T_{\rm rh}^{\rm ins}$ are fully consistent with the general baryogenesis results, see Fig. 8, provided that

$f_\phi \lesssim 0.03\, M_{\rm pl}$.

In the presence of extra couplings of the inflaton to matter, the predictions for the inflaton decay width, Eqs. (4.23) and (4.24), and the reheating temperature, Eqs. (4.26) and (4.27), will change in a model-dependent way, as well as the model predictions concerning the generation of the baryon asymmetry.

Of course in the hypothetical case where the explosive production of gauge fields should have prevailed over the perturbative inflaton decays, gauge preheating would have taken place over a few e-folds after the end of inflation. As we see from the previous results, this is never the case and gauge preheating is never strong enough to reheat the Universe after the period of cosmological inflation. This result does not preclude that, in the presence of a strong coupling λ of the inflaton with some other field, e.g. a scalar (or a fermion), there could exist an explosive production of that scalar (or fermion), triggering preheating of the Universe after inflation [31].

4.5 Baryon asymmetry

Before concluding this paper we wish to make a small comment on the baryogenesis issue at the electroweak phase transition. In Ref. [18], we presented a model of inflation that leads to a successful BAU. The effective potential for the inflaton, labeled therein as χ, was the Starobinsky potential[9], and we did consider the Schwinger equilibrium and maximal estimates. Hence it is straightforward, using our numerical analysis in this paper, to make an update of the final results for the BAU for inflation driven by the α-attractor models with $\alpha = 1$.

As all details are explained in Secs. 6 and 7 of Ref. [18], we skip them here and go straight to the final result. First of all we show in Fig. 8 the analogous plot to Fig. 9 of Ref. [18], namely the parameter space that provides a successful BAU. In particular, we display in blue the region where

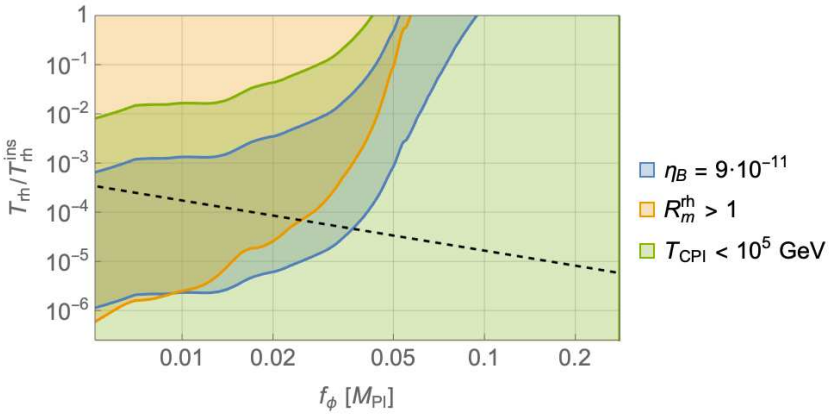

Figure 8: *The baryogenesis window in the parameter space* $(f_\phi, T_{\rm rh}/T_{\rm rh}^{\rm ins})$ *for the Starobinsky potential* (α*-attractor model with* $\alpha = 1$*). The dashed line corresponds to Eq. (4.26).*

[9] In fact, we used in Ref. [18] an scalar field ϕ non-minimally coupled with gravity as $\mathcal{L} = -\frac{1}{2} g\phi^2 R + \ldots$, which yields for the canonically normalized field χ in the Einstein frame an α-attractor potential with $\alpha = 1 + \frac{1}{6g} \in [4.3, 17.6]$, where the lower bound was coming from imposing the naive unitarity bound $g\phi^2 < M_{\rm pl}^2$. As the dependence in α (hence in g) is tiny, we choose to show in the present paper the result for $\alpha = 1$, hence for the Starobinsky potential (which would correspond in Ref. [18] to the limit $g \gg 1$).

the asymmetry parameter meets its observational value given by

$$\eta_B \simeq 4 \cdot 10^{-12}\, f_{\theta_W} \frac{\mathcal{H}}{H_E^3} \left(\frac{H_E}{10^{13}\,\mathrm{GeV}}\right)^{\frac{3}{2}} \left(\frac{T_{\rm rh}}{T_{\rm rh}^{\rm ins}}\right) \simeq 9 \cdot 10^{-11}, \tag{4.28}$$

where we have imposed the observed value [32] in the right-hand side. Following Refs. [16, 17] we define the parameter f_{θ_W}, which encodes all the details of the EW phase transition and its uncertainties, as

$$f_{\theta_W} = -\sin(2\theta_W)\, \frac{d\theta_W}{d\ln T}\bigg|_{T=135\ \mathrm{GeV}}, \quad 5.6 \cdot 10^{-4} \lesssim f_{\theta_W} \lesssim 0.32. \tag{4.29}$$

In addition to their dependence on the gauge sector observables, the quantities used in this section vary according to the ratio of the reheating over the instant reheating temperature. This parameter hence adds to f_ϕ in the parameter space. The reheating temperature is computed as

$$T_{\rm rh} = \left(\frac{90}{\pi^2 g_*}\right)^{\frac{1}{4}} \sqrt{\Gamma_\phi M_{\rm pl}}, \tag{4.30}$$

where $g_* = 106.75$ is the SM number of relativistic degrees of freedom, and we define $T_{\rm rh}^{\rm ins}$ as a reference temperature given by the above equation with $\Gamma_\phi \simeq H_E$, which is obtained from the simulation. It would correspond to the reheating temperature for instant reheating, and takes the value $T_{\rm rh}^{\rm ins} \simeq 2.87 \cdot 10^{15}$ GeV. Using Eq. (4.26) it is possible to link the reheat temperature to the parameter f_ϕ. The corresponding plot is shown in Fig. 8 which shows that it provides a wide window for baryogenesis.

Second, we display in orange the region where the magnetic Reynold's number at reheating $\mathcal{R}_m^{\rm rh}$ is bigger than one, hence ensuring that the required magnetohydrodynamical conditions are fulfilled for the (hyper)magnetic fields to survive until the electroweak crossover. As we are in the viscous regime, it can be computed as [18]

$$\mathcal{R}_m^{\rm rh} \approx 5.9 \cdot 10^{-6}\, \frac{\rho_B \ell_B^2}{H_E^2} \left(\frac{H_E}{10^{13}\,\mathrm{GeV}}\right) \left(\frac{T_{\rm rh}}{T_{\rm rh}^{\rm ins}}\right)^{\frac{2}{3}}, \tag{4.31}$$

where ℓ_B is the physical correlation length of the magnetic field given by

$$\ell_B = \frac{2\pi}{\rho_B\, a^3} \int^{k_c} dk\, \frac{k^3}{4\pi^2} \left(|A_+|^2 + |A_-|^2\right), \tag{4.32}$$

which can be numerically computed during the simulation in the same way as the other observables.

Third, and last[10], we show in green the condition on the chiral plasma instability (CPI) temperature, ensuring that the CPI time scale is long enough to allow all right-handed fermionic states to come into chemical equilibrium with the left-handed ones via Yukawa coupling interactions (so that sphalerons can erase their corresponding asymmetries in particle number densities) before CPI can happen. The estimated temperature at which CPI takes place is

$$T_{\rm CPI}/\mathrm{GeV} \approx 4 \cdot 10^{-7}\, \frac{\mathcal{H}^2}{H_E^6} \left(\frac{H_E}{10^{13}\,\mathrm{GeV}}\right)^3 \left(\frac{T_{\rm rh}}{T_{\rm rh}^{\rm ins}}\right)^2. \tag{4.33}$$

The constraint $T_{\rm CPI} \lesssim 10^5$ GeV (the temperature at which e_R comes into chemical equilibrium) guarantees that the CPI cannot occur before the smallest Yukawa coupling reaches equilibrium and

[10] Besides, we checked that the generation of baryon isocurvature perturbation provides no constraint.

all particle number density asymmetries are erased, preventing thus the cancellation of the helicity generated at the reheating temperature.

Therefore, as we can see from Fig. 8, the resulting baryogenesis window for the Starobinsky potential is close to the Schwinger equilibrium estimate for $f_\phi \lesssim 0.06\, M_{\rm pl}$, just as the corresponding results on helicity and magnetic energy density suggest (see the green dots of Fig. 3). However, for $f_\phi \gtrsim 0.06\, M_{\rm pl}$ there is no space for the BAU, as the production of gauge fields is too weak, unlike in the previous results from Ref. [18]. In addition to this we have seen that the reheating temperature is constrained by the model, see Eq. (4.26), as we can see from Fig. 8 and compatibility of the model reheating temperature with the baryogenesis results translates into the baryogenesis region on the parameter f_ϕ

$$f_\phi \lesssim 0.03\, .M_{\rm pl} \tag{4.34}$$

Finally, one of the results of this paper is then that baryogenesis at the electroweak phase transition is favored by low reheating temperatures, in the range $10^{-6}\, T_{\rm rh}^{\rm ins} \lesssim T_{\rm rh} \lesssim 10^{-3}\, T_{\rm rh}^{\rm ins}$.

5 Conclusions

In this paper, we have studied by means of numerical computations the effect of the Schwinger particle production on the helical hypermagnetic fields produced at the end of inflation. The inflaton field ϕ can decay, through its coupling to the Chern-Simons density $\frac{\phi}{4f_\phi} Y_{\mu\nu}\tilde{Y}^{\mu\nu}$, into helical hypermagnetic fields in a nonperturbative process. When exiting the vacuum, the gauge modes are strong enough to create particle/antiparticle pairs of light fermions, which contribute to the electrical conductivity of the plasma. The backreaction of fermion currents on the produced gauge fields acts as a damping force in the explosive production of helical gauge fields. This effect, called *Schwinger effect*, was already considered in numerous studies of inflation and/or baryogenesis, where some analytical and numerical estimates were computed, mainly in configuration space while our calculation is done in momentum space.

The equations of motion are in fact a nontrivial integro-differential system. It was solved numerically by using a fourth order Runge-Kutta method, with details being displayed in the Appendices. The computed observables of interest are the electric and magnetic energy density, the helicity as well as the helicity time derivative. We assumed a homogeneous inflaton with only zero mode, hence we did not treat any spatial effects. Besides, we also ensured the convergence of the algorithm and its invariance to the initial conditions.

First of all we have checked that we recover previous results in the slow roll inflation regime by making the same approximations required by an analytical resolution. In this way, we validate our code, i.e. we verify that our code produces the right results in known cases such as the backreactionless case, where the Schwinger effect is turned off, and the gradient expansion formalism, where the Bunch-Davies parameter Δ was first introduced.

In a second step, still in the slow roll regime, we considered a specific model of inflation, namely the Starobinsky potential, in order to account for the instability parameter as a function, $\xi(a)$, instead of the constant imposed by the analytical approximations. That way, we could also implement the effects of a function $\Delta(a)$ obtained from the plasma evolution on the gauge production itself.

We then simulated, in a third step, the full system, where neither the slow roll conditions nor the Universe geometry (e.g. de Sitter) are imposed. In order words, the inflaton equation of motion was computed alongside with the gauge one, taking the backreaction of the latter to the former into account along with the Schwinger effect. We compare our result to the previous setup and found

perfect agreement as long as the slow roll conditions are met. When inflation is near its end, the full solution diverges from the slow roll results and produces, as expected, less energy density and helicity.

Finally we will comment on the implication about two related topics: gauge preheating and baryogenesis. As our code is free from any geometrical issues, and only requires a model of inflation, we let the simulations run until the onset of reheating to compute the electromagnetic to total energy density ratio. We choose two well-known classes of models that satisfy the cosmological constraints as illustrative examples. Previous studies have quoted a sufficient criterion for gauge preheating to happen, namely that this fraction should be at least $\gtrsim 80\%$ [12]. However, our numerical estimates suggest that the Schwinger effect significantly reduces the share of electromagnetic energy for the considered models and preheating is unlikely to occur. Moreover, since we are neglecting all spatial effects, any negative statement concerning the possibility of gauge preheating due to the lack of electromagnetic energy should be a conservative one. On the other hand our results do apply to the considered class of inflationary models. They show a certain degree of model dependence, so we cannot exclude a qualitatively different result for models of inflation other than the considered ones.

On the other hand, as a successful baryogenesis does depend on a delicate equilibrium between the amount of helicity, magnetic energy density, and magnetic correlation length, damped fields do not necessarily mean no baryon asymmetry in the late Universe. Actually, as a result of our numerical calculation, we have found there is still a window in the parameter space for baryogenesis to happen as long as $f_\phi \lesssim 0.05\, M_{\rm pl}$, while consistency from the perturbative decay channel of the inflaton into hypergauge bosons implies the bound $f_\phi \lesssim 0.03\, M_{\rm pl}$. Moreover, baryogenesis is favored for low enough values of the reheating temperature $T_{\rm rh} \lesssim 10^{-3}\, T_{\rm rh}^{\rm ins}$. Of course, the baryogenesis predictions should, to some extent, depend on the model of inflation. In this way, our result here is restricted to the Starobinsky model and should be considered just as a "proof of existence" for baryogenesis in the presence of the Schwinger effect.

These two comments should be viewed as hints for future studies that address the production of gauge fields at the end of inflation. Of course, a full lattice simulation of the Schwinger effect involving fermions remains to be done.

Acknowledgments

YC would like to thank Adrien Florio, for interesting discussions at the early stage of this work. MQ is indebted to Daniel Figueroa for interesting discussions, full of new ideas, on the subject. This work is supported by the Departament d'Empresa i Coneixement, Generalitat de Catalunya Grant No. 2017SGR1069, by the Ministerio de Economía y Competitividad Grant No. FPA2017-88915-P. IFAE is partially funded by Centres de Recerca de Catalunya. YC is supported by the European Union's Horizon 2020 research and innovation programme under the Marie Sklodowska-Curie Actions No. 754558.

A Numerical method: the slow roll case

We provide here the technical details for the solution of Eq. (3.10) subject to the initial condition (3.11). For convenience, we implement the numerical computation in units of H_E. Writing

$$x_\lambda(a) = A_\lambda(a), \qquad\qquad y_\lambda(a) = \frac{dA_\lambda}{da}(a), \tag{A.1}$$

Eq. (3.10) becomes the following system:

$$\frac{d}{da}\begin{pmatrix} x_\lambda \\ y_\lambda \end{pmatrix} = \begin{pmatrix} 0 & 1 \\ \frac{k}{a^3}\left(2\lambda\xi - \frac{k}{a}\right) & -\frac{1}{a}\left(\frac{\sigma}{a}+2\right) \end{pmatrix}\begin{pmatrix} x_\lambda \\ y_\lambda \end{pmatrix} \quad \Leftrightarrow \quad \frac{d\boldsymbol{x}}{da} = \boldsymbol{f}(a,\boldsymbol{x}). \tag{A.2}$$

To perform each time step Δa, we use the fourth order Runge-Kutta (`RK4`) algorithm:

$$\boldsymbol{\lambda}_1 = \boldsymbol{f}(a_i, \boldsymbol{x}_i) \tag{A.3a}$$
$$\boldsymbol{\lambda}_2 = \boldsymbol{f}\left(a_i + \tfrac{1}{2}\Delta a, \boldsymbol{x}_i + \tfrac{1}{2}\Delta a\boldsymbol{\lambda}_1\right) \tag{A.3b}$$
$$\boldsymbol{\lambda}_3 = \boldsymbol{f}\left(a_i + \tfrac{1}{2}\Delta a, \boldsymbol{x}_i + \tfrac{1}{2}\Delta a\boldsymbol{\lambda}_2\right) \tag{A.3c}$$
$$\boldsymbol{\lambda}_4 = \boldsymbol{f}\left(a_i + \Delta a, \boldsymbol{x}_i + \Delta a\boldsymbol{\lambda}_3\right) \tag{A.3d}$$
$$a_{i+1} = a_i + \Delta a \tag{A.3e}$$
$$\boldsymbol{x}_{i+1} = \boldsymbol{x}_i + \tfrac{1}{6}\Delta a(\boldsymbol{\lambda}_1 + 2\boldsymbol{\lambda}_2 + 2\boldsymbol{\lambda}_3 + \boldsymbol{\lambda}_4) \tag{A.3f}$$

Note that $\boldsymbol{x}$ is complex, hence we solve the above system for both real and imaginary parts but with their specific initial conditions. These are mode-dependent as it takes longer for modes with bigger wave number to leave the BD vacuum. Therefore, we choose as initial condition for each mode

$$a_{k,0} = \frac{k}{x_{\rm BD}}, \tag{A.4}$$

where we choose the factor $x_{\rm BD}$ in order to make sure that we initialize the gauge field sufficiently deep inside the Hubble radius. Its exact value is subject to analysis and is discussed later. As we can see from (2.8) and (2.9), high values of k are dominating the integral hence large modes are negligible compared to small ones. This makes us to choose a lower bound on the k range such that the initial time of the simulation is

$$a_0 = \frac{k_{\rm min}}{x_{\rm BD}}. \tag{A.5}$$

In that way, at a_0 we make sure that all the modes are in their respective vacua, which implies $\sigma = 0$ as explained above.

In practice, this means that the modes with $k > x_{\rm BD}a$ are given by the following relations

$$\mathrm{Re}(x^{\rm BD}_{\lambda,i}) = \sqrt{\frac{\Delta_i}{2k}}\cos\frac{k}{a_i}, \tag{A.6a}$$
$$\mathrm{Im}(x^{\rm BD}_{\lambda,i}) = \sqrt{\frac{\Delta_i}{2k}}\sin\frac{k}{a_i}, \tag{A.6b}$$
$$\mathrm{Re}(y^{\rm BD}_{\lambda,i}) = \frac{1}{a_i^2}\sqrt{\frac{\Delta_i}{2}}\left(\sqrt{k}\sin\frac{k}{a_i} - \frac{\sigma_i}{2\sqrt{k}}\cos\frac{k}{a_i}\right), \tag{A.6c}$$
$$\mathrm{Im}(y^{\rm BD}_{\lambda,i}) = \frac{1}{a_i^2}\sqrt{\frac{\Delta_i}{2}}\left(-\sqrt{k}\cos\frac{k}{a_i} - \frac{\sigma_i}{2\sqrt{k}}\sin\frac{k}{a_i}\right) \tag{A.6d}$$

while the others are evolving with the `RK4` algorithm.

The time steps are distributed on a logarithmic scale

$$\log a_i - \log a_{i-1} = \log a_{i+1} - \log a_i, \tag{A.7}$$

so that the discretization is the same for each order of magnitude. This means Δa grows exponentially with a. The advantage of this method is that there is a refinement of the grid for small values of a, at the beginning of inflation. The same is done for the discretization in k.

We explored the numerical convergence of the solution, both in the number of a_i's, labeled as N_a, and in the number of k_j's, labeled as N_k. Provided that $N_a > 2000$ and $N_k > 200$, the simulations are very stable and the output does not depend on the discretization. For big values of f_ϕ, $f_\phi \gtrsim 0.1$, we can even lower the number of time steps needed.

Besides, we must choose the BD penetration factor $x_{\rm BD}$ such that it produces trustable results. We have done a numerical analysis and conclude that depending on the value of N_a, a range $20 < x_{\rm BD} < 50$ yields trustable results. We hence choose throughout this work the following values

$$x_{\rm BD} = 20, \qquad N_a = 500,\, 1000,\, 2000, \qquad N_k = 300. \tag{A.8}$$

At each time step, we compute the electric and magnetic energy density as

$$\rho_E^i = \int_{k_{\rm min}}^{k_c^i} dk\, \frac{k^2}{4\pi^2} \left(|y_i^+(k)|^2 + |y_i^-(k)|^2\right), \tag{A.9a}$$

$$\rho_B^i = \frac{1}{a_i^4} \int_{k_{\rm min}}^{k_c^i} dk\, \frac{k^4}{4\pi^2} \left(|x_i^+(k)|^2 + |x_i^-(k)|^2\right), \tag{A.9b}$$

where we choose

$$k_c^i = a_i\xi + \sqrt{(a_i\xi)^2 + \frac{a_i^2}{2}\left[\frac{\sigma_i - \sigma_{i-1}}{a_i - a_{i-1}} + \frac{\sigma_i}{a_i}\left(\frac{\sigma_i}{2a_i} + 1\right)\right]}. \tag{A.10}$$

such that we cut off the spectra to retain only modes outside the horizon. The helicity (2.9a) and its derivative (2.9b) become

$$\mathcal{H}_i = \frac{1}{a_i^3} \int_{k_{\rm min}}^{k_c^i} dk\, \frac{k^3}{2\pi^2} \left(|x_i^+(k)|^2 - |x_i^-(k)|^2\right), \tag{A.11a}$$

$$\mathcal{G}_i = \frac{1}{a_i^2} \int_{k_{\rm min}}^{k_c^i} dk\, \frac{k^3}{2\pi^2} \left(|x_i^+(k) y_i^+(k)| - |x_i^-(k) y_i^-(k)|\right). \tag{A.11b}$$

In the numerics, these integrals are performed numerically over the range of k that takes N_k discrete values. If the Schwinger effect is taken into account, we turn on the possibility of having σ computed at each time step a_i of the numerical computation with

$$\sigma_{i+1} = \frac{41\, g'^3}{72\,\pi^2}\, a_i \sqrt{2\rho_B^i}\, \coth\left(\pi\sqrt{\frac{\rho_B^i}{\rho_E^i}}\right) \tag{A.12}$$

and injected into the calculation of the next step. Otherwise, we keep it zero. Last, the fermion energy density is computed as

$$\rho_\psi^i = \frac{\sigma_i}{a_i^2} \int_{k_{\rm min}}^{k_c^i} dk\, \frac{k^2}{\pi^2} \sum_{\lambda=\pm} \left[{\rm Re}(x_i^\lambda){\rm Re}(y_i^\lambda) + {\rm Im}(x_i^\lambda){\rm Im}(y_i^\lambda)\right]. \tag{A.13}$$

Finally, we stop the simulation at $a = a_E$. Quantities at that time are compared to the known analytical results. The color matching dashed vertical lines in Fig. 2 show the cutoff values k_c^i computed from (A.10). They agree perfectly with the point where the BD vacuum modes become dominant for large k.

B Numerical method: full analysis

The numerical implementation follows from the previous case. Defining the variables

$$w = \phi, \qquad x = \frac{d\phi}{da}, \qquad y_\lambda = A_\lambda, \qquad z_\lambda = \frac{dA_\lambda}{da} \tag{B.1}$$

we transform the above coupled system of differential equations (4.6) into the system

$$\frac{dw}{da} = x \tag{B.2a}$$

$$\frac{dx}{da} = -\frac{\mathcal{G}}{a^2 H^2 f_\phi} - \frac{4-\mathcal{F}}{a}\, x - \frac{V'(w)}{a^2 H^2} \tag{B.2b}$$

$$\frac{dy_\lambda}{da} = z_\lambda \tag{B.2c}$$

$$\frac{dz_\lambda}{da} = \frac{k}{a^2 H}\left(\frac{\lambda}{f_\phi}\, x - \frac{k}{a^2 H}\right) y_\lambda - \frac{1}{a}\left(2 - \mathcal{F} + \frac{\sigma}{aH}\right) z_\lambda \tag{B.2d}$$

which is equivalent to writing

$$\frac{d\boldsymbol{x}}{da} = \boldsymbol{f}(a, \boldsymbol{x}). \tag{B.3}$$

We recall that w, $x \in \mathbb{R}$ and y_λ, $z_\lambda \in \mathbb{C}$. Similarly to the previous calculation with the slow roll approximation, we use the `RK4` algorithm (A.3) with the values of H, σ, $\mathcal{F}$ and $\mathcal{G}$ computed at each time step.

Inflaton initial condition could be set to

$$w_0 = \phi_*, \qquad\qquad x_0 = 0. \tag{B.4}$$

However, the number of e-folds sets the initial time as $a_0 = \mathrm{e}^{-|N_*|} \sim 10^{-26}$, which is too small a number for the numerical implementation. We then proceed as follows. For $a \lesssim k_{\rm min}/x_{\rm BD}$, and sufficiently low $k_{\rm min}$, the gauge field modes stay in their vacuum and the total contribution to $\Delta(a)$ is negligible. Hence we do not need to perform the numerical simulation before that time, as the inflaton is the main player, so we can solve its equation of motion analytically. Instead, we fix the start of the simulation like before, at $a_0 = k_{\rm min}/x_{\rm BD}$ and we compute the corresponding number of e-folds N which leads us to the corresponding value of $\phi(N)$. Therefore, the initial condition must be set to w_0 such that

$$\int_{\phi_E}^{w_0} \frac{V(\phi)}{V'(\phi)}\, d\phi = -M_{\rm pl}^2 \log a_0 \tag{B.5}$$

and, using $\dot\phi \simeq -\frac{V'(\phi)}{3H}$ which is valid at the early stages of inflation,

$$x_0 = -\frac{V'(w_0)}{3a_0 H_0^2}. \tag{B.6}$$

As for the gauge field, initial conditions are set in the same way as in the slow roll approximation, see App. A.

References

[1] A. H. Guth, *The Inflationary Universe: A Possible Solution to the Horizon and Flatness Problems*, *Phys. Rev. D* **23** (1981) 347–356.

[2] A. D. Linde, *A New Inflationary Universe Scenario: A Possible Solution of the Horizon, Flatness, Homogeneity, Isotropy and Primordial Monopole Problems*, *Phys. Lett. B* **108** (1982) 389–393.

[3] A. Albrecht and P. J. Steinhardt, *Cosmology for Grand Unified Theories with Radiatively Induced Symmetry Breaking*, *Phys. Rev. Lett.* **48** (1982) 1220–1223.

[4] Planck collaboration, Y. Akrami et al., *Planck 2018 results. X. Constraints on inflation*, *Astron. Astrophys.* **641** (2020) A10, [1807.06211].

[5] P. Adshead, J. T. Giblin, M. Pieroni and Z. J. Weiner, *Constraining axion inflation with gravitational waves from preheating*, *Phys. Rev. D* **101** (2020) 083534, [1909.12842].

[6] P. Adshead, J. T. Giblin, M. Pieroni and Z. J. Weiner, *Constraining Axion Inflation with Gravitational Waves across 29 Decades in Frequency*, *Phys. Rev. Lett.* **124** (2020) 171301, [1909.12843].

[7] M. M. Anber and L. Sorbo, *Naturally inflating on steep potentials through electromagnetic dissipation*, *Phys. Rev. D* **81** (2010) 043534, [0908.4089].

[8] M. M. Anber and E. Sabancilar, *Hypermagnetic Fields and Baryon Asymmetry from Pseudoscalar Inflation*, *Phys. Rev. D* **92** (2015) 101501, [1507.00744].

[9] Y. Cado and E. Sabancilar, *Asymmetric Dark Matter and Baryogenesis from Pseudoscalar Inflation*, *JCAP* **04** (2017) 047, [1611.02293].

[10] P. Adshead, J. T. Giblin, T. R. Scully and E. I. Sfakianakis, *Gauge-preheating and the end of axion inflation*, *JCAP* **12** (2015) 034, [1502.06506].

[11] E. I. Sfakianakis and J. van de Vis, *Preheating after Higgs Inflation: Self-Resonance and Gauge boson production*, *Phys. Rev. D* **99** (2019) 083519, [1810.01304].

[12] J. R. C. Cuissa and D. G. Figueroa, *Lattice formulation of axion inflation. Application to preheating*, *JCAP* **06** (2019) 002, [1812.03132].

[13] K. Kamada and A. J. Long, *Baryogenesis from decaying magnetic helicity*, *Phys. Rev. D* **94** (2016) 063501, [1606.08891].

[14] K. Kamada and A. J. Long, *Evolution of the Baryon Asymmetry through the Electroweak Crossover in the Presence of a Helical Magnetic Field*, *Phys. Rev. D* **94** (2016) 123509, [1610.03074].

[15] D. Jiménez, K. Kamada, K. Schmitz and X.-J. Xu, *Baryon asymmetry and gravitational waves from pseudoscalar inflation*, *JCAP* **12** (2017) 011, [1707.07943].

[16] V. Domcke, B. von Harling, E. Morgante and K. Mukaida, *Baryogenesis from axion inflation*, *JCAP* **10** (2019) 032, [1905.13318].

[17] Y. Cado, B. von Harling, E. Massó and M. Quirós, *Baryogenesis via gauge field production from a relaxing Higgs*, *JCAP* **07** (2021) 049, [2102.13650].

[18] Y. Cado and M. Quirós, *Baryogenesis from combined Higgs – scalar field inflation*, *Phys. Rev. D* **106** (2022) 055018, [2201.06422].

[19] V. Domcke and K. Mukaida, *Gauge Field and Fermion Production during Axion Inflation*, *JCAP* **11** (2018) 020, [1806.08769].

[20] H. Kitamoto and M. Yamada, *Semiclassical analysis of axion-assisted and axion-driven pair production*, *JHEP* **06** (2022) 103, [2109.14782].

[21] T. D. Cohen and D. A. McGady, *The Schwinger mechanism revisited*, *Phys. Rev. D* **78** (2008) 036008, [0807.1117].

[22] O. O. Sobol, E. V. Gorbar and S. I. Vilchinskii, *Backreaction of electromagnetic fields and the Schwinger effect in pseudoscalar inflation magnetogenesis*, *Phys. Rev. D* **100** (2019) 063523, [1907.10443].

[23] E. V. Gorbar, K. Schmitz, O. O. Sobol and S. I. Vilchinskii, *Gauge-field production during axion inflation in the gradient expansion formalism*, *Phys. Rev. D* **104** (2021) 123504, [2109.01651].

[24] E. V. Gorbar, K. Schmitz, O. O. Sobol and S. I. Vilchinskii, *Hypermagnetogenesis from axion inflation: Model-independent estimates*, *Phys. Rev. D* **105** (2022) 043530, [2111.04712].

[25] T. Fujita, J. Kume, K. Mukaida and Y. Tada, *Effective treatment of U(1) gauge field and charged particles in axion inflation*, 2204.01180.

[26] J. R. Espinosa, G. F. Giudice, E. Morgante, A. Riotto, L. Senatore, A. Strumia et al., *The cosmological Higgstory of the vacuum instability*, *JHEP* **09** (2015) 174, [1505.04825].

[27] M. M. Anber and L. Sorbo, *N-flationary magnetic fields*, *JCAP* **10** (2006) 018, [astro-ph/0606534].

[28] R. Durrer and A. Neronov, *Cosmological Magnetic Fields: Their Generation, Evolution and Observation*, *Astron. Astrophys. Rev.* **21** (2013) 62, [1303.7121].

[29] R. Kallosh, A. Linde and D. Roest, *Superconformal Inflationary α-Attractors*, *JHEP* **11** (2013) 198, [1311.0472].

[30] L. Boubekeur and D. H. Lyth, *Hilltop inflation*, *JCAP* **07** (2005) 010, [hep-ph/0502047].

[31] C. Cosme, D. G. Figueroa and N. Loayza, *Gravitational wave production from preheating with trilinear interactions*, 2206.14721.

[32] Particle Data Group collaboration, P. Zyla et al., *Review of Particle Physics*, *PTEP* **2020** (2020) 083C01.

Baryogenesis in R^2-Higgs Inflation: the Gravitational Connection

Yann Cado,[1] Christoph Englert,[2] Tanmoy Modak,[3] and Mariano Quirós[4]

[1] *Laboratoire de Physique Théorique et Hautes Energies (LPTHE), Sorbonne Université et CNRS UMR 7589, 4 place Jussieu, 75252 Paris CEDEX 05, France*

[2] *School of Physics & Astronomy, University of Glasgow, Glasgow G12 8QQ, UK*

[3] *Institut für Theoretische Physik, Universität Heidelberg, 69120 Heidelberg, Germany*

[4] *Institut de Física d'Altes Energies (IFAE) and The Barcelona Institute of Science and Technology (BIST), Campus UAB, 08193 Bellaterra, Barcelona, Spain*

R^2-Higgs inflation stands out as one of the best-fit models of Planck data. Using a covariant formalism for the inflationary dynamics and the production of helical gauge fields, we show that the observed baryon asymmetry of the Universe (BAU) can be obtained when this model is supplemented by a dimension-six CP-violating term $\sim (R/\Lambda^2)\, B_{\mu\nu}\widetilde{B}^{\mu\nu}$ in the hypercharge sector. At linear order, values of $\Lambda \simeq 2.5\times 10^{-5}\, M_{\rm P}$ produce, in the R^2-like regime, sufficient helical hypermagnetic fields to create the observed matter-antimatter asymmetry during the electroweak crossover. However, the Schwinger effect of fermion pair production can play a critical role in this context, and that scale is significantly lowered when the backreaction of the fermion fields on the gauge field production is included. In all cases, the helical field configurations can remain robust against washout after the end of inflation.

Contents

1. Introduction 2

2. The Starobinsky-Higgs Action 4

3. Inflationary Dynamics in the Covariant Formalism 8

4. Gauge Field Production 14

5. Baryogenesis 20

6. Summary and Conclusions 24

A. The Vierbein Fields 25

B. Field-Space Metric and Christoffel Symbols 25

C. Einstein Equation and Stress-Energy Tensor 25

D. The Valley Approximation 26

E. Numerical Solutions of the Electromagnetic Equations 26

References 28

1 Introduction

Cosmic inflation [1–3] elegantly addresses a plethora of observations, ranging from the flatness of the Universe, over resolving the horizon and exotic relics problems, all the way to seeding the primordial density perturbations giving rise to the large-scale structure of the Universe that we see today. In parallel, it can explain the cosmic microwave background (CMB) anisotropies measured by experiments such as Planck [4]. While there are several alternatives to inflation, among these models, Starobinsky or R^2 [1, 5–8] inflation, where pure General Relativity (GR) is extended by an additional scalar curvature term R^2, is one of the best-fitting models of current data [4].

In the dual scalar-tensor theory, the presence of the R^2 term makes the scalar degree of freedom dynamical, which can account for cosmic inflation. After the discovery of the Higgs boson at the Large Hadron Collider (LHC) [9, 10], the theory essentially contains two scalar degrees of freedom. Indeed, if the Higgs field Φ couples non-minimally to the Ricci scalar R via a term $\xi_H R|\Phi|^2$, with ξ_H as the nonminimal coupling, the Higgs field itself can induce inflation [11–17] (for earlier works which employed similar mechanisms, see [18–25]). In pure Higgs inflation, i.e. without the presence of such R^2 term, a scale of unitarity violation emerges [26–29]. This may not pose a threat to inflationary dynamics, see Ref. [30]. However, during the preheating stage, longitudinal gauge bosons with momenta beyond the unitarity cut-off scale are violently produced [31–33]. The perturbative unitarity is restored up to the Planck scale due to the presence of R^2 term in R^2-Higgs inflation [34] (see also e.g. [35–46]). Moreover, R^2-Higgs inflation (or the Starobinsky-Higgs

inflation), which features both the R^2 and $R|\Phi|^2$ terms, is also the best-fit model for the Planck data.

Following on from these successes, it is not unreasonable to correlate the R^2-Higgs inflation to the other shortcomings of the current microscopic theory of interactions, the Standard Model of Particle Physics (SM). One such shortfall is the observed matter-antimatter asymmetry (or the Baryon asymmetry) of the Universe, BAU. The existence of the BAU is a strong indicator of the presence of interactions beyond the SM. A range of particle physics experiments, chiefly at the LHC, are searching for such interactions at the currently largest available energy scales of $\mathcal{O}$(TeV). If the fundamental scale of the mechanism behind the BAU is tied to a higher scale, it might be possible that tell-tale effects at present or even future colliders could remain absent. In the SM, the CP-violation from the CKM matrix is not sufficient for baryogenesis [47–49]. Further, the electroweak phase transition in the SM is a continuous crossover [50] rather than the typically desired strong first-order transition to drive the departure from thermal equilibrium condition as part of Sakharov's criteria [51]. However, even at the crossover, the out-of-equilibrium condition can be met if the source and washout decay rates are different and shut off at different epochs [52, 53]. If the inflaton field couples to the CP-odd hypercharge Chern-Simons density $F\tilde{F}$, with F and $\tilde{F}$ denoting the field-stress tensor of a $U(1)$ gauge field (which mixes with the hypercharge gauge field) and its dual, respectively, helical hypermagnetic fields can be abundantly produced at the end of inflation [54–59]. The helical hypermagnetic fields may then create the observed baryon asymmetry at the electroweak crossover [53, 60–65].

In this article, we investigate baryogenesis in R^2-Higgs inflation from CP-violating dimension-six Chern-Simons density $\sim (R/\Lambda^2)B_{\mu\nu}\widetilde{B}^{\mu\nu}$, where R is the Ricci scalar and $B_{\mu\nu}$ is the field stress tensor of $U(1)_Y$ hypercharge in the Jordan frame (see also Refs. [66–70] for similar discussions). This term can be considered within the context extended theories of gravity (or rather, $f(R, \phi, B_\mu)$ gravity), and it elegantly connects high-scale BAU to inflationary dynamics without requiring additional fields beyond the SM. Adopting the covariant formalism due to the non-canonical kinetic terms in R^2-Higgs inflation, our linear order analysis, with $\Lambda \sim 10^{-5}M_{\rm P}$, demonstrates that the produced helical hypermagnetic fields are sufficient to account for the BAU. We take into account effects that could lead to a washout of the helicity stored in the gauge sector (e.g. the chiral plasma instability) alongside observational bounds on a range of associated phenomena that prevent total freedom of the possible field configurations.

In the presence of strong gauge fields, light fermions charged under the gauge group are produced by the backreaction of gauge fields that source the fermions equation of motion [71, 72]. The corresponding currents can then, in turn, backreact on the produced gauge fields, a phenomenon called the *Schwinger effect*, see e.g. Ref. [73]. The backreaction of fermion currents on the produced gauge fields acts as a damping force during the explosive production of helical gauge fields, and many of the conclusions from the gauge field production should be revised in the presence of the Schwinger effect. In particular, it has been shown that, although the amount of gauge energy density is suppressed, which jeopardizes the gauge preheating capabilities, there is still a window for the baryogenesis mechanism, see Ref. [65]. Also, one possible way out is if there are no light, charged fermion fields when gauge fields are produced, for instance by the use of a special Froggatt-Nielsen mechanism such that all fermion Yukawa couplings stay large at the end of inflation, while they relax after inflation to the measured values [74]. However, in this paper, we will stay agnostic on the fermions effect in the plasma and provide the results with and without the Schwinger effect.

We organize this paper as follows. We start with outlining the action and derive the relevant equations of motion (EoM) for different fields in Sec. 2, followed by the inflationary dynamics in the covariant formalism in Sec. 3. The production of hypermagnetic fields and subsequent generation

of the BAU are discussed, respectively, in Sec. 4 and Sec. 5. We summarize with some discussion in Sec. 6. Finally, we present some technical computational details through appendices A-E.

2 The Starobinsky-Higgs Action

In pure GR with a canonically coupled scalar theory, without the presence of R^2, the conformal mode of the metric is known to have a wrong-sign kinetic term. The Starobinsky inflation model, which extends pure GR with an additional scalar curvature term R^2, falls within the so-called general $f(R)$ theory of gravity. In its dual scalar-tensor theory, the presence of the R^2 term makes the scalar degree of freedom dynamical, which can then account for cosmic inflation. R^2-Higgs inflation (or Starobinsky-Higgs inflation), which features all possible dimension-four terms i.e. both the R^2 and $R|\Phi|^2$ terms also provide best-fit models of the Planck data. The model has two dynamical scalar degrees of freedom, one appearing from the gravity sector and one entering as part of the Higgs field Φ.

We briefly discuss the action and its transformation properties in the metric formalism assuming the affine connection to be the Levi-Civita connection. The action in the Jordan frame of R^2-Higgs inflation, along with a dimension-six CP-odd term coupling Ricci scalar and $U(1)_Y$ gauge boson, is given by

$$S_J = \int d^4x\sqrt{-g_J}\Big[\frac{M_{\rm P}^2}{2}f(R_J,\Phi,B_\mu) - g_J^{\mu\nu}(\nabla_\mu\Phi)^\dagger\nabla_\nu\Phi - V(\Phi,\Phi^\dagger) - \frac{1}{4}g_J^{\mu\rho}g_J^{\nu\sigma}B_{\mu\nu}B_{\rho\sigma} - \frac{1}{4}g_J^{\mu\rho}g_J^{\nu\sigma}W^i_{\mu\nu}W^i_{\rho\sigma} - \sum_f g_J^{\mu\nu}\bar{f}e^a_\mu\tilde{\gamma}_a\nabla^f_\nu f\Big], \tag{2.1}$$

and we adopt a mostly-plus convention for the metric $(-1,+1,+1,+1)$. From here on, for notational simplicity, we will remove the sum over fermions $\sum_f$ in the fermion quadratic terms, which will remain implicit. The $B_{\mu\nu}$ and $W^i_{\mu\nu}$ are field stress tensors of the $U(1)_Y$ and $SU(2)_L$ gauge groups, respectively, Φ is the Higgs field, R_J the Ricci scalar in the Jordan frame, and $M_{\rm P} = \sqrt{1/(8\pi G)} = 2.435\times10^{18}$ GeV, where G is the Newton's constant and $M_{\rm P}$ the reduced Planck mass. We use the convention $\epsilon^{0123} = 1$ for the Levi-Civita tensor. The covariant derivatives are defined as

$$\nabla_\mu = D_\mu + ig'\frac{1}{2}Q_{Y_f}B_\mu + ig\frac{1}{2}\boldsymbol{\tau}\cdot\boldsymbol{W}_\mu, \tag{2.2a}$$

$$\nabla^f_\mu f = \left(D^f_\mu + ig'\frac{1}{2}Q_{Y_f}B_\mu + ig\frac{1}{2}\boldsymbol{\tau}\cdot\boldsymbol{W}_\mu\right)f, \tag{2.2b}$$

with Q_{Y_f} denoting the $U(1)_Y$ hypercharge, $\boldsymbol{\tau}$ are the Pauli matrices, and g' and g are respective gauge couplings. D_μ is the usual covariant derivative with respect to the space-time metric $g_{J\mu\nu}$ and $D^f_\mu \equiv \partial_\mu + \Gamma_\mu$ is the covariant derivative of spinors, with Γ_μ as the spin affine connection. Here e^a_μ is the so-called vierbein and $\tilde{\gamma}_a$ is Minkowski space gamma matrices (see Appendix A for details of the formalism and the definition of Γ_μ). The corresponding field-stress tensors for the $U(1)_Y$ and $SU(2)_L$ gauge fields are

$$B_{\mu\nu} = D_\mu B_\nu - D_\nu B_\mu, \qquad W^i_{\mu\nu} = D_\mu W^i_\nu - D_\nu W^i_\mu - g\sum_{j,k=1}^{3}\epsilon_{ijk}W^j_\mu W^k_\nu. \tag{2.3}$$

The Higgs potential $V(\Phi,\Phi^\dagger)$ and $f(R_J,\Phi,B_\mu)$ are given as[1]

$$V(\Phi,\Phi^\dagger) = \lambda|\Phi|^4, \tag{2.4a}$$

[1] For large configuration values of the Higgs field we can consistently neglect the mass term of the Higgs potential, which triggers electroweak symmetry breaking.

$$f(R_J,\Phi,B_\mu) \;=\; R_J+\frac{\xi_R}{2M_{\rm P}^2}R_J^2+\frac{2\xi_H}{M_{\rm P}^2}|\Phi|^2R_J-\frac{2}{\Lambda^2M_{\rm P}^2}\frac{\epsilon^{\mu\nu\rho\sigma}}{\sqrt{-g_J}}B_{\mu\nu}B_{\rho\sigma}R_J. \tag{2.4b}$$

The Higgs field has hypercharge +1 and is decomposed in the standard way (we will comment on our gauge choice further below)

$$\Phi=\frac{1}{\sqrt{2}}\begin{pmatrix}0\\h\end{pmatrix}. \tag{2.5}$$

With this choice, Eq. (2.1) becomes

$$\begin{aligned}S_J=\int d^4x\sqrt{-g_J}\Big[&\frac{M_{\rm P}^2}{2}f(R_J,h,B_\mu)-\frac{1}{2}g_J^{\mu\nu}(D_\mu h)D_\nu h-V(h)\\&-\frac{1}{4}g_J^{\mu\nu}g^2h^2\frac{(W_\mu^1-iW_\mu^2)}{\sqrt{2}}\frac{(W_\nu^1+iW_\nu^2)}{\sqrt{2}}-\frac{1}{8}g_J^{\mu\nu}h^2\left(gW_\mu^3-g'B_\mu\right)\left(gW_\nu^3-g'B_\nu\right)\\&-\frac{1}{4}g_J^{\mu\rho}g_J^{\nu\sigma}B_{\mu\nu}B_{\rho\sigma}-\frac{1}{4}g_J^{\mu\rho}g_J^{\nu\sigma}W_{\mu\nu}^iW_{\rho\sigma}^i-g_J^{\mu\nu}\bar{f}e_\mu^a\tilde{\gamma}_a\nabla_\nu^f f\Big],\end{aligned} \tag{2.6}$$

with

$$V(h)=\frac{\lambda}{4}h^4,\quad f(R_J,h,B_\mu)=R_J+\frac{\xi_R}{2M_{\rm P}^2}R_J^2+\frac{\xi_H}{M_{\rm P}^2}h^2R_J-\frac{2}{\Lambda^2M_{\rm P}^2}\frac{\epsilon^{\mu\nu\rho\sigma}}{\sqrt{-g_J}}B_{\mu\nu}B_{\rho\sigma}R_J. \tag{2.7}$$

The dynamics of the scalar degrees of freedom are easily captured once we move from the Jordan frame to the Einstein frame via a Weyl transformation. We first introduce an auxiliary field Ψ and rewrite the action in Eq. (2.6) as

$$\begin{aligned}S_J=\int d^4x\sqrt{-g_J}\Big[&\frac{M_{\rm P}^2}{2}\left(f(\Psi,h,B_\mu)+\frac{\partial f(\Psi,h,B_\mu)}{\partial\Psi}(R_J-\Psi)\right)-\frac{1}{2}g_J^{\mu\nu}(D_\mu h)(D_\nu h)-V(h)\\&-\frac{1}{4}g_J^{\mu\nu}g^2h^2\frac{(W_\mu^1-iW_\mu^2)}{\sqrt{2}}\frac{(W_\nu^1+iW_\nu^2)}{\sqrt{2}}-\frac{1}{8}g_J^{\mu\nu}h^2\left(gW_\mu^3-g'B_\mu\right)\left(gW_\nu^3-g'B_\nu\right)\\&-\frac{1}{4}g_J^{\mu\rho}g_J^{\nu\sigma}B_{\mu\nu}B_{\rho\sigma}-\frac{1}{4}g_J^{\mu\rho}g_J^{\nu\sigma}W_{\mu\nu}^iW_{\rho\sigma}^i-g_J^{\mu\nu}\bar{f}e_\mu^a\tilde{\gamma}_a\nabla_\nu^f f\Big].\end{aligned} \tag{2.8}$$

The variation with respect to Ψ gives the constraint $\Psi=R_J$ as long as $\partial^2 f(\Psi,h,B_\mu)/\partial\Psi^2\neq 0$. We now define a physical degree of freedom Θ as

$$\Theta=\frac{\partial f(\Psi,h,B_\mu)}{\partial\Psi} \tag{2.9}$$

such that the action Eq. (2.8) can be cast into

$$\begin{aligned}S_J=\int d^4x\sqrt{-g_J}\Big[&\frac{M_{\rm P}^2}{2}\Theta R_J-U(\Theta,h,B_\mu)-\frac{1}{2}g_J^{\mu\nu}(D_\mu h)(D_\nu h)-V(h)-\frac{1}{4}g_J^{\mu\rho}g_J^{\nu\sigma}B_{\mu\nu}B_{\rho\sigma}\\&-\frac{1}{4}g_J^{\mu\nu}g^2h^2\frac{(W_\mu^1-iW_\mu^2)}{\sqrt{2}}\frac{(W_\nu^1+iW_\nu^2)}{\sqrt{2}}-\frac{1}{8}g_J^{\mu\nu}h^2\left(gW_\mu^3-g'B_\mu\right)\left(gW_\nu^3-g'B_\nu\right)\\&-\frac{1}{4}g_J^{\mu\rho}g_J^{\nu\sigma}W_{\mu\nu}^iW_{\rho\sigma}^i-g_J^{\mu\nu}\bar{f}e_\mu^a\tilde{\gamma}_a\nabla_\nu^f f\Big],\end{aligned} \tag{2.10}$$

with the definition

$$\begin{aligned} U(\Theta, h, B_\mu) &= \frac{M_{\rm P}^2}{2}\left[\Psi(\Theta)\Theta - f(\Psi(\Theta), h, B_\mu)\right] \\ &= \frac{M_{\rm P}^4}{4\xi_R}\left(1 - \Theta + \frac{\xi_H}{M_{\rm P}^2}h^2 - \frac{2}{\Lambda^2 M_{\rm P}^2}\frac{\epsilon^{\mu\nu\rho\sigma}}{\sqrt{-g_J}}B_{\mu\nu}B_{\rho\sigma}\right)^2. \end{aligned} \tag{2.11}$$

To formulate the action in the Einstein frame, we perform the metric redefinition (Weyl transformation)

$$g_{J\mu\nu} = \frac{1}{\Theta}\, g_{E\mu\nu}, \quad g_J^{\mu\nu} = \Theta\, g_E^{\mu\nu}, \text{ and } \sqrt{-g_J} = \frac{1}{\Theta^2}\sqrt{-g_E}. \tag{2.12}$$

Under this transformation, the Ricci scalar transforms as

$$R_J = \Theta\left[R_E + 3\Box_E\Theta - \frac{3}{2}g_E^{\mu\nu}D_\mu(\ln\Theta)D_\nu(\ln\Theta)\right], \tag{2.13}$$

with $\Box_E = g_E^{\mu\nu}D_\mu D_\nu$. Ignoring the surface term, the action of Eq. (2.8) now becomes

$$\begin{aligned} S_E = \int d^4x\sqrt{-g_E}\Big[&\frac{M_{\rm P}^2}{2}R_E - \frac{3M_{\rm P}^2}{4}g_E^{\mu\nu}D_\mu(\ln\Theta)D_\nu(\ln\Theta) - \frac{1}{2\Theta}g_E^{\mu\nu}(D_\mu h)(D_\nu h) - V_E \\ &- \frac{1}{4}g_E^{\mu\rho}g_E^{\nu\sigma}B_{\mu\nu}B_{\rho\sigma} - \frac{1}{4\Theta}g_E^{\mu\nu}g^2h^2\frac{(W_\mu^1 - iW_\mu^2)}{\sqrt{2}}\frac{(W_\nu^1 + iW_\nu^2)}{\sqrt{2}} \\ &- \frac{1}{8\Theta}g_E^{\mu\nu}h^2\left(gW_\mu^3 - g'B_\mu\right)\left(gW_\nu^3 - g'B_\nu\right) - \frac{1}{4}g_E^{\mu\rho}g_E^{\nu\sigma}W_{\mu\nu}^iW_{\rho\sigma}^i - \frac{1}{\Theta}g_E^{\mu\nu}\bar{f}e_\mu^a\tilde{\gamma}_a\nabla_\nu^f f\Big], \end{aligned} \tag{2.14}$$

with

$$V_E = \frac{1}{\Theta^2}\left[V(h) + U(\Theta, h, B_\mu)\right]. \tag{2.15}$$

Finally, we perform the field redefinition

$$\phi = M_{\rm P}\sqrt{\frac{3}{2}}\ln\Theta. \tag{2.16}$$

to arrive at the action in the form

$$\begin{aligned} S_E = \int d^4x\sqrt{-g_E}\,\Big[&\frac{M_{\rm P}^2}{2}R_E - \frac{1}{2}G_{IJ}g_E^{\mu\nu}D_\mu\phi^I D_\nu\phi^J - V_E(\phi^I) - \frac{1}{4}g_E^{\mu\rho}g_E^{\nu\sigma}B_{\mu\nu}B_{\rho\sigma} \\ &- \frac{1}{4}g_E^{\mu\rho}g_E^{\nu\sigma}W_{\mu\nu}^iW_{\rho\sigma}^i - \frac{1}{4}e^{-\sqrt{\frac{2}{3}}\frac{\phi}{M_{\rm P}}}g_E^{\mu\nu}g^2h^2\frac{(W_\mu^1 - iW_\mu^2)}{\sqrt{2}}\frac{(W_\nu^1 + iW_\nu^2)}{\sqrt{2}} \\ &- \frac{1}{8}e^{-\sqrt{\frac{2}{3}}\frac{\phi}{M_{\rm P}}}g_E^{\mu\nu}h^2\left(gW_\mu^3 - g'B_\mu\right)\left(gW_\nu^3 - g'B_\nu\right) - e^{-\sqrt{\frac{2}{3}}\frac{\phi}{M_{\rm P}}}g_E^{\mu\nu}\bar{f}e_\mu^a\tilde{\gamma}_a\nabla_\nu^f f\Big]. \end{aligned} \tag{2.17}$$

The multi-field $\phi^I \in \{\phi, h\}$ alongside the field-space metric G_{IJ}

$$G_{\phi\phi} = 1,\ G_{\phi h} = G_{h\phi} = 0,\ G_{hh} = e^{-\sqrt{\frac{2}{3}}\frac{\phi}{M_{\rm P}}} \tag{2.18}$$

highlight that we are working with a non-canonical kinetic term as alluded to above (see Appendix B for the corresponding field-space Christoffel symbols). The potential $V_E(\phi^I)$, consistently truncated at dimension-six level, reads

$$V_E(\phi^I) = e^{-2\sqrt{\frac{2}{3}}\frac{\phi}{M_{\rm P}}}\left[\frac{\lambda}{4}h^4 + \frac{M_{\rm P}^4}{4\xi_R}\left(1 - e^{\sqrt{\frac{2}{3}}\frac{\phi}{M_{\rm P}}} + \frac{\xi_H}{M_{\rm P}^2}h^2 - \frac{2}{\Lambda^2M_{\rm P}^2}\frac{\epsilon^{\mu\nu\rho\sigma}}{\sqrt{-g_E}}e^{2\sqrt{\frac{2}{3}}\frac{\phi}{M_{\rm P}}}B_{\mu\nu}B_{\rho\sigma}\right)^2\right]$$

$$= V_0(\phi^I) + \frac{2M_{\rm P}^2}{\xi_R \Lambda^2} F(\phi^I) e^{\sqrt{\frac{2}{3}}\frac{\phi}{M_{\rm P}}} B_{\mu\nu}\tilde{B}^{\mu\nu}, \tag{2.19}$$

with

$$V_0(\phi^I) = \frac{\lambda}{4} h^4 e^{-2\sqrt{\frac{2}{3}}\frac{\phi}{M_{\rm P}}} + \frac{M_{\rm P}^4}{4\xi_R} F^2(\phi^I), \tag{2.20a}$$

$$F(\phi^I) = 1 - e^{-\sqrt{\frac{2}{3}}\frac{\phi}{M_{\rm P}}} + \frac{\xi_H}{M_{\rm P}^2} h^2 e^{-\sqrt{\frac{2}{3}}\frac{\phi}{M_{\rm P}}}, \quad \tilde{B}^{\mu\nu} = \frac{1}{2\sqrt{-g_E}} \epsilon^{\mu\nu\rho\sigma} B_{\rho\sigma}. \tag{2.20b}$$

Note that the unmodified Starobinsky potential is recovered when the term that contains $B_{\mu\nu}\tilde{B}^{\mu\nu}$ is absent.

We can now turn to the EoMs of the different fields in Eq. (2.17). By varying Eq. (2.17) with respect to the field ϕ, we obtain

$$\Box\phi^K + \Gamma^K_{IJ}\, g_E^{\alpha\nu} D_\alpha \phi^I D_\nu \phi^J - G^{KM} V_{E,M} + g_E^{\mu\nu} \mathcal{X}^K_{\mu\nu} = 0, \tag{2.21}$$

identifying Γ^K_{IJ} as the field-space Christoffel symbols and

$$\begin{aligned}
\mathcal{X}^K_{\mu\nu} = {} & \frac{1}{4}\sqrt{\frac{2}{3}}\frac{1}{M_{\rm P}} G^{K1} e^{-\sqrt{\frac{2}{3}}\frac{\phi}{M_{\rm P}}} g^2 h^2 \frac{(W^1_\mu - iW^2_\mu)}{\sqrt{2}} \frac{(W^1_\nu + iW^2_\nu)}{\sqrt{2}} \\
& - \frac{1}{2} e^{-\sqrt{\frac{2}{3}}\frac{\phi}{M_{\rm P}}} G^{K2} g^2 h \frac{(W^1_\mu - iW^2_\mu)}{\sqrt{2}} \frac{(W^1_\nu + iW^2_\nu)}{\sqrt{2}} \\
& + \frac{1}{8}\sqrt{\frac{2}{3}}\frac{1}{M_{\rm P}} G^{K1} e^{-\sqrt{\frac{2}{3}}\frac{\phi}{M_{\rm P}}} h^2 \left(gW^3_\mu - g' B_\mu\right)\left(gW^3_\nu - g' B_\nu\right) \\
& - \frac{1}{4} G^{K2} e^{-\sqrt{\frac{2}{3}}\frac{\phi}{M_{\rm P}}} h \left(gW^3_\mu - g' B_\mu\right)\left(gW^3_\nu - g' B_\nu\right) \\
& + \sqrt{\frac{2}{3}}\frac{1}{M_{\rm P}} \delta_1{}^K e^{-\sqrt{\frac{2}{3}}\frac{\phi}{M_{\rm P}}} g_E^{\mu\nu} \bar{f} t^a_\mu \tilde{\gamma}_a \nabla_\nu f.
\end{aligned} \tag{2.22}$$

Note that all the terms in $\mathcal{X}^K_{\mu\nu}$ are quadratic in the gauge fields.

The energy-momentum tensor $T_{\mu\nu}$ describes relevant quantities of the inflationary dynamics such as energy density or pressure. One can derive the Einstein-Hilbert equation from the action S_E by varying it with respect to $g_E^{\mu\nu}$

$$R_{E\mu\nu} - \frac{1}{2} g_{E\mu\nu} R_E = \frac{1}{M_{\rm P}^2}\left(\mathcal{L}_M g_{E\mu\nu} - 2\frac{\delta(\mathcal{L}_M)}{\delta g_E^{\mu\nu}}\right) \tag{2.23}$$

and identify $T_{\mu\nu}$ as

$$T_{\mu\nu} = \left(\mathcal{L}_M g_{E\mu\nu} - 2\frac{\delta(\mathcal{L}_M)}{\delta g_E^{\mu\nu}}\right). \tag{2.24}$$

Appendix C provides the full expression of $T_{\mu\nu}$ for the model considered in this work.

The EoM for the gauge field B_μ is given as

$$\begin{aligned}
g_E^{\mu\alpha} g_E^{\nu\beta} D_\alpha B_{\mu\nu} + \frac{8M_{\rm P}^2}{\xi_R \Lambda^2} D_\alpha \left(F(\phi^I) e^{\sqrt{\frac{2}{3}}\frac{\phi}{M_{\rm P}}}\right) \tilde{B}^{\alpha\beta} + \left[\frac{g'}{4} e^{-\sqrt{\frac{2}{3}}\frac{\phi}{M_{\rm P}}} g_E^{\mu\beta} h^2 (gW^3_\mu - g' B_\mu)\right] \\
- \frac{ig' Q_{Y_f}}{2} e^{-\sqrt{\frac{2}{3}}\frac{\phi}{M_{\rm P}}} g_E^{\mu\beta} \bar{f} e^a_\mu \tilde{\gamma}_a f = 0,
\end{aligned} \tag{2.25}$$

and those for the W^i_μ fields are found to be

$$g_E^{\mu\alpha}g_E^{\nu\beta}D_\alpha W^i_{\mu\nu} - g g_E^{\mu\beta}g_E^{\nu\sigma}\sum_{j,k=1}^{3}\epsilon_{ijk}W^j_{\mu\nu}W^k_\sigma - \frac{g}{4}g_E^{\mu\beta}e^{-\sqrt{\frac{2}{3}}\frac{\phi}{M_{\rm P}}}h^2\mathcal{W}^i_\mu + \frac{ig}{2}e^{-\sqrt{\frac{2}{3}}\frac{\phi}{M_{\rm P}}}g_E^{\mu\beta}\bar{f}e^a_\mu\tilde{\gamma}_a\tau^i f = 0,$$
$$\text{with } \mathcal{W}^i_\mu = \begin{cases} gW^i_\mu, \text{if } \ i=1,2 \\ gW^3_\mu - g'B_\mu, \text{if } i=3 \end{cases} . \quad (2.26)$$

We define W_μ, Z_μ and A_μ in the usual way

$$W_\mu = \frac{W^1_\mu - iW^2_\mu}{\sqrt{2}}, \quad W^\dagger_\mu = \frac{W^1_\mu + iW^2_\mu}{\sqrt{2}}$$
$$A_\mu = \sin\theta_W W^3_\mu + \cos\theta_W B_\mu, \quad Z_\mu = \cos\theta_W W^3_\mu - \sin\theta_W B_\mu, \quad (2.27)$$

with $e = g\sin\theta_W = g'\cos\theta_W$, and electroweak angle θ_W. We can express the W^i_μ and B_μ fields in terms of W_μ, Z_μ and A_μ by inverting the above equations.

Given that we are in the broken phase, for which $h_0 \neq 0$, where h_0 is the homogeneous background field as we shall see shortly, we can consider the trivial solution $\mathcal{W}^i_\mu = 0$ from the mass term in Eq. (2.26) as the variation is small compared to the background field. This means that we can set $W_\mu = W^\dagger_\mu = 0$ and $Z_\mu = \cos\theta_W W^3_\mu - \sin\theta_W B_\mu = 0$ which implies that $B_\mu = \cos\theta_W A_\mu$ and $W^3_\mu = \sin\theta_W A_\mu$. We will therefore retain only the photon field A_μ, replacing B_μ with $\cos\theta_W A_\mu$ in the corresponding Chern-Simons term. Put differently, the production of photon fields proceeds unsuppressed compared to the other heavy gauge bosons.

We now turn to some comments related to the gauge fixing in Eq. (2.5). The Higgs doublet contains, apart from the radial degree of freedom h, three Goldstone bosons $\vec{\chi}$. Using $SU(2)_L$ gauge invariance, and fixing the corresponding gauge parameter $\vec{\alpha}(x)$ as $\vec{\alpha}(x) = -\vec{\chi}(x)$ (unitary gauge), the Goldstone bosons disappear from the Lagrangian and the Higgs doublet reduces to Eq. (2.5). There is still the $U(1)$ gauge invariance that can be used to fix the Coulomb gauge for the electromagnetic field $\partial^i A_i = 0$. This is done by fixing the hypercharge gauge field B_μ as $\partial^i B_i = -\tan\theta_W \partial^i W^3_i$. Moreover, in regions where the electric charge density is zero, it turns out that $A_0 = 0$ (the radiation gauge we use in this paper). Therefore, the EoM for the A_μ field simplifies to

$$g_E^{\mu\alpha}g_E^{\nu\beta}D_\alpha F_{A\mu\nu} + \frac{8\cos^2\theta_W M_{\rm P}^2}{\xi_R\Lambda^2}\partial_\alpha\left(F(\phi^I)e^{\sqrt{\frac{2}{3}}\frac{\phi}{M_{\rm P}}}\right)\tilde{F}_A^{\alpha\beta}$$
$$= ieQ_f\, e^{-\sqrt{\frac{2}{3}}\frac{\phi}{M_{\rm P}}}g_E^{\mu\beta}\bar{f}e^a_\mu\tilde{\gamma}_a f, \quad (2.28)$$

with $Q_f = \frac{1}{2}Q_{Y_f} + T_{3f}$, where T_3 is the third component of weak isospin.

Similarly, one can find the general covariant Dirac equation as

$$g_E^{\mu\nu}e^a_\mu\tilde{\gamma}_a(\nabla^f_\nu f) = 0. \quad (2.29)$$

3 Inflationary Dynamics in the Covariant Formalism

We now study the inflationary dynamics of our two-field scenario with the non-canonical kinetic term (i.e. with a nontrivial field-space manifold) following the covariant formalism discussed in

Refs. [33, 75, 76] (see also Refs. [31, 77–88]). Focussing on linear order perturbations, we decompose the fields into classical background (φ^I) and perturbation parts ($\delta\phi^I$) as

$$\phi^I(x^\mu) = \varphi^I(t) + \delta\phi^I(x^\mu), \tag{3.1}$$

with $\varphi^I(t) = \{\varphi(t), h_0(t)\}$. The space-time dynamics can be described by the perturbed spatially flat Friedmann-Robertson-Walker (FRW) metric, which is expanded as [89–91]

$$ds^2 = -(1+2\mathcal{A})dt^2 + 2a(t)(\partial_i\mathcal{B})dx^i dt + a(t)^2\left[(1-2\psi)\delta_{ij} + 2\partial_i\partial_j\mathcal{E}\right]dx^i dx^j. \tag{3.2}$$

$a(t)$ denotes the scale factor, t parametrizes cosmic time, and $\mathcal{A}, \mathcal{B}, \psi$ and $\mathcal{E}$ characterize the scalar metric perturbations. Like the scalar fields, the space-time metric is also considered up to first order in the perturbations. In the following, when deriving the background and perturbation equations for scalar and gauge fields, we shall adopt the longitudinal gauge, i.e. $\mathcal{B} = \mathcal{E} = 0$.

One may define covariant field fluctuations $\mathcal{Q}^I$ (covariant with respect to the field-space metric) that connect $\phi^I(x^\mu)$ and $\varphi^I(t)$ along the geodesic of the field-space manifold with affine connection κ. Concretely, we can take $\phi^I(\kappa = 0) = \varphi^I$, $\phi^I(\kappa = \kappa') = \varphi^I + \delta\phi^I$ and $D_\kappa\phi^I|_{\kappa=0} = d\phi^I/d\kappa|_{\kappa=0} \equiv \mathcal{Q}^I$, such that with these conditions, the unique field-space vector $\mathcal{Q}^I$ connects ϕ^I and φ^I [75]. Note here, that D_κ is the covariant derivative with respect to the affine connection. The field fluctuations $\delta\phi^I$ can be expressed in a series of $\mathcal{Q}^I$ as [75, 85]

$$\delta\phi^I = \mathcal{Q}^I - \frac{1}{2}\Gamma^I_{JK}\mathcal{Q}^I\mathcal{Q}^J + \frac{1}{3!}\left(\Gamma^I_{MN}\Gamma^N_{JK} - \Gamma^I_{JK,M}\right)\mathcal{Q}^I\mathcal{Q}^J\mathcal{Q}^M + \ldots, \tag{3.3}$$

where the Christoffel symbols Γ^I_{JK} are evaluated at the background field order. The field fluctuations $\delta\phi^I(x^\mu)$ are gauge-dependent quantities under both the field-space transformation $\varphi^I \to \varphi'^I$, as well as the space-time transformation $x^\mu \to x'^\mu$. This is motivation to formulate gauge-independent Mukhanov-Sasaki variables, which are a linear combinations of space-time metric perturbation ψ and covariant field fluctuations $\mathcal{Q}^I$ as [90, 92, 93]

$$Q^I = \mathcal{Q}^I + \frac{\dot\varphi^I}{H}\psi. \tag{3.4}$$

We remark that, while φ^I is not a vector of the field-space manifold, $\mathcal{Q}^I$, $\dot\varphi^I$ and Q^I all transform, indeed, as vectors of the field-space manifold. The Q^I is doubly covariant with respect to both space-time and field-space transformations to first order in the perturbations. It is useful to define the covariant derivative of vectors S^I and S_I in the field-space as

$$\mathcal{D}_J S^I \equiv \partial_J S^I + \Gamma^I_{JK}S^K, \qquad \mathcal{D}_J S_I \equiv \partial_J S_I - \Gamma^K_{IJ}S_K. \tag{3.5}$$

It is convenient to also define a covariant derivative with respect to cosmic time t

$$\mathcal{D}_t S^I \equiv \dot\varphi^J\mathcal{D}_J S^I = \dot S^I + \Gamma^I_{JK}S^J\dot\varphi^K, \tag{3.6}$$

see also Refs. [83, 84, 94–96].

We turn to the stress-energy tensor $T_{\mu\nu}$, which can be written for the homogeneous, isotropic and spatially flat metric $\tilde g_{E\mu\nu} = \mathrm{diag}(-1, a^2(t), a^2(t), a^2(t))$ as

$$T_{\mu\nu} = (p+\rho)U_\mu U_\nu + p\, g_{\mu\nu}, \tag{3.7}$$

with a choice of $U_\mu = (1,0,0,0)$ for the fluid four-velocity. For a spatially flat metric, employing Eq. (3.7) and the Einstein equations, we get the Friedmann equations for the background order

$$H^2 = \left(\frac{\dot a}{a}\right)^2 = \frac{1}{3M_{\rm P}^2}\rho, \quad \text{and} \quad \dot H = -\frac{1}{2M_{\rm P}^2}(p+\rho), \tag{3.8}$$

where p and ρ are pressure and energy density, respectively. We can compare the 00 and ij component of Eq. (2.24) and Eq. (3.7) to get expressions for pressure p and energy density ρ,

$$\rho = T_{00}, \quad p = \frac{1}{3a^2}\sum_{i=1}^{3} T_{ii}. \tag{3.9}$$

At the considered background order, employing the explicit expression of Eq. (C.5) (see Appendix C), the (inflaton) pressure and energy density reduce to

$$\rho = \frac{1}{2}G_{IJ}\dot{\varphi}^I\dot{\varphi}^J + V_0(\varphi^I), \tag{3.10a}$$

$$p = \frac{1}{2}G_{IJ}\dot{\varphi}^I\dot{\varphi}^J - V_0(\varphi^I), \tag{3.10b}$$

yielding the equation of state

$$w = \frac{p}{\rho} = \frac{G_{IJ}\dot{\varphi}^I\dot{\varphi}^J - 2V_0}{G_{IJ}\dot{\varphi}^I\dot{\varphi}^J + 2V_0}. \tag{3.11}$$

Furthermore, the Hubble parameter and its derivative with respect to cosmic time take the form

$$H^2 = \left(\frac{\dot{a}}{a}\right)^2 = \frac{1}{3M_{\rm P}^2}\left(\frac{1}{2}G_{IJ}\dot{\varphi}^I\dot{\varphi}^J + V_0(\varphi^I)\right), \tag{3.12a}$$

$$\dot{H} = -\frac{1}{2M_{\rm P}^2}\left(G_{IJ}\dot{\varphi}^I\dot{\varphi}^J\right). \tag{3.12b}$$

The EoMs for the background fields φ^I and the perturbations Q^I at linear order can be derived utilizing Eq. (3.4), and Eq. (2.21)

$$\mathcal{D}_t\dot{\varphi}^I + 3H\dot{\varphi}^I + G^{IJ}V_{0,J} = 0, \tag{3.13a}$$

$$\mathcal{D}_t^2 Q^I + 3HD_tQ^I + \frac{k^2}{a^2}\delta^I_J Q^J + \mathcal{M}^I_L Q^L = 0, \tag{3.13b}$$

with

$$\mathcal{M}^I_L = G^{IJ}(\mathcal{D}_L\mathcal{D}_J V_0) - \mathcal{R}^I_{JKL}\dot{\varphi}^J\dot{\varphi}^K - \frac{1}{M_{\rm P}^2 a^3}\mathcal{D}_t\left(\frac{a^3}{H}\dot{\varphi}^I\dot{\varphi}_L\right), \tag{3.14}$$

and the field-space Riemann tensor $\mathcal{R}^I_{JKL}$. All relevant quantities such as V_0, G^{IJ}, Γ^I_{JK}, $\mathcal{R}^I_{JKL}$ in Eqs. (3.13) are evaluated at background order. Moreover, as the field-space metric G^{IJ} and M^{IJ} are diagonal in this approximation, the first-order perturbations do not mix the different Q^I. Note also that the EoMs for background and perturbations do not depend on the gauge fields for our linear-order considerations.

To study perturbations, we can find a set of unit vectors that differentiate between adiabatic and entropy directions. Firstly, we define the length of the velocity vector $\dot{\varphi}^I$ in field-space defined as

$$\dot{\sigma} = \sqrt{G_{IJ}\dot{\varphi}^I\dot{\varphi}^J} = \sqrt{\rho + p} \tag{3.15}$$

and the corresponding unit vector

$$\hat{\sigma}^I = \frac{\dot{\varphi}^I}{\dot{\sigma}}. \tag{3.16}$$

With this, we can rewrite Eq. (3.13a) to reproduce a single-field model with a canonically normalized kinetic term. The slow-roll parameters ϵ and η are

$$\epsilon = -\frac{\dot{H}}{H^2} = \frac{3\dot{\sigma}^2}{\dot{\sigma}^2 + 2V_0}, \tag{3.17a}$$

$$\eta = M_{\rm P}^2 \frac{\mathcal{M}_{\sigma\sigma}}{V_0}, \tag{3.17b}$$

with $\mathcal{M}_{\sigma\sigma} \equiv \hat{\sigma}_I \hat{\sigma}^J \mathcal{M}^I_J = \hat{\sigma}^I \hat{\sigma}^J (\mathcal{D}_I \mathcal{D}_J V_0)$. Inflation ends when the slow-roll parameter reaches $\epsilon = 1$, and we denote the corresponding cosmological time as $t_{\rm end}$ in the following.

The field-space directions orthogonal to $\hat{\sigma}^I$ are given by

$$\hat{s}^{IJ} = G^{IJ} - \hat{\sigma}^I \hat{\sigma}^J, \tag{3.18}$$

and $\hat{\sigma}^I$ and $\hat{s}^{IJ}$ tensors are related by relations [31]

$$\hat{\sigma}^I \hat{\sigma}_I = 1, \quad \hat{s}^{IJ} \hat{s}_{IJ} = N - 1, \quad \hat{\sigma}_I \hat{s}^{IJ} = 0 \text{ for each } J. \tag{3.19}$$

$N = 2$, and $I, J = 1, 2$ in our two-field scenario. We can now decompose the perturbations in the directions of $\hat{\sigma}^I$ and $\hat{s}^{IJ}$ as

$$Q_\sigma = \hat{\sigma}_I Q^I, \tag{3.20}$$

$$\delta s^I = \hat{s}^I{}_J Q^J, \tag{3.21}$$

with Q_σ and δs^I being referred to as adiabatic and entropy perturbations, respectively. We also define a "turning vector" ω^I as the covariant rate of change of $\hat{\sigma}^I$,

$$\omega^I = \mathcal{D}_t \hat{\sigma}^I. \tag{3.22}$$

The turning vector is orthogonal with respect to $\hat{\sigma}^I$, $\omega_I \hat{\sigma}^I = 0$, the corresponding unit vector is

$$\hat{\omega}^I = \frac{\omega^I}{\omega}, \tag{3.23}$$

with $\omega = |\omega^I| = \sqrt{G_{IJ} \omega^I \omega^J}$.

With these definitions in place, we can now define the entropy perturbations as

$$Q_s = \hat{\omega}_I Q^I, \tag{3.24}$$

which are conveniently normalized to give

$$\mathcal{S} = \frac{H}{\dot{\sigma}} Q_s. \tag{3.25}$$

The gauge-invariant curvature (adiabatic) perturbation $\mathcal{R}$ [90, 91, 97]

$$\mathcal{R} = \psi - \frac{H}{\rho + p} \delta q, \tag{3.26}$$

with ρ, p as defined above, and δq given by $\partial_i \delta q = -T_{0i}$ evaluated at background order (cf. Appendix C) together with Eqs. (3.3) and (3.4)

$$\delta q = -G_{IJ} \dot{\varphi}^I \delta\phi^J = -\dot{\sigma} \hat{\sigma}_I \left(Q^I - \frac{\dot{\varphi}^I}{H} \psi \right). \tag{3.27}$$

Therefore, $\mathcal{R}$ takes the compact form

$$\mathcal{R} = \psi + \frac{H}{\dot{\sigma}^2}\dot{\sigma}\hat{\sigma}_I\left(Q^I - \dot{\sigma}\frac{\hat{\sigma}^I}{H}\psi\right) = \frac{H}{\dot{\sigma}}Q_\sigma, \tag{3.28}$$

at linear order. In the presence of entropy perturbations, the gauge-invariant curvature perturbation does not need to be conserved, $\dot{\mathcal{R}} \neq 0$. The non-adiabatic pressure perturbation is given by [91, 97]

$$\delta p_{\rm nad} = \delta p - \frac{\dot{p}}{\dot{\rho}}\delta\rho = -\frac{2\hat{\sigma}^I\partial_I V}{3H\dot{\sigma}}\epsilon_m + 2\dot{\sigma}\left(\omega_I\delta s^I\right). \tag{3.29}$$

with ϵ_m as the comoving density perturbation. For super-horizon scales $k \ll aH$, the only source of non-adiabatic pressure stems from δs^I. This means that $\dot{\mathcal{R}} \neq 0$ will not vanish even at the $k \ll aH$ scale and $\omega_I\delta s^I$ will source Q_σ and hence $\dot{\mathcal{R}}$.

The gauge invariant curvature perturbation is defined as [90, 97]

$$\langle\mathcal{R}(\boldsymbol{k}_1)\mathcal{R}(\boldsymbol{k}_2)\rangle = (2\pi)^3\delta^{(3)}(\boldsymbol{k}_1+\boldsymbol{k}_2)P_{\mathcal{R}}(t;k_1) \tag{3.30}$$

and $P_{\mathcal{R}}(t;k) = |\mathcal{R}|^2$. The dimensionless power spectrum for the adiabatic perturbation is given by

$$\mathcal{P}_{\mathcal{R}}(t;k) = \frac{k^3}{2\pi^2}|\mathcal{R}|^2. \tag{3.31}$$

Similarly, the power spectrum for the entropy perturbations is

$$\mathcal{P}_{\mathcal{S}}(t;k) = \frac{k^3}{2\pi^2}|\mathcal{S}|^2. \tag{3.32}$$

To find the power spectra of the curvature and isocurvature (entropy) perturbations, Eqs. (3.31) and (3.32), we utilize the quantities H, ϵ and unit vectors such as $\hat{\sigma}^I$, $\hat{\omega}^I$,..., from the solutions of the Eqs. (3.12a) and (3.13a) while Q_σ and Q_s are evaluated using the solutions of mode equations from Eq. (3.13b). For a given Fourier mode k, we calculate the different power spectra at the $t = t_{\rm end}$ numerically as a function of k as

$$\mathcal{P}_{\mathcal{R}}(k) = \mathcal{P}_{\mathcal{R}}(t_{\rm end};k), \qquad \mathcal{P}_{\mathcal{S}}(k) = \mathcal{P}_{\mathcal{S}}(t_{\rm end};k), \tag{3.33}$$

where $t_{\rm end}$ denotes the time when inflation ends, i.e. when $\epsilon = 1$.

The spectral index n_s of the power spectrum of the curvature perturbation is defined as

$$n_s = 1 + \frac{d\ln\mathcal{P}_{\mathcal{R}}(k)}{d\ln k}. \tag{3.34}$$

As we will discuss in the next section, although our scenario involves scalar fields h and ϕ, we shall primarily focus on a scenario where the dynamics are essentially described by single field-like inflation. In such a case, the spectral index can be calculated as

$$n_s(t_*) \approx 1 - 6\epsilon(t_*) + 2\eta(t_*), \tag{3.35}$$

where t_* denotes the time when the reference scale exited the horizon and the tensor-to-scalar ratio is given by $r \approx 16\epsilon$.

We choose three benchmark points to highlight quantitatively the implications of consistent inflation parameter choices when contextualized with baryogenesis. These are summarized in Tab. I

BP	ξ_R	ξ_H	$\varphi(t_{\rm in})$ $[M_{\rm P}]$	$h_0(t_{\rm in})$ $[M_{\rm P}]$
a	2.35×10^9	10^{-3}	5.5	2×10^{-4}
b	2.55×10^9	1	5.5	8.94×10^{-4}
c	2.2×10^9	10	5.4	5.00×10^{-3}

TABLE I: Benchmark points chosen for our analysis. Scales are given in units of the Planck mass $M_{\rm P}$. See text for details.

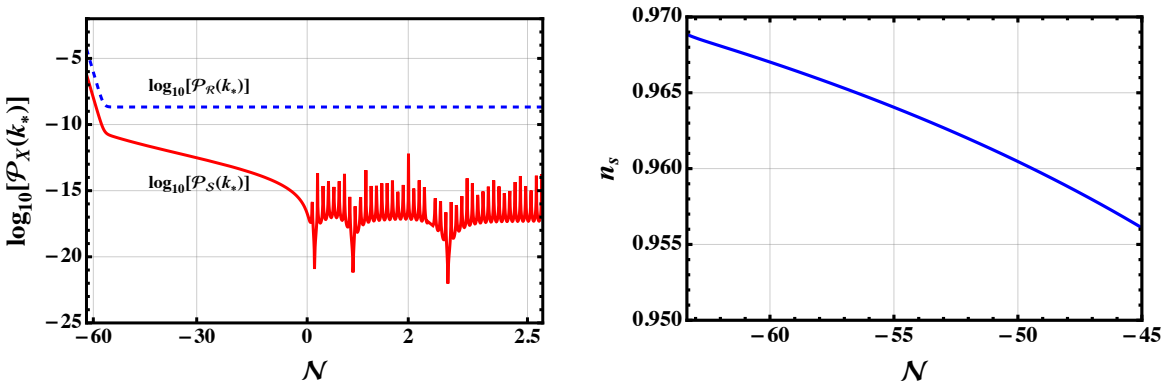

FIG. 1: The power spectra of the adiabatic and isocurvature modes and the spectral index n_s for the parameter values of BPa in Tab. I.

alongside the required initial field values to satisfy Planck 2018 measurements: At the pivot scale $k = k_*$, the amplitude of $\mathcal{P}_\mathcal{R}(k)$ should match the scalar amplitude measurement of Ref. [4]

$$A_s = (2.099 \pm 0.014) \times 10^{-9} \text{ at } 68\% \text{ CL}. \tag{3.36}$$

As a guideline for our parameter choices and the initial values of the background fields, we follow the valley approximation that we discuss in Appendix D. We note that, whilst finding the parameter sets, we also ensure that the isocurvature mode remains orders of magnitude smaller than the curvature perturbation. The background equations are solved with initial conditions $\varphi(t_{\rm in})$ and $h_0(t_{\rm in})$ as in Tab. I, with vanishing time derivatives; $t_{\rm in}$ denotes the initial time for our numerical analysis in the following. The perturbation equations (3.13b) are solved with approximate initial conditions for a Fourier mode k

$$Q^I(t) \simeq \frac{H}{\sqrt{2k^3}}\left(i + \frac{k}{aH}\right) \exp\left\{i\frac{k}{aH}\right\}, \tag{3.37}$$

sufficiently in the past such that the Hubble parameter at $t_{\rm in}$ remains approximately constant. In practice, we initialize the Q^I and their derivatives about four e-foldings before they exit the horizon for each mode.

In Fig. 1, we show the evolution of power spectra $\mathcal{P}_\mathcal{R}$ and $\mathcal{P}_\mathcal{S}$ (for the pivot scale $k = k_*$) and the spectral index n_s for BPa. Note, when calculating both power spectra, we solve Eq. (3.31) and Eq. (3.32) numerically without any assumption related to slow-roll. It is clear from Fig. 1 that the isocurvature mode is orders of magnitude smaller than the adiabatic mode and both power spectra freeze out once they exit the horizon. We remark that while finding the power spectrum we always check the orthogonality conditions of Eq. (3.19) in our numerical analysis. In the following, we interchangeably use the cosmological time t and the number of e-foldings before the end of inflation

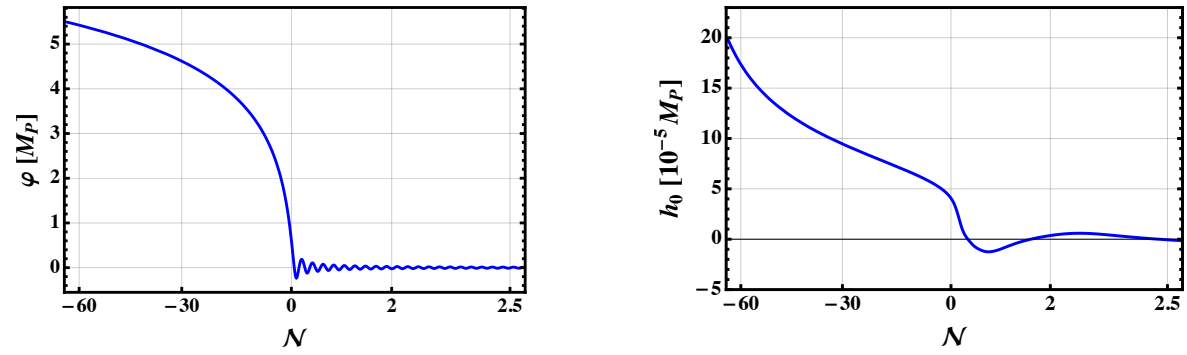

FIG. 2: The evolution of the background fields φ and the h_0 for the parameter values of BPa in Tab. I.

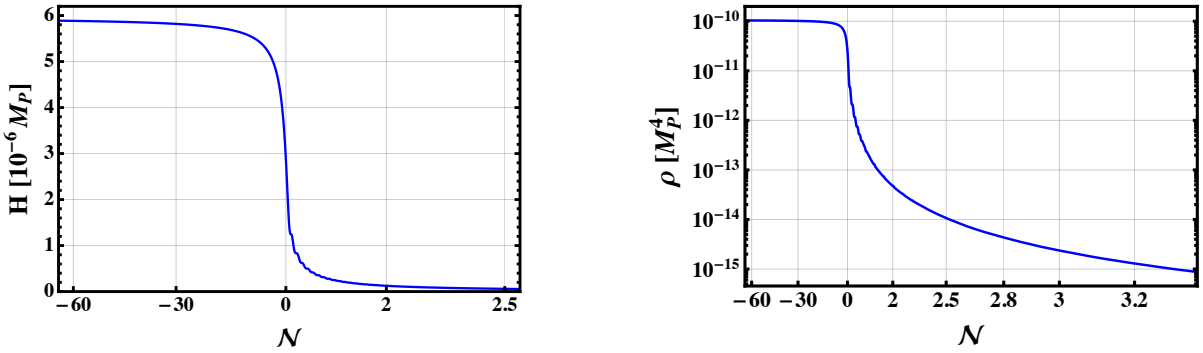

FIG. 3: The Hubble function H and the inflaton energy density ρ as in Eq. (3.10a) for the parameter values of BPa given in Tab. I.

which is defined as

$$\mathcal{N} \equiv \ln \frac{a(t)}{a(t_{\rm end})}. \tag{3.38}$$

The pivot scale k_* exits the horizon $\mathcal{N}_* = 57,\ 59.3,\ 54.9$ e-foldings before the end of inflation for BPa, BPb, and BPc, respectively. For illustration, we also show the fields' time evolution in Fig. 2 for BPa, while, the evolution of the Hubble parameter and the inflaton energy density are shown in Fig. 3. It is also clear from Fig. 1 that the spectral index n_s lies within the Planck 2018 range when the reference scale exits the horizon. The corresponding values of the tensor-to-scalar ratios are $r_* \sim 0.003$, which is consistent with expected values for R^2-Higgs inflation.

4 Gauge Field Production

The EoM for the gauge field A_μ of Eq. (2.28) can be rewritten as

$$\begin{aligned}\frac{1}{\sqrt{-g_E}}\partial_\alpha\left(\sqrt{-g_E}g_E^{\mu\alpha}g_E^{\nu\beta}F_{A\mu\nu}\right) + \frac{8\cos^2\theta_W M_{\rm P}^2}{\xi_R\Lambda^2}\partial_\alpha\left(F(\phi^I)e^{\sqrt{\frac{2}{3}}\frac{\phi}{M_{\rm P}}}\right)\tilde{F}_A^{\alpha\beta} \\ - ieQ_f\, e^{-\sqrt{\frac{2}{3}}\frac{\phi}{M_{\rm P}}} g_E^{\mu\beta}\bar{f}e_\mu^a\tilde{\gamma}_a f = 0,\end{aligned} \tag{4.1}$$

without the presence of a torsion term $F_{A\mu\nu} = D_\mu A_\nu - D_\nu A_\mu = \partial_\mu A_\nu - \partial_\nu A_\mu$. One can identify the fermion current

$$j^\mu = \sum_f ieQ_f\, e^{-\sqrt{\frac{2}{3}}\frac{\phi}{M_{\rm P}}} g_E^{\mu\nu}\bar{f}e_\nu^a\tilde{\gamma}_a f \tag{4.2}$$

that sources the Schwinger effect.

Neglecting the Schwinger effect

First, we consider the scenario without Schwinger effect i.e. when the fermion current is negligible. This is possible if the fermion field values are small. One can now separate the space and time component of the A_μ field. The time component of Eq. (2.25) at linear order in the perturbations is

$$-\frac{1}{a^2}\partial_i\left(\partial_i A_0 - \partial_0 A_i\right) = 0, \tag{4.3}$$

which, in temporal gauge $A_0 = 0$, reduces to $\partial_i \dot{A}_i = 0$. The spatial components of Eq. (2.25) are found to be

$$\ddot{A}_i + H\dot{A}_i - \frac{1}{a^2}\partial_j\left(\partial_j A_i - \partial_i A_j\right) - \frac{\xi H}{a}\epsilon^{ijk}\left(\partial_j A_k - \partial_k A_j\right) = 0. \tag{4.4}$$

where

$$H = \frac{\dot{a}}{a}, \qquad \xi = \frac{4\cos^2\theta_W M_{\rm P}^2}{\xi_R \Lambda^2 H}\,\partial_0\left(F(\varphi^I)e^{\sqrt{\frac{2}{3}}\frac{\varphi}{M_{\rm P}}}\right). \tag{4.5}$$

In momentum space, using the notation $\mathbf{A} \equiv \vec{A}$

$$\mathbf{A}(t,\mathbf{x}) = \int \frac{d^3\mathbf{k}}{(2\pi)^{3/2}}\tilde{\mathbf{A}}(t,\mathbf{k})e^{-i\mathbf{k}\cdot\mathbf{x}}, \tag{4.6}$$

with $|\mathbf{k}| = k$, Eq. (4.4) reads

$$\ddot{\tilde{\mathbf{A}}} + H\dot{\tilde{\mathbf{A}}} + \frac{k^2}{a^2}\tilde{\mathbf{A}} + \frac{2i\xi H}{a}(\mathbf{k}\times\tilde{\mathbf{A}}) = 0. \tag{4.7}$$

The $\tilde{\mathbf{A}}$ field can be written in terms of transverse components as

$$\tilde{\mathbf{A}} = \sum_{\lambda=\pm}\tilde{A}^\lambda(t,\mathbf{k})\;\hat{\epsilon}^\lambda(\mathbf{k}), \;\text{ with } \mathbf{k}\cdot\hat{\epsilon}^\lambda(\mathbf{k}) = 0, \quad i\mathbf{k}\times\hat{\epsilon}^\lambda(\mathbf{k}) = \lambda k\;\hat{\epsilon}^\lambda(\mathbf{k}). \tag{4.8}$$

so that, using conformal time τ (with $\partial_0 = \partial_t = a^{-1}\partial_\tau$), the EoM for the transverse components becomes

$$\partial_\tau^2\tilde{A}^\lambda + \omega_\lambda^2\tilde{A}^\lambda = 0, \tag{4.9}$$

with

$$\omega_\lambda^2(\tau,k) = k^2 + 2\lambda\xi H a k. \tag{4.10}$$

In order to quantize the gauge fields, we first integrate Eq. (4.9) by parts to get the action quadratic in the fields

$$S^\lambda = \int d\tau\,\mathcal{L}_\lambda = \int d\tau\,d^3\mathbf{k}\left[\frac{1}{2}|\partial_\tau\tilde{A}^\lambda|^2 - \frac{1}{2}\omega_\lambda^2(\tau,k)|\tilde{A}^\lambda|^2\right]. \tag{4.11}$$

As we deal with non-canonical kinetic terms, we apply the quantization procedure detailed in Ref. [98]. The canonical momentum of the transverse modes are

$$\pi_\lambda(\tau,\mathbf{k}) = \frac{\delta\mathcal{L}_\lambda}{\delta\left(\partial_\tau\tilde{A}^\lambda(\tau,-\mathbf{k})\right)}, \tag{4.12}$$

with the commutation relation expressed as

$$\left[\tilde{A}^{\lambda}(\tau,\mathbf{k}),\partial_{\tau}\tilde{A}^{\lambda'}(\tau,\mathbf{q})\right]=i\delta_{\lambda\lambda'}\delta(\mathbf{k}+\mathbf{q}). \tag{4.13}$$

The field operator $\tilde{A}^{\lambda}(\tau,\mathbf{k})$ can be written as creation and annihilation operators

$$\tilde{A}^{\lambda}(\tau,\mathbf{k})=\hat{a}^{\lambda}_{\mathbf{k}}u^{\lambda}_{k}(\tau)+\hat{a}^{\lambda}_{-\mathbf{k}}u^{\lambda}_{k}(\tau), \tag{4.14}$$

and the mode equations for the gauge fields are then

$$\ddot{u}^{\lambda}+H\dot{u}^{\lambda}+\frac{\omega^{2}_{\lambda}}{a^{2}}\,u^{\lambda}=0. \tag{4.15}$$

From these mode functions, we can compute the gauge observables, namely the magnetic and electric fields' energy densities, magnetic helicity and its derivative, defined as

$$\rho_{B} = \frac{1}{a^{4}}\int_{k_{\rm min}}^{k_{c}}dk\frac{k^{4}}{4\pi^{2}}\sum_{\lambda}|u^{\lambda}|^{2}, \tag{4.16a}$$

$$\rho_{E} = \frac{1}{a^{4}}\int_{k_{\rm min}}^{k_{c}}dk\frac{k^{2}}{4\pi^{2}}\sum_{\lambda}|\partial_{\tau}u^{\lambda}|^{2}, \tag{4.16b}$$

$$\mathcal{H} = \frac{1}{a^{3}}\int_{k_{\rm min}}^{k_{c}}dk\frac{k^{3}}{2\pi^{2}}\left(|u^{+}|^{2}-|u^{-}|^{2}\right), \tag{4.16c}$$

$$\mathcal{G} = \frac{1}{2}\frac{\partial\mathcal{H}}{\partial t}, \tag{4.16d}$$

with the cut-off value given by [65, 99]

$$k_{c}=2\left|aH\,\xi\right|, \tag{4.17}$$

defined by the condition $\omega^{2}_{\lambda}(\tau,k_{c})=0$ satisfied by the helicity λ such that $\mathrm{sign}(\lambda\xi)=-1$. The corresponding $U(1)_{Y}$ quantities are linked to the electromagnetic ones via

$$\begin{aligned}\rho_{B_{Y}}&=\rho_{B}\,\cos^{2}\theta_{W} & \rho_{E_{Y}}&=\rho_{E}\,\cos^{2}\theta_{W}\\ \mathcal{H}_{Y}&=\mathcal{H}\,\cos^{2}\theta_{W} & \mathcal{G}_{Y}&=\mathcal{G}\,\cos^{2}\theta_{W}\end{aligned} \tag{4.18}$$

In general, the integration limits should cover all modes from zero to infinity, however, not all modes are amplified during inflation. At the time t, the cut-off mode k_{c} is found by the solution of $\omega_{\lambda}=0$; essentially this is when a mode $k=k_{c}$ crosses the horizon for the first time (at least for one helicity). The modes $k\gg k_{c}$ are not excited during inflation and can be neglected for the estimation of the above observable quantities. We will discuss $k_{\rm min}$ shortly.

In order to find ρ_{B}, ρ_{E}, $\mathcal{H}$ and $\mathcal{G}$ we solve Eq. (4.15) numerically via fourth-order Runge-Kutta (RK4) method in discrete time steps. We outline the details in Appendix E. For the i-th time step, the gauge field modes are initialized with the Bunch-Davies (BD) initial condition as [100]

$$u_{\lambda}(k,t_{i})\simeq\frac{1}{\sqrt{2k}}e^{-i\omega_{i}t_{i}}, \qquad \dot{u}_{\lambda}\simeq-i\frac{\omega_{i}}{\sqrt{2k}}e^{-i\omega_{i}t_{i}}, \tag{4.19}$$

with $\omega_{i}=ka^{-1}(t_{i})$. It is practically not possible to go to the infinite past. Hence, to ensure that all modes remain well within the horizon at the initial time step $t_{\rm in}$, we chose $k_{\rm min}=x_{\rm BD}a(t_{\rm in})H(t_{\rm in})$ with $x_{\rm BD}=100$. On the one hand, if a mode k remains well within the horizon, $k>x_{\rm BD}\,a(t_{i})H(t_{i})$,

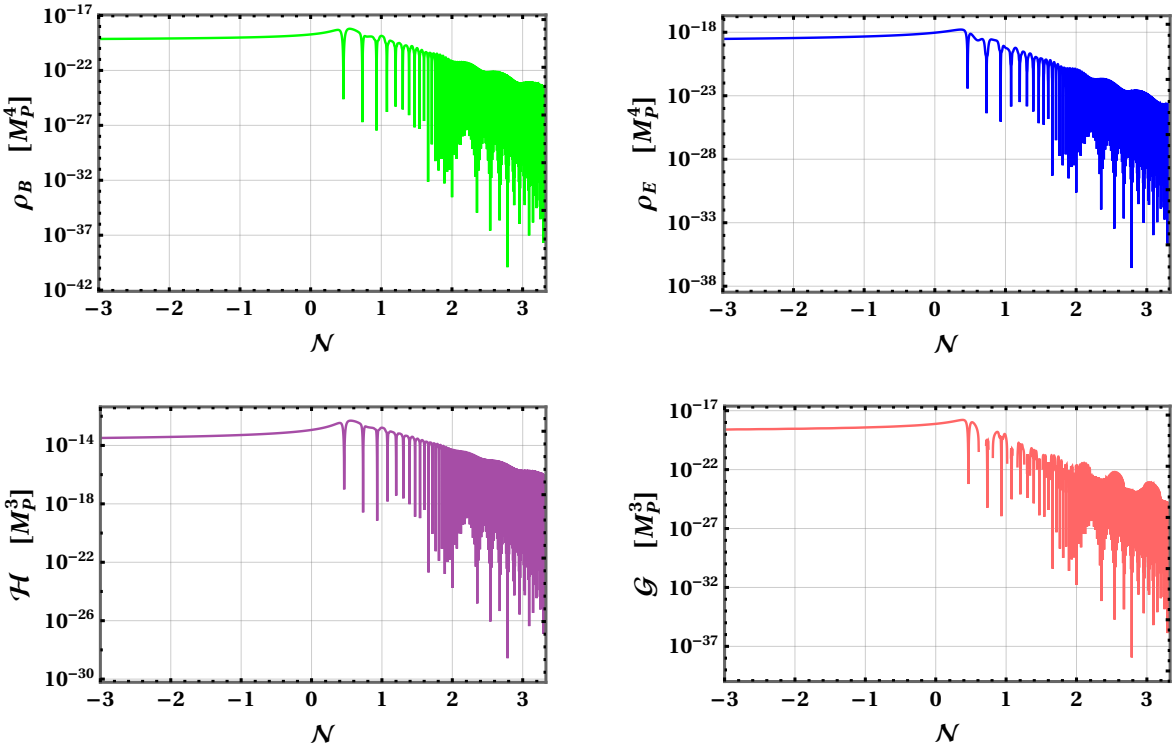

FIG. 4: In the upper panel we plot the energy densities ρ_B and ρ_E with $\Lambda = 2.55 \times 10^{-5}\ M_{\rm P}$ for the BPa summarized in Tab. I. The lower panel corresponds to the hyperhelical magnetic fields $\mathcal{H}$ and $\mathcal{G}$ for identical parameter choices.

we directly assume the BD solutions for the modes instead of applying the RK4 method for any subsequent time step. On the other hand, all superhorizon modes are solved with the RK4 method. For the numerical solution discussed below, we employ 25k time steps.

In Fig. 4, we show the evolution of ρ_B, ρ_E, $\mathcal{H}$ and $\mathcal{G}$ for BPa with $\Lambda = 2.55 \times 10^{-5} M_{\rm P}$ for illustration. Similar values are found for the other benchmark points. We remark that we have compared our numerical results to the analytical approximation of the magnetic and electric fields' energy densities, magnetic helicity, and its derivative as in Ref. [65] and find good agreement.

Relevance of the Schwinger effect

We now turn to the impact of the Schwinger effect. The fermion current of Eq. (4.2) can be expressed as

$$j^\mu = (\rho_{\rm c}, \boldsymbol{J}) \tag{4.20}$$

The current and the gauge field are related by Ohm's law

$$\boldsymbol{J} = \sigma_{\rm c}\, \boldsymbol{E} = -\sigma_{\rm c}\, \partial_\tau \boldsymbol{A}, \tag{4.21}$$

where the conductivity $\sigma_{\rm c}$ has been defined as a comoving quantity. The physical conductivity $\sigma_{\rm ph}$ relates to the comoving one via $\sigma_{\rm c} = a\, \sigma_{\rm ph}$. In the case of one Dirac fermion f with mass m_f and charge Q_f under a $U(1)$ group with coupling g, the comoving conductivity associated to f can be written as [71]

$$\sigma_f^{\rm c} = \frac{|g\, Q_f|^3}{6\pi^2} \frac{a}{H} \sqrt{2\rho_B}\, \coth\left(\pi \sqrt{\frac{\rho_B}{\rho_E}}\right) \exp\left\{ -\frac{\pi m_f^2}{\sqrt{2\rho_E}\, |g\, Q_f|} - \sqrt{\frac{2}{3}} \frac{\varphi}{M_{\rm P}} \right\}, \tag{4.22}$$

where $m_f \equiv m_f(h_0) = m_f(v)h_0/v$ and so that

$$\sigma_{\rm c} = \sum_f \sigma_f^{\rm c} = \sum_\ell \sigma_\ell^{\rm c} + N_c \sum_q \sigma_q^c, \tag{4.23}$$

with $\ell = e, \mu, \tau$; $q = u, d, c, s, t, b$, $N_c = 3$ being the number of colors. Last, since we are in the broken phase, we identify g as the electric charge $g \equiv e \simeq 0.71$ at the scale in which inflation takes place.

This conductivity is to be distinguished from the conductivity of a thermal plasma after reheating in a radiation-dominated universe. We stress that the above is the conductivity at the end of inflation, before the reheating, produced by fermion pair formation from the magnetic field. Also, this estimation is valid in the case of collinear electric and magnetic fields, an assumption that we have numerically checked. Finally, the electric and magnetic fields are assumed to be slowly varying, as we expect the hypercharge gauge field to reach a stationary configuration, where the tachyonic instability and the induced current balance each other. We have verified in our numerical simulation that this is indeed the case.

In the presence of the fermion current, Eq. (4.7) becomes

$$\ddot{\tilde{\mathbf{A}}} + (H + \sigma_{\rm ph})\,\dot{\tilde{\mathbf{A}}} + \frac{k^2}{a^2}\,\tilde{\mathbf{A}} + \frac{2iH\xi}{a}\,(\mathbf{k}\times\tilde{\mathbf{A}}) = 0, \tag{4.24}$$

which, for the transverse components in conformal time reads as

$$\partial_\tau^2 \tilde{A}^\lambda + \sigma_{\rm c}\,\partial_\tau \tilde{A}^\lambda + \omega_\lambda^2 \tilde{A}^\lambda = 0, \tag{4.25}$$

which can be recast as

$$\partial_\tau^2 \tilde{A}^\lambda + \left(\frac{\partial}{\partial\tau}\log(\Delta(\tau))\right)\partial_\tau \tilde{A}^\lambda + \omega_\lambda^2 \tilde{A}^\lambda = 0, \tag{4.26}$$

with

$$\Delta(\tau) = \exp\left\{\int_{-\infty}^{\tau} \sigma_{\rm c}(\tau')\,d\tau'\right\}. \tag{4.27}$$

Integrating Eq. (4.26) by parts as in the previous subsection, one can now define the canonical momentum for the transverse modes as

$$\pi_\lambda(\tau,\mathbf{k}) = \frac{\delta\mathcal{L}_\lambda}{\delta\left(\partial_\tau \tilde{A}^\lambda(\tau,-\mathbf{k})\right)} = \Delta(\tau)\partial_\tau \tilde{A}^{\lambda\prime}(\tau,\mathbf{k}), \tag{4.28}$$

and the commutation relation now becomes [98]

$$\left[\tilde{A}^\lambda(\tau,\mathbf{k}), \partial_\tau \tilde{A}^{\lambda'}(\tau,\mathbf{q})\right] = i\frac{1}{\Delta(\tau)}\delta_{\lambda\lambda'}\delta(\mathbf{k}+\mathbf{q}), \quad \text{with, } \tilde{A}^\lambda(\tau,\mathbf{k}) = \hat{a}^\lambda_{\mathbf{k}} u^\lambda_k(\tau) + \hat{a}^\lambda_{-\mathbf{k}} u^\lambda_k(\tau). \tag{4.29}$$

The mode equations for the gauge fields in the presence of the Schwinger effect become

$$\ddot{u}^\lambda + (H+\sigma_{\rm c})\dot{u}^\lambda + \frac{k}{a}\left(\frac{k}{a} + 2\lambda H\xi\right)u^\lambda = 0, \tag{4.30}$$

and the cut-off momenta k_c is now modified to

$$k_c = |aH\,\xi| + \sqrt{(aH\,\xi)^2 + \frac{a^2}{2}\left[\dot{\sigma}_{\rm ph} + \sigma_{\rm ph}\left(\frac{\sigma_{\rm ph}}{2} + H\right)\right]}\,. \tag{4.31}$$

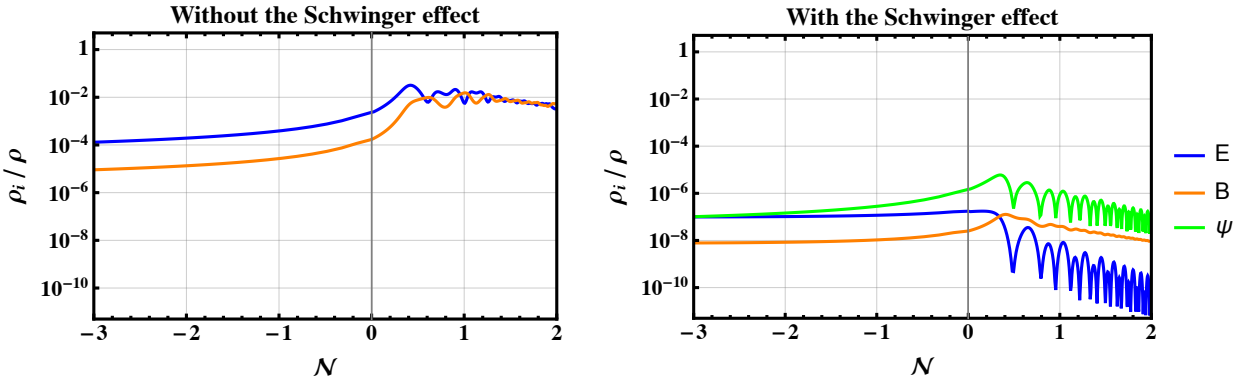

FIG. 5: Energy breakdown for $\xi_R = 2.35 \times 10^9$, $\xi_H = 10^{-3}$ and $\Lambda = 2 \times 10^{-5} M_{\rm P}$ at the end of inflation and the onset of reheating. We show a comparison between the absence and the presence of the Schwinger effect for the quantities $\rho_i(\mathcal{N})/\rho(\mathcal{N})$, $i = E, B, \psi$. When the Schwinger effect is strong, like here, the fermion energy density can dominate over the gauge density. Still, all energy shares are reduced in the presence of the Schwinger effect.

At early times solution of the mode equations of Eq. (4.30) are represented by WKB solution [33, 98]

$$u^\lambda(\tau) = \frac{1}{\sqrt{2}} \frac{1}{\sqrt{\Delta(\tau)\omega_\lambda(\tau,k)}}\, e^{-i\int_{\tau_{\rm in}}^{\tau} d\tau' \omega_\lambda(\tau',k)} \tag{4.32}$$

as long as $|\frac{\partial_\tau \omega_\lambda}{\omega_\lambda}| \ll 1$. In practice, we utilize the early-time solution for the modes

$$u^\lambda(\tau) = \frac{1}{\sqrt{2}} \frac{1}{\sqrt{\Delta(\tau)\omega_\lambda(\tau,k)}}\, e^{-ik\tau} \tag{4.33}$$

to find relevant, observable quantities. From Eq. (4.30) and Eq. (4.31), we find the energy densities for BPa and display them in the right panel of Fig. 5.

Due to the coupling between the fermion and gauge sectors, massless hypercharged fermions are continuously produced during inflation. They are massless as long as the EW symmetry remains intact and thus contribute to the energy density of relativistic radiation as

$$\rho_\psi = \lim_{V\to\infty} \frac{\sigma_{\rm c}}{V} \int_V d^3x\, \frac{\langle \boldsymbol{A}\cdot\boldsymbol{E}\rangle}{a^4} = \frac{\sigma_{\rm c}}{a^4} \int_{k_{\rm min}}^{k_c} dk\, \frac{k^2}{2\pi^2} \frac{d}{d\tau} \sum_\lambda |u^\lambda|^2. \tag{4.34}$$

It has been shown in Ref. [99] that the fermion energy density can easily dominate over the energy densities of E and B fields at the end of inflation. This situation has been chosen as an example in Fig. 5 where we display the energy fraction $\rho_i(\mathcal{N})/\rho(\mathcal{N})$, $i = E, B, \psi$ at the end of inflation and the onset of reheating. We show a direct comparison between the presence and the absence of the Schwinger effect. While for $\Lambda \gtrsim 4 \times 10^{-5} M_{\rm P}$ the difference is an order one factor, the Schwinger effect reduces the amount of electromagnetic energy and helicity up to two orders of magnitude for $\Lambda \simeq 2.4 \times 10^{-5} M_{\rm P}$, see Fig. 7. This is because the presence of the Schwinger effect trades an exponential behaviour in ξ with a polynomial one.

When the gauge share dominates at least by 80%, the Universe will reheat before the perturbative decay of the inflaton [100], a phenomenon called *gauge preheating*. As in Ref. [65], we found that preheating is unlikely since the ratio is $\sim 10^{-6}$ at most. However, the huge damping in both energy and helicity does not preclude a window in the parameter space where the BAU is achieved, as we will see in the next section.

5 Baryogenesis

To generate a baryon asymmetry, the Sakharov conditions [51] must be met: *(i)* the system must contain a process that violates the baryon number, *(ii)*, this process also violates C/CP symmetries, *(iii)* this process occurs out of thermal equilibrium. In the SM, the CP-violating term from the CKM matrix phase is too small to induce a significant baryon asymmetry at a low energy scale, hence we included the dimension-six CP-odd term between Ricci scalar and $U(1)_Y$ gauge boson. On the other hand, in the symmetric phase of the EW plasma, the SM exhibits a chiral anomaly that is enough to source the present-day BAU. The anomaly expresses the fact that the $B+L$ anomaly, the $U(1)_Y$ helicity and the weak sphaleron are connected as

$$\Delta N_B = \Delta N_L = N_g \left(\Delta N_{\rm CS} - \frac{g'^2}{16\pi^2}\, \Delta \mathcal{H}_Y \right). \tag{5.1}$$

The factor $N_g = 3$ is the number of fermion generations and g' is the $U(1)_Y$ gauge coupling. Under the thermal fluctuation of the $SU(2)_L$ gauge fields, the Chern-Simons number $N_{\rm CS}$ is diffusive, resulting in the rapid washout of both lepton N_L and baryon N_B numbers. On the contrary, a helical primordial magnetic field acts as a source, and a net baryon asymmetry can remain after the EW phase transition.

In Refs. [53, 60], the effects of the helicity decay and sphaleron washout balance have been studied within a careful analysis of the transport equations for all SM species during the EWPT. As a result, a non-zero baryon-to-entropy ratio η_B remains in the broken phase while the transformation of baryon asymmetry back into helicity is avoided. The novelty of the mechanism lies in the introduction of a time-dependent (temperature-dependent) weak mixing angle $\theta_W(T)$ which enters an additional source of the baryon number into the kinetic equation. When the EW symmetry breaking occurs at $T \simeq 160$ GeV, the primordial hypermagnetic field becomes an electromagnetic field. However, the electroweak sphaleron remains in equilibrium until $T \simeq 130$ GeV and threatens to washout the baryon asymmetry. Therefore proper modeling of the epoch 160 GeV $\gtrsim T \gtrsim$ 130 GeV is critical to an accurate prediction of the relic BAU.

The behavior of $\theta_W(T)$ is confirmed by analytic calculations [50], and numerical lattice simulations [101]. We follow Refs. [60, 61] and model it with a smooth step function

$$\cos^2\theta_W = \frac{g^2}{g'^2+g^2} + \frac{1}{2}\frac{g'^2}{g'^2+g^2}\left(1+\tanh\left[\frac{T-T_{\rm step}}{\Delta T}\right]\right) \tag{5.2}$$

which, for $155\,{\rm GeV} \lesssim T_{\rm step} \lesssim 160\,{\rm GeV}$ and $5\,{\rm GeV} \lesssim \Delta T \lesssim 20\,{\rm GeV}$, describes reasonably well the analytical and lattice results for the temperature dependence. Consequently, it is possible to generate the observed BAU from a maximally helical magnetic field that was generated before the EW crossover. Indeed, including all contributions, the Boltzmann equation for the baryon-to-entropy ratio η_B reads

$$\frac{d\eta_B}{dx} = -\frac{111}{34}\gamma_{W\rm sph}\,\eta_B + \frac{3}{16\pi^2}(g'^2+g^2)\sin(2\theta_W)\frac{d\theta_W}{dx}\frac{\mathcal{H}_Y}{s}, \tag{5.3}$$

where $x = T/H(T)$, with $H(T)$ being the Hubble rate at temperature T, $\mathcal{H}_Y$ the hypermagnetic helicity that is initially present and s the comoving entropy density of the SM plasma given by $s = (2\pi^2/45)g_* T^3$. Furthermore, $\gamma_{W\rm sph} = 6\,\Gamma_{W\rm sph}/T^4$ is the dimensionless transport coefficient for the EW sphaleron which, for temperatures $T < 161$ GeV, is found from lattice simulations to be [102]

$$\gamma_{W\rm sph} \simeq \exp\left\{-147.7 + 107.9\,\frac{T}{130\,{\rm GeV}}\right\}. \tag{5.4}$$

The Boltzmann equation (5.3) has been numerically solved in Ref. [60] and the baryon-to-entropy ratio η_B was found to become frozen, i.e. $\dot{\eta}_B = 0$, at a temperature $T \simeq 135$ GeV. As expected, this is close to the temperature $T \simeq 130$ GeV at which EW sphalerons freeze out. Setting the RHS of Eq. (5.3) to zero and solving for η_B yields

$$\eta_B \simeq 4 \cdot 10^{-12}\, f_{\theta_W} \frac{\mathcal{H}_Y}{H^3(t_{\rm end})} \left(\frac{H(t_{\rm end})}{10^{13}\,{\rm GeV}}\right)^{\frac{3}{2}} \left(\frac{T_{\rm rh}}{T_{\rm rh}^{\rm ins}}\right), \tag{5.5}$$

where the (instant) reheating temperature is

$$T_{\rm rh} = \left(\frac{90}{\pi^2 g_*}\right)^{\frac{1}{4}} \sqrt{\Gamma_\phi}, \qquad T_{\rm rh}^{\rm ins} = \left(\frac{90}{\pi^2 g_*}\right)^{\frac{1}{4}} \sqrt{H(t_{\rm end})}, \tag{5.6}$$

and Γ_ϕ is the total decay width of the inflaton that reheats the universe after inflation.

All the details on the EWPT dynamics are encoded in the parameter f_{θ_W} which is subject to significant uncertainties

$$f_{\theta_W} = -\sin(2\theta_W) \left.\frac{d\theta_W}{d\log T}\right|_{T=135\ {\rm GeV}}, \qquad 5.6 \cdot 10^{-4} \lesssim f_{\theta_W} \lesssim 0.32. \tag{5.7}$$

The bounds on f_{θ_W} are given by varying $T_{\rm step}$ and ΔT in the ranges given below Eq. (5.2). The result Eq. (5.5) is a main ingredient of this work as it directly relates the amount of the final BAU to the amount of hypermagnetic helicity available at the EWPT.

The production of hypermagnetic fields nevertheless happens at the inflationary scale, hence one must ensure that the helicity is preserved as the Universe cools down in the radiation-dominated era that follows reheating. A rough estimate is to require that the magnetic Reynolds number $\mathcal{R}_m$ is bigger than unity, as this implies that the effects of magnetic induction are dominating over magnetic diffusion in the thermal plasma. On the other hand, the electric Reynolds number $\mathcal{R}_e$ determines in which regime the plasma evolves and informs us how to calculate the magnetic Reynolds number, see e.g. Refs. [62, 64]. In our work, we found that we are in the viscous regime, $\mathcal{R}_e < 1$, and hence we need to satisfy the constraint

$$\mathcal{R}_m^{\rm rh} \approx 5.9 \cdot 10^{-6}\, \frac{\rho_{B_Y} \ell_{B_Y}^2}{H(t_{\rm end})^2} \left(\frac{H(t_{\rm end})}{10^{13}\,{\rm GeV}}\right) \left(\frac{T_{\rm rh}}{T_{\rm rh}^{\rm ins}}\right)^{\frac{2}{3}} > 1, \tag{5.8}$$

where ℓ_{B_Y} is the hypermagnetic characteristic size given by

$$\ell_{B_Y} = \frac{2\pi}{\rho_B\, a^3} \int_{k_{\rm min}}^{k_c} dk\, \frac{k^3}{4\pi^2} \sum_\lambda |u^\lambda|^2. \tag{5.9}$$

The magnetohydrodynamics description of the plasma also admits a CP-odd term that can induce a helicity cancellation because of the fermion asymmetry back-transformation into helical gauge fields with opposite sign. This is because the energy configuration in the gauge sector is more favorable than in the fermion sector [103], a phenomenon called chiral plasma instability (CPI). Thus, one must ensure that all fermion asymmetry created alongside the helical field during inflation is erased by the action of the weak sphaleron for 10^{12} GeV $\gtrsim T \gtrsim 130$ GeV. Because the weak interaction only couples to left-handed fermions, the right-handed fermions are protected from the washout until their Yukawa interaction becomes relevant in thermal equilibrium. The right-handed electron e_R is the last species to come into chemical equilibrium, at temperatures $\sim 10^5$ GeV, thus its asymmetry survives the longest. Therefore, to efficiently erase the fermion asymmetry, while

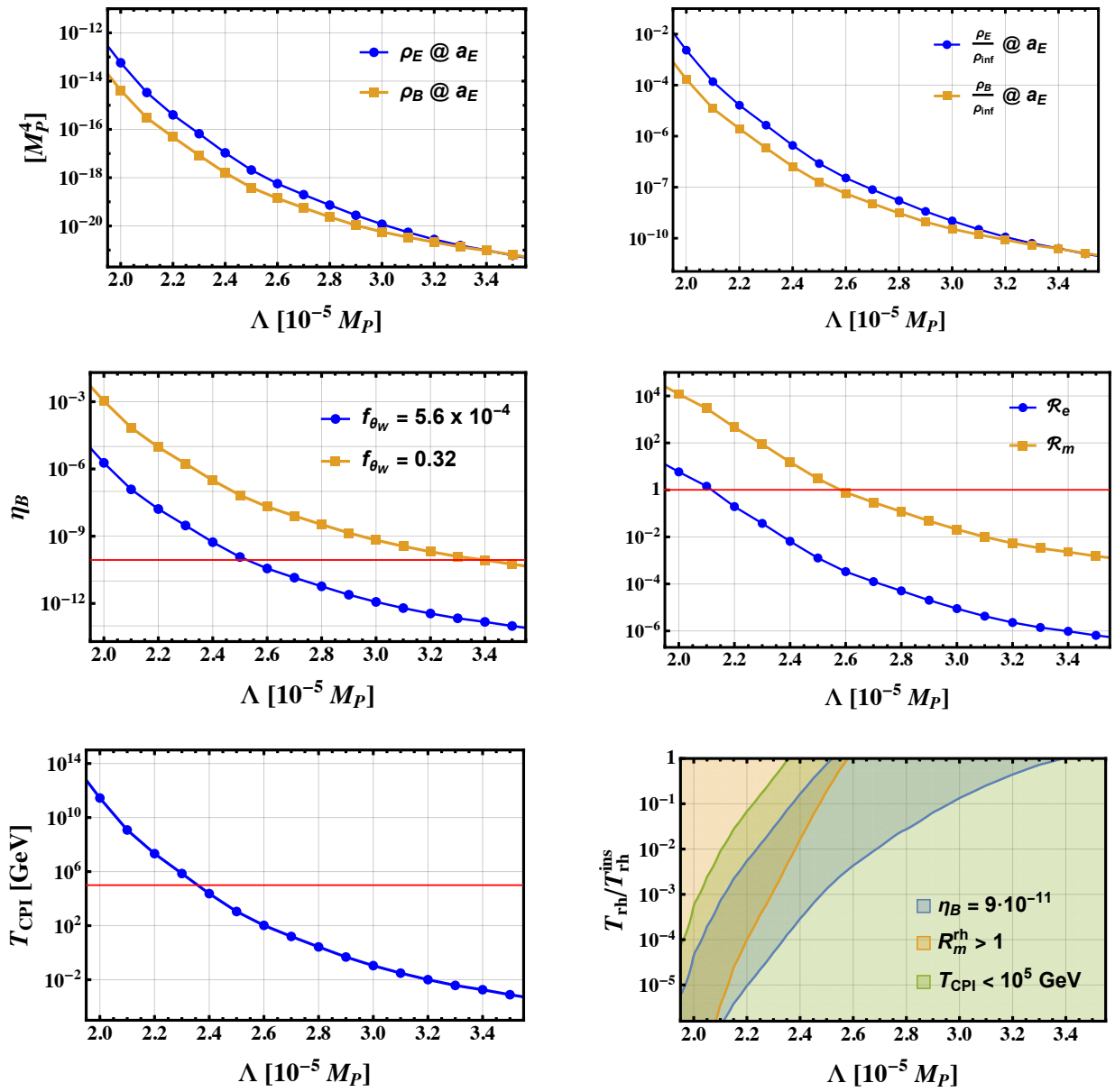

FIG. 6: These figures display a scan of the parameter Λ with the first set of initial conditions, see BPa in Tab. I without Schwinger effect. Top panels: Magnetic and electric energy density (left) and their ratio with the inflation energy density (right). Middle panel: baryon asymmetry η_B (left) and Reynolds numbers (right) with their corresponding constraints in red. Bottom panels: CPI temperature with constraint in red (left) and baryogenesis parameter space (right).

preserving the helicity in the gauge sector, before the CPI can happen, one must require that [62, 103]

$$T_{\rm CPI} \approx (4 \cdot 10^{-7}\ {\rm GeV})\ \frac{\mathcal{H}_Y^2}{H(t_{\rm end})^6}\left(\frac{H(t_{\rm end})}{10^{13}\ {\rm GeV}}\right)^3\left(\frac{T_{\rm rh}}{T_{\rm rh}^{\rm ins}}\right)^2 \lesssim 10^5\ {\rm GeV}. \tag{5.10}$$

In Figs. 6 and 7, we display the main results for the baryogenesis mechanism both in the presence and absence of the Schwinger effect. In both figures, the top panels display the electromagnetic energy and energy ratio to the background energy density. In the middle panels we show the quantities $\eta_B(\Lambda, f_{\theta_W})$, $\mathcal{R}_m(\Lambda)$ and $\mathcal{R}_e(\Lambda)$. On the left, the red line must be in between the two

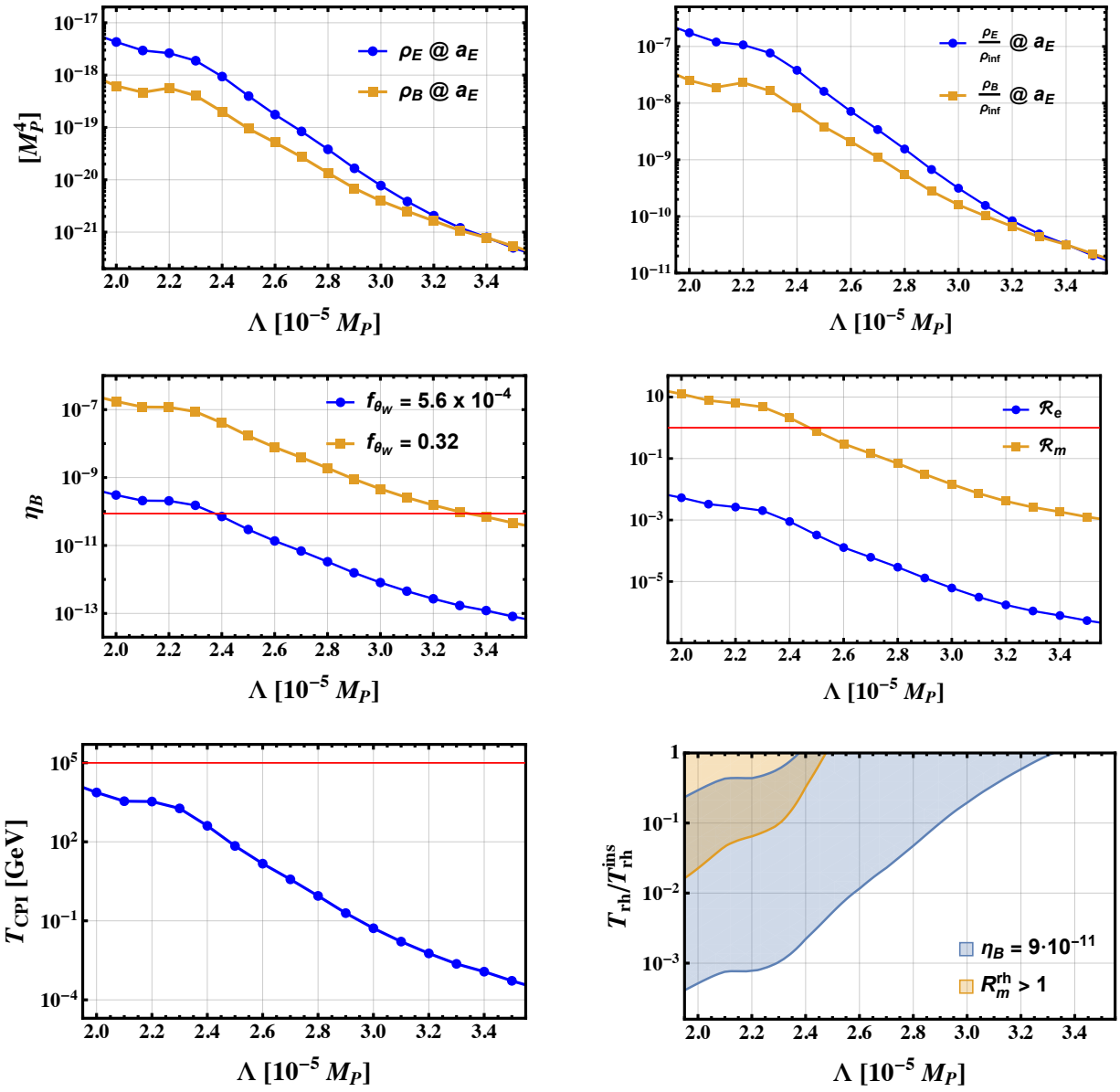

FIG. 7: Similar to Fig. 6, these figures again display a scan of the parameter Λ with the first set of initial conditions, BPa in Tab. I including the Schwinger effect. Top panels: Magnetic and electric energy density (left) and their ratio with the inflation energy density (right). Middle panel: baryon asymmetry η_B (left) and Reynolds numbers (right) with their corresponding constraints in red. Bottom panels: CPI temperature with constraint in red (left) and baryogenesis parameter space (right). We did not display the CPI temperature on this last plot as the CPI is no longer a constraint.

curves to meet the constraint. On the right, the only constraint is that $\mathcal{R}_m$ is above the red line. Finally, at the bottom, we present the CPI temperature as a function of Λ and the regions where the different constraints are met. On the bottom left panel, the curve should be below the red line. On the right one, we shall seek the overlapping region. In this last plot, we add the temperature ratio $T_{\rm rh}\,/\,T_{\rm rh}^{\rm ins}$ as a supplementary parameter. We see that the window is larger in the presence of the Schwinger, which also totally removes the constraint on $T_{\rm CPI}$. Indeed, the backreactionless mechanism tends to overshoot the BAU, an issue addressed by the presence of the Schwinger effect which therefore acts as a BAU facilitator.

6 Summary and Conclusions

We have discussed baryogenesis in the context of R^2-Higgs inflation, involving the CP-violating dimension-six term proportional to $(R/\Lambda^2)\, B_{\mu\nu}\tilde{B}^{\mu\nu}$. We adopt a fully covariant formalism for both inflationary dynamics and gauge field production. Our linear order analysis shows that if $\Lambda \sim 3\times10^{-5}M_{\rm P}$, sufficient helical hypermagnetic fields are produced, which can lead to the observed BAU during the electroweak crossover. Smaller values of Λ imply an overproduction of baryons. Once the Schwinger effect is included, the energy densities ρ_E and ρ_B are suppressed, but there is a subtlety: the Schwinger effect is exponentially suppressed by a factor $\sim \exp\left(-\sqrt{(2/3)}\,\varphi/M_{\rm P}\right)$, which dilutes its relevance during the inflationary epoch, but becomes pronounced around and after the end of inflation. The Schwinger effect can then lead to baryogenesis for smaller values $\Lambda \sim 2.2\times10^{-5}M_{\rm P}$. We also find that when the Schwinger effect is included, the radiation density ρ_ψ can dominate over the electromagnetic densities ρ_E and ρ_B, cf. Fig. 5.

We have primarily focused on the Starobinsky-like regime in our linear order analysis. In the mixed R^2-Higgs scenario, a smaller Λ may generate BAU without the Schwinger effect. This can be understood from Eq. (2.25) where a smaller ξ_R and moderately large ξ_H (i.e. the mixed R^2-Higgs like regime) can induce inflation, while BAU can be triggered by a larger scale Λ. However, a larger ξ_H may lead to an exponential growth of isocurvature modes (see e.g. Refs. [78, 104, 105]) in our backreactionless scenario although such a mode is suppressed during inflation. Moreover, in such a scenario, one would need to take into account non-perturbative effects. In our analysis, we have not considered the impact of decay and self-resonance. Thus, the ratio $T_{\rm rh}/T_{\rm rh}^{\rm ins}$ is essentially a free parameter in our analysis. We leave a more detailed analysis of (p)reheating and particle production for future work. It has been pointed out that the helical gauge fields may source non-gaussianity [106, 107], which may result in moderate constraint to the parameter space for baryogenesis without the Schwinger effect [64]. In the presence of the Schwinger effect, the produced helical gauge fields are much weaker and we expect those constraints to be harmless. However, one needs to be careful when interpreting results from Refs. [106, 107] as they focus on a single field. In our multi-field model, a proper estimation of non-gaussianity requires considering perturbations up to third order. This would induce several new contributions from field-space Riemann tensor [76] and is beyond the scope of our work.

While there are many avenues to achieve the observed BAU, baryogenesis driven by a dimension-six CP-odd term $\sim (R/\Lambda^2)\, B_{\mu\nu}\tilde{B}^{\mu\nu}$ provides a motivated approach to address BAU within the framework of R^2-Higgs inflation. This approach critically rests on the presence of an effective dimension-six term, but it does not require additional degrees of freedom beyond the SM. In parallel, such dimension-six terms can also shed light on the UV sensitivity of R^2-Higgs inflation as discussed in, e.g. Refs. [108, 109].

Acknowledgments — YC acknowledges funding support from the Initiative Physique des Infinis (IPI), a research training program of the Idex SUPER at Sorbonne Université. CE is supported by the UK Science and Technology Facilities Council (STFC) under grant ST/X000605/1 and the Leverhulme Trust under RPG-2021-031. TM is funded by the Deutsche Forschungsgemeinschaft (DFG, German Research Foundation) under grant 396021762 — TRR 257: Particle Physics Phenomenology after the Higgs Discovery and Germany's Excellence Strategy EXC 2181/1 — 390900948 (the Heidelberg STRUCTURES Excellence Cluster). The work of MQ is partly supported by Spanish MICIN under Grant PID2020-115845GB-I00, and by the Catalan Government under Grant 2021SGR00649. IFAE is partially funded by the CERCA program of the Generalitat de Catalunya.

A The Vierbein Fields

The vierbein fields e^a_μ are defined as follows: The metric in the Jordan frame $g_{J\mu\nu}$ can be related at every point to a Minkowski tangent space η_{ab} via the vierbein, which obeys the following orthogonality conditions

$$e^a_\mu e^\nu_a = \delta^\nu_\mu, \quad e^a_\mu e^\mu_b = \delta^a_b, \quad g_{J\mu\nu} = e^a_\mu e^b_\nu \eta_{ab} \text{ and } \gamma_\mu = e^a_\mu \tilde{\gamma}_a, \tag{A.1}$$

where $\tilde{\gamma}_a$ are the Minkowski γ-matrices. The γ_μ satisfy $\{\gamma^\mu, \gamma^\nu\} = 2g_J^{\mu\nu}$ in curved space-time. The spin-affine connection is given by

$$\Gamma_\mu = \frac{1}{2}\omega_{\mu\, ab}\sigma^{ab} \text{ with } \sigma^{ab} = \frac{1}{4}[\tilde{\gamma}^a, \tilde{\gamma}^b]. \tag{A.2}$$

The spin-connection $\omega_\mu^{\ a}{}_b$ is defined as [110]

$$\omega_\mu^{\ a}{}_b \equiv \left(e^a_\nu e^\beta_b \Gamma^\nu_{\mu\beta} - e^\beta_b \partial_\mu e^a_\beta\right). \tag{A.3}$$

B Field-Space Metric and Christoffel Symbols

The field-space G^{IJ} metric is given by

$$G^{\phi\phi} = 1, \quad G^{hh} = e^{\sqrt{\frac{2}{3}}\frac{\phi}{M_\mathrm{P}}}, \quad G^{\phi h} = G^{h\phi} = 0. \tag{B.1}$$

The corresponding non-vanishing Christoffel symbols are therefore

$$\Gamma^\phi_{hh} = \frac{e^{-\sqrt{\frac{2}{3}}\frac{\phi}{M_\mathrm{P}}}}{\sqrt{6}M_\mathrm{P}}, \quad \Gamma^h_{\phi h} = \Gamma^h_{h\phi} = -\frac{1}{\sqrt{6}M_\mathrm{P}}. \tag{B.2}$$

C Einstein Equation and Stress-Energy Tensor

The action S_E can be rewritten in the following way

$$S_E = \int d^4x\sqrt{-g_E}\left(\frac{M_\mathrm{P}^2}{2}R_E + \mathcal{L}_M\right), \tag{C.1}$$

where $\mathcal{L}_M$ is all terms in the action other than R_E. Varying the action with respect to $g_E^{\mu\nu}$ we get

$$\begin{aligned} 0 &= \delta S_E \\ &= \int d^4x \left(\frac{M_\mathrm{P}^2}{2}\frac{\delta(\sqrt{-g_E}R_E)}{\delta g_E^{\mu\nu}} + \frac{\delta(\sqrt{-g_E}\mathcal{L}_M)}{\delta g_E^{\mu\nu}}\right)\delta g_E^{\mu\nu} \\ &= \int d^4x \left(\frac{M_\mathrm{P}^2}{2}\left(R_E\frac{\delta(\sqrt{-g_E})}{\delta g_E^{\mu\nu}} + \sqrt{-g_E}\frac{\delta(R_E)}{\delta g_E^{\mu\nu}}\right) + \sqrt{-g_E}\frac{\delta(\mathcal{L}_M)}{\delta g_E^{\mu\nu}} + \mathcal{L}_M\frac{\delta(\sqrt{-g_E})}{\delta g_E^{\mu\nu}}\right)\delta g_E^{\mu\nu}. \end{aligned} \tag{C.2}$$

Utilizing $\frac{\delta(\sqrt{-g_E})}{\delta g_E^{\mu\nu}} = -\frac{1}{2}\sqrt{-g_E}g_{E\mu\nu}$, $\frac{\delta(R_E)}{\delta g_E^{\mu\nu}} = R_{E\mu\nu}$ and ignoring the surface term we get

$$R_{E\mu\nu} - \frac{1}{2}g_{E\mu\nu}R_E = \frac{1}{M_\mathrm{P}^2}T_{\mu\nu} \tag{C.3}$$

where

$$T_{\mu\nu} = \left(\mathcal{L}_M g_{E\mu\nu} - 2\frac{\delta \mathcal{L}_M}{\delta g_E^{\mu\nu}} \right), \tag{C.4}$$

which is found to be

$$\begin{aligned} T_{\mu\nu} = & \Bigg[G_{IJ} D_\mu \phi^I D_\nu \phi^J + g_E^{\alpha\beta} B_{\alpha\mu} B_{\beta\nu} + g_E^{\alpha\beta} W^i_{\alpha\mu} W^i_{\beta\nu} + \frac{1}{2} e^{-\sqrt{\frac{2}{3}}\frac{\phi}{M_{\rm P}}} g^2 h^2 \frac{(W^1_\mu - iW^2_\mu)}{\sqrt{2}} \frac{(W^1_\nu + iW^2_\nu)}{\sqrt{2}} \\ & + \frac{2M_{\rm P}^2}{\xi_R \Lambda^2 \sqrt{-g_E}} F(\phi^I) e^{\sqrt{\frac{2}{3}}\frac{\phi}{M_{\rm P}}} \left(2 g_{E\mu\alpha} \epsilon^{\alpha\beta\rho\sigma} B_{\nu\beta} B_{\rho\sigma} + \frac{1}{8} g_{E\mu\nu} \epsilon^{\alpha\beta\rho\sigma} B_{\alpha\beta} B_{\rho\sigma} \right) \\ & + \frac{1}{4} e^{-\sqrt{\frac{2}{3}}\frac{\phi}{M_{\rm P}}} h^2 \left(g W^3_\mu - g' B_\mu \right) \left(g W^3_\nu - g' B_\nu \right) \Bigg] - \\ & g_{E\mu\nu} \Bigg(\frac{1}{2} G_{IJ} g_E^{\alpha\beta} D_\alpha \phi^I D_\beta \phi^J + V_0(\phi^I) + \frac{2M_{\rm P}^2}{\xi_R \Lambda^2 \sqrt{-g_E}} F(\phi^I) e^{\sqrt{\frac{2}{3}}\frac{\phi}{M_{\rm P}}} B_{\alpha\beta} \tilde{B}^{\alpha\beta} \\ & + \frac{1}{4} g_E^{\alpha\rho} g_E^{\beta\sigma} B_{\alpha\beta} B_{\rho\sigma} + \frac{1}{4} g_E^{\alpha\rho} g_E^{\beta\sigma} W^i_{\alpha\beta} W^i_{\rho\sigma} + \frac{1}{4} e^{-\sqrt{\frac{2}{3}}\frac{\phi}{M_{\rm P}}} g_E^{\alpha\beta} g^2 h^2 \frac{(W^1_\alpha - iW^2_\alpha)}{\sqrt{2}} \frac{(W^1_\beta + iW^2_\beta)}{\sqrt{2}} \\ & + \frac{1}{8} e^{-\sqrt{\frac{2}{3}}\frac{\phi}{M_{\rm P}}} g_E^{\alpha\beta} h^2 \left(g W^3_\alpha - g' B_\alpha \right) \left(g W^3_\beta - g' B_\beta \right) \Bigg) + e^{-\sqrt{\frac{2}{3}}\frac{\phi}{M_{\rm P}}} \bar{f} e^a_\mu \tilde{\gamma}_a \nabla^f_\nu f. \end{aligned} \tag{C.5}$$

D The Valley Approximation

In this section, we detail aspects of the so-called valley approximation for V_0. In this approximation, the system essentially behaves as a single-field scenario. Firstly, for positivity of the potential at the inflationary scale, one requires

$$\lambda + \frac{\xi_H^2}{4\xi_R} > 0. \tag{D.1}$$

For solving the background equations and the inflationary dynamics we focus on the R^2-like regime and the initial condition of the valley approximation derives from

$$\frac{\partial V_0}{\partial h} = 0, \tag{D.2}$$

which gives three solutions

$$h = 0, \quad \text{and} \quad h = \pm \frac{\sqrt{e^{\sqrt{\frac{2}{3}}\frac{\phi}{M_{\rm P}}} - 1}}{\sqrt{4\lambda + \frac{\xi_H^2}{\xi_R}}} \sqrt{\frac{\xi_H}{\xi_R}} M_{\rm P}. \tag{D.3}$$

One may choose the trivial solution $h = 0$, or the solution with a positive sign for convenience.

E Numerical Solutions of the Electromagnetic Equations

In the following, we summarize the details of solving the mode equation of Eq. (4.15) in cosmological time t using the RK4 method

$$\ddot{u}^\lambda + H\dot{u}^\lambda + \left(\frac{k^2}{a^2} + \frac{8\cos^2\theta_W M_{\rm P}^2}{\xi_R \Lambda^2 a} \partial_0 \left(F(\varphi^I) e^{\sqrt{\frac{2}{3}}\varphi/M_{\rm P}} \right) \lambda k \right) u^\lambda = 0. \tag{E.1}$$

Firstly, as required for the RK4 method, we rewrite the above equation as two first order equations

$$\frac{du^\lambda}{dt} = y^\lambda \quad \text{and,} \quad \frac{dy^\lambda}{dt} = -y^\lambda H - \left(\frac{k^2}{a^2} + \frac{8\cos^2\theta_W M_{\rm P}^2}{\xi_R \Lambda^2 a}\partial_0\left(F(\varphi^I)e^{\sqrt{\frac{2}{3}}\varphi/M_{\rm P}}\right)\lambda k\right)u^\lambda \tag{E.2}$$

The equations are essentially in the form of

$$\frac{du^\lambda}{dt} = f(u^\lambda, y^\lambda, t), \quad \text{and} \quad \frac{dy^\lambda}{dt} = g(u^\lambda, y^\lambda, t), \tag{E.3}$$

with

$$\begin{aligned} f(u^\lambda, y^\lambda, t) &= y^\lambda, \\ g(u^\lambda, y^\lambda, t) &= -y^\lambda H - \left(\frac{k^2}{a^2} + \frac{8\cos^2\theta_W M_{\rm P}^2}{\xi_R \Lambda^2 a}\partial_0\left(F(\varphi^I)e^{\sqrt{\frac{2}{3}}\varphi/M_{\rm P}}\right)\lambda k\right)u^\lambda. \end{aligned} \tag{E.4}$$

Now the task is to find out u^λ and y for each time step utilizing the RK4 method. This is provided by

$$\begin{aligned} u^\lambda_{i+1} &= u^\lambda_i + \frac{1}{6}\left(l_0 + 2l_1 + 2l_2 + l_3\right), \\ y^\lambda_{i+1} &= y^\lambda_i + \frac{1}{6}\left(m_0 + 2m_1 + 2m_2 + m_3\right), \end{aligned} \tag{E.5}$$

with

$$\begin{aligned} l_0 &= \delta t\ f(u^\lambda_i, y^\lambda_i, t_i), \\ m_0 &= \delta t\ g(u^\lambda_i, y^\lambda_i, t_i), \\ l_1 &= \delta t\ f(u^\lambda_i + \frac{1}{2}l_0, y^\lambda_i + \frac{1}{2}m_0, t_i + \frac{1}{2}\delta t), \\ m_1 &= \delta t\ g(u^\lambda_i + \frac{1}{2}l_0, y^\lambda_i + \frac{1}{2}m_0, t_i + \frac{1}{2}\delta t), \\ l_2 &= \delta t\ f(u^\lambda_i + \frac{1}{2}l_1, y^\lambda_i + \frac{1}{2}m_1, t_i + \frac{1}{2}\delta t), \\ m_2 &= \delta t\ g(u^\lambda_i + \frac{1}{2}l_1, y^\lambda_i + \frac{1}{2}m_1, t_i + \frac{1}{2}\delta t), \\ l_3 &= \delta t\ f(u^\lambda_i + l_2, y_i + m_2, t_i), \\ m_3 &= \delta t\ g(u^\lambda_i + l_2, y_i + m_3, t_i), \end{aligned} \tag{E.6}$$

where δt is the time step. The Bunch-Davis initial conditions for the modes u^λ and y are given in Eq. (4.19).

One can in principle fix the number of modes N_k in each time step within $[k_{\rm min}, k_c]$ for the integration of Eqs. (4.16). However, this makes the initialization of the modes in the next time step more involved. This is because as k_c increases in each time step, keeping N_k fixed each time would require some more involved initialization for subsequent time steps. We can take a simpler route and keep the number of k modes the same for all time steps. This ensures that the number of modes N_k and the corresponding modes are identical at each time step. In practice, we take a large range $[k_{\rm min}, k_{\rm max}]$ with $k_{\rm max} = Ca(t_{\rm numend})H(t_{\rm numend})$ where $t_{\rm numend}$ is the numerical end of our simulation. We chose $C = 100$ to ensure that $k_c(t_{\rm numend}) < k_{\rm max}$ and divide the range $[k_{\rm min}, k_{\rm max}]$ into $N_k = 200$ intervals. In each time step, we then numerically interpolate Eqs. (4.16) in $[k_{\rm min}, k_{\rm max}]$ and truncate the numerical integration up to the corresponding k_c values. Increasing

N_k to higher values does not significantly impact our results. For further details of the numerical procedure, we refer the reader to Ref. [65].

In the presence of the Schwinger effect the corresponding equation of motion, Eq. (4.30), is solved numerically using similar methods as those described above.

---

[1] A. A. Starobinsky, Phys. Lett. B **91**, 99 (1980).
[2] K. Sato, Mon. Not. Roy. Astron. Soc. **195**, 467 (1981).
[3] A. H. Guth, Phys. Rev. D **23**, 347 (1981).
[4] Y. Akrami et al. (Planck), Astron. Astrophys. **641**, A10 (2020), arXiv:1807.06211 [astro-ph.CO].
[5] A. A. Starobinsky, Sov. Astron. Lett. **9**, 302 (1983).
[6] A. Vilenkin, Phys. Rev. D **32**, 2511 (1985).
[7] M. B. Mijic, M. S. Morris, and W.-M. Suen, Phys. Rev. D **34**, 2934 (1986).
[8] K.-i. Maeda, Phys. Rev. D **37**, 858 (1988).
[9] G. Aad et al. (ATLAS), Phys. Lett. B **716**, 1 (2012), arXiv:1207.7214 [hep-ex].
[10] S. Chatrchyan et al. (CMS), Phys. Lett. B **716**, 30 (2012), arXiv:1207.7235 [hep-ex].
[11] F. L. Bezrukov and M. Shaposhnikov, Phys. Lett. B **659**, 703 (2008), arXiv:0710.3755 [hep-th].
[12] A. O. Barvinsky, A. Y. Kamenshchik, and A. A. Starobinsky, JCAP **11**, 021 (2008), arXiv:0809.2104 [hep-ph].
[13] F. Bezrukov, A. Magnin, M. Shaposhnikov, and S. Sibiryakov, JHEP **01**, 016 (2011), arXiv:1008.5157 [hep-ph].
[14] F. Bezrukov, Class. Quant. Grav. **30**, 214001 (2013), arXiv:1307.0708 [hep-ph].
[15] A. De Simone, M. P. Hertzberg, and F. Wilczek, Phys. Lett. B **678**, 1 (2009), arXiv:0812.4946 [hep-ph].
[16] F. L. Bezrukov, A. Magnin, and M. Shaposhnikov, Phys. Lett. B **675**, 88 (2009), arXiv:0812.4950 [hep-ph].
[17] A. O. Barvinsky, A. Y. Kamenshchik, C. Kiefer, A. A. Starobinsky, and C. F. Steinwachs, Eur. Phys. J. C **72**, 2219 (2012), arXiv:0910.1041 [hep-ph].
[18] B. L. Spokoiny, Phys. Lett. B **147**, 39 (1984).
[19] T. Futamase and K.-i. Maeda, Phys. Rev. D **39**, 399 (1989).
[20] D. S. Salopek, J. R. Bond, and J. M. Bardeen, Phys. Rev. D **40**, 1753 (1989).
[21] R. Fakir and W. G. Unruh, Phys. Rev. D **41**, 1783 (1990).
[22] L. Amendola, M. Litterio, and F. Occhionero, Int. J. Mod. Phys. A **5**, 3861 (1990).
[23] D. I. Kaiser, Phys. Rev. D **52**, 4295 (1995), arXiv:astro-ph/9408044.
[24] J. L. Cervantes-Cota and H. Dehnen, Nucl. Phys. B **442**, 391 (1995), arXiv:astro-ph/9505069.
[25] E. Komatsu and T. Futamase, Phys. Rev. D **59**, 064029 (1999), arXiv:astro-ph/9901127.
[26] C. P. Burgess, H. M. Lee, and M. Trott, JHEP **09**, 103 (2009), arXiv:0902.4465 [hep-ph].
[27] J. L. F. Barbon and J. R. Espinosa, Phys. Rev. D **79**, 081302 (2009), arXiv:0903.0355 [hep-ph].
[28] C. P. Burgess, H. M. Lee, and M. Trott, JHEP **07**, 007 (2010), arXiv:1002.2730 [hep-ph].
[29] M. P. Hertzberg, JHEP **11**, 023 (2010), arXiv:1002.2995 [hep-ph].
[30] I. Antoniadis, A. Guillen, and K. Tamvakis, JHEP **08**, 018 (2021), [Addendum: JHEP 05, 074 (2022)], arXiv:2106.09390 [hep-th].
[31] M. P. DeCross, D. I. Kaiser, A. Prabhu, C. Prescod-Weinstein, and E. I. Sfakianakis, Phys. Rev. D **97**, 023526 (2018), arXiv:1510.08553 [astro-ph.CO].
[32] Y. Ema, R. Jinno, K. Mukaida, and K. Nakayama, JCAP **02**, 045 (2017), arXiv:1609.05209 [hep-ph].
[33] E. I. Sfakianakis and J. van de Vis, Phys. Rev. D **99**, 083519 (2019), arXiv:1810.01304 [hep-ph].
[34] Y. Ema, Phys. Lett. B **770**, 403 (2017), arXiv:1701.07665 [hep-ph].
[35] A. Salvio and A. Mazumdar, Phys. Lett. B **750**, 194 (2015), arXiv:1506.07520 [hep-ph].
[36] S. Pi, Y.-l. Zhang, Q.-G. Huang, and M. Sasaki, JCAP **05**, 042 (2018), arXiv:1712.09896 [astro-ph.CO].
[37] D. Gorbunov and A. Tokareva, Phys. Lett. B **788**, 37 (2019), arXiv:1807.02392 [hep-ph].
[38] A. Gundhi and C. F. Steinwachs, Nucl. Phys. B **954**, 114989 (2020), arXiv:1810.10546 [hep-th].

[39] M. He, A. A. Starobinsky, and J. Yokoyama, JCAP **05**, 064 (2018), arXiv:1804.00409 [astro-ph.CO].
[40] M. He, R. Jinno, K. Kamada, S. C. Park, A. A. Starobinsky, and J. Yokoyama, Phys. Lett. B **791**, 36 (2019), arXiv:1812.10099 [hep-ph].
[41] D. Y. Cheong, S. M. Lee, and S. C. Park, JCAP **01**, 032 (2021), arXiv:1912.12032 [hep-ph].
[42] F. Bezrukov, D. Gorbunov, C. Shepherd, and A. Tokareva, Phys. Lett. B **795**, 657 (2019), arXiv:1904.04737 [hep-ph].
[43] M. He, R. Jinno, K. Kamada, A. A. Starobinsky, and J. Yokoyama, JCAP **01**, 066 (2021), arXiv:2007.10369 [hep-ph].
[44] F. Bezrukov and C. Shepherd, JCAP **12**, 028 (2020), arXiv:2007.10978 [hep-ph].
[45] M. He, JCAP **05**, 021 (2021), arXiv:2010.11717 [hep-ph].
[46] S. Aoki, H. M. Lee, A. G. Menkara, and K. Yamashita, JHEP **05**, 121 (2022), arXiv:2202.13063 [hep-ph].
[47] G. R. Farrar and M. E. Shaposhnikov, Phys. Rev. Lett. **70**, 2833 (1993), [Erratum: Phys.Rev.Lett. 71, 210 (1993)], arXiv:hep-ph/9305274.
[48] G. R. Farrar and M. E. Shaposhnikov, Phys. Rev. D **50**, 774 (1994), arXiv:hep-ph/9305275.
[49] M. B. Gavela, P. Hernandez, J. Orloff, and O. Pene, Mod. Phys. Lett. A **9**, 795 (1994), arXiv:hep-ph/9312215.
[50] K. Kajantie, M. Laine, K. Rummukainen, and M. E. Shaposhnikov, Nucl. Phys. B **493**, 413 (1997), arXiv:hep-lat/9612006.
[51] A. D. Sakharov, Pisma Zh. Eksp. Teor. Fiz. **5**, 32 (1967).
[52] M. E. Shaposhnikov, Nucl. Phys. B **287**, 757 (1987).
[53] K. Kamada and A. J. Long, Phys. Rev. D **94**, 063501 (2016), arXiv:1606.08891 [astro-ph.CO].
[54] M. M. Anber and L. Sorbo, JCAP **10**, 018 (2006), arXiv:astro-ph/0606534.
[55] K. Bamba, Phys. Rev. D **74**, 123504 (2006), arXiv:hep-ph/0611152.
[56] K. Bamba, C. Q. Geng, and S. H. Ho, Phys. Lett. B **664**, 154 (2008), arXiv:0712.1523 [hep-ph].
[57] M. M. Anber and L. Sorbo, Phys. Rev. D **81**, 043534 (2010), arXiv:0908.4089 [hep-th].
[58] M. M. Anber and E. Sabancilar, Phys. Rev. D **92**, 101501 (2015), arXiv:1507.00744 [hep-th].
[59] Y. Cado and E. Sabancilar, JCAP **04**, 047 (2017), arXiv:1611.02293 [hep-ph].
[60] K. Kamada and A. J. Long, Phys. Rev. D **94**, 123509 (2016), arXiv:1610.03074 [hep-ph].
[61] D. Jiménez, K. Kamada, K. Schmitz, and X.-J. Xu, JCAP **12**, 011 (2017), arXiv:1707.07943 [hep-ph].
[62] V. Domcke, B. von Harling, E. Morgante, and K. Mukaida, JCAP **10**, 032 (2019), arXiv:1905.13318 [hep-ph].
[63] Y. Cado, B. von Harling, E. Massó, and M. Quirós, JCAP **07**, 049 (2021), arXiv:2102.13650 [hep-ph].
[64] Y. Cado and M. Quirós, Phys. Rev. D **106**, 055018 (2022), arXiv:2201.06422 [hep-ph].
[65] Y. Cado and M. Quirós, Phys. Rev. D **106**, 123527 (2022), arXiv:2208.10977 [hep-ph].
[66] R. Durrer, O. Sobol, and S. Vilchinskii, Phys. Rev. D **106**, 123520 (2022), arXiv:2207.05030 [gr-qc].
[67] R. Durrer, O. Sobol, and S. Vilchinskii, Phys. Rev. D **108**, 043540 (2023), arXiv:2303.04583 [gr-qc].
[68] O. Savchenko and Y. Shtanov, JCAP **10**, 040 (2018), arXiv:1808.06193 [astro-ph.CO].
[69] K. Subramanian, Rept. Prog. Phys. **79**, 076901 (2016), arXiv:1504.02311 [astro-ph.CO].
[70] R. Durrer and A. Neronov, Astron. Astrophys. Rev. **21**, 62 (2013), arXiv:1303.7121 [astro-ph.CO].
[71] V. Domcke and K. Mukaida, JCAP **11**, 020 (2018), arXiv:1806.08769 [hep-ph].
[72] H. Kitamoto and M. Yamada, JHEP **06**, 103 (2022), arXiv:2109.14782 [hep-ph].
[73] T. D. Cohen and D. A. McGady, Phys. Rev. D **78**, 036008 (2008), arXiv:0807.1117 [hep-ph].
[74] Y. Cado and M. Quirós, Phys. Rev. D **108**, 023508 (2023), arXiv:2303.12932 [hep-ph].
[75] J.-O. Gong and T. Tanaka, JCAP **03**, 015 (2011), [Erratum: JCAP 02, E01 (2012)], arXiv:1101.4809 [astro-ph.CO].
[76] D. I. Kaiser, E. A. Mazenc, and E. I. Sfakianakis, Phys. Rev. D **87**, 064004 (2013), arXiv:1210.7487 [astro-ph.CO].
[77] M. Sasaki and E. D. Stewart, Prog. Theor. Phys. **95**, 71 (1996), arXiv:astro-ph/9507001.
[78] C. Gordon, D. Wands, B. A. Bassett, and R. Maartens, Phys. Rev. D **63**, 023506 (2000), arXiv:astro-ph/0009131.
[79] S. Groot Nibbelink and B. J. W. van Tent, (2000), arXiv:hep-ph/0011325.
[80] S. Groot Nibbelink and B. J. W. van Tent, Class. Quant. Grav. **19**, 613 (2002), arXiv:hep-ph/0107272.
[81] D. Wands, N. Bartolo, S. Matarrese, and A. Riotto, Phys. Rev. D **66**, 043520 (2002), arXiv:astro-ph/0205253.

[82] D. Seery and J. E. Lidsey, JCAP **09**, 011 (2005), arXiv:astro-ph/0506056.
[83] C. M. Peterson and M. Tegmark, Phys. Rev. D **83**, 023522 (2011), arXiv:1005.4056 [astro-ph.CO].
[84] C. M. Peterson and M. Tegmark, Phys. Rev. D **87**, 103507 (2013), arXiv:1111.0927 [astro-ph.CO].
[85] J. Elliston, D. Seery, and R. Tavakol, JCAP **11**, 060 (2012), arXiv:1208.6011 [astro-ph.CO].
[86] M. P. DeCross, D. I. Kaiser, A. Prabhu, C. Prescod-Weinstein, and E. I. Sfakianakis, Phys. Rev. D **97**, 023527 (2018), arXiv:1610.08868 [astro-ph.CO].
[87] M. P. DeCross, D. I. Kaiser, A. Prabhu, C. Prescod-Weinstein, and E. I. Sfakianakis, Phys. Rev. D **97**, 023528 (2018), arXiv:1610.08916 [astro-ph.CO].
[88] S. M. Lee, T. Modak, K.-y. Oda, and T. Takahashi, Eur. Phys. J. C **82**, 18 (2022), arXiv:2108.02383 [hep-ph].
[89] H. Kodama and M. Sasaki, Prog. Theor. Phys. Suppl. **78**, 1 (1984).
[90] V. F. Mukhanov, H. A. Feldman, and R. H. Brandenberger, Phys. Rept. **215**, 203 (1992).
[91] K. A. Malik and D. Wands, Phys. Rept. **475**, 1 (2009), arXiv:0809.4944 [astro-ph].
[92] M. Sasaki, Prog. Theor. Phys. **76**, 1036 (1986).
[93] V. F. Mukhanov, Sov. Phys. JETP **67**, 1297 (1988).
[94] R. Easther and J. T. Giblin, Phys. Rev. D **72**, 103505 (2005), arXiv:astro-ph/0505033.
[95] D. Langlois and S. Renaux-Petel, JCAP **04**, 017 (2008), arXiv:0801.1085 [hep-th].
[96] C. M. Peterson and M. Tegmark, Phys. Rev. D **84**, 023520 (2011), arXiv:1011.6675 [astro-ph.CO].
[97] B. A. Bassett, S. Tsujikawa, and D. Wands, Rev. Mod. Phys. **78**, 537 (2006), arXiv:astro-ph/0507632.
[98] K. D. Lozanov and M. A. Amin, JCAP **06**, 032 (2016), arXiv:1603.05663 [hep-ph].
[99] E. V. Gorbar, K. Schmitz, O. O. Sobol, and S. I. Vilchinskii, Phys. Rev. D **104**, 123504 (2021), arXiv:2109.01651 [hep-ph].
[100] J. R. C. Cuissa and D. G. Figueroa, JCAP **06**, 002 (2019), arXiv:1812.03132 [astro-ph.CO].
[101] M. D'Onofrio and K. Rummukainen, Phys. Rev. D **93**, 025003 (2016), arXiv:1508.07161 [hep-ph].
[102] M. D'Onofrio, K. Rummukainen, and A. Tranberg, Phys. Rev. Lett. **113**, 141602 (2014), arXiv:1404.3565 [hep-ph].
[103] M. Joyce and M. E. Shaposhnikov, Phys. Rev. Lett. **79**, 1193 (1997), arXiv:astro-ph/9703005.
[104] B. A. Bassett, C. Gordon, R. Maartens, and D. I. Kaiser, Phys. Rev. D **61**, 061302 (2000), arXiv:hep-ph/9909482.
[105] A. R. Liddle, D. H. Lyth, K. A. Malik, and D. Wands, Phys. Rev. D **61**, 103509 (2000), arXiv:hep-ph/9912473.
[106] N. Barnaby and M. Peloso, Phys. Rev. Lett. **106**, 181301 (2011), arXiv:1011.1500 [hep-ph].
[107] N. Barnaby, E. Pajer, and M. Peloso, Phys. Rev. D **85**, 023525 (2012), arXiv:1110.3327 [astro-ph.CO].
[108] T. Modak, L. Röver, B. M. Schäfer, B. Schosser, and T. Plehn, SciPost Phys. **15**, 047 (2023), arXiv:2210.05698 [astro-ph.CO].
[109] S. M. Lee, T. Modak, K.-y. Oda, and T. Takahashi, JCAP **08**, 045 (2023), arXiv:2303.09866 [hep-ph].
[110] P. Collas and D. Klein, The Dirac Equation in Curved Spacetime: A Guide for Calculations, SpringerBriefs in Physics (Springer, 2019) arXiv:1809.02764 [gr-qc].

Implication of preheating on gravity assisted baryogenesis in R^2-Higgs inflation

Yann Cado,[1] Christoph Englert,[2] Tanmoy Modak,[3] and Mariano Quirós[4]

[1] *Laboratoire de Physique Théorique et Hautes Energies (LPTHE), Sorbonne Université et CNRS UMR 7589, 4 place Jussieu, 75252 Paris CEDEX 05, France*

[2] *School of Physics & Astronomy, University of Glasgow, Glasgow G12 8QQ, UK*

[3] *Department of Physical Sciences, Indian Institute of Science Education and Research Berhampur, Berhampur 760010, Odisha, India*

[4] *Institut de Física d'Altes Energies (IFAE) and The Barcelona Institute of Science and Technology (BIST), Campus UAB, 08193 Bellaterra, Barcelona, Spain*

We investigate the impact of preheating on baryogenesis in R^2-Higgs inflation. In this scenario, the inclusion of a dimension-six operator $(R/\Lambda^2)B_{\mu\nu}\widetilde{B}^{\mu\nu}$ abundantly generates helical hypermagnetic fields during inflation, leading to a baryon asymmetric Universe at the electroweak crossover. Focusing on the R^2-like regime, we first derive the relevant dynamics of preheating using a doubly-covariant formalism. We find that preheating can happen for the Higgs, transverse gauge and Goldstone bosons, however, it is dependent on the value of the non-minimal coupling ξ_H between the Standard Model Higgs field and the Ricci scalar. We identify the preheating temperature to determine the appropriate scale Λ for driving baryogenesis, which is around $\Lambda \sim 2.2\,(2.6) \times 10^{-5}\, M_{\rm P}$ for $\xi_H \sim 1\,(10)$. Our results represent the most accurate estimation of the scale of gravity induced baryogenesis in R^2-Higgs inflation to date. Areas for further improvement are identified.

Contents

1. Introduction 2

2. The action 3

3. Inflationary dynamics 6
   1. Gauge choice and equations of motion of the gauge and Goldstone bosons 8
      1. Z bosons 9
      2. $W^{\pm}$ bosons 10
      3. Goldstone bosons 11

4. Inflaton and Higgs quanta production 12

5. Production of Z, W and Goldstone bosons 19
   1. Equations of motion and quantization 19
   2. Energy density 21
      1. Z and W bosons 22
      2. Goldstone bosons 23

6. Production of the electromagnetic field 25

7. Reheating temperature 28

8. Baryogenesis 30

9. Summary and Outlook 34

A. Gauge boson spectra 35

References 35

1 Introduction

The existence of the baryon asymmetry of the Universe (BAU) is firmly established by various cosmological observations such as the cosmic microwave background and big-bang nucleosynthesis. However, its origin still remains unclear. If the fundamental scale of the mechanism behind the BAU is tied to a higher scale than the electroweak one, it might be possible that telltale effects at present, or even future, colliders could remain absent. One such high-scale mechanism provides, in the Jordan frame [1], an additional source of CP violation via a (CP-odd) dimension-six operator $(R/\Lambda^2)B_{\mu\nu}\widetilde{B}^{\mu\nu}$, where R is the Ricci scalar and $B_{\mu\nu}$ is the field stress tensor of the hypercharge $U(1)_Y$. We will refer to this mechanism as gravity assisted baryogenesis from here onwards. In this case, even at the electroweak crossover of the Standard Model (SM), the out-of-equilibrium condition can be met if the source and washout decay rates are different and shut off at different epochs [2, 3]. The CP-violating dimension-six Chern-Simons density can abundantly produce helical hypermagnetic fields at the end of inflation [#1]. These helical hypermagnetic fields [#2] may then create the observed baryon asymmetry at the electroweak crossover [3, 15–20].

This mechanism can seamlessly be integrated into inflationary scenarios such as R^2-Higgs inflation [21–29] since the $(R/\Lambda^2)B_{\mu\nu}\widetilde{B}^{\mu\nu}$ term can also be considered within the context of $f(R)$ gravity (or, rather here, $f(R,\Phi,B_\mu)$ gravity). In the dual scalar-tensor theory, the R^2 term is manifest as a dynamical scalar degree of freedom, which, along with the Higgs field Φ, couples to the Chern-Simons density, resulting in the production of hypermagnetic fields at the end of inflation. It should also be noted that R^2-Higgs inflation, like R^2 [30–34] inflation and Higgs inflation [35–41] (for similar mechanisms, see e.g. [42–49]), is one of the best-fit models of the Planck data [50]. Further, unlike Higgs

[#1] This term, not directly connected to BAU but in the context of hypermagnetic field production, has been discussed in, e.g., Refs. [4–8].
[#2] See also Refs. [9–14] for the production of helical hypermagnetic fields due to inflaton dynamics.

inflation, where longitudinal gauge bosons are violently produced well beyond the unitarity cut-off scale [51–53], the unitarity scale is restored up to the Planck scale in R^2-Higgs inflation [22]. Thus, high-scale baryogenesis via $(R/\Lambda^2)B_{\mu\nu}\widetilde{B}^{\mu\nu}$ can be elegantly connected to the R^2-Higgs model without requiring additional degrees of freedom beyond the SM ones.

It is not surprising that, in the gravity assisted baryogenesis, the production of hypermagnetic fields highly depends on the inflationary dynamics. The baryon-to-entropy ratio is also highly sensitive to the value of the magnetic Reynolds number which in turn highly depends on the exact (p)reheating temperature [1, 15, 18–20]. In addition, the latter is also highly dependent on the value of quantum hypermagnetic energy density when preheating is complete. Therefore, the exact amount of baryon asymmetry will be model-dependent as it makes use of specific (p)reheating results [#3]. An improved understanding of these dynamics brings about major improvements in the precision of predictions since we do not need to rely on estimates as in previous studies but directly determine the thermal plasma temperature, the relevant energy densities and the scale factor ratio at reheating and the end of inflation. Previous studies performed by the current authors treated such effects as effective parameters [1], while a detailed analysis of how (p)reheating impacts gravity assisted baryogenesis was missing. This will entail us to find a more precise value for the Λ required for baryogenesis.

In this work, taking R^2-Higgs inflation as a benchmark model for inflation, and focusing primarily on the R^2-like regime, we study the impact of preheating and particle production in the mechanism of gravity assisted baryogenesis. Adopting the doubly-covariant formalism and including all perturbations at the linear order, we study the preheating dynamics of the scalar and gauge sectors. In Ref. [53], Sfakianakis and van de Vis did provide a similar detailed analysis of linear fluctuations during preheating in Higgs inflation in the Einstein frame. In our case, the field space of the inflationary dynamics consists of five fields: one dynamical scalar degree of freedom arising due to the R^2 term and four from the Higgs $SU(2)_L$ doublet, corresponding to the physical Higgs and the three Goldstone bosons. The background dynamics are governed by the R^2 scalar alongside the physical Higgs boson; the three would-be Goldstone bosons are treated as perturbations. Our results include the full $SU(2)_L \times U(1)_Y$ gauge dynamics in a complete analysis.

The inflaton's self-resonance turns out to not be efficient enough for preheating. However, Higgs fluctuations can lead to preheating if the non-minimal coupling ξ_H between the Ricci scalar R and the Higgs is $\gtrsim 10$. We also show that for $\xi_H \sim 10$, the transverse modes of the Z and W boson can lead to gauge preheating. For tiny ξ_H values, gauge preheating might be induced if Λ is sufficiently small. We shall see that such a small value of Λ would, however, lead to an overproduction of baryon asymmetry. Further, Goldstone bosons may also preheat the Universe even for $\xi_H \sim 1$ (see also Refs. [28, 52, 54–58] for Goldstone/longitudinal gauge boson preheating in R^2-Higgs inflation). Our results show that the Goldstone bosons can preheat the Universe mildly faster than any other fields and, hence, they determine the reheating temperature needed for the baryogenesis computation.

We organize this paper as follows. First, we start with outlining the action and derive the relevant equations of motion (EoM) for the different fields in Sec. 2. We discuss the inflationary dynamics in the covariant formalism in Sec. 3. The production of inflaton and Higgs fluctuations are studied in Sec. 4, and the production of the Z, W and Goldstone bosons is presented in Sec. 5. The production of hypermagnetic fields and subsequent generation of the BAU are discussed, respectively, in Sec. 6 and Sec. 8. We discuss reheating in Sec. 7. Finally, we summarize and conclude in Sec. 9. Some technical and computational details are relegated to App. A.

2 The action

We start with the action in the Jordan frame given by

$$S_J = \int d^4x\sqrt{-g_J}\left[\frac{M_{\rm P}^2}{2}f(R_J,\Phi,B_\mu,W^i_\mu) - g_J^{\mu\nu}(\nabla_\mu\Phi)^\dagger\nabla_\nu\Phi - V(\Phi,\Phi^\dagger) - \frac{1}{4}g_J^{\mu\rho}g_J^{\nu\sigma}B_{\mu\nu}B_{\rho\sigma} - \frac{1}{4}g_J^{\mu\rho}g_J^{\nu\sigma}W^i_{\mu\nu}W^i_{\rho\sigma}\right], \tag{2.1}$$

where $M_{\rm P} = \sqrt{1/(8\pi G)} \approx 2.4\times10^{18}$ GeV is the reduced Planck mass and G is Newton's constant. Throughout this work, we follow the mostly-plus convention $(-1,+1,+1,+1)$ for the metric, $\sqrt{-g_J}$ is the determinant of the metric, and we choose the $\epsilon^{0123} = 1$ convention for the Levi-Civita tensor. R_J and Φ denote the space-time Ricci scalar and

[#3] In the absence of efficient preheating, thermalization proceeds through perturbative reheating.

the Higgs doublet, $B_{\mu\nu}$ and $W^i_{\mu\nu}$ are the field stress tensors of the $U(1)_Y$ and $SU(2)_L$ gauge groups, respectively. The covariant derivative with the SM gauge groups is defined as

$$\nabla_\mu = D_\mu + ig'\frac{1}{2}Q_{Y_f}B_\mu + ig\boldsymbol{T}\cdot\boldsymbol{W}_\mu, \tag{2.2}$$

where g' and g are $U(1)_Y$ and $SU(2)_L$ couplings. Q_{Y_f} is $U(1)_Y$ hypercharge and $\boldsymbol{T} = \boldsymbol{\tau}/2$ are the weak isospin generators derived from the three Pauli matrices $\boldsymbol{\tau}$. The field-stress tensors for the $U(1)_Y$ and $SU(2)_L$ gauge fields can be written as

$$B_{\mu\nu} = D_\mu B_\nu - D_\nu B_\mu, \qquad W^i_{\mu\nu} = D_\mu W^i_\nu - D_\nu W^i_\mu - g\sum_{j,k=1}^{3}\epsilon_{ijk}W^j_\mu W^k_\nu, \tag{2.3}$$

where D_μ is the covariant derivative of the space-time metric $g_{J\mu\nu}$. We have thus far ignored the fermions in Eq. (2.1) but shall return later part of the paper. The Higgs potential $V(\Phi,\Phi^\dagger)$ and $f(R_J,\Phi,B_\mu,W^i_\mu)$ are given as

$$V(\Phi,\Phi^\dagger) = \lambda|\Phi|^4, \tag{2.4a}$$

$$f(R_J,\Phi,B_\mu,W^i_\mu) = R_J + \frac{\xi_R}{2M_{\rm P}^2}R_J^2 + \frac{2\xi_H}{M_{\rm P}^2}|\Phi|^2R_J - \frac{2}{\Lambda^2M_{\rm P}^2}\frac{\epsilon^{\mu\nu\rho\sigma}}{\sqrt{-g_J}}B_{\mu\nu}B_{\rho\sigma}R_J - \frac{2}{\Lambda^2M_{\rm P}^2}\frac{\epsilon^{\mu\nu\rho\sigma}}{\sqrt{-g_J}}W^i_{\mu\nu}W^i_{\rho\sigma}R_J. \tag{2.4b}$$

The mass term in the Higgs potential is neglected as it plays no role for the inflationary dynamics.

To transition from a generic $f(R_J,\Phi,B_\mu,W^i_\mu)$ gravity to the respective scalar-tensor theory, we perform a Legendre transformation by first introducing an auxiliary field Ψ and rewrite Eq. (2.1) as

$$\begin{aligned} S_J = \int d^4x\sqrt{-g_J}\Big[\frac{M_P^2}{2}\left(f(\Psi,\Phi,B_\mu,W^i_\mu) + \frac{\partial f(\Psi,\Phi,B_\mu,W^i_\mu)}{\partial\Psi}(R_J-\Psi)\right) \\ - g_J^{\mu\nu}(\nabla_\mu\Phi)^\dagger\nabla_\nu\Phi - V(\Phi,\Phi^\dagger) - \frac{1}{4}g_J^{\mu\rho}g_J^{\nu\sigma}B_{\mu\nu}B_{\rho\sigma} - \frac{1}{4}g_J^{\mu\rho}g_J^{\nu\sigma}W^i_{\mu\nu}W^i_{\rho\sigma}\Big]. \end{aligned} \tag{2.5}$$

We can introduce a physical degree of freedom

$$\Theta = \frac{\partial f(\Psi,\Phi,B_\mu,W^i_\mu)}{\partial\Psi} \tag{2.6}$$

and re-express Eq. (2.5) as

$$\begin{aligned} S_J = \int d^4x\sqrt{-g_J}\Big[\frac{M_P^2}{2}\Theta R_J - U(\Theta,\Phi,B_\mu,W^i_\mu) - g_J^{\mu\nu}(\nabla_\mu\Phi)^\dagger\nabla_\nu\Phi - V(\Phi,\Phi^\dagger) \\ - \frac{1}{4}g_J^{\mu\rho}g_J^{\nu\sigma}B_{\mu\nu}B_{\rho\sigma} - \frac{1}{4}g_J^{\mu\rho}g_J^{\nu\sigma}W^i_{\mu\nu}W^i_{\rho\sigma}\Big] \end{aligned} \tag{2.7}$$

with

$$\begin{aligned} U(\Theta,\Phi,B_\mu,W^i_\mu) &= \frac{M_{\rm P}^2}{2}\left[\Psi(\Theta)\Theta - f(\Psi(\Theta),\Phi,B_\mu)\right] \\ &= \frac{M_{\rm P}^4}{4\xi_R}\left[\left(1-\Theta+\frac{\xi_H}{M_{\rm P}^2}|\Phi|^2 - \frac{2}{\Lambda^2M_{\rm P}^2}\frac{\epsilon^{\mu\nu\rho\sigma}}{\sqrt{-g_J}}B_{\mu\nu}B_{\rho\sigma} - \frac{2}{\Lambda^2M_{\rm P}^2}\frac{\epsilon^{\mu\nu\rho\sigma}}{\sqrt{-g_J}}W^i_{\mu\nu}W^i_{\rho\sigma}\right)^2\right]. \end{aligned} \tag{2.8}$$

Next, we Weyl-rescale the metric

$$g_{J\mu\nu} = \frac{1}{\Theta}\,g_{E\mu\nu}, \qquad g_J^{\mu\nu} = \Theta\,g_E^{\mu\nu}, \qquad \sqrt{-g_J} = \frac{1}{\Theta^2}\sqrt{-g_E}, \tag{2.9}$$

to write the action Einstein frame as

$$\begin{aligned} S_E = \int d^4x\sqrt{-g_E}\Big[\frac{M_{\rm P}^2}{2}R_E - \frac{3M_{\rm P}^2}{4}g_E^{\mu\nu}D_\mu(\ln\Theta)D_\nu(\ln\Theta) - \frac{1}{2\Theta}g_E^{\mu\nu}(\nabla_\mu\Phi)^\dagger\nabla_\nu\Phi - V_E \\ - \frac{1}{4}g_E^{\mu\rho}g_E^{\nu\sigma}B_{\mu\nu}B_{\rho\sigma} - \frac{1}{4}g_E^{\mu\rho}g_E^{\nu\sigma}W^i_{\mu\nu}W^i_{\rho\sigma}\Big] \end{aligned} \tag{2.10}$$

with

$$V_E = \frac{1}{\Theta^2}\left[V(\Phi,\Phi^\dagger) + U(\Theta,\Phi,B_\mu,W^i_\mu)\right], \tag{2.11}$$

$$R_J = \Theta\left[R_E + 3\Box_E\Theta - \frac{3}{2}g_E^{\mu\nu}D_\mu(\ln\Theta)D_\nu(\ln\Theta)\right]. \tag{2.12}$$

We have ignored the surface term $\Box_E = g_E^{\mu\nu}D_\mu D_\nu$ in the action S_E. With the field redefinition

$$\phi = M_{\rm P}\sqrt{\frac{3}{2}}\ln\Theta, \tag{2.13}$$

Eq. (2.10) finally becomes

$$\begin{aligned} S_E = \int d^4x\sqrt{-g_E}\Big[&\frac{M_{\rm P}^2}{2}R_E - \frac{1}{2}g_E^{\mu\nu}D_\mu\phi D_\nu\phi - e^{-\sqrt{\frac{2}{3}}\frac{\phi}{M_{\rm P}}}g_E^{\mu\nu}(\nabla_\mu\Phi)^\dagger\nabla_\nu\Phi - V_E \\ &- \frac{1}{4}g_E^{\mu\rho}g_J^{\nu\sigma}B_{\mu\nu}B_{\rho\sigma} - \frac{1}{4}g_E^{\mu\rho}g_E^{\nu\sigma}W^i_{\mu\nu}W^i_{\rho\sigma}\Big]. \end{aligned} \tag{2.14}$$

We now turn our attention to the Higgs and gauge fields. The $Q_Y = +1$ Higgs field decomposes as

$$\Phi = \frac{1}{\sqrt{2}}\begin{pmatrix}\phi_3 + i\phi_4 \\ h + i\phi_2\end{pmatrix}. \tag{2.15}$$

It is customary to perform a basis transformation for gauge bosons from the electroweak W^i_μ, B_μ to the mass and QED charge basis W_μ, Z_μ, A_μ as

$$\begin{aligned} W^1_\mu &= \frac{W^+_\mu + W^-_\mu}{\sqrt{2}}, & W^2_\mu &= \frac{i}{\sqrt{2}}\left(W^+_\mu - W^-_\mu\right), \\ W^3_\mu &= s_W A_\mu + c_W Z_\mu, & B_\mu &= c_W A_\mu - s_W Z_\mu, \end{aligned} \tag{2.16}$$

where $e = s_W g = c_W g'$ with shorthand s_W and c_W for the sine and cosine of the electroweak Weinberg angle θ_W. In the following, we will consider equations of motion (EoM) at the linear order. We therefore expand the action Eq. (2.14) to quadratic order

$$\begin{aligned} S_E = \int d^4x\sqrt{-g_E}\Big[&\frac{M_{\rm P}^2}{2}R_E - \frac{1}{2}G_{IJ}g_E^{\mu\nu}D_\mu\phi^I D_\nu\phi^J - V_E(\phi^I) - \frac{1}{4}g_E^{\mu\rho}g_E^{\nu\sigma}F_{A\mu\nu}F_{A\rho\sigma} - \frac{1}{4}g_E^{\mu\rho}g_E^{\nu\sigma}F_{Z\mu\nu}F_{Z\rho\sigma} \\ &- \frac{1}{2}g_E^{\mu\rho}g_E^{\nu\sigma}F^+_{W\mu\nu}F^-_{W\rho\sigma} - e^{-\sqrt{\frac{2}{3}}\frac{\phi}{M_{\rm P}}}g_E^{\mu\nu}\Big(\frac{g_Z^2}{8}h^2Z_\mu Z_\nu + \frac{g_Z}{2}\left[(D_\mu h)\,\phi_2 - (D_\mu\phi_2)h\right]Z_\nu + \frac{e^2}{4s_W^2}h^2W^+_\mu W^-_\nu + \\ &\frac{ie}{2\sqrt{2}s_W}D_\mu h\left[W^-_\nu(\phi_3 + i\phi_4) - W^+_\nu(\phi_3 - i\phi_4)\right] - \frac{ie}{2\sqrt{2}s_W}\left[W^-_\nu D_\mu(\phi_3 + i\phi_4) - W^+_\nu D_\mu(\phi_3 - i\phi_4)\right]h\Big), \end{aligned} \tag{2.17}$$

introducing $\phi^I \in \{\phi, h, \phi_2, \phi_3, \phi_4\}$, $g_Z = e/(s_W c_W)$, and the 5×5 field space metric G_{IJ} whose non-vanishing elements are

$$G_{\phi\phi} = 1, \qquad G_{hh} = e^{-\sqrt{\frac{2}{3}}\frac{\phi}{M_{\rm P}}}, \qquad G_{\phi_i\phi_i} = e^{-\sqrt{\frac{2}{3}}\frac{\phi}{M_{\rm P}}} \quad \text{with } i = 2,3,4. \tag{2.18}$$

We have treated Goldstone and gauge bosons as perturbations, i.e. they do not acquire any background values while deriving Eq (2.17). The potential $V_E(\phi^I)$ reads

$$\begin{aligned} V_E(\phi^I) = e^{-2\sqrt{\frac{2}{3}}\frac{\phi}{M_{\rm P}}}\Bigg[&\frac{\lambda}{4}\left(h^2 + \sum_{i=2}^4\phi_i^2\right)^2 + \frac{M_{\rm P}^4}{4\xi_R}\Bigg\{1 - e^{\sqrt{\frac{2}{3}}\frac{\phi}{M_{\rm P}}} + \frac{\xi_H}{M_{\rm P}^2}\left(h^2 + \sum_{i=2}^4\phi_i^2\right) \\ &- \frac{2}{\Lambda^2M_{\rm P}^2}\frac{\epsilon^{\mu\nu\rho\sigma}}{\sqrt{-g_E}}e^{2\sqrt{\frac{2}{3}}\frac{\phi}{M_{\rm P}}}B_{\mu\nu}B_{\rho\sigma} - \frac{2}{\Lambda^2M_{\rm P}^2}\frac{\epsilon^{\mu\nu\rho\sigma}}{\sqrt{-g_E}}e^{2\sqrt{\frac{2}{3}}\frac{\phi}{M_{\rm P}}}W^i_{\mu\nu}W^i_{\rho\sigma}\Bigg\}^2\Bigg] \\ \approx V_0(\phi^I) + &\frac{2M_{\rm P}^2}{\xi_R\Lambda^2}F(\phi^I)e^{\sqrt{\frac{2}{3}}\frac{\phi}{M_{\rm P}}}\left(F_{A\mu\nu}\widetilde{F}_A^{\mu\nu} + F_{Z\mu\nu}\widetilde{F}_Z^{\mu\nu} + 2F^+_{W\mu\nu}\widetilde{F}_W^{-\mu\nu}\right), \end{aligned} \tag{2.19}$$

where we have further introduced

$$F(\phi^I) = 1 - e^{-\sqrt{\frac{2}{3}}\frac{\phi}{M_{\rm P}}} - \frac{\xi_H}{M_{\rm P}^2}\left(h^2 + \sum_{i=2}^{4}\phi_i^2\right)e^{-\sqrt{\frac{2}{3}}\frac{\phi}{M_{\rm P}}}, \tag{2.20}$$

$$V_0(\phi^I) = \frac{\lambda}{4}\left(h^2 + \sum_{i=2}^{4}\phi_i^2\right)^2 e^{-2\sqrt{\frac{2}{3}}\frac{\phi}{M_{\rm P}}} + \frac{M_{\rm P}^4}{4\xi_R}F^2(\phi^I), \tag{2.21}$$

$$\widetilde{F}_A^{\mu\nu} = \frac{1}{2\sqrt{-g_E}}\epsilon^{\mu\nu\rho\sigma}F_{A\rho\sigma}, \quad \widetilde{F}_Z^{\mu\nu} = \frac{1}{2\sqrt{-g_E}}\epsilon^{\mu\nu\rho\sigma}F_{Z\rho\sigma}, \quad \widetilde{F}_W^{\pm\mu\nu} = \frac{1}{2\sqrt{-g_E}}\epsilon^{\mu\nu\rho\sigma}F_{W\rho\sigma}^{\pm}. \tag{2.22}$$

The field stress tensors for the massive and massless gauge bosons are

$$F_{A\mu\nu} = D_\mu A_\nu - D_\nu A_\mu = \partial_\mu A_\nu - \partial_\nu A_\mu, \tag{2.23a}$$

$$F_{Z\mu\nu} = D_\mu Z_\nu - D_\nu Z_\mu = \partial_\mu Z_\nu - \partial_\nu Z_\mu, \tag{2.23b}$$

$$F_{W\mu\nu}^{\pm} = D_\mu W_\nu^{\pm} - D_\nu W_\mu^{\pm} = \partial_\mu W_\nu^{\pm} - \partial_\nu W_\mu^{\pm}. \tag{2.23c}$$

Since the field-stress tensors are torsionless, the covariant derivatives become partial derivatives. Furthermore, in the linearized approximation, the field-stress tensors have reduced to the abelian case.

Varying the action, the equation of motion of the scalars fields ϕ^I can be written as

$$\begin{aligned}
&\Box\phi^K + \Gamma^K_{IJ}\, g_E^{\alpha\nu} D_\alpha\phi^I D_\nu\phi^J - G^{KM}V_{E,M} \\
&+ G^{KM}e^{-\sqrt{\frac{2}{3}}\frac{\phi}{M_{\rm P}}}\left(\sqrt{\frac{2}{3}}\frac{1}{M_{\rm P}}\right) g_E^{\alpha\nu}(\partial_\alpha\phi)\Big(\frac{g_Z}{2}\delta^3_M h Z_\nu + \frac{ie}{2\sqrt{2}s_W}\left[W_\nu^-(\delta^4_M + i\delta^5_M) - W_\nu^+(\delta^4_M - i\delta^5_M)\right]h\Big) \\
&- G^{KM}e^{-\sqrt{\frac{2}{3}}\frac{\phi}{M_{\rm P}}} g_E^{\alpha\nu}\Big(\frac{g_Z}{2}\; D_\alpha\left(\delta^3_M h Z_\nu\right) + \frac{ie}{2\sqrt{2}s_W}D_\alpha\left[\left(W_\nu^-(\delta^4_M + i\delta^5_M) - W_\nu^+(\delta^4_M - i\delta^5_M)\right]h\right)\Big) \\
&- G^{KM}\Big[e^{-\sqrt{\frac{2}{3}}\frac{\phi}{M_{\rm P}}} g_E^{\mu\nu}\delta^3_M\Big(\frac{g_Z}{2}(D_\mu h)Z_\nu\Big) + e^{-\sqrt{\frac{2}{3}}\frac{\phi}{M_{\rm P}}} g_E^{\mu\nu}\delta^4_M\Big(\frac{ie}{2\sqrt{2}s_W}D_\mu h\,(\,W_\nu^- - W_\nu^+)\Big) \\
&+ e^{-\sqrt{\frac{2}{3}}\frac{\phi}{M_{\rm P}}} g_E^{\mu\nu}\delta^5_M\Big(\frac{ie}{2\sqrt{2}s_W}D_\mu h\,(\,iW_\nu^- + iW_\nu^+)\Big)\Big] = 0,
\end{aligned} \tag{2.24}$$

where Γ^K_{IJ} are the Christoffel symbols associated with field-space metric. The EoMs for the Z boson, $W^\pm$ bosons and photon are

$$g_E^{\mu\alpha}g_E^{\nu\beta}D_\alpha F_{Z\mu\nu} + \frac{8M_{\rm P}^2}{\xi_R\Lambda^2}\partial_\alpha\left(F(\phi^I)e^{\sqrt{\frac{2}{3}}\,\phi/M_{\rm P}}\right)\widetilde{F}_Z^{\alpha\beta} - e^{-\sqrt{\frac{2}{3}}\frac{\phi}{M_{\rm P}}}g_E^{\mu\beta}\Big(\frac{g_Z^2}{4}h^2Z_\mu + \frac{g_Z}{2}\left(\phi_2 D_\mu h - h D_\mu\phi_2\right)\Big) = 0, \tag{2.25}$$

$$\begin{aligned}
g_E^{\mu\alpha}g_E^{\nu\beta}D_\alpha F_{W\mu\nu}^{\pm} + \frac{8M_{\rm P}^2}{\xi_R\Lambda^2}\partial_\alpha\left(F(\phi^I)e^{\sqrt{\frac{2}{3}}\,\phi/M_{\rm P}}\right)\widetilde{F}_W^{\pm\alpha\beta} - e^{-\sqrt{\frac{2}{3}}\frac{\phi}{M_{\rm P}}}g_E^{\mu\beta}\Big(\frac{e^2}{4s_W^2}h^2W_\mu^\pm \pm \frac{ie}{2\sqrt{2}s_W}D_\mu h\,(\phi_3 \pm i\phi_4) \\
\mp \frac{ie}{2\sqrt{2}s_W}D_\mu(\phi_3 \pm i\phi_4)h\Big) = 0,
\end{aligned} \tag{2.26}$$

$$g_E^{\mu\alpha}g_E^{\nu\beta}D_\alpha F_{A\mu\nu} + \frac{8M_{\rm P}^2}{\xi_R\Lambda^2}\partial_\alpha\left(F(\phi^I)e^{\sqrt{\frac{2}{3}}\,\phi/M_{\rm P}}\right)\widetilde{F}_A^{\alpha\beta} = 0. \tag{2.27}$$

3 Inflationary dynamics

The preheating after inflation depends on the background and perturbation dynamics. We closely follow covariant formalism as discussed in Ref. [53, 59, 60], which is suited for multifield inflation with non-canonical kinetic terms as encountered in our scenario. We decompose the $\phi^I(x^\mu)$ fields into a homogeneous classical background part (φ^I) and a perturbation ($\delta\phi^I$) part

$$\phi^I(x^\mu) = \varphi^I(t) + \delta\phi^I(x^\mu). \tag{3.1}$$

In the following, t labels the cosmic time and $\varphi^I(t) = \{\varphi(t), h_0(t)\}$, i.e. only the Higgs and inflaton fields acquire background field values while the Goldstone modes ϕ_2, ϕ_3 and ϕ_4 are perturbations. The perturbed spatially flat Friedmann-Robertson-Walker (FRW) metric can be expanded to linear order as [61–63]

$$ds^2 = -(1+2\mathcal{A})dt^2 + 2a(t)(\partial_i\mathcal{B})dx^i dt + a(t)^2\left[(1-2\psi)\delta_{ij} + 2\partial_i\partial_j\mathcal{E}\right]dx^i dx^j, \tag{3.2}$$

where $a(t)$ is scale factor. $\mathcal{A}, \mathcal{B}, \psi$ and $\mathcal{E}$ characterize the scalar metric perturbations. In this work, we adopt the longitudinal gauge where the scalar perturbations $\mathcal{B}$ and $\mathcal{E}$ vanish.

Utilizing Eq. (2.24) and Eq. (3.1), we find the EoMs for the background fields as

$$\mathcal{D}_t\dot{\varphi} + 3H\dot{\varphi} + G^{\phi J}V_{0,J} = 0, \tag{3.3a}$$
$$\mathcal{D}_t\dot{h}_0 + 3H\dot{h}_0 + G^{hJ}V_{0,J} = 0, \tag{3.3b}$$

where

$$\mathcal{D}_t A^I \equiv \dot{\varphi}^J \mathcal{D}_J A^I = \dot{A}^I + \Gamma^I{}_{JK}\dot{\varphi}^J A^K, \tag{3.4a}$$
$$\mathcal{D}_J A^I \equiv \partial_J A^I + \Gamma^I{}_{JK} A^K. \tag{3.4b}$$

We draw the reader's attention to the fact that the covariant derivative $\mathcal{D}_I$ of field space G_{IJ} shall not be confused with the covariant derivative D_μ of space-time metric $g_{J\mu\nu}$. The Hubble function is defined as

$$H^2 = \left(\frac{\dot{a}}{a}\right)^2 = \frac{1}{3M_{\rm P}^2}\left(\frac{1}{2}G_{IJ}\dot{\varphi}^I\dot{\varphi}^J + V_0(\varphi^I)\right), \tag{3.5}$$
$$\dot{H} = -\frac{1}{2M_{\rm P}^2}\left(G_{IJ}\dot{\varphi}^I\dot{\varphi}^J\right). \tag{3.6}$$

We solve the equations (3.3) and (3.5) together while simultaneously performing consistency check such that $\dot{H}$ estimated from Eq. (3.5) matches Eq. (3.6) with adequate precision. We define the number of e-foldings relative to the end of inflation as

$$\mathcal{N} \equiv \ln\frac{a(t)}{a(t_{\rm end})}, \tag{3.7}$$

which we will use in the following interchangeably with the cosmic time t. The background energy density is

$$\rho_{\rm inf} = \frac{1}{2}G_{IJ}\dot{\varphi}^I\dot{\varphi}^J + V_0(\varphi^I), \tag{3.8}$$

where G_{IJ} is evaluated at the background field order.

The field fluctuations $\delta\phi^I(x^\mu)$ are gauge-dependent quantities. However, we can construct covariant field fluctuations $\mathcal{Q}^I(x^\mu)$ which connect the scalar fields $\phi^I(x^\mu)$ with their background fields $\varphi^I(t)$ along a unique geodesic of the field-space manifold such that the field fluctuations can be written as [59, 64]

$$\delta\phi^I = \mathcal{Q}^I - \frac{1}{2}\Gamma^I{}_{JK}\mathcal{Q}^K\mathcal{Q}^J + \frac{1}{3!}\left(\Gamma^I{}_{MN}\Gamma^N{}_{JK} - \Gamma^I{}_{JK,M}\right)\mathcal{Q}^K\mathcal{Q}^J\mathcal{Q}^M + \dots\ . \tag{3.9}$$

This motivates one to consider gauge-independent Mukhanov-Sasaki variables for the field fluctuations expressed as [62, 65, 66]

$$Q^I = \mathcal{Q}^I + \frac{\dot{\varphi}^I}{H}\psi, \tag{3.10}$$

which is doubly covariant with respect to field-space and space-time transformations. The quantities $\mathcal{Q}^I$, $\dot{\varphi}^I$ and Q^I transform like vectors in the field-space manifold. In our five-field case, at the linear order, we thus have

$$Q^\phi = \mathcal{Q}^\phi + \frac{\dot{\varphi}}{H}\psi = \delta\varphi + \frac{\dot{\varphi}}{H}\psi, \tag{3.11a}$$
$$Q^h = \mathcal{Q}^h + \frac{\dot{h}_0}{H}\psi = \delta h + \frac{\dot{h}_0}{H}\psi, \tag{3.11b}$$
$$Q^{\phi_i} = \mathcal{Q}^{\phi_i} = \delta\phi_i = \phi_i, \qquad (i = 2, 3, 4) \tag{3.11c}$$

Inserting Eq. (3.10) and Eq. (3.2) in Eq. (2.24), we find the EoMs for the gauge independent Q^I at linear order as

$$\mathcal{D}_t^2 Q^\phi + 3H\mathcal{D}_t Q^\phi - \frac{\nabla^2}{a^2}Q^\phi + \mathcal{M}^\phi{}_\phi Q^\phi = 0, \tag{3.12}$$

$$\mathcal{D}_t^2 Q^h + 3H\mathcal{D}_t Q^h - \frac{\nabla^2}{a^2}Q^h + \mathcal{M}^h{}_h Q^h = 0, \tag{3.13}$$

$$\mathcal{D}_t^2 Q^{\phi_2} + 3H\mathcal{D}_t Q^{\phi_2} - \frac{\nabla^2}{a^2}Q^{\phi_2} + \mathcal{M}^{\phi_2}{}_{\phi_2} Q^{\phi_2} + \frac{g_Z}{2}\left[\left(\sqrt{\frac{2}{3}}\frac{1}{M_{\rm P}}\right)\dot\varphi h_0 Z_0 - 2\dot h_0 Z_0 + h_0 g_E^{\alpha\nu}(D_\alpha Z_\nu)\right] = 0, \tag{3.14}$$

$$\mathcal{D}_t^2 Q^{\phi_3} + 3H\mathcal{D}_t Q^{\phi_3} - \frac{\nabla^2}{a^2}Q^{\phi_3} + \mathcal{M}^{\phi_3}{}_{\phi_3} Q^{\phi_3} + \frac{ie}{2\sqrt{2}s_W}\left[\left(\sqrt{\frac{2}{3}}\frac{1}{M_{\rm P}}\right)\dot\varphi h_0\left(W_0^- - W_0^+\right) - 2\dot h_0\left(W_0^- - W_0^+\right)\right.$$
$$\left. + g_E^{\alpha\nu} h_0 D_\alpha\left(W_\nu^- - W_\nu^+\right)\right] = 0, \tag{3.15}$$

$$\mathcal{D}_t^2 Q^{\phi_4} + 3H\mathcal{D}_t Q^{\phi_4} - \frac{\nabla^2}{a^2}Q^{\phi_4} + \mathcal{M}^{\phi_4}{}_{\phi_4} Q^{\phi_4} + \frac{ie}{2\sqrt{2}s_W}\left[\left(\sqrt{\frac{2}{3}}\frac{1}{M_{\rm P}}\right)\dot\varphi h_0\left(iW_0^- + iW_0^+\right) - 2\dot h_0\left(iW_0^- + iW_0^+\right)\right.$$
$$\left. + g_E^{\alpha\nu} h_0 D_\alpha\left(iW_\nu^- + iW_\nu^+\right)\right] = 0, \tag{3.16}$$

with

$$\mathcal{M}^I{}_L = G^{IJ}(\mathcal{D}_L\mathcal{D}_J V_E) - \mathcal{R}^I{}_{JKL}\dot\varphi^J\dot\varphi^K - \frac{1}{M_{\rm P}^2 a^3}\mathcal{D}_t\left(\frac{a^3}{H}\dot\varphi^I\dot\varphi_L\right), \tag{3.17}$$

where the $\mathcal{R}^I{}_{JKL}$ is the field-space Riemann tensor. Here all relevant quantities such as V_0, G^{IJ}, $\Gamma^I{}_{JK}$, $\mathcal{R}^I{}_{JKL}$ are evaluated at background order. In contrast to Ref. [1], which focused on the unitary gauge for the Higgs sector, the EoMs for the perturbations Q^{ϕ_2}, Q^{ϕ_3} and Q^{ϕ_4} now depend on the Z and W bosons at linear order. Reference [1] solely focused on the production of the hypermagnetic fields *at the end of inflation*; the reheating temperature was treated as a free parameter. Therefore, the choice of unitary gauge was not relevant for the estimation of baryon asymmetry. However, for the present study of preheating, as is clear from the last terms involving Z and W bosons in the respective Eqs. (3.14), (3.15) and (3.16), the unitary gauge becomes ill-defined (specifically at zero crossings of the background fields).

Finally, and for later convenience, we re-express the EoMs of the scalar field fluctuations in conformal time τ such that line element becomes $ds^2 = a^2(\tau)\eta_{\mu\nu}dx^\mu dx^\nu$ with the rescaled variables $X^I(x^\mu) \equiv a(t)Q^I(x^\mu)$. Hence, performing the replacements $Z_0 \to Z_0/a$, $W_0^\pm \to W_0^\pm/a$ and $\partial_0 \to \partial_\tau/a$, we find new EoMs

$$\mathcal{D}_\tau^2 X^\phi - \left[\nabla^2 - a^2\left(\mathcal{M}^\phi{}_\phi - \frac{1}{6}R_E G^\phi{}_\phi\right)\right]X^\phi = 0, \tag{3.18}$$

$$\mathcal{D}_\tau^2 X^h - \left[\nabla^2 - a^2\left(\mathcal{M}^h{}_h - \frac{1}{6}R_E G^h{}_h\right)\right]X^h = 0, \tag{3.19}$$

$$\mathcal{D}_\tau^2 X^{\phi_2} - \left[\nabla^2 - a^2\left(\mathcal{M}^{\phi_2}{}_{\phi_2} - \frac{1}{6}R_E G^{\phi_2}{}_{\phi_2}\right)\right]X^{\phi_2} + a\, g_Z h_0\left(\Upsilon Z_0 - Z_0'\right) = 0, \tag{3.20}$$

$$\mathcal{D}_\tau^2 X^{\phi_3} - \left[\nabla^2 - a^2\left(\mathcal{M}^{\phi_3}{}_{\phi_3} - \frac{1}{6}R_E G^{\phi_3}{}_{\phi_3}\right)\right]X^{\phi_3} + a\,\frac{ie}{\sqrt{2}s_W}h_0\left[\Upsilon\left(W_0^- - W_0^+\right) - \left(W_0^{-\prime} - W_0^{+\prime}\right)\right] = 0, \tag{3.21}$$

$$\mathcal{D}_\tau^2 X^{\phi_4} - \left[\nabla^2 - a^2\left(\mathcal{M}^{\phi_4}{}_{\phi_4} - \frac{1}{6}R_E G^{\phi_4}{}_{\phi_4}\right)\right]X^{\phi_4} + a\,\frac{ie}{\sqrt{2}s_W}h_0\left[\Upsilon\left(iW_0^- + iW_0^+\right) - \left(iW_0^{-\prime} + iW_0^{+\prime}\right)\right] = 0, \tag{3.22}$$

where we defined

$$\Upsilon(\tau) = \frac{\varphi'}{\sqrt{6}M_{\rm P}} - \frac{a'}{a} - \frac{h_0'}{h_0}. \tag{3.23}$$

In these equations, as in the following, we have introduced the shorthand notation ($'$) for derivatives with respect to conformal time τ.

3.1 Gauge choice and equations of motion of the gauge and Goldstone bosons

We have already mentioned that the unitary gauge becomes ill-defined at the zero crossing of the background field h_0 (see also Refs. [52, 53]). We, therefore, choose the Coulomb gauge to study the dynamics of field fluctuations. In the Coulomb gauge, we have $\partial_i Z^i = 0$ and $\partial_i W^{\pm i} = 0$ and the Goldstone bosons are dynamical.

3.1.1 Z bosons

We begin with the EoM for the Z boson. The time (i.e. $\beta = 0$) and space (i.e. $\beta = i$) components of Eq. (2.25) at linear perturbation order in conformal time are

$$-\partial_i\left(\partial_i Z_0 - Z_i'\right) + a^2\, e^{-\sqrt{\frac{2}{3}}\frac{\varphi}{M_{\rm P}}}\left(\frac{g_Z^2}{4}h_0^2 Z_0 + \frac{g_Z}{2}\left(\phi_2 h_0' - h_0\phi_2'\right)\right) = 0, \tag{3.24}$$

$$\begin{aligned}-\partial_\tau\left(\partial_\tau Z_i - \partial_i Z_0\right) + \partial_j\left(\partial_j Z_i - \partial_i Z_j\right) - a^2\, e^{-\sqrt{\frac{2}{3}}\frac{\varphi}{M_{\rm P}}}\left(\frac{g_Z^2}{4}h_0^2 Z_i - \frac{g_Z}{2}h_0\partial_i\phi_2\right)\\ + \frac{4M_{\rm P}^2}{\xi_R\Lambda^2}\partial_\tau\left(F(\varphi^I)e^{\sqrt{\frac{2}{3}}\frac{\varphi}{M_{\rm P}}}\right)\epsilon^{ijk}\left(\partial_j Z_k - \partial_k Z_j\right) = 0.\end{aligned} \tag{3.25}$$

One can move to momentum space by considering

$$Z_0(\tau,\mathbf{x}) = \int \frac{d^3k}{(2\pi)^3}\widetilde{Z}_0(\tau,\mathbf{k})e^{-i\mathbf{k}\cdot\mathbf{x}}, \qquad Z_i(\tau,\mathbf{x}) = \int \frac{d^3k}{(2\pi)^3}\widetilde{Z}_i(\tau,\mathbf{k})e^{-i\mathbf{k}\cdot\mathbf{x}}, \tag{3.26}$$

where the $\widetilde{\mathbf{Z}} \equiv \left(\widetilde{Z}_i(\tau,\vec{k})\right)$ field can be written in terms of transverse and longitudinal components as

$$\widetilde{\mathbf{Z}}(\tau,\mathbf{k}) = \sum_{\lambda=\pm,L}\widetilde{Z}^\lambda(\tau,\mathbf{k})\;\hat{\epsilon}_Z^\lambda(\mathbf{k}), \tag{3.27}$$

with

$$i\mathbf{k}\cdot\hat{\epsilon}_Z^\pm(\mathbf{k}) = 0, \qquad i\mathbf{k}\cdot\hat{\epsilon}_Z^L(\mathbf{k}) = |\mathbf{k}| = k, \qquad i\mathbf{k}\times\hat{\epsilon}_Z^\pm(\mathbf{k}) = \pm k\;\hat{\epsilon}_Z^\pm(\mathbf{k}), \qquad \hat{\epsilon}_Z^\lambda(\mathbf{k})^* = \hat{\epsilon}_Z^\lambda(-\mathbf{k}). \tag{3.28}$$

The Coulomb gauge condition for the Z boson then implies

$$\partial_i Z^i = \partial_i\left(\overline{g}_E^{ik}Z_k\right) = \overline{g}_E^{ik}\partial_i Z_k = \frac{1}{a^2}\partial_i Z_i = 0, \tag{3.29}$$

which translates in the momentum space to

$$k_i\widetilde{Z}_i = \eta_{ij}k_i\widetilde{Z}^j = k_j\widetilde{Z}^j = \mathbf{k}\cdot\widetilde{\mathbf{Z}} = 0. \tag{3.30}$$

Inserting Eq. (3.27) in Eq. (3.30), we get $\widetilde{Z}^L = 0$ as a consequence of the gauge condition and Eq. (3.28). Using the gauge condition of Eq. (3.29) in Eqs. (3.24)-(3.25) and going to momentum space, we find

$$\widetilde{Z}_0 = e^{-\sqrt{\frac{2}{3}}\frac{\varphi}{M_{\rm P}}}\frac{g_Z}{2\mathcal{K}_Z}\left(h_0\widetilde{\phi}_2' - \widetilde{\phi}_2 h_0'\right), \tag{3.31}$$

$$\widetilde{Z}_i'' + a^2\mathcal{K}_Z\widetilde{Z}_i + ik_i\left(\widetilde{Z}_0' + a^2\, e^{-\sqrt{\frac{2}{3}}\frac{\varphi}{M_P}}\frac{g_Z}{2}h_0\widetilde{\phi}_2\right) + i\,\frac{4M_{\rm P}^2}{\xi_R\Lambda^2}\;\partial_\tau\left(F(\varphi^I)e^{\sqrt{\frac{2}{3}}\frac{\varphi}{M_P}}\right)\epsilon^{ijm}(k_j\widetilde{Z}_m - k_m\widetilde{Z}_j) = 0, \tag{3.32}$$

where we have defined

$$\mathcal{K}_Z = \frac{k^2}{a^2} + m_Z^2, \qquad m_Z^2 = \frac{g_Z^2}{4}e^{-\sqrt{\frac{2}{3}}\frac{\varphi}{M_{\rm P}}}h_0^2. \tag{3.33}$$

The three-components of Eq. (3.32) can then be brought to the form

$$\left[\widetilde{\mathbf{Z}}'' + a^2\mathcal{K}_Z\widetilde{\mathbf{Z}}\right] + i\mathbf{k}\left\{\widetilde{Z}_0' + a^2\, e^{-\sqrt{\frac{2}{3}}\frac{\varphi}{M_P}}\frac{g_Z}{2}h_0\widetilde{\phi}_2\right\} + \frac{8iM_{\rm P}^2}{\xi_R\Lambda^2}\partial_\tau\left(F(\varphi^I)e^{\sqrt{\frac{2}{3}}\frac{\varphi}{M_P}}\right)\left(\mathbf{k}\times\widetilde{\mathbf{Z}}\right) = \mathbf{0}. \tag{3.34}$$

This is a system of three differential equations. A linear combination of them is obtained by multiplying both sides of Eq. (3.34) by $i\mathbf{k}$ and utilizing Eq. (3.30): all terms in square bracket go to zero since $i\mathbf{k}\cdot\hat{\epsilon}_Z^\pm(\mathbf{k}) = 0$ and $\widetilde{Z}^L = 0$. The last term vanishes due to $\mathbf{k}\cdot\left(\mathbf{k}\times\widetilde{\mathbf{Z}}\right) \equiv 0$. In the end, we obtain the equation

$$\widetilde{Z}_0' = -a^2\, e^{-\sqrt{\frac{2}{3}}\frac{\varphi}{M_P}}\frac{g_Z}{2}h_0\widetilde{\phi}_2. \tag{3.35}$$

Together, Eqs. (3.31) and (3.35) imply a constraint for the scalar fields. We can now use these Eqs. (3.31) and (3.35) alongside the gauge condition to remove the Z fields from the EoM of X^{ϕ_2}. This makes $\widetilde{\phi}_2$ dynamical in place of the longitudinal component of the Z boson. Finally, multiplying $\hat{\epsilon}_Z^{\pm}(\mathbf{k})$ to both sides of Eq. (3.34), we obtain the EoM for the transverse modes (the two remaining equations)

$$\partial_\tau^2 \widetilde{Z}^\lambda + (\omega_Z^\lambda)^2 \ \widetilde{Z}^\lambda = 0, \qquad \text{with } (\lambda = \pm), \tag{3.36}$$

where

$$(\omega_Z^\lambda(\tau,k))^2 = a^2\mathcal{K}_Z + \lambda k \ \frac{8M_{\rm P}^2}{\xi_R\Lambda^2}\partial_\tau\left(F(\varphi^I)e^{\sqrt{\frac{2}{3}}\frac{\varphi}{M_{\rm P}}}\right) = k^2 + a^2\, m_Z^2(\tau) + \zeta^\lambda(\tau,k), \tag{3.37}$$

where, we identify

$$\zeta^\lambda(\tau,k) = \lambda k \ \frac{8M_{\rm P}^2}{\xi_R\Lambda^2}\partial_\tau\left(F(\varphi^I)e^{\sqrt{\frac{2}{3}}\frac{\varphi}{M_{\rm P}}}\right). \tag{3.38}$$

We shall return to the impact of different terms in $(\omega_Z^\lambda(\tau,k))^2$ shortly.

3.1.2 $W^\pm$ bosons

An identical consideration as for the Z bosons leads for the time and space components of Eq. (2.26) to

$$-\partial_i\left(\partial_i W_0^\pm - W_i^{\pm\prime}\right) + a^2\, e^{-\sqrt{\frac{2}{3}}\frac{\varphi}{M_{\rm P}}}\left(\frac{e^2}{4s_W^2}h_0^2 W_0^\pm \pm \frac{ie}{2\sqrt{2}s_W}\Big[(\phi_3 \pm i\phi_4)h_0' - h_0(\phi_3' \pm i\phi_4')\Big]\right) = 0, \tag{3.39}$$

$$\begin{aligned}-\partial_\tau\left(\partial_\tau W_i^\pm - \partial_i W_0^\pm\right) + \partial_j\left(\partial_j W_i^\pm - \partial_i W_j^\pm\right) - a^2\, e^{-\sqrt{\frac{2}{3}}\frac{\varphi}{M_{\rm P}}}\left(\frac{e^2}{2s_W^2}h_0^2 W_i^\pm \mp \frac{ie}{2\sqrt{2}s_W}h_0(\partial_i\phi_3 \pm i\partial_i\phi_4)\right)\\ + \frac{4M_{\rm P}^2}{\xi_R\Lambda^2}\ \partial_\tau\left(F(\varphi^I)e^{\sqrt{\frac{2}{3}}\frac{\varphi}{M_{\rm P}}}\right)\epsilon^{ijk}\left(\partial_j W_k^\pm - \partial_k W_j^\pm\right) = 0.\end{aligned} \tag{3.40}$$

We can again go in the momentum space, where the $\widetilde{\mathbf{W}}^\pm$ fields can be written in terms of transverse and longitudinal components as

$$\widetilde{\mathbf{W}}^\pm(\tau,\mathbf{k}) = \sum_{\lambda=\pm,L}\widetilde{W}^{\pm,\lambda}(\tau,\mathbf{k})\ \hat{\epsilon}_W^\lambda(\mathbf{k}), \tag{3.41}$$

with

$$i\mathbf{k}\cdot\hat{\epsilon}_W^\pm(\mathbf{k}) = 0, \qquad i\mathbf{k}\cdot\hat{\epsilon}_W^L(\mathbf{k}) = |\mathbf{k}| = k, \qquad i\mathbf{k}\times\hat{\epsilon}_W^\pm(\mathbf{k}) = \pm k\ \hat{\epsilon}_W^\pm(\mathbf{k}), \qquad \hat{\epsilon}_W^\lambda(\mathbf{k})^* = \hat{\epsilon}_W^\lambda(-\mathbf{k}). \tag{3.42}$$

The Coulomb gauge condition gives

$$\partial_i W^{\pm i} = \partial_i\left(\overline{g}_E^{ik}W_k^\pm\right) = \overline{g}_E^{ik}\partial_i W_k^\pm = \frac{1}{a^2}\partial_i W_i^\pm = 0 \tag{3.43}$$

and it translates to

$$k_i\widetilde{W}_i^\pm = \eta_{ij}k_i\widetilde{W}^{\pm j} = k_j\widetilde{W}^{\pm j} = \mathbf{k}\cdot\widetilde{\mathbf{W}}^\pm = 0. \tag{3.44}$$

Inserting Eq. (3.41) in Eq. (3.44), we obtain again $\widetilde{W}^{\pm,L} = 0$ similar to the previous section. Using the gauge condition of Eq. (3.43) in Eq. (3.39) and going to momentum space, we then find

$$\widetilde{W}_0^\pm = \mp\, e^{-\sqrt{\frac{2}{3}}\frac{\varphi}{M_{\rm P}}}\frac{ie}{2\sqrt{2}s_W\mathcal{K}_W}\Big[(\phi_3 \pm i\phi_4)h_0' - h_0(\phi_3' \pm i\phi_4')\Big], \tag{3.45}$$

$$\begin{aligned}\widetilde{W}_i^{\pm\prime\prime} + a^2\mathcal{K}_W\widetilde{W}_i^\pm + ik_i\left(\widetilde{W}_0^{\pm\prime} \pm a^2\, e^{-\sqrt{\frac{2}{3}}\frac{\varphi}{M_P}}\frac{ie}{2\sqrt{2}s_W}h_0(\widetilde{\phi}_3 \pm i\widetilde{\phi}_4)\right)\\ + ik_i\ \frac{4M_{\rm P}^2}{\xi_R\Lambda^2}\ \partial_\tau\left(F(\varphi^I)e^{\sqrt{\frac{2}{3}}\frac{\varphi}{M_P}}\right)\epsilon^{ijm}(k_j\widetilde{W}_m^\pm - k_m\widetilde{W}_j^\pm) = 0,\end{aligned} \tag{3.46}$$

with

$$\mathcal{K}_W = \frac{k^2}{a^2} + m_W^2, \qquad\qquad m_W^2 = \frac{e^2}{4s_W^2} e^{-\sqrt{\frac{2}{3}}\frac{\varphi}{M_P}} h_0^2. \tag{3.47}$$

Likewise, the three components of Eqs. (3.46) read as

$$\begin{aligned}\left[\widetilde{\mathbf{W}}^{\pm\prime\prime} + a^2\mathcal{K}_W\widetilde{\mathbf{W}}^{\pm}\right] + i\mathbf{k}\left\{\widetilde{W}_0^{\pm\prime} \pm a^2\, e^{-\sqrt{\frac{2}{3}}\frac{\varphi}{M_P}} \frac{ie}{2\sqrt{2}s_W} h_0(\widetilde{\phi}_3 \pm i\widetilde{\phi}_4)\right\} \\ + \frac{8iM_{\rm P}^2}{\xi_R\Lambda^2}\partial_\tau\left(F(\varphi^I)e^{\sqrt{\frac{2}{3}}\frac{\varphi}{M_P}}\right)\left(\mathbf{k}\times\widetilde{\mathbf{W}}^{\pm}\right) = \mathbf{0}.\end{aligned} \tag{3.48}$$

Applying the same procedure as for the Z boson, and using Eq. (3.48), we find

$$\widetilde{W}_0^{\pm\prime} = \mp\, a^2\, e^{-\sqrt{\frac{2}{3}}\frac{\varphi}{M_P}} \frac{ie}{2\sqrt{2}s_W} h_0(\widetilde{\phi}_3 \pm i\widetilde{\phi}_4). \tag{3.49}$$

Combing Eqs. (3.45) and (3.49), we can remove two degrees of freedom each from $W^\pm$ making the Goldstone ϕ_3 and ϕ_4 dynamical, leaving a constraint on the Goldstone fields $\widetilde{\phi}_3$ and $\widetilde{\phi}_4$. Finally, from Eq. (3.48) we get the EoM for the transverse modes

$$\partial_\tau^2\widetilde{W}^{\pm,\lambda} + (\omega_W^\lambda)^2\,\widetilde{W}^{\pm,\lambda} = 0 \text{ with } (\lambda = \pm). \tag{3.50}$$

where

$$(\omega_W^\lambda(\tau,k))^2 = a^2\mathcal{K}_W + \lambda k\,\frac{8M_{\rm P}^2}{\xi_R\Lambda^2}\partial_\tau\left(F(\varphi^I)e^{\sqrt{\frac{2}{3}}\frac{\varphi}{M_P}}\right) = k^2 + a^2\, m_W^2(\tau) + \zeta^\lambda(\tau,k). \tag{3.51}$$

3.1.3 Goldstone bosons

As discussed earlier, the Goldstone bosons are dynamical in the Coulomb gauge. The gauge choices remove the longitudinal components of the Z and $W^\pm$ and constraint equations for each fields. In the case of the Z boson, these equations, namely Eq. (3.31) and Eq. (3.35), can be used to make the ϕ_2 field dynamical. This is obtained as follows: We first rewrite the Eq. (3.20) in momentum space as

$$\mathcal{D}_\tau^2\widetilde{X}^{\phi_2} + \left(k^2 + a^2 m_{\text{eff},(\phi_2)}^2\right)\widetilde{X}^{\phi_2} + a\, g_Z h_0\left(\Upsilon\widetilde{Z}_0 - \widetilde{Z}_0'\right) = 0, \tag{3.52}$$

where we used the gauge condition $\partial_i\widetilde{Z}_i = 0$ and defined

$$m_{\text{eff},(\phi_i)}^2 = \mathcal{M}^{\phi_i}{}_{\phi_i} - \frac{1}{6}R_E G^{\phi_i}{}_{\phi_i}, \qquad\qquad (i = 2,3,4). \tag{3.53}$$

We then employ Eqs. (3.31) and (3.35) to get the EoM of the $\widetilde{X}^{\phi_2}$ as

$$\mathcal{D}_\tau^2\widetilde{X}^{\phi_2} + \mathcal{E}_{(\phi_2)}(\tau,k)\mathcal{D}_\tau\widetilde{X}^{\phi_2} + \omega_{(\phi_2)}^2(\tau,k)\widetilde{X}^{\phi_2} = 0, \tag{3.54}$$

where

$$\mathcal{E}_{(\phi_2)}(\tau,k) = 2\,\frac{m_Z^2}{\mathcal{K}_Z}\,\Upsilon, \tag{3.55a}$$

$$\omega_{(\phi_2)}^2(\tau,k) = k^2 + a^2\left(m_{\text{eff},(\phi_2)}^2 + m_Z^2\right) + \mathcal{E}_{(\phi_2)}\Upsilon. \tag{3.55b}$$

Similarly, Eqs. (3.21) and (3.22) lead to

$$\mathcal{D}_\tau^2\widetilde{X}^{\phi_3} + \mathcal{E}_{(\phi_3)}(\tau,k)\mathcal{D}_\tau\widetilde{X}^{\phi_3} + \omega_{(\phi_3)}^2(\tau,k)\widetilde{X}^{\phi_3} = 0, \tag{3.56a}$$

$$\mathcal{D}_\tau^2\widetilde{X}^{\phi_4} + \mathcal{E}_{(\phi_4)}(\tau,k)\mathcal{D}_\tau\widetilde{X}^{\phi_4} + \omega_{(\phi_4)}^2(\tau,k)\widetilde{X}^{\phi_4} = 0, \tag{3.56b}$$

with

$$\mathcal{E}_{(\phi_3)}(\tau,k) = \mathcal{E}_{(\phi_4)}(\tau,k) = 2\,\frac{m_W^2}{\mathcal{K}_W}\,\Upsilon, \tag{3.57a}$$

$$\omega^2_{(\phi_3)}(\tau,k) = k^2 + a^2\left(m^2_{\text{eff},(\phi_3)} + m^2_W\right) + \mathcal{E}_{(\phi_3)}\Upsilon, \tag{3.57b}$$

$$\omega^2_{(\phi_4)}(\tau,k) = k^2 + a^2\left(m^2_{\text{eff},(\phi_4)} + m^2_W\right) + \mathcal{E}_{(\phi_4)}\Upsilon. \tag{3.57c}$$

It is clear that all gauge bosons are decoupled from Eqs. (3.54) and (3.56). Furthermore, as only ϕ and h acquire background field values, the EoMs of the Goldstone bosons are decoupled not only from the EoMs of $\widetilde{X}^\phi$ and $\widetilde{X}^h$, they are also decoupled from each other.

4 Inflaton and Higgs quanta production

We now proceed with the quantization of the ϕ and h fields, and the production of the respective particles. For this, we follow closely Refs. [51, 67], which consider non-trivial field space manifolds relevant to our analysis. The G_{IJ} matrix is diagonal and only depends on $\phi^1 = \phi$, whereas the 3×3 lower block of $\mathcal{M}^I_J$ matrix involving the Goldstones is diagonal. Therefore, we can reduce the upper 2×2 block of $\mathcal{M}^I_J$ in our scenario to a two field model with ϕ and h. Quantization of the three Goldstone bosons is discussed separately in the following section alongside the massive gauge bosons. One may still have nonzero $\mathcal{M}^\phi{}_h$ and $\mathcal{M}^h{}_\phi$ if h_0 and ξ_H are not vanishingly small. The second order action involving the inflaton and Higgs fluctuations Q^I (with $I = \{1,2\}$) can be derived as in [51, 59]

$$S^{(2)}_{(\phi h)} = \int d^3x\, dt\, a^3\Big[-\frac{1}{2}\overline{g}^{\mu\nu}_E G_{IJ}\mathcal{D}_\mu Q^I \mathcal{D}_\nu Q^J - \frac{1}{2}\mathcal{M}_{IJ}Q^I Q^J\Big], \tag{4.1}$$

where G_{IJ}, $\mathcal{M}_{IJ}$ are evaluated at background order and $\overline{g}^{\mu\nu}_E \equiv (-1, a^2(t), a^2(t), a^2(t))$ is the unperturbed spatially flat FLRW metric. The latter action can be written in conformal time and with the rescaled variables $X^I(x^\mu)$ as

$$S^{(2)}_{(\phi h)} = \int d^3x\, d\tau\left[-\frac{1}{2}\eta^{\mu\nu}G_{IJ}(\mathcal{D}_\mu X^I)(\mathcal{D}_\nu X^J) - \frac{1}{2}\mathscr{M}_{IJ}X^I X^J\right], \tag{4.2}$$

with

$$\mathscr{M}_{IJ} = a^2\Big(\mathcal{M}_{IJ} - \frac{1}{6}G_{IJ}R_E\Big), \quad \text{with} \quad R_E = \frac{6a''}{a^3}. \tag{4.3}$$

The energy momentum tensor for the field fluctuation is given for the linearized theory as

$$T^{(\phi h)}_{\mu\nu} = G_{IJ}(\mathcal{D}_\mu X^I)(\mathcal{D}_\nu X^J) + \eta_{\mu\nu}\left[-\frac{1}{2}\eta^{\alpha\beta}G_{IJ}(\mathcal{D}_\alpha X^I)(\mathcal{D}_\beta X^J) - \frac{1}{2}\mathscr{M}_{IJ}X^I X^J\right], \tag{4.4}$$

with $T^{(\phi h)}_{00}$ denoting the associated energy density.

Transforming to momentum space, one can recast Eq. (4.2) into the form

$$S_{(\phi h)} = \int d\tau\, \mathcal{L}_{(\phi h)} = \int d\tau\, \frac{d^3k}{(2\pi)^3}\left[\frac{1}{2}\left|\partial_\tau \widetilde{X}^I\right|^2 - \frac{1}{2}\omega^2_{(I)}(\tau,k)\left|\widetilde{X}^I\right|^2\right], \tag{4.5}$$

with

$$\omega^2_{(I)}(\tau,k) = \left(k^2 + a^2 m^2_{\text{eff},(I)}(\tau)\right). \tag{4.6}$$

The effective masses are given by

$$m^2_{\text{eff},(\phi)}(\tau) = \mathcal{M}^\phi_\phi - \frac{1}{6}R_E = \frac{1}{a^2}\,\mathscr{M}^\phi{}_\phi, \qquad m^2_{\text{eff},(h)}(\tau) = \mathcal{M}^h_h - \frac{1}{6}R_E = \frac{1}{a^2}\,\mathscr{M}^h{}_h. \tag{4.7}$$

We identify

$$m^2_{1,(I)} = G^{(I)J}(\mathcal{D}_{(I)}\mathcal{D}_J V_E), \tag{4.8a}$$

$$m^2_{2,(I)} = -\mathcal{R}^{(I)}{}_{JK(I)}\dot{\varphi}^J\dot{\varphi}^K, \tag{4.8b}$$

$$m^2_{3,(I)} = -\frac{1}{M_{\rm P}^2 a^3}\mathcal{D}_t\left(\frac{a^3}{H}\dot{\varphi}^{(I)}\dot{\varphi}_{(I)}\right), \tag{4.8c}$$

$$m^2_{4,(I)} = -\frac{R_E}{6}, \tag{4.8d}$$

without summing over (I), such that

$$m^2_{\text{eff},(I)} = \sum_k m^2_{k,(I)}. \tag{4.9}$$

One advantage of writing the action in Eq. (4.5) (and consequently also Eqs. (3.18) and (3.19)) in conformal time as opposed to cosmic time is the absence of terms linear in $\mathcal{D}_\tau \widetilde{X}^I$. Hence, the canonical momentum in momentum space is found as

$$\hat{\widetilde{\pi}}^I(\tau,\mathbf{k}) = \partial_\tau \hat{\widetilde{X}}^I(\tau,\mathbf{k}), \tag{4.10}$$

$$\text{with } \left[\hat{\widetilde{X}}^I(\tau,\mathbf{k}), \hat{\widetilde{\pi}}^J(\tau,\mathbf{q})\right] = i(2\pi)^3\delta^{IJ}\delta^{(3)}(\mathbf{k}+\mathbf{q}), \tag{4.11}$$

where we have elevated the classical field fluctuations $\widetilde{X}^I$ to their respective quantized $\hat{\widetilde{X}}^I$ versions.

The quantized fluctuations $\hat{\widetilde{X}}^I(\tau,\mathbf{k})$ can be decomposed in momentum space as

$$\hat{\widetilde{X}}^I(\tau,\mathbf{k}) = \sum_m \left[u^I_m(\tau,k)\hat{a}_m(\mathbf{k}) + u^{I*}_m(\tau,k)\hat{a}^\dagger_m(-\mathbf{k})\right], \tag{4.12}$$

where $m \in \{1,2\}$ for $\{\phi, h\}$. $u^I_m(\tau,k)$ corresponds to the associated mode functions of the creation and annihilation operators $\hat{a}_m(\mathbf{k})$ and $\hat{a}^\dagger_m(-\mathbf{k})$. These are defined as

$$\hat{a}_m(\mathbf{k})\,|0\rangle = 0, \qquad\qquad \langle 0|\,\hat{a}^\dagger_m(\mathbf{k}) = 0, \tag{4.13}$$

and obey the usual commutator relationships

$$[\hat{a}_m(\mathbf{k}), \hat{a}_n(\mathbf{q})] = \left[\hat{a}^\dagger_m(\mathbf{k}), \hat{a}^\dagger_n(\mathbf{q})\right] = 0, \qquad \left[\hat{a}_m(\mathbf{k}), \hat{a}^\dagger_n(\mathbf{q})\right] = (2\pi)^3\delta_{mn}\delta^{(3)}(\mathbf{k}-\mathbf{q}). \tag{4.14}$$

Note that, we have $N = 2$ second order differential equations for the $\widetilde{X}^\phi$ and $\widetilde{X}^h$, the parametrization in Eq. (4.12) leads to N^2 complex mode functions $u^I_m(\tau,k)$, and hence $2N^2$ real-valued scalar functions. However, these two fluctuations are coupled through the EoMs via $\mathcal{M}^I{}_J$. This implies $2N(N-1)$ constraints, leading to $2N^2-2N(N-1) = 2N = 4$ independent solutions. The mode functions can be parametrized as

$$u^I_m(\tau,k) = t_{(m,I)}(\tau,k)e^I_m(\tau), \tag{4.15}$$

where the $t_{(m,I)}(\tau,k)$ are complex scalar functions and $e^I_m(\tau)$ are vielbeins of the field-space metric. Note, $x_{(m,I)}$ is not a field space vector, but the index I in brackets denotes individual species and is not summed over. The vielbeins satisfy the following conditions

$$\delta^{mn}e^I_m(\tau)e^J_n(\tau) = G^{IJ}(\tau), \tag{4.16}$$

and are real functions. For any arbitrary vector A^I in field space, we have,

$$\begin{aligned} A^m &= e^m_I A^I, & A^I &= e^I_m A^m, \\ e^m_I e^I_n &= \delta^m_n, & e^m_I e^J_m &= \delta^I_J. \end{aligned} \tag{4.17}$$

The covariant derivative of the vielbeins in terms of the spin connection reads

$$\mathcal{D}_I e^m_J = -\omega^{mn}_I e_{nJ}, \tag{4.18}$$

with $\omega^{mn}_I = -\omega^{nm}_I$ antisymmetric in the internal indices. Further, since the ω^{mn}_I is antisymmetric, the covariant derivative with respect to conformal time vanishes

$$\mathcal{D}_\tau e^m_J = 0, \tag{4.19}$$

for all m and J.

We take $t_{(1,\phi)}(\tau,k)=v_{1k}(\tau)$, $t_{(2,\phi)}(\tau,k)=v_{2k}(\tau)$, $t_{(1,h)}(\tau,k)=y_{1k}(\tau)$ and $t_{(2,h)}(\tau,k)=y_{2k}(\tau)$ for the quantization of Eq. (4.12). Hence, we get,

$$\widehat{\widetilde{X}}^{\phi}=\Big[\Big(v_{1k}(\tau)e_1^{\phi}(\tau)\hat{a}_1(\mathbf{k})+v_{2k}(\tau)e_2^{\phi}(\tau)\hat{a}_2(\mathbf{k})\Big)+\Big(v_{1k}^{*}(\tau)e_1^{\phi}(\tau)\hat{a}_1^{\dagger}(-\mathbf{k})+v_{2k}^{*}(\tau)e_2^{\phi}(\tau)\hat{a}_2^{\dagger}(-\mathbf{k})\Big)\Big]\,, \tag{4.20a}$$

$$\widehat{\widetilde{X}}^{h}=\Big[\Big(y_{1k}(\tau)e_1^{h}(\tau)\hat{a}_1(\mathbf{k})+y_{2k}(\tau)e_2^{h}(\tau)\hat{a}_2(\mathbf{k})\Big)+\Big(y_{1k}^{*}(\tau)e_1^{h}(\tau)\hat{a}_1^{\dagger}(-\mathbf{k})+y_{2k}^{*}(\tau)e_2^{h}(\tau)\hat{a}_2^{\dagger}(-\mathbf{k})\Big)\Big]\,. \tag{4.20b}$$

Going into momentum space and utilizing the quantization above, from the EoMs in Eq. (3.18) and (3.19) we get

$$v_{1k}''+\omega_{(\phi)}^2\,v_{1k}\,e_1^{\phi}=-a^2\mathcal{M}^{\phi}{}_{h}\;y_{1k}\,e_1^{h}, \tag{4.21a}$$

$$v_{2k}''+\omega_{(\phi)}^2\,v_{2k}\,e_2^{\phi}=-a^2\mathcal{M}^{\phi}{}_{h}\;y_{2k}\,e_2^{h}, \tag{4.21b}$$

$$y_{1k}''+\omega_{(h)}^2\,y_{1k}\,e_1^{h}=-a^2\mathcal{M}^{h}{}_{\phi}\;v_{1k}\,e_1^{\phi}, \tag{4.21c}$$

$$y_{2k}''+\omega_{(h)}^2\,y_{2k}\,e_2^{h}=-a^2\mathcal{M}^{h}{}_{\phi}\;v_{2k}\,e_2^{\phi}, \tag{4.21d}$$

with $\omega_{(I)}^2$ given by Eq. (4.6).

We are now equipped with necessary tools to derive the energy density. The comoving vacuum averaged energy density is defined as

$$\rho_{(\phi h)}=\int d^3x\,\big\langle T_{00}^{(\phi h)}\big\rangle=\int\frac{d^3k}{(2\pi)^3}\,\big\langle\rho_{k,(\phi h)}\big\rangle=\int\frac{d^3k}{(2\pi)^3}\;\rho^{\rm vev}_{k,(\phi h)}, \tag{4.22}$$

where we recall we are only considering $\phi^I\in\{\phi,h\}$ in this section. Taking the 00-component of $T_{00}^{(\phi h)}$ and expressing different fluctuation fields in momentum space via

$$F(t,\vec{x})=\int\frac{d^3k}{(2\pi)^3}\widetilde{f}(t,\mathbf{k})e^{-i\mathbf{k}\cdot\mathbf{x}},$$

we can perform one momentum integration via the Dirac delta function that appears after performing the position space integral. In $\rho_{k,(\phi h)}$, which is a quadratic function of fluctuations, one fluctuation is $\widetilde{X}^J(\tau,-\mathbf{k})$. The energy density spectra is therefore read

$$\rho_{k,(\phi h)}=\frac{1}{2}G_{IJ}\left(\mathcal{D}_\tau\widetilde{X}^I(\tau,\mathbf{k})\right)\left(\mathcal{D}_\tau\widetilde{X}^J(\tau,-\mathbf{k})\right)+\frac{1}{2}\left(k^2G_{IJ}+\mathscr{M}_{IJ}\right)\widetilde{X}^I(\tau,\mathbf{k})\widetilde{X}^J(\tau,-\mathbf{k}). \tag{4.23}$$

Inserting Eq. (4.12) in Eq. (4.23) we get energy density per mode k of the quantized fluctuations as

$$\begin{aligned}\rho^{\rm vev}_{k,(\phi h)}&=\big\langle\rho_{k,(\phi h)}\big\rangle=\frac{1}{2}\sum_{m,n}\left[\delta^{mn}\Big(G_{IJ}t'_{(m,I)}t^{*\prime}{}_{(n,J)}+\left(k^2G_{IJ}+\mathscr{M}_{IJ}\right)t_{(m,I)}t^{*}_{(n,J)}\Big)e^I_m e^J_n\right]\\&=\rho_k^{(\phi)}+\rho_k^{(h)}+\rho_k^{\rm int},\end{aligned} \tag{4.24}$$

with

$$\rho_k^{(\phi)}=\frac{1}{2}G_{\phi\phi}\left[(|v'_{1k}|^2+\omega^2_{(\phi)}\,|v_{1k}|^2)e_1^{\phi}e_1^{\phi}+(|v'_{2k}|^2+\omega^2_{(\phi)}\,|v_{2k}|^2)e_2^{\phi}e_2^{\phi}\right], \tag{4.25a}$$

$$\rho_k^{(h)}=\frac{1}{2}G_{hh}\left[(|y'_{1k}|^2+\omega^2_{(h)}\,|y_{1k}|^2)e_1^{h}e_1^{h}+(|y'_{2k}|^2+\omega^2_{(h)}\,|y_{2k}|^2)e_2^{h}e_2^{h}\right], \tag{4.25b}$$

$$\rho_k^{\rm int}=\frac{1}{2}(\mathscr{M}_{\phi h}+\mathscr{M}_{h\phi})\left[v_{1k}y^*_{1k}e_1^{h}e_1^{\phi}+v_{2k}y^*_{2k}e_2^{h}e_2^{\phi}\right], \tag{4.25c}$$

where we used Eq. (4.6) and Eq. (4.7).

As we already discussed, in this paper we primarily focus on the R^2-like regime and assume that the background value of h_0 is much smaller than φ, which essentially reduces our scenario to a single field attractor-like scenario. We consider three benchmark points (BP) [1] for our analysis, summarized in Tab. I. The BPa is deep in the R^2-like

BP	ξ_R	ξ_H	$\varphi(t_{\rm in})$ $[M_{\rm P}]$	$h_0(t_{\rm in})$ $[M_{\rm P}]$
a	2.35×10^9	10^{-3}	5.5	2×10^{-4}
b	2.55×10^9	1	5.5	8.94×10^{-4}
c	2.2×10^9	10	5.4	5.00×10^{-3}

Table I. Benchmark points chosen for our analysis. Scales are given in units of the Planck mass $M_{\rm P}$. See text for details.

regime with ξ_H being negligibly small. We can therefore expect this scenario to behave practically like Starobinsky inflation. BPb and BPc parametrize mixed R^2-Higgs scenarios, with $\xi_H = 1$ for BPb and $\xi_H = 10$ for BPc. For all three BPs, the corresponding scalar amplitude, spectral index and tensor-to-scalar ratio are in agreement with the Planck 2018 data [50] within the 95% confidence level (CL) interval [1]. We have checked that the off-diagonal elements $\mathcal{M}^{\phi}{}_{h} \sim 0$ and $\mathcal{M}^{h}{}_{\phi} \sim 0$ and, hence, $\mathcal{M}^{I}{}_{J}$ is essentially diagonal for all three BPs. Consequently, the vielbeins also are diagonal, $e_2^{\phi} \sim 0$, $e_1^{h} \sim 0$ and $\widetilde{X}^{\phi}$ and $\widetilde{X}^{h}$ depend only on the scalar mode functions $v_{1k}(\tau)$ and $y_{2k}(\tau)$, respectively. Therefore, Eq. (4.21a) and Eq. (4.21d) essentially satisfy source-free EoMs while Eq. (4.21b) and Eq. (4.21c) vanish. We are left with

$$v_{1k}'' + \omega_{(\phi)}^2\, v_{1k} \simeq 0, \tag{4.26a}$$
$$y_{2k}'' + \omega_{(h)}^2\, y_{2k} \simeq 0, \tag{4.26b}$$

and the energy densities for the inflaton and Higgs fluctuations per mode read

$$\rho_k^{(\phi)} = \frac{1}{2}G_{\phi\phi}\left(|v_{1k}'|^2 + \omega_{(\phi)}^2|v_{1k}|^2\right) e_1^{\phi}e_1^{\phi} = \frac{1}{2}\left(|v_{1k}'|^2 + \omega_{(\phi)}^2|v_{1k}|^2\right), \tag{4.27a}$$
$$\rho_k^{(h)} = \frac{1}{2}G_{hh}\left(|y_{2k}'|^2 + \omega_{(h)}^2|y_{2k}|^2\right) e_2^{h}e_2^{h} = \frac{1}{2}\left(|y_{2k}'|^2 + \omega_{(h)}^2|y_{2k}|^2\right), \tag{4.27b}$$
$$\rho_k^{\rm int} = \mathcal{O}(h^2) \sim 0. \tag{4.27c}$$

Note that equation of motion of the mode functions are decoupled for all three BPs. It is worth noting that, in the single field like regime v_{1k} corresponds to the mode function for the adiabatic mode while y_{2k} corresponds to isocurvature mode [1, 68].

Let us take a closer look at the different contributions to $m^2_{{\rm eff},(\phi)}$ and $m^2_{{\rm eff},(h)}$ as displayed in Fig. 1 for all three BPs. The dominant contribution to $m^2_{{\rm eff},(\phi)}$ for all three BPs before the end of inflation arises from $m^2_{4,(I)}$, which turns $m^2_{{\rm eff},(\phi)}$ large and negative. After inflation, $m^2_{1,(\phi)}$ provides the largest but positive contributions to $m^2_{{\rm eff},(\phi)}$ for all three BPs. The same behavior is observed for the Higgs field for BPa, the dominant contribution to $m^2_{{\rm eff},(h)}$ before the end of the inflation stems again from $m^2_{4,(h)}$. However, for BPb and BPc, $m^2_{1,({\rm h})}$ overpowers $m^2_{4,({\rm h})}$. After the end of inflation, $m^2_{1,({\rm h})}$ constitutes the largest contribution to $m^2_{{\rm eff},(h)}$ for all three BPs, which oscillates around the minimum. This oscillation, makes $m^2_{{\rm eff},(h)}$ negative periodically with largest amplitude for BPc, due to the comparably larger value of ξ_H for BPc. We note that if $m^2_{{\rm eff},(I)} < 0$, modes with $k^2/a^2 < \left|m^2_{{\rm eff},(I)}\right|$ will experience tachyonic instability, which may lead to exponential growth in energy density. In the case of a tachyonic regime, we shall use the definition

$$\omega^2_{(I)}(\tau, k) = \left(k^2 + \left|a^2 m^2_{{\rm eff},(I)}(\tau)\right|\right), \tag{4.28}$$

instead of Eq. (4.6) when computing the energy density [69]. This is because the standard definition of the occupation number, which was extensively used in modeling preheating, is only valid for $m^2_{{\rm eff},(I)} \geqslant 0$. We shall return to the impact of $m^2_{{\rm eff},(I)}$ on preheating shortly.

The energy densities in Eqs. (4.40) are not vacuum-subtracted. To identify the latter, we first define the Bunch-Davies (BD) vacuum as

$$v_{1k} = c_1^{\phi}\left(1 - \frac{i}{k\tau}\right)e^{-ik\tau} + c_2^{\phi}\left(1 + \frac{i}{k\tau}\right)e^{ik\tau}, \tag{4.29a}$$
$$y_{2k} = c_1^{h}\left(1 - \frac{i}{k\tau}\right)e^{-ik\tau} + c_2^{h}\left(1 + \frac{i}{k\tau}\right)e^{ik\tau}. \tag{4.29b}$$

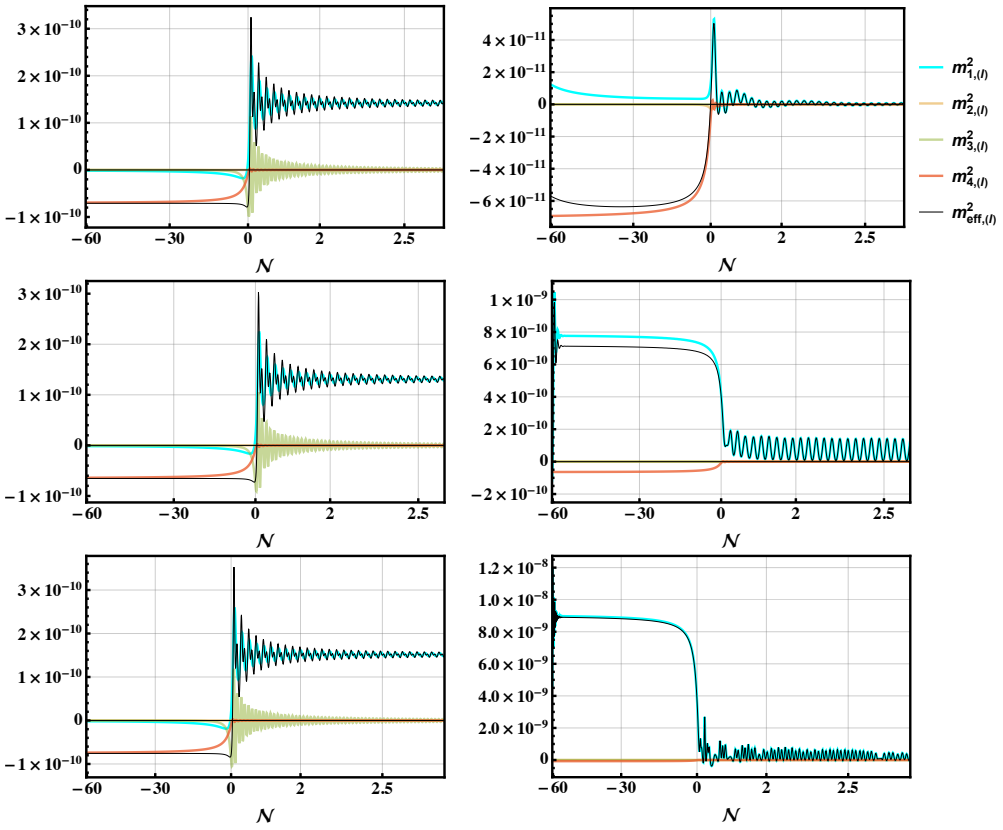

Figure 1. The effective masses $m^2_{\text{eff},(I)}$ (black) for ϕ (left) and h (right) as in Eq. (4.7) and their respective contributions (4.8) for BPa (upper row), BPb (middle row) and BPc (lower row). See text for details.

The normalization $v_{1k}v^{*\prime}_{1k} - v^{\prime}_{1k}v^{*}_{1k} = i$ and $y_{2k}y^{*\prime}_{2k} - y^{\prime}_{2k}y^{*}_{2k} = i$ yields constraints

$$|c_1^{\phi}|^2 - |c_2^{\phi}|^2 = \frac{1}{2k}, \tag{4.30a}$$

$$|c_1^{h}|^2 - |c_2^{h}|^2 = \frac{1}{2k}. \tag{4.30b}$$

Here, variations in the mode functions v_{1k} and y_{2k} could be accompanied by respective annihilation operators such that $\widetilde{X}^{\phi}$ and $\widetilde{X}^{h}$ remains unchanged. Each such solution corresponds to a different vacuum, however, we may require that the vacuum state $|0\rangle$ is the minimum energy state (ground state) of the Hamiltonian.

The Hamiltonian for the inflaton and Higgs fluctuations is written as

$$\begin{aligned}\hat{\mathcal{H}} &= \int \frac{d^3k}{(2\pi)^3} \left\langle T_{00}^{(\phi h)} \right\rangle \\ &= \frac{1}{2}\int \frac{d^3k}{(2\pi)^3} \left[\left(|v^{\prime}_{1k}|^2 + \omega^2_{(\phi)}|v_{1k}|^2 \right) \left(\hat{a}_1^{\dagger}(\mathbf{k})\hat{a}_1(\mathbf{k}) + \delta^3(\mathbf{0}) \right) + \left(|y^{\prime}_{2k}|^2 + \omega^2_{(h)}|y_{2k}|^2 \right) \left(\hat{a}_2^{\dagger}(\mathbf{k})\hat{a}_2(\mathbf{k}) + \delta^3(\mathbf{0}) \right) \right]. \end{aligned} \tag{4.31}$$

The vacuum expectation value of the Hamiltonian is

$$\left\langle \hat{\mathcal{H}} \right\rangle = \int \frac{d^3k}{(2\pi)^3} \left[\rho_k^{(\phi)}\delta^3(\mathbf{0}) + \rho_k^{(h)}\delta^3(\mathbf{0}) \right], \tag{4.32}$$

where $\delta^3(\mathbf{0})$ is divergent and arises due to integrating an infinite volume as usual. At sufficiently early times i.e. $\tau \to -\infty$, the vacuum choice of Eqs. (4.29) leads to

$$v_{1k} = c_1^{\phi} e^{-ik\tau} + c_2^{\phi} e^{ik\tau}, \tag{4.33a}$$

$$y_{2k} = c_1^h e^{-ik\tau} + c_2^h e^{ik\tau}, \tag{4.33b}$$

where along with the constraints Eqs. (4.30), $\left\langle \hat{\mathcal{H}} \right\rangle$ minimized if

$$c_1^\phi = \frac{1}{\sqrt{2k}}, \qquad c_2^\phi = 0, \qquad c_1^h = \frac{1}{\sqrt{2k}}, \qquad c_2^h = 0. \tag{4.34}$$

Therefore, the desired vacuum solutions (i.e. the so-called BD vacuum) at early times become

$$v_{1k}^{\rm BD} = \frac{1}{\sqrt{2k}} e^{-ik\tau}, \qquad y_{2k}^{\rm BD} = \frac{1}{\sqrt{2k}} e^{-ik\tau}. \tag{4.35}$$

The physical BD-vacuum energy is identified as

$$\rho_{(\phi)}^{\rm BD} = \frac{1}{2a^4} \int \frac{d^3k}{(2\pi)^3} \left(|v_{1k}^{\rm BD\prime}|^2 + \omega_{(\phi)}^2 |v_{1k}^{\rm BD}|^2 \right), \tag{4.36a}$$

$$\rho_{(h)}^{\rm BD} = \frac{1}{2a^4} \int \frac{d^3k}{(2\pi)^3} \left(|y_{2k}^{\rm BD\prime}|^2 + \omega_{(h)}^2 |y_{2k}^{\rm BD}|^2 \right). \tag{4.36b}$$

At sufficiently early times and for large modes we have $k^2/a^2 \gg |m_{{\rm eff},(I)}^2(t)|$. Hence $\omega_{(I)}^2 \simeq k^2$, and the vacuum energy becomes for both fields

$$\rho_{(I)}^{\rm BD} = \int dk \, \frac{k^2}{2\pi^2 a^4} \rho_{k,(I)}^{\rm BD} = \frac{1}{a^4} \int dk \, \frac{k^3}{4\pi^2}. \tag{4.37}$$

The energy density of the inflaton and Higgs quanta is then obtained by removing the BD vacuum from the classical solution as

$$\rho_{(\phi)}^q = \rho_{(\phi)} - \rho_{(\phi)}^{\rm BD}, \tag{4.38a}$$

$$\rho_{(h)}^q = \rho_{(h)} - \rho_{(h)}^{\rm BD}. \tag{4.38b}$$

It is, however, computationally less challenging to solve Eqs. (4.26) in cosmic time. Therefore, we rewrite them in cosmic time as

$$\ddot{v}_{1k} + H\dot{v}_{1k} + \left(\frac{k^2}{a^2} + m_{{\rm eff},(\phi)}^2(t) \right) v_{1k} \simeq 0, \tag{4.39a}$$

$$\ddot{y}_{2k} + H\dot{y}_{2k} + \left(\frac{k^2}{a^2} + m_{{\rm eff},(h)}^2(t) \right) y_{2k} \simeq 0. \tag{4.39b}$$

Utilizing, Eq. (4.22), and Eqs. (4.27c), we can find the corresponding (physical) energy densities for ϕ and h fluctuations in cosmic time

$$\rho_{(\phi)} = \frac{\left\langle \rho_c^\phi(x^\mu) \right\rangle}{a^4} = \frac{1}{a^2} \int \frac{k^2}{4\pi^2} dk \left[|\dot{v}_{1k}|^2 + \left(\frac{k^2}{a^2} + \left| m_{{\rm eff},(\phi)}^2(t) \right| \right) |v_{1k}|^2 \right], \tag{4.40a}$$

$$\rho_{(h)} = \frac{\left\langle \rho_c^h(x^\mu) \right\rangle}{a^4} = \frac{1}{a^2} \int \frac{k^2}{4\pi^2} dk \left[|\dot{y}_{2k}|^2 + \left(\frac{k^2}{a^2} + \left| m_{{\rm eff},(h)}^2(t) \right| \right) |y_{2k}|^2 \right]. \tag{4.40b}$$

To solve the Eqs. (4.39) in cosmic time we use the BD initial condition and initialize all relevant modes about ~ 5 e-foldings before the end of inflation, $\mathcal{N} \sim -5$

$$\lim_{t\to-\infty} v_{1k}(k,t) = \lim_{t\to-\infty} y_{2k}(k,t) = \frac{e^{-\frac{ikt}{a}}}{\sqrt{2k}}, \qquad \lim_{t\to-\infty} \dot{v}_{1k}(k,t) = \lim_{t\to-\infty} \dot{y}_{2k}(k,t) = -\frac{i}{a}\sqrt{\frac{k}{2}}\, e^{-\frac{ikt}{a}}. \tag{4.41}$$

After solving Eqs. (4.39) and evaluating $\rho_{(\phi)}$ and $\rho_{(h)}$ in cosmic time, one can plug them in Eqs. (4.38) to find respective energy densities.

In Fig. 2, we plot the spectra (solid) of the energy densities for ϕ and h alongside the BD spectra (dashed) for all three BPs for different $\mathcal{N}$. The figure allows us to identify the upper limit of the k, i.e., the corresponding value where the bare spectra match the BD ones. Once the upper limit is identified, we evaluate the quantum energy densities for ϕ

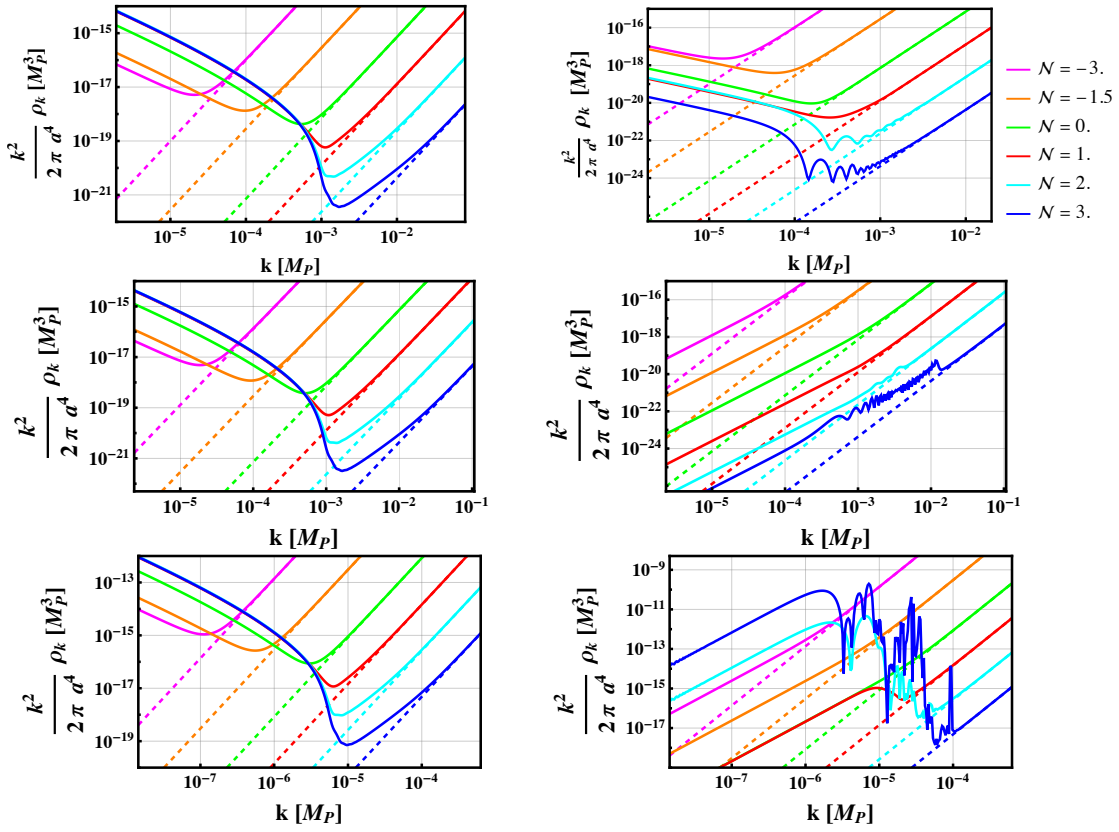

Figure 2. Spectra of $\frac{k^2}{2\pi^2 a^4}\rho_{k,(I)}$ (solid) and $\frac{k^2}{2\pi^2 a^4}\rho^{\rm BD}_{k,(I)}$ (dashed) for ϕ (left) and h (right) as given in Eqs. (4.37) and (4.38) for BPa (upper row), BPb (middle row) and BPc (lower row).

and h via Eqs. (4.38). In practice, we generate all spectra with wave number close to the unitarity cut-off $k_{\rm UV}$ (which is $M_{\rm P}$ in case of R^2-Higgs inflation [22, 24]). However, to find the quantum energy density from Eqs. (4.38), we utilize an adaptive numerical code that considers only those modes for which the relative error between ρ_k and $\rho_k^{\rm BD}$ is about 10% with $\rho_k > \rho_k^{\rm BD}$, ensuring vacuum is subtracted properly. The lower limit of the relevant modes in Eqs. (4.38), on the other hand, is chosen from different dynamics. Since thermalization during (p)reheating proceeds through particle interactions, the relevant modes are those which reside within the horizon at the time of consideration. Modes that are super-horizon are so-called frozen-in and cannot take part in such processes [53]. In our numerical analysis, this is done via the same adaptive code that only includes modes that have large enough physical wave-numbers to be inside the horizon at the time that we are considering. Further, for solving Eqs. (4.39), we have ensured that all modes are initialized deep inside the horizon such that the dynamics at the onset of preheating is captured.

We show the energy densities $\rho^q_{(\phi)}$ (blue), $\rho^q_{(h)}$ (red) and the background energy density $\rho_{\rm inf}$ (black) in Fig. 3. For BPa and BPb, both $\rho^q_{(\phi)}$ and $\rho^q_{(h)}$ are much smaller than $\rho_{\rm inf}$, which is well above the plotted range and not displayed. The $\rho^q_{(\phi)}$ remains practically unchanged between all the BPs primarily because of the value of ξ_R, which is practically the same for all three BPs. Around the end of inflation, $\rho^q_{(\phi)}$ receives a tachyonic (exponential) amplification, which can be easily understood as $m^2_{{\rm eff},(\phi)} < 0$ in Fig. 1. This is due to $m^2_{4,(\phi)}$ dominating over all other terms in $m^2_{{\rm eff},(\phi)}$ before the end of inflation. After inflation, $m^2_{1,(\phi)}$ dominates and oscillates but never goes below zero. We then find the production of inflaton quanta will not preheat the Universe.

The situation changes for $\rho^q_{(h)}$ due to the range of ξ_H values for different BPs. For BPa, $m^2_{{\rm eff},(h)}$ remains negative before the end of inflation due to negative $m^2_{4,({\rm h})}$, however, after the end of inflation $m^2_{1,({\rm h})}$ dominates and becomes periodically negative due to zero crossing of h_0 condensate, as can be seen from Fig. 1. But this is not sufficient to drive tachyonic growth of $\rho^q_{(h)}$ due to a small amplitude, rather we observe a damping of $\rho^q_{(h)}$ as displayed in Fig. 3. This is chiefly due to the smallness of $\xi_H \sim 10^{-3}$ for BPa, which is essentially deep inside R^2-like regime. In contrast,

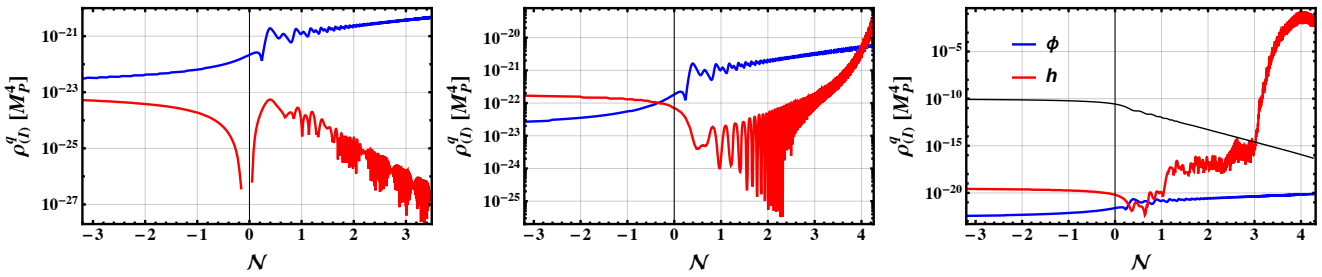

Figure 3. The energy densities $\rho^q_{(\phi)}$ (blue) and $\rho^q_{(h)}$ (red) as defined in Eqs. (4.38) for the three benchmark points. The black line displays the background energy density $\rho_{\rm inf}$.

for BPb and BPc, $m^2_{{\rm eff},(h)}$ is large positive for $\mathcal{N} < 0$ but oscillates for $\mathcal{N} \gtrsim 0$. For BPb, after the end of inflation, $m^2_{{\rm eff},(h)}$ does not go below zero in the plotted range $\mathcal{N} \lesssim 3$ (see Fig. 1). Thus, $\rho^q_{(h)}$ does not undergo tachyonic growth for BPb and $\rho^q_{(h)}$ still remains much smaller than $\rho_{\rm inf}$. As a result, for BPb, Higgs production will lead to inefficient and incomplete preheating. In contrast, for BPc, $m^2_{{\rm eff},(h)}$ turns negative for $\mathcal{N} \gtrsim 0$, but the amplitude becomes small as we approach $\mathcal{N} \gtrsim 1.5$. Therefore, in the initial stage of preheating, $\rho^q_{(h)}$ experiences tachyonic growth, but parametric resonance takes over for the later part of the preheating. We find successful preheating for BPc which is completed at $\mathcal{N} \sim 3$. Here we understand "completion" of preheating as the point in the time evolution when $\rho^q_{(h)}$ becomes equal to the background energy density $\rho_{\rm inf}$. A more conservative approach is adopted by Ref. [53] where the authors understand completion of preheating as $\rho^q_{(h)} \sim 0.1\rho_{\rm inf}$ (the linear analysis is not reliable when $\rho^q_{(h)}$ approaches $\rho_{\rm inf}$). Our results for baryogenesis are not significantly impacted by the choice between these conventions. We also remark that the growth in $\rho^q_{(h)}$ beyond $\mathcal{N} \sim 3$ for BPc is indicative of the breakdown of our linear order estimation. This growth is expected to be shut off once the decay of the produced particles, backreaction and rescattering effects are taken into account. We shall discuss this in more detail in Sec. 7.

5 Production of Z, W and Goldstone bosons

In this section, we focus on a detailed discussion of particle production of gauge and Goldstone bosons.

5.1 Equations of motion and quantization

We consider the second-order action involving Goldstone and gauge bosons

$$\begin{aligned} S^{(2)}_{\rm G} = \int d^3x\, dt\, a^3 \Bigg[& -\frac{1}{2}\overline{g}^{\mu\nu}_E G_{IJ}\mathcal{D}_\mu Q^I \mathcal{D}_\nu Q^J - \frac{1}{2}\mathcal{M}_{IJ}Q^I Q^J \\ & - e^{-\sqrt{\frac{2}{3}}\frac{\varphi}{M_{\rm P}}}\overline{g}^{\mu\nu}_E \Bigg\{ \left(Q^J\partial_\mu h_0 - h_0\partial_\mu Q^J\right)\left(\delta^3_J\frac{g_Z}{2}Z_\nu + \frac{ie}{2\sqrt{2}s_W}\left[(\delta^4_J + i\delta^5_J)W^-_\nu - (\delta^4_J - i\delta^5_J)W^+_\nu\right]\right) \\ & + \frac{g_Z^2}{8}h_0^2 Z_\mu Z_\nu + \frac{e^2}{4s_W^2}h_0^2 W^+_\mu W^-_\nu \Bigg\} - \frac{1}{4}\overline{g}^{\mu\rho}_E\overline{g}^{\nu\sigma}_E F_{Z\mu\nu}F_{Z\rho\sigma} - \frac{1}{2}\overline{g}^{\mu\rho}_E\overline{g}^{\nu\sigma}_E F^+_{W\mu\nu}F^-_{W\rho\sigma} \\ & - \frac{M_{\rm P}^2}{\xi_R\Lambda^2}F(\varphi^I)e^{\sqrt{\frac{2}{3}}\frac{\varphi}{M_{\rm P}}}\frac{\epsilon^{\mu\nu\rho\sigma}}{a^3}F_{Z\mu\nu}F_{Z\rho\sigma} - \frac{2M_{\rm P}^2}{\xi_R\Lambda^2}F(\varphi^I)e^{\sqrt{\frac{2}{3}}\frac{\varphi}{M_{\rm P}}}\frac{\epsilon^{\mu\nu\rho\sigma}}{a^3}F^+_{W\mu\nu}F^-_{W\rho\sigma}\Bigg], \end{aligned} \tag{5.1}$$

where $I, J = \{3, 4, 5\}$ everywhere, except inside $F(\varphi^I)$ where $\varphi^I \in \{\varphi, h_0\}$. In conformal time, the action becomes

$$\begin{aligned} S^{(2)}_{\rm G} = \int d^3x\, d\tau \Bigg[& -\frac{1}{2}\eta^{\mu\nu}G_{IJ}(\mathcal{D}_\mu X^I)(\mathcal{D}_\nu X^J) - \frac{1}{2}\mathscr{M}_{IJ}X^I X^J \\ & - a\, e^{-\sqrt{\frac{2}{3}}\frac{\varphi}{M_{\rm P}}}\eta^{00}\left(X^J(\partial_\tau h_0) - h_0(\partial_\tau X^J) + \frac{\partial_\tau a}{a}h_0 X^J\right)\left(\delta^3_J\frac{g_Z}{2}Z_0 + \frac{ie}{2\sqrt{2}s_W}\left[(\delta^4_J + i\delta^5_J)W^-_0 - (\delta^4_J - i\delta^5_J)W^+_0\right]\right) \\ & - a^2\, e^{-\sqrt{\frac{2}{3}}\frac{\varphi}{M_{\rm P}}}\eta^{\mu\nu}\left(\frac{g_Z^2}{8}h_0^2 Z_\mu Z_\nu + \frac{e^2}{4s_W^2}h_0^2 W^+_\mu W^-_\nu\right) - \frac{1}{4}\eta^{\mu\rho}\eta^{\nu\sigma}F_{Z\mu\nu}F_{Z\rho\sigma} - \frac{1}{2}\eta^{\mu\rho}\eta^{\nu\sigma}F^+_{W\mu\nu}F^-_{W\rho\sigma} \end{aligned} \tag{5.2}$$

$$- \frac{M_{\rm P}^2}{\xi_R \Lambda^2} F(\varphi^I) e^{\sqrt{\frac{2}{3}} \frac{\varphi}{M_{\rm P}}} \epsilon^{\mu\nu\rho\sigma} F_{Z\mu\nu} F_{Z\rho\sigma} - \frac{2M_{\rm P}^2}{\xi_R \Lambda^2} F(\varphi^I) e^{\sqrt{\frac{2}{3}} \frac{\varphi}{M_{\rm P}}} \epsilon^{\mu\nu\rho\sigma} F^+_{W\mu\nu} F^-_{W\rho\sigma} \Bigg].$$

We first proceed to quantize the Z and W bosons. With Eq. (5.2), and aided by Eqs. (3.36) and (3.50), the quadratic actions for the respective fields can be written as

$$\begin{aligned} S^\lambda_{W,Z} = \int d\tau\, \mathcal{L}^\lambda_{W,Z} = \int d\tau\, \frac{d^3k}{(2\pi)^3} \Bigg[\left(\frac{1}{2} |\partial_\tau \widetilde{Z}^\lambda|^2 - \frac{1}{2} (\omega^\lambda_Z(\tau,k))^2 |\widetilde{Z}^\lambda|^2 \right) \\ + \left(\frac{1}{2} |\partial_\tau \widetilde{W}^{+,\lambda}|^2 - \frac{1}{2} (\omega^\lambda_W(\tau,k))^2 |\widetilde{W}^{+,\lambda}|^2 \right) + \left(\frac{1}{2} |\partial_\tau \widetilde{W}^{-,\lambda}|^2 - \frac{1}{2} (\omega^\lambda_W(\tau,k))^2 |\widetilde{W}^{-,\lambda}|^2 \right) \Bigg]. \end{aligned} \tag{5.3}$$

The canonical momenta for the Z and W in Fourier space are therefore

$$\hat{\widetilde{\pi}}^\lambda_Z(\tau,\mathbf{k}) = \partial_\tau \hat{\widetilde{Z}}^\lambda(\tau,\mathbf{k}), \tag{5.4a}$$

$$\hat{\widetilde{\pi}}^\lambda_{W^\pm}(\tau,\mathbf{k}) = \partial_\tau \hat{\widetilde{W}}^{\mp,\lambda}(\tau,\mathbf{k}), \tag{5.4b}$$

with the commutation relations

$$\left[\hat{\widetilde{Z}}^\lambda(\tau,\mathbf{k}), \hat{\widetilde{\pi}}^{\lambda\prime}_Z(\tau,\mathbf{q}) \right] = i(2\pi)^3 \delta^{\lambda\lambda\prime} \delta(\mathbf{k}+\mathbf{q}), \tag{5.5a}$$

$$\left[\hat{\widetilde{W}}^{\pm,\lambda}(\tau,\mathbf{k}), \hat{\widetilde{\pi}}^{\lambda\prime}_{W^\pm}(\tau,\mathbf{q}) \right] = i(2\pi)^3 \delta^{\lambda\lambda\prime} \delta(\mathbf{k}+\mathbf{q}), \tag{5.5b}$$

where the field operators are given as

$$\hat{\widetilde{Z}}^\lambda = z^\lambda_k(\tau) \hat{a}^\lambda_Z(\mathbf{k}) + z^{\lambda *}_k(\tau) \hat{a}^{\lambda\dagger}_Z(-\mathbf{k}), \qquad (\lambda = \pm) \tag{5.6a}$$

$$\hat{\widetilde{W}}^{+,\lambda} = w^\lambda_k(\tau) \hat{a}^\lambda_W(\mathbf{k}) + w^{\lambda *}_k(\tau) \hat{b}^{\lambda\dagger}_W(-\mathbf{k}), \qquad (\lambda = \pm) \tag{5.6b}$$

where $\hat{a}^\dagger_W$, $\hat{b}^\dagger_W$ are the creation operators for W^+ and W^-, respectively. These obey the usual commutation relations

$$\left[\hat{a}^\lambda_Z(\mathbf{k}), \hat{a}^{\lambda\prime}_Z(\mathbf{q}) \right] = 0, \qquad \left[\hat{a}^{\dagger\lambda}_Z(\mathbf{k}), \hat{a}^{\dagger\lambda\prime}_Z(\mathbf{q}) \right] = 0, \qquad \left[\hat{a}^\lambda_Z(\mathbf{k}), \hat{a}^{\lambda'\dagger}_Z(\mathbf{q}) \right] = (2\pi)^3 \delta^{\lambda\lambda\prime} \delta^3(\mathbf{k}-\mathbf{q}), \tag{5.7a}$$

$$\left[\hat{a}^\lambda_W(\mathbf{k}), \hat{a}^{\lambda\prime}_W(\mathbf{q}) \right] = 0, \qquad \left[\hat{a}^{\dagger\lambda}_W(\mathbf{k}), \hat{a}^{\dagger\lambda\prime}_W(\mathbf{q}) \right] = 0, \qquad \left[\hat{a}^\lambda_W(\mathbf{k}), \hat{a}^{\lambda'\dagger}_W(\mathbf{q}) \right] = (2\pi)^3 \delta^{\lambda\lambda\prime} \delta^3(\mathbf{k}-\mathbf{q}). \tag{5.7b}$$

Similar commutation relations hold for $\hat{b}^\lambda_W$ while all commutation relationships between $\hat{a}_W$, $\hat{b}_W$ vanish. Inserting Eqs. (5.6) in the Eq. (3.36) and Eq. (3.50), the mode equations of the W and Z fields can be found as

$$z^{\lambda\,\prime\prime}_k + (\omega^\lambda_Z)^2 z^\lambda_k = 0 \qquad (\lambda = \pm), \tag{5.8a}$$

$$w^{\lambda\,\prime\prime}_k + (\omega^\lambda_W)^2 w^\lambda_k = 0 \qquad (\lambda = \pm). \tag{5.8b}$$

The quantization of the Goldstone bosons is a bit more involved. This is due to the presence of friction term $\mathcal{D}_\tau \widetilde{X}^I$ (with $I = \phi_2, \phi_3, \phi_4$) in the respective EoMs. We start by recasting Eqs. (3.54), (3.56a) and (3.56b) into the form

$$S_{(\phi_i)} = \int d\tau\, L_{(\phi_i)} = \int d\tau\, \frac{d^3k}{(2\pi)^3}\, \Delta_{(I)} \left[\frac{1}{2} \left| \partial_\tau X^I \right|^2 - \frac{1}{2} \omega^2_{(I)}(\tau,k) \left| X^I \right|^2 \right], \tag{5.9}$$

with

$$\Delta_{(I)} = \exp\left\{ \int_{-\infty}^{\tau} \mathcal{E}_{(I)}(\tau',k)\, d\tau' \right\}. \tag{5.10}$$

$\mathcal{E}_{(I)}(\tau,k)$ and $\omega^2_{(I)}(\tau,k)$ are provided in Sec. 3.1.3. As we deal with non-canonical kinetic terms, we apply the quantization procedure detailed in Ref. [70]. We can quantize the fields as in before as

$$\hat{\widetilde{X}}^{\phi_2} = \left[s_k(\tau) e^{\phi_2}(\tau) \hat{a}_3(\mathbf{k}) + s^*_k(\tau) e^{\phi_2}(\tau) \hat{a}^\dagger_3(-\mathbf{k}) \right], \tag{5.11a}$$

$$\widehat{\widetilde{X}}^{\phi_3} = \left[q_k(\tau)e^{\phi_3}(\tau)\hat{a}_4(\mathbf{k}) + q_k^*(\tau)e^{\phi_3}(\tau)\hat{a}_4^\dagger(-\mathbf{k})\right], \tag{5.11b}$$

$$\widehat{\widetilde{X}}^{\phi_4} = \left[r_k(\tau)e^{\phi_4}(\tau)\hat{a}_5(\mathbf{k}) + r_k^*(\tau)e^{\phi_4}(\tau)\hat{a}_5^\dagger(-\mathbf{k})\right], \tag{5.11c}$$

and the canonical momentum can be found as

$$\hat{\widetilde{\pi}}^I(\tau,\mathbf{k}) = \Delta_{(I)}\partial_\tau\widehat{\widetilde{X}}^I(\tau,\mathbf{k}), \tag{5.12}$$

with

$$\left[\widehat{\widetilde{X}}^I(\tau,\mathbf{k}),\hat{\widetilde{\pi}}^J(\tau,\mathbf{q})\right] = \frac{i}{\Delta_{(I)}}(2\pi)^3\delta^{IJ}\delta(\mathbf{k}+\mathbf{q}), \tag{5.13}$$

and similar commutation relations between creation and annihilation operators as in the previous section. From Eqs. (3.54), (3.56a) and (3.56b), we obtain the EoMs of the mode functions as

$$s_k'' + \mathcal{E}_{(\phi_2)}(\tau,k)\ s_k' + \omega^2_{(\phi_2)}(\tau,k)\, s_k = 0, \tag{5.14a}$$

$$q_k'' + \mathcal{E}_{(\phi_3)}(\tau,k)\ q_k' + \omega^2_{(\phi_3)}(\tau,k)\, q_k = 0, \tag{5.14b}$$

$$r_k'' + \mathcal{E}_{(\phi_4)}(\tau,k)\ r_k' + \omega^2_{(\phi_4)}(\tau,k)\, r_k = 0. \tag{5.14c}$$

We have checked numerically that the constraints imposed by Eqs. (3.31) and (3.35) on the Goldstone boson $\widetilde{\phi}_2$, and (3.46) and (3.49) on the Goldstones $\widetilde{\phi}_3$ and $\widetilde{\phi}_4$, are consistent with the EoM of the corresponding mode functions Eqs. (3.54) and (3.56a)-(3.56b), respectively.

5.2 Energy density

We can define the physical energy density associated with the Goldstone and gauge bosons as

$$\rho_{\rm G} = \frac{1}{a^4}\int d^3x\,\langle T^{\rm G}_{00}\rangle = \frac{1}{a^4}\int\frac{d^3k}{(2\pi)^3}\,\langle\rho_{k,{\rm G}}\rangle = \frac{1}{a^4}\int\frac{d^3k}{(2\pi)^3}\rho^{\rm vev}_{k,{\rm G}}, \tag{5.15}$$

where the energy-momentum tensor can be derived from Eq. (5.2) as

$$\begin{aligned}
T^{\rm G}_{\mu\nu} =\ & G_{IJ}(\mathcal{D}_\mu X^I)(\mathcal{D}_\nu X^J) + 2a\,e^{-\sqrt{\frac{2}{3}}\frac{\varphi}{M_{\rm P}}}\ \delta^0_\mu\delta^0_\nu\left(X^J(\partial_\tau h_0) - h_0(\partial_\tau X^J) + \frac{\partial_\tau a}{a}h_0X^J\right)\\
&\left(\delta^3_J\frac{g_Z}{2}Z_0 + \frac{ie}{2\sqrt{2}s_W}\left[(\delta^4_J+i\delta^5_J)W_0^- - (\delta^4_J-i\delta^5_J)W_0^+\right]\right) + 2a^2\,e^{-\sqrt{\frac{2}{3}}\frac{\varphi}{M_{\rm P}}}\left(\frac{g_Z^2}{8}h_0^2Z_\mu Z_\nu + \frac{e^2}{4s_W^2}h_0^2W_\mu^+W_\nu^-\right)\\
&+\eta^{\rho\sigma}F_{Z\mu\rho}F_{Z\nu\sigma} + 2\eta^{\rho\sigma}F^+_{W\mu\rho}F^-_{W\nu\sigma} + \eta_{\mu\nu}\left[-\frac{1}{2}\eta^{\alpha\beta}G_{IJ}(\mathcal{D}_\alpha X^I)(\mathcal{D}_\beta X^J) - \frac{1}{2}\mathscr{M}_{IJ}X^IX^J\right.\\
&+a\,e^{-\sqrt{\frac{2}{3}}\frac{\varphi}{M_{\rm P}}}\left(X^J(\partial_\tau h_0) - h_0(\partial_\tau X^J) + \frac{\partial_\tau a}{a}h_0X^J\right)\left(\delta^3_J\frac{g_Z}{2}Z_0 + \frac{ie}{2\sqrt{2}s_W}\left[(\delta^4_J+i\delta^5_J)W_0^- - (\delta^4_J-i\delta^5_J)W_0^+\right]\right)\\
&\left.-a^2\,e^{-\sqrt{\frac{2}{3}}\frac{\varphi}{M_{\rm P}}}\eta^{\alpha\beta}\left(\frac{g_Z^2}{8}h_0^2Z_\alpha Z_\beta + \frac{e^2}{4s_W^2}h_0^2W^+_\alpha W^-_\beta\right) - \frac{1}{4}\eta^{\alpha\rho}\eta^{\beta\sigma}F_{Z\alpha\beta}F_{Z\rho\sigma} - \frac{1}{2}\eta^{\alpha\rho}\eta^{\beta\sigma}F^+_{W\alpha\beta}F^-_{W\rho\sigma}\right].
\end{aligned} \tag{5.16}$$

We can also find the energy density per Fourier mode of the of scalar field fluctuations in momentum space

$$\begin{aligned}
\rho_{k,{\rm G}} =\ & \frac{1}{2}G_{IJ}(\mathcal{D}_\tau\widetilde{X}^I)(\mathcal{D}_\tau\widetilde{X}^J) + \frac{1}{2}\left(k^2G_{IJ}+\mathscr{M}_{IJ}\right)\widetilde{X}^I\widetilde{X}^J - \frac{1}{2}\,e^{-2\sqrt{\frac{2}{3}}\frac{\varphi}{M_{\rm P}}}\left(h_0'\widetilde{X}^I + h_0\frac{a'}{a}\widetilde{X}^I - h_0\partial_\tau\widetilde{X}^I\right)\\
&\left(h_0'\widetilde{X}^J + h_0\frac{a'}{a}\widetilde{X}^J - h_0\partial_\tau\widetilde{X}^J\right)\left[\frac{g_Z^2}{4\mathcal{K}_Z}\delta^3_I\delta^3_J + \frac{e^2}{4s_W^2\mathcal{K}_W}\left(\delta^4_I\delta^4_J+\delta^5_I\delta^5_J\right)\right] + \frac{1}{2}\widetilde{Z}_i'\widetilde{Z}_i' + \widetilde{W}_i^{+\prime}\widetilde{W}_i^{-\prime}\\
&+a^2\left[\frac{\mathcal{K}_Z}{2}\widetilde{Z}_i\widetilde{Z}_i + \mathcal{K}_W\widetilde{W}_i^+\widetilde{W}_i^-\right] + \mathcal{O}(\widetilde{X}^3),
\end{aligned} \tag{5.17}$$

where we have used Eqs. (3.31) and (3.44), as well as the gauge conditions described in Eqs. (3.30) and (3.44). As the different fields do not mix, we can decompose $\rho^{\rm vev}_{k,\rm G}$ into gauge and Goldstone energy densities

$$\rho^{\rm vev}_{k,\rm G} = \rho^Z_k + \rho^W_k + \rho^{(\phi_i)}_k. \tag{5.18}$$

We are now ready to consider the Z and W boson cases before turning to the Goldstone bosons.

5.2.1 Z and W bosons

From Eq. (5.17), we see that the energy densities for W and Z bosons are separated out as

$$\rho^Z_k = \sum_{\lambda=\pm}\left[\left|z^{\lambda\prime}_k\right|^2 + a^2\mathcal{K}_Z\left|z^\lambda_k\right|^2\right], \tag{5.19a}$$

$$\rho^W_k = 2\sum_{\lambda=\pm}\left(\left|w^{\lambda\prime}_k\right|^2 + a^2\mathcal{K}_W\left|w^\lambda_k\right|^2\right). \tag{5.19b}$$

To find the respective vacuum-subtracted energy densities, we have to minimize the associated Hamiltonian

$$\begin{aligned}\hat{\mathcal{H}}_{W,Z} = \int d^3x\,\langle T^{\rm G}_{00,\ WZ}\rangle = \frac{1}{2}\int\frac{d^3k}{(2\pi)^3}\sum_{\lambda=\pm}\Big[&\left(|z^{\lambda\prime}_k|^2 + (\omega^\lambda_Z)^2|z^\lambda_k|^2\right)\left(\hat{a}^{\lambda\dagger}_Z(\mathbf{k})\hat{a}^\lambda_Z(\mathbf{k}) + \delta^3(\mathbf{0})\right)\\ &+ 2\left(|w^{\lambda\prime}_k|^2 + (\omega^\lambda_W)^2|w^\lambda_k|^2\right)\left(\hat{a}^{\lambda\dagger}_W(\mathbf{k})\hat{a}^\lambda_W(\mathbf{k}) + \delta^3(\mathbf{0})\right)\Big],\end{aligned} \tag{5.20}$$

($T^{\rm G}_{00,\ WZ}$ is the energy associated with Z and W). As before, $\hat{\mathcal{H}}_{W,Z}$ can be minimized by the BD vacuum solution

$$z^\lambda_{k,\rm BD} = \frac{1}{\sqrt{2k}}e^{-ik\tau}, \qquad w^\lambda_{k,\rm BD} = \frac{1}{\sqrt{2k}}e^{-ik\tau}. \tag{5.21}$$

The corresponding energy densities, obtained from Eqs. (5.19), are

$$\rho^{\rm BD}_Z = \int dk\frac{k^2}{2\pi^2a^4}\,\rho^{\rm BD}_{k,Z} = \frac{1}{a^4}\int dk\,\frac{k^3}{\pi^2}, \tag{5.22a}$$

$$\rho^{\rm BD}_W = \int dk\frac{k^2}{2\pi^2a^4}\,\rho^{\rm BD}_{k,W} = \frac{1}{a^4}\int dk\,\frac{2k^3}{\pi^2}, \tag{5.22b}$$

where, at sufficiently early times and for large modes, $(\omega^\lambda_{Z,W})^2 \to k^2$. The quantum gauge energy density is obtained by removing the BD vacuum from the classical solution as

$$\rho^q_Z = \rho_Z - \rho^{\rm BD}_Z, \tag{5.23a}$$

$$\rho^q_W = \rho_W - \rho^{\rm BD}_W. \tag{5.23b}$$

When finding the energy densities, we solve Eqs. (5.8a) and (5.8b) in cosmic time.

In Fig. 4, we display the different contributions to ${\omega^+_Z}^2$, Eq. (3.37), for all three BPs. For BPa (first column of Fig. 4), as the non-minimal coupling ξ_H is small, the impact of m^2_Z is suppressed compared to ζ^+ (see Eq.(3.37)). This is visible from the cyan and orange solid lines, respectively. However, for BPb and BPc, the larger non-minimal coupling renders m^2_Z more dominant compared to ζ^λ. This can be seen from the second and third columns of Fig. 4. ${\omega^-_Z}^2$ shows a similar behavior, except for a sign change of the CS term. We also find that the different contributions of ${\omega^\lambda_W}^2$ follow a similar pattern, and we choose to not repeat these here.

The behavior of $(\omega^+_Z)^2$ of Fig. 4 has severe implications for the energy densities of the Z and W bosons, Fig. 5. For BPa, as the ζ^λ term dominantes, ρ^q_Z and ρ^q_W both scale as $1/\Lambda$. However, for BPb and BPc, as the non-minimal coupling becomes larger, the m^2_Z term overpowers ζ^λ. We, therefore, see parametric resonance taking over. We find that Z boson production can preheat the Universe within 2 e-foldings after the end of inflation for both BPb and BPc. For W production, the preheating is completed within $\mathcal{N}\approx 4$ ($\mathcal{N}\approx 2$) for BPb (BPc). We remark that gauge preheating is also possible for BPa if $\Lambda \lesssim 2\times 10^{-5}\ M_{\rm P}$, however, we shall see below that such values of Λ will overproduce hypermagnetic fields and imply an overproduction of the observed baryon asymmetry. Note that the produced Z boson W boson can decay into SM matter. We will return to this in Sec. 7.

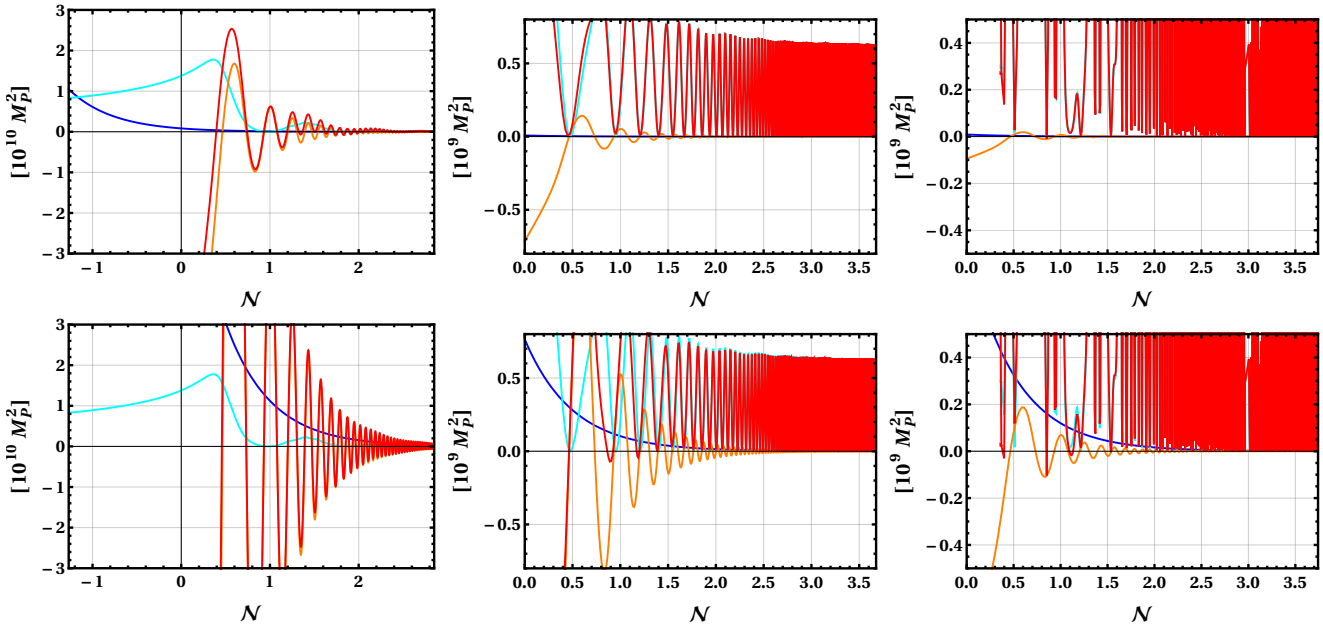

Figure 4. Relative strength of different terms of $(\omega_Z^+)^2$ in Eq. (3.37) for BPa (left panel), BPb (middle panel) and BPc (right panel). The upper panel conforms $k = a(t_{\rm end})H(t_{\rm end})$ while the lower panel is for $k = 10\,a(t_{\rm end})H(t_{\rm end})$. The blue, cyan, orange, and red lines in each figure display k^2/a^2, m_Z^2, ζ^+ and a combination of m_Z^2 plus ζ^+. We set $\Lambda = 2 \times 10^{-5}\ M_{\rm P}$ throughout.

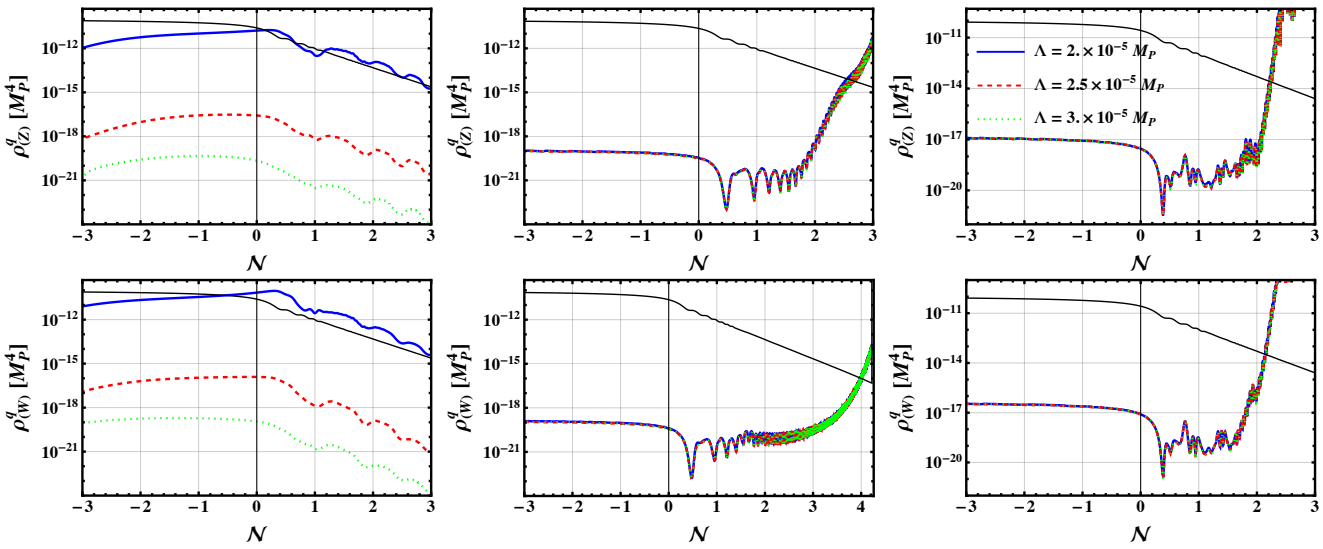

Figure 5. The energy densities ρ_Z^q (upper row) and ρ_W^q (lower row) for various values of Λ for the benchmark points BPa (left column), BPb (middle column) and BPc (right column). The black line displays the background energy density $\rho_{\rm inf}$.

5.2.2 Goldstone bosons

The Goldstone fields do not mix. Therefore, we can further decompose VEV energy density $\rho_k^{(\phi_i)}$ from Eq. (5.18) into the ϕ_i VEV energy density as

$$\rho_k^{(\phi_i)} = \rho_k^{(\phi_2)} + \rho_k^{(\phi_3)} + \rho_k^{(\phi_4)} \tag{5.24}$$

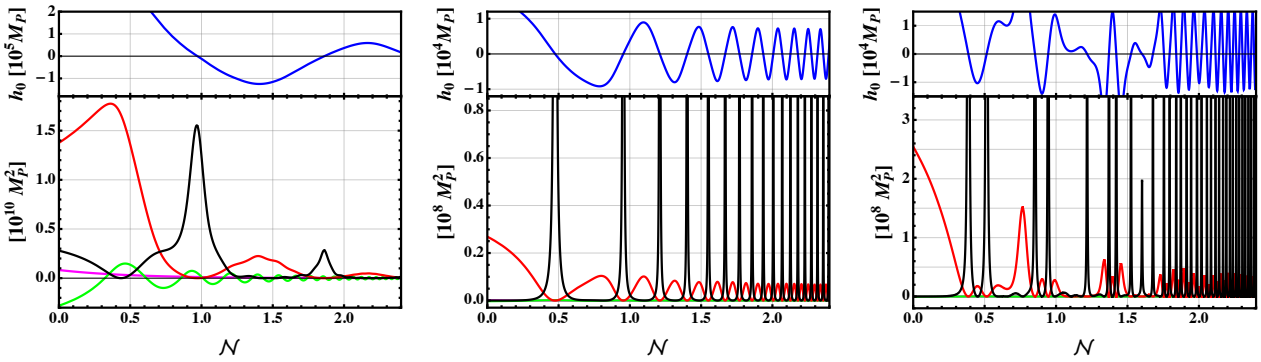

Figure 6. Different terms in $\omega^2_{(\phi_2)}(\tau,k)/a^2$. On the bottom panels, the magenta, green, red and black lines correspond to k^2/a^2, $m^2_{\text{eff},(\phi_2)}$, m_Z^2 and $\mathcal{E}_{(\phi_2)}\Upsilon/a^2$, see Eq. (3.55b), for all three BPs. Here as a reference we set $k = a(t_{\rm end})H(t_{\rm end})$. We can see that the spikes correspond to the zero-crossings of h_0 (blue lines) displayed on the upper panels. See text for detailed explanation.

with

$$\rho_k^{(\phi_2)} = \frac{1}{2}\left\{\left(1-\frac{m_Z^2}{\mathcal{K}_Z}\right)|s_k'|^2+\left[k^2+a^2m^2_{\text{eff},(\phi_2)}-\frac{m_Z^2}{\mathcal{K}_Z}\,\Upsilon^2\right]|s_k|^2-\frac{m_Z^2}{\mathcal{K}_Z}\,\Upsilon\,(s_k's_k^*+s_k^{*\prime}s_k)\right\}, \tag{5.25a}$$

$$\rho_k^{(\phi_3)} = \frac{1}{2}\left\{\left(1-\frac{m_W^2}{\mathcal{K}_W}\right)|q_k'|^2+\left[k^2+a^2m^2_{\text{eff},(\phi_3)}-\frac{m_W^2}{\mathcal{K}_W}\,\Upsilon^2\right]|q_k|^2-\frac{m_W^2}{\mathcal{K}_W}\,\Upsilon\,(q_k'q_k^*+q_k^{*\prime}q_k)\right\}, \tag{5.25b}$$

$$\rho_k^{(\phi_4)} = \frac{1}{2}\left\{\left(1-\frac{m_W^2}{\mathcal{K}_W}\right)|r_k'|^2+\left[k^2+a^2m^2_{\text{eff},(\phi_4)}-\frac{m_W^2}{\mathcal{K}_W}\,\Upsilon^2\right]|r_k|^2-\frac{m_W^2}{\mathcal{K}_W}\,\Upsilon\,(r_k'r_k^*+r_k^{*\prime}r_k)\right\}, \tag{5.25c}$$

where Υ was defined in Eq. (3.23).

Before solving Eqs. (5.14) to find the energy densities, let us briefly discuss the different contributions to $\omega^2_{(I)}$ and their impact on preheating. For this purpose, we take ϕ_2 as a representative field for the Goldstone bosons, and we checked that ϕ_3 and ϕ_4 show a similar behavior (with m_Z^2 replaced by m_W^2). In Fig. 6, we have plotted the different contributions to $\omega^2_{(\phi_2)}(\tau,k)$ for $k = a(t_{\rm end})H(t_{\rm end})$ for illustration. It is clear, around the end of inflation, m_Z^2 dominates over all other terms but soon after, the last term associated with $\mathcal{E}_{(\phi_2)}$ dominates every time h_0 crosses zero, resulting in spike-like structures. The spikes have the amplitude

$$\omega^2_{(\phi_2)}\Big|_{h_0=0} = k^2+a^2\left[m^2_{\text{eff},(\phi_2)}+\frac{g_Z^2}{2}\frac{a^2}{k^2}e^{-\sqrt{\frac{2}{3}}\frac{\varphi}{M_{\rm P}}}h_0'^2\right], \tag{5.26}$$

which is well below the unitarity cut-off scale. For comparison, we have also plotted k^2/a^2 for the $k = a(t_{\rm end})H(t_{\rm end})$ in magenta in the lower panels and the evolution of h_0 in blue in the upper panels. It is clear that the spikes are smaller for BPa, which is deep in the R^2-like regime with $\xi_H \ll 1$. However, they increase significantly for BPb and BPc due to a comparably larger ξ_H. As we will see shortly, such spikes induce a growth of the corresponding modes leading to preheating of the Goldstone bosons (see Refs. [26, 28, 52–54, 56] for similar discussions) without violating unitarity.

To solve Eqs. (5.14), we make the change of variable $\bar{s}_k = \sqrt{\Delta_{(\phi_2)}}\,s_k$ to write

$$\bar{s}_k''(\tau,k)+\bar{\omega}^2_{(\phi_2)}\bar{s}_k(\tau,k) = 0, \tag{5.27a}$$

$$\bar{q}_k''(\tau,k)+\bar{\omega}^2_{(\phi_3)}\bar{q}_k(\tau,k) = 0, \tag{5.27b}$$

$$\bar{r}_k''(\tau,k)+\bar{\omega}^2_{(\phi_4)}\bar{r}_k(\tau,k) = 0, \tag{5.27c}$$

where

$$\bar{\omega}^2_{(I)} = \omega^2_{(I)}-\frac{\mathcal{E}'_{(I)}}{2}-\frac{\mathcal{E}^2_{(I)}}{4}. \tag{5.28}$$

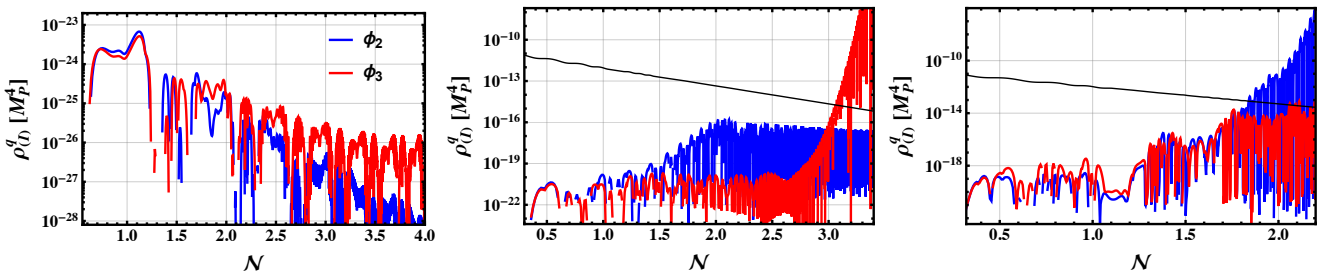

Figure 7. The energy densities $\rho^q_{(\phi_2)}$ and $\rho^q_{(\phi_3)}$ for the benchmark points BPa through c from left to right. We recall that $\rho^q_{(\phi_3)} = \rho^q_{(\phi_4)}$. The black line displays the background energy density $\rho_{\rm inf}$.

At sufficiently early times, when all modes of interest are deep inside the horizon (i.e. $k \gg aH$), the frequencies become $\bar{\omega}^2_{(I)} \to k^2$ and the solutions of Eqs. (5.27) reduce to plane waves

$$s_k = \frac{e^{-ik\tau}}{\sqrt{2k\Delta_{(\phi_2)}}}, \qquad q_k = \frac{e^{-ik\tau}}{\sqrt{2k\Delta_{(\phi_3)}}}, \qquad r_k = \frac{e^{-ik\tau}}{\sqrt{2k\Delta_{(\phi_4)}}}. \tag{5.29}$$

Hence, by taking Eq. (5.29) as the initial conditions, Eqs. (5.27) will enable us to find the evolution of the relevant modes from sub-horizon to super-horizon scales. Here, unlike the BD solution of all other fields, the appearance of the $\Delta_{(I)}$s is due to the presence of additional friction terms in Eqs. (5.14) as shown above. At early times, for the relevant modes, we simultaneously have $k^2/a^2 \gg |m^2_{{\rm eff},(I)}(t)|$ and $m^2_{Z,W}/\mathcal{K}_{Z,W} \to 0$. As before, Eq. (5.29) will minimize the associated Hamiltonian.

The energy density associated with vacuum for the Goldstone modes reads

$$\rho^{\rm BD}_{(\phi_i)} = \frac{1}{4\pi^2 a^4} \int dk\, \frac{k^3}{\Delta_{(\phi_i)}(k,\tau)}. \tag{5.30}$$

The quantum Goldstone energy densities are obtained by removing the BD vacua from the respective classical solutions as

$$\rho^q_{(\phi_i)} = \rho_{(\phi_i)} - \rho^{\rm BD}_{(\phi_i)}, \qquad \text{with } i = 2,3,4. \tag{5.31}$$

Note that we have solved the respective EoMs in cosmic time.

We show the $\rho^q_{(\phi_2)}$ and $\rho^q_{(\phi_3)}$ as function of $\mathcal{N}$ in Fig. 7 in blue and red, respectively. We recall that $\omega^2_{(\phi_3)} = \omega^2_{(\phi_4)}$ and $\rho^q_{(\phi_3)} = \rho^q_{(\phi_4)}$. We find that for all of our BPs no particles are produced before the end of inflation. However, the spike behavior in $\omega^2_{(\phi_2)}$ and $\omega^2_{(\phi_3)}$ induces a growth of the energy densities for BPb and BPc. We find that preheating is possible for both BPb and BPc. In case of BPb, the preheating is complete for $\mathcal{N} \approx 3$ ($\mathcal{N} \approx 1.9$ for the BPc). However, there is a subtlety. For BPb, the preheating is completed via the ϕ_3 field, whereas, for BPc it is completed by ϕ_2. This is primarily due to $m_Z > m_W$ and the evolution of h_0. For both these BPs, initially $\rho^q_{(\phi_2)}$ rises faster due to the heaviness of the Z boson while $\rho^q_{(\phi_3)}$ remains constant. At a later time, the "spike forest" becomes denser which overpowers the mild mass difference between Z and W. Therefore, the delayed growth of $\rho^q_{(\phi_3)}$ plateaus when the spikes are more abundant. The exponential growth of $\rho^q_{(\phi_3)}$ for BPc is not shown in the right panel of Fig. 7 because the initial growth of $\rho^q_{(\phi_2)}$ is sufficiently high enough to preheat the Universe. We stress again that our linearized result here does not include decay, which we shall discuss in Sec. 7.

6 Production of the electromagnetic field

Following the same steps as in the previous sections, we now consider the production of electromagnetic (EM) field. The time component ($\beta = 0$) of Eq. (2.27) at linear order in the perturbations is

$$-\frac{1}{a^2}\partial_i\left(\partial_i A_0 - \partial_0 A_i\right) = 0, \tag{6.1}$$

and the spatial components ($\beta = i$) are

$$-\frac{\dot{a}}{a}\left(\partial_0 A_i - \partial_i A_0\right) - \partial_0\left(\partial_0 A_i - \partial_i A_0\right) + \frac{1}{a^2}\partial_j\left(\partial_j A_i - \partial_i A_j\right) + \frac{4M_{\rm P}^2}{\xi_R \Lambda^2 a}\partial_0\left(F(\varphi^I)e^{\sqrt{\frac{2}{3}}\frac{\varphi}{M_{\rm P}}}\right)\epsilon^{ijk}\left(\partial_j A_k - \partial_k A_j\right) = 0. \tag{6.2}$$

We move to conformal time $d\tau = dt/a(t)$ such that the line element becomes $ds^2 = a^2(\tau)\eta_{\mu\nu}dx^\mu dx^\nu$. Hence, performing the replacements $A_0 \to A_0/a$, $\partial_0 \to \partial_\tau/a$, we find that the above two equations written in comoving coordinates are

$$-\partial_i\left(\partial_i A_0 - A_i'\right) = 0, \tag{6.3}$$

$$-\partial_0\left(\partial_0 A_i - \partial_i A_0\right) + \partial_j\left(\partial_j A_i - \partial_i A_j\right) + \frac{4M_{\rm P}^2}{\xi_R\Lambda^2}\partial_\tau\left(F(\varphi^I)e^{\sqrt{\frac{2}{3}}\frac{\varphi}{M_{\rm P}}}\right)\epsilon^{ijk}\left(\partial_j A_k - \partial_k A_j\right) = 0. \tag{6.4}$$

As before, we can transform to momentum space by

$$A_0(x^\mu) = \int \frac{d^3k}{(2\pi)^3}\widetilde{A}_0(\tau,\mathbf{k})e^{-i\mathbf{k}\cdot\mathbf{x}}, \qquad A_i(x^\mu) = \int \frac{d^3k}{(2\pi)^3}\widetilde{A}_i(\tau,\mathbf{k})e^{-i\mathbf{k}\cdot\mathbf{x}}, \tag{6.5}$$

where the $\widetilde{\mathbf{A}}$ field can be written in terms of transverse and longitudinal components as

$$\widetilde{\mathbf{A}}(\tau,\mathbf{k}) = \sum_{\lambda=\pm,L}\widetilde{A}^\lambda(\tau,\mathbf{k})\;\hat{\epsilon}_A^\lambda(\mathbf{k}), \tag{6.6}$$

with

$$i\mathbf{k}\cdot\hat{\epsilon}_A^\pm(\mathbf{k}) = 0, \qquad i\mathbf{k}\cdot\hat{\epsilon}_A^L(\mathbf{k}) = |\mathbf{k}| = k, \qquad i\mathbf{k}\times\hat{\epsilon}_A^\pm(\mathbf{k}) = \pm k\;\hat{\epsilon}_A^\pm(\mathbf{k}), \qquad \hat{\epsilon}_A^\lambda(\mathbf{k})^* = \hat{\epsilon}_A^\lambda(-\mathbf{k}). \tag{6.7}$$

We are free to choose any gauge for the EM field regardless of our choice of gauge for the massive gauge bosons. Choosing the Coulomb gauge for the EM field, we have $\partial_j A^j = \frac{1}{a^2}\partial_j A_j = 0$. This reduces in momentum space to $i\mathbf{k}\cdot\widetilde{\mathbf{A}} = 0$, and removes one degree of freedom from the EM field. Utilizing Eq. (6.7), the gauge condition $i\mathbf{k}\cdot\widetilde{\mathbf{A}} = 0$ translates to $\widetilde{A}^L(t,\mathbf{k}) = 0$, i.e. the longitudinal component of the photon vanishes. Further, inserting the gauge condition $\widetilde{A}^L(t,\mathbf{k}) = 0$ in Eq. (6.1), we find that $A_0 = 0$, so that the photon is left with two independent (transverse) degrees of freedom. This is unchanged by the presence of $F\widetilde{F}$ term as expected. Notice the stark difference between the photon and the massive gauge bosons discussed earlier. In the former case the constraint equations from the gauge condition render the Goldstone bosons ϕ_2, ϕ_3 and ϕ_3 dynamical, while for the photon only two transverse degrees of freedom are dynamical.

In momentum space and conformal time, Eq. (6.4) reads

$$\left[\widetilde{\mathbf{A}}'' + k^2\widetilde{\mathbf{A}}\right] + \frac{8iM_{\rm P}^2}{\xi_R\Lambda^2}\partial_\tau\left(F(\varphi^I)e^{\sqrt{\frac{2}{3}}\frac{\varphi}{M_{\rm P}}}\right)\left(\mathbf{k}\times\widetilde{\mathbf{A}}\right) = \mathbf{0}. \tag{6.8}$$

The EoM for the transverse components becomes

$$\partial_\tau^2\widetilde{A}^\lambda + (\omega_A^\lambda)^2\widetilde{A}^\lambda = 0, \qquad (\lambda = \pm) \tag{6.9}$$

with

$$(\omega_A^\lambda(\tau,k))^2 = k^2 + \zeta^\lambda(\tau,k), \tag{6.10}$$

where $\zeta^\lambda(\tau,k)$ is given by Eq. (3.38), as well as $\widetilde{A}^L = 0$.

In order to quantize the EM fields, we first integrate the photon part of the Lagrangian by parts to get the action quadratic in the fields

$$S_A^\lambda = \int d\tau\,\mathcal{L}_A^\lambda = \int d\tau\,\frac{d^3k}{(2\pi)^3}\left[\frac{1}{2}|\partial_\tau\widetilde{A}^\lambda|^2 - \frac{1}{2}(\omega_A^\lambda)^2|\widetilde{A}^\lambda|^2\right]. \tag{6.11}$$

The canonical momentum of the transverse modes are

$$\hat{\pi}_A^\lambda(\tau,\mathbf{x}) = \frac{\partial \mathcal{L}_A^\lambda}{\partial\left(\partial_\tau \hat{A}^\lambda(\tau,\mathbf{x})\right)} = \partial_\tau \hat{A}^\lambda(\tau,\mathbf{x}), \tag{6.12}$$

with the commutation relation expressed as

$$\left[\hat{A}^\lambda(\tau,\mathbf{x}), \hat{\pi}_A^\lambda(\tau,\mathbf{y})\right] = i\delta^{\lambda\lambda\prime}\delta(\mathbf{x}-\mathbf{y}). \qquad (\lambda=\pm) \tag{6.13}$$

In momentum space these expressions become

$$\hat{\tilde{\pi}}_A^\lambda(\tau,\mathbf{k}) = \partial_\tau \widehat{\tilde{A}^\lambda}(\tau,\mathbf{k}), \tag{6.14}$$

$$\left[\widehat{\tilde{A}^\lambda}(\tau,\mathbf{k}), \hat{\tilde{\pi}}_A^\lambda(\tau,\mathbf{q})\right] = i(2\pi)^3\delta^{\lambda\lambda\prime}\delta(\mathbf{k}+\mathbf{q}) \qquad (\lambda=\pm). \tag{6.15}$$

The field operator $\widehat{\tilde{A}^\lambda}(\tau,\mathbf{k})$ can be written as creation and annihilation operators

$$\widehat{\tilde{A}^\lambda}(\tau,\mathbf{k}) = u_k^\lambda(\tau)\hat{a}_A^\lambda(\mathbf{k}) + u_k^{\lambda *}(\tau)\hat{a}_A^{\lambda\dagger}(-\mathbf{k}) \qquad (\lambda=\pm) \tag{6.16}$$

that obey

$$\left[\hat{a}_A^\lambda(\mathbf{k}), \hat{a}_A^{\lambda\prime}(\mathbf{q})\right] = 0, \qquad \left[\hat{a}_A^{\dagger\lambda}(\mathbf{k}), \hat{a}_A^{\dagger\lambda\prime}(\mathbf{q})\right] = 0, \qquad \left[\hat{a}_A^\lambda(\mathbf{k}), \hat{a}_A^{\lambda\prime\dagger}(\mathbf{q})\right] = (2\pi)^3\delta^{\lambda\lambda\prime}\delta^3(\mathbf{k}-\mathbf{q}). \tag{6.17}$$

Inserting Eq. (6.16) in Eq. (6.9), the mode equations of A can be found as

$$u_k^{\lambda\prime\prime} + (\omega_A^\lambda)^2\, u_k^\lambda = 0 \qquad (\lambda=\pm). \tag{6.18}$$

As in the last section, we can define the physical energy density as

$$\rho_A = \frac{1}{a^4}\int d^3x\, \langle T_{00}^A\rangle = \frac{1}{a^4}\int \frac{d^3k}{(2\pi)^3}\,\langle \rho_{k,A}\rangle = \frac{1}{a^4}\int dk\, \frac{k^2}{2\pi^2}\,\rho_{k,A}^{\rm vev}, \tag{6.19}$$

where the EM energy-momentum tensor can be derived from the action (2.17)

$$S_A^{(2)} = \int d^3x\, d\tau \left[-\frac{1}{4}\,\eta^{\mu\rho}\eta^{\nu\sigma}F_{A\mu\nu}F_{A\rho\sigma} - \frac{M_{\rm P}^2}{\xi_R\Lambda^2}F(\varphi^I)e^{\sqrt{\frac{2}{3}}\frac{\varphi}{M_{\rm P}}}\,\epsilon^{\mu\nu\rho\sigma}F_{A\mu\nu}F_{A\rho\sigma}\right] \tag{6.20}$$

as

$$T_{\mu\nu}^A = \eta_{\mu\nu}\left[-\frac{1}{4}\,\eta^{\alpha\rho}\eta^{\beta\sigma}F_{A\alpha\beta}F_{A\rho\sigma}\right] + \eta^{\rho\sigma}F_{A\mu\rho}F_{A\nu\sigma}. \tag{6.21}$$

Moving to momentum space and the helical basis (6.7), we find that the EM energy density is

$$\rho_{k,A}^{\rm vev} = \sum_{\lambda=\pm}\left[\frac{1}{2}\left|u_k^{\lambda\prime}\right|^2 + \frac{k^2}{2}\left|u_k^\lambda\right|^2\right], \tag{6.22}$$

where we used Eq. (6.16) and the gauge conditions $A_0=0$ and $\partial_i A_i = 0$. The first term is the electric component, and the second is the magnetic one. The BD vacuum solution as before is

$$u_{k,\rm BD}^\lambda = \frac{e^{-ik\tau}}{\sqrt{2k}}, \qquad u_{k,\rm BD}^{\lambda\prime} = \sqrt{\frac{k}{2}}\,e^{-ik\tau} \tag{6.23}$$

with energy density

$$\rho_A^{\rm BD} = \int dk\,\frac{k^2}{2\pi^2 a^4}\rho_{k,A}^{\rm BD} = \frac{1}{a^4}\int dk\,\frac{k^3}{2\pi^2}. \tag{6.24}$$

As in the other cases, the quantum EM energy density is obtained by removing the BD vacuum from the classical solution as

$$\rho_A^q = \rho_A - \rho_A^{\rm BD}. \tag{6.25}$$

We display the result in Fig. 8 for all the BPs. Preheating from photon production seems then possible only for low values of the scale Λ. We will not consider this case in this paper as for such low values of the cutoff the rate of baryon asymmetry production is too large. See also discussion in Sec. 9.

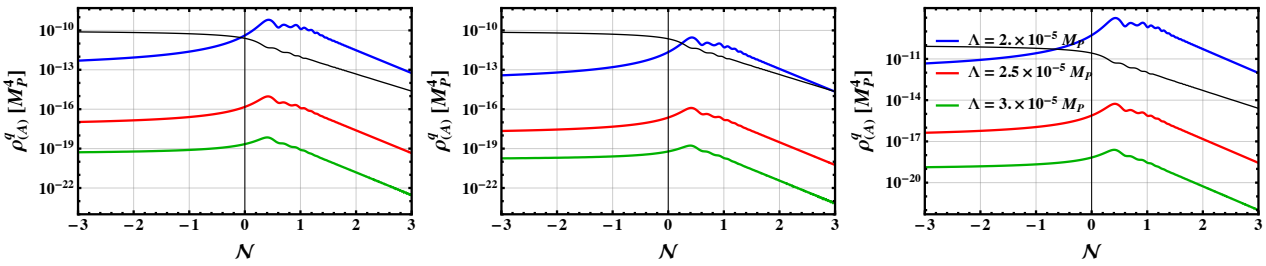

Figure 8. The energy densities ρ^q_A for various values of Λ and all the benchmark points. The black line displays the background energy density $\rho_{\rm inf}$.

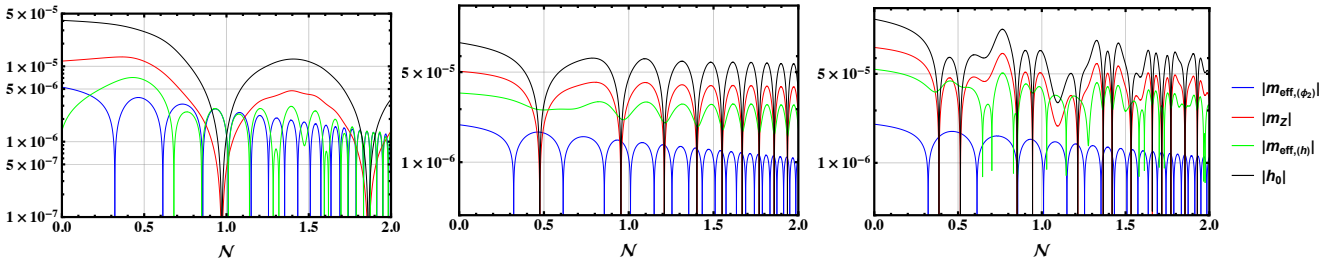

Figure 9. Comparison of different masses for the three BPs after end of inflation.

7 Reheating temperature

Our discussion in the preceding sections regarding preheating for different fields did not include effects such as decay and scattering of the produced particles. These interactions are, of course, not summarized in the action of Eq. (2.17) since they are beyond the linearized approximation we adopted throughout this paper. Nonetheless, these nonlinear effects may indeed dampen the strength of preheating and, in some cases may completely shut down preheating for certain species. We leave out a detailed estimation for separate work but briefly discuss their qualitative impact, in particular for those fields which display the capability of preheating the Universe.

Let us begin with the decay of the produced particles. For the case of Higgs and inflaton quanta, both Higgs and Goldstone bosons can preheat for BPc and BPb but the Goldstones preheat faster. The produced Higgs as well as the Goldstone particles may decay into SM fermions and gauge bosons. For pure Higgs inflation, it has been found that the decay of Higgs particles into gauge bosons ZZ, WW is kinematically disallowed [53]. Our model is quite similar in this regard. In Fig. 9, we plot how $|m_{\text{eff},(h)}|$, $|m_{\text{eff},(\phi_2)}|$ and $|m_Z|$ evolve in comparison to h_0. It is clear that $|m_Z|$ is heavier than both $|m_{\text{eff},(h)}|$ and $|m_{\text{eff},(\phi_2)}|$ for most times during preheating except when $h_0 = 0$. For the case of the Higgs in our qualitative discussion, we find that the duration when $|m_Z| < |m_{\text{eff},(h)}|$ is too small to deplete the energy density of the Higgs. The same holds for $|m_{\text{eff},(\phi_3)}|$ ($|m_{\text{eff},(\phi_2)}|$) for BP$b$ (BPc), where the effective masses of the respective gauge bosons are larger than those of Goldstone bosons such that decays into gauge bosons are not allowed. The situation is different for the case of decays to fermions as discussed in Ref. [53]. For lighter fermions, the decays of the Higgs and Goldstone quanta into fermions are kinematically allowed. However, one needs a decay rate much greater than the Hubble expansion rate for the decay to efficiently deplete the energy densities. This is only possible for the heaviest fermions due to the largeness of their Yukawa couplings. However, even in this instance, as in Ref. [53], we find the duration is too small to deplete the produced particles in our back-reactionless analysis.

The decays of the Z and W bosons into fermions may lead to a significant reduction of the energy densities. Similarly, the Z boson can decay to two scalar bosons. To illustrate the impact of these decays, we consider Z and W boson decays into fermions [55, 71][#4]

$$\Gamma_Z(\tau) = \frac{g_Z^2}{8\pi^2\cos^2\theta_W}\, m_Z(\tau)\left(\frac{7}{2} - \frac{11}{3}\sin^2\theta_W + \frac{49}{9}\sin^4\theta_W\right), \tag{7.1}$$

[#4] Note here that Z and W decay rates include decay to all fermions and averaged over all polarization. We ignore the polarization averaging effect and utilize these expressions for the transverse modes.

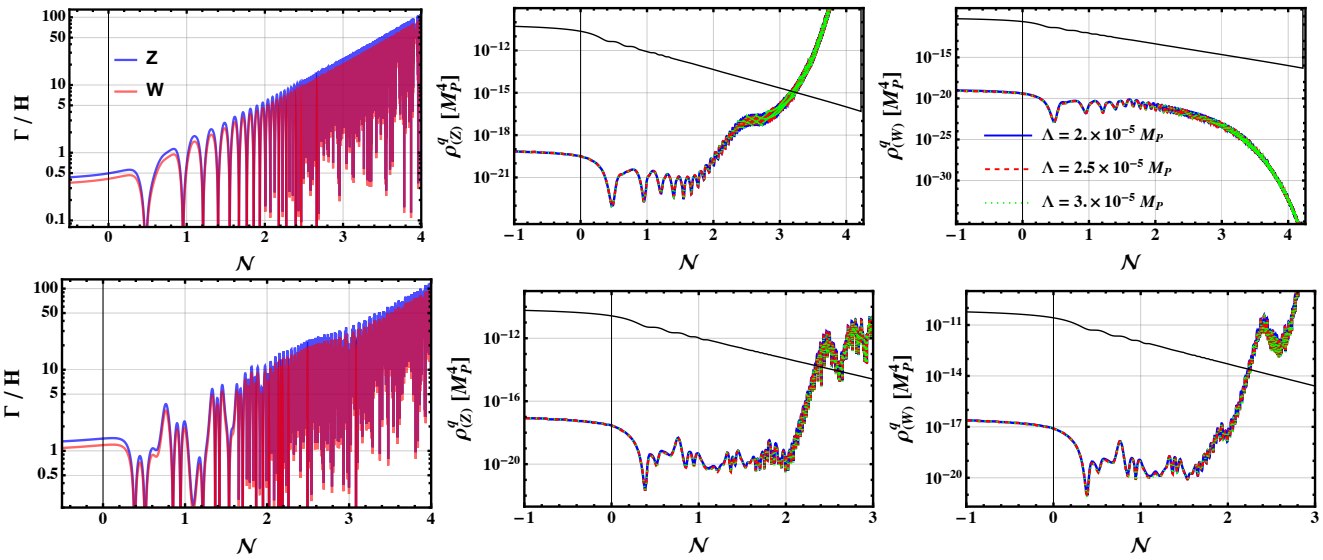

Figure 10. The Γ_Z/H and Γ_W/H shown, in the left panels, in blue and red respectively for BPb (top) and BPc (bottom). The energy densities of the Z (middle) and W (right) taking into account the particle decay for the BPb (top) and BPc (bottom), see Eq. (7.3). The black line displays the background energy densities $\rho_{\rm inf}$ for the respective BPs.

$$\Gamma_W(\tau) = \frac{3g^2}{16\pi} m_W(\tau), \tag{7.2}$$

where the time-dependent Z and W masses have been defined in Eqs. (3.33) and (3.47). These decays may deplete the density of the produced gauge quanta if $\Gamma_{Z,W}/H \gg 1$. While these decay rates can be directly incorporated into the respective mode equations to estimate their impact, for simplicity we follow the approximate expression for the modified energy densities as in [53]

$$\rho^q(\tau) \to \rho^q(\tau)\, \exp\left\{-\int_{\tau_0}^{\tau} d\tau'\, \Gamma(\tau')\right\} \tag{7.3}$$

where τ_0 is the time when $\Gamma_{Z,W}/H$ becomes $\gg 1$ for the respective particles. The modified energy densities of the W and Z bosons are shown in Fig. 10. It is clear that the completion of the Z preheating takes longer for the BPs, in comparison with the results shown in Fig. 5. For the W boson, the decay may completely shut off preheating for BPb; completion takes longer for BPc. The case of BPa is more involved as for small Λ there will be an explosive production of all the gauge fields. However, it was shown that the gauge fields will trigger the production of fermion anti-fermion pairs in the electromagnetic plasma that will strongly reduce the energy density, see e.g. Refs. [20, 72]. This backreaction (dubbed the Schwinger effect) may jeopardize any gauge preheating. Hence, we will conservatively consider that there is no preheating for the BPa benchmark point.

Finally, while a more detailed study is required for the consideration of nonlinear effects, we turn to a qualitative discussion of rescattering and its potential relevance for preheating. In Fig. 11, we combine the effective mass information at a representative time of Fig. 9 into a computation of representative $2 \to 2$ scattering processes. The rate of particle conversion can be approximated as

$$\Gamma = n\sigma\beta, \tag{7.4}$$

in natural units where β is the velocity of a representative W in the plasma. We can further estimate the number density as

$$n_i \simeq \frac{\rho_i}{m_i} \tag{7.5}$$

for a particle species i. The energy densities for, e.g., the gauge bosons are collected in Sec. 5.2.1. We obtain the cross section in Eq. (7.4) keeping the full mass, background field, and centre-of-mass dependencies. There is interesting phenomenology toward the end of inflation; W particles can quickly convert into fermions and Higgs bosons, and vice versa. If the low-mass particles are sufficiently relativistic, they can convert back to vector bosons as indicated

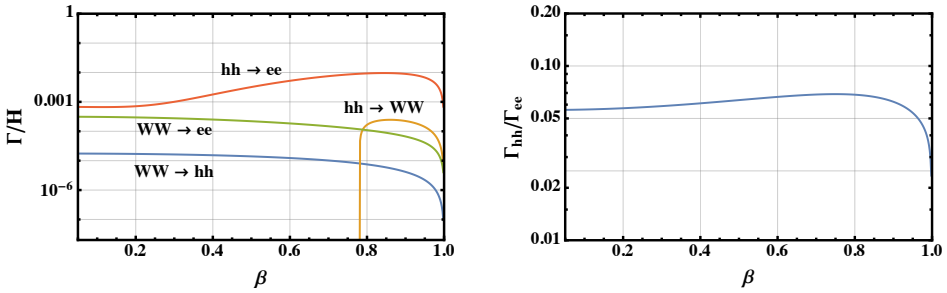

Figure 11. Representative conversion rates $WW \to ee$, $WW \to hh$, and $hh \to ee$ as a function of the Hubble constant and the W/h velocity β for a typical epoch at the end of inflation characterized by $h_0 \simeq 10^{-5} M_P$, $m_{\text{eff},(h)} \sim 2.5 \times 10^{-5} M_P$, $m_W \sim 4 \times 10^{-5} M_P$, from Fig. 9. (Right) comparison of $WW \to hh$ and $WW \to ee$ conversion as a function of the W velocity.

BP	preheating field(s)	$\mathcal{N}_{\rm rh}$	$a_{\rm rh}$	$\rho_{\rm rh}$ $[M_{\rm P}^4]$	$T_{\rm rh}$ [GeV]
a	–	–	–	–	–
b	ϕ_3, ϕ_4	3.05	21	5×10^{-14}	5×10^{14}
c	ϕ_2	1.83	6.2	10^{-13}	6×10^{14}

Table II. Preheating summary in the benchmark points chosen for our analysis. Values given are approximate.

in Fig. 11 (left). This is also true for fermions with sufficient energy very close to unity to transfer kinetic energy to heavy particle creation (these processes are not shown) as well as for any other crossed process shown in Fig. 11. Compared to the change of occupation number resulting from the particle decay discussed above, however, we see that particle conversion turns out to be insignificant and will not quantitatively impact the preheating implications that are derived from the particle decay in isolation. Again this is consistent with the findings of Ref. [53].

In the following, for definiteness, we take the completion of preheating exactly when $\rho_{\rm inf} = \rho^{(q)}_{(X)}$ (with X is any fields), corresponding to a cosmic time $t_{\rm rh}$, i.e. $a_{\rm rh}$, i.e. $\mathcal{N}_{\rm rh}$. The energy density at the time $a_{\rm rh}$, namely $\rho_{\rm rh}$ is therefore identified with the thermal bath energy density

$$\rho_{\rm inf}(a_{\rm rh}) \equiv \rho_{\rm rh} = \frac{g_{\rm rh}\pi^2}{30}\, T_{\rm rh}^4, \tag{7.6}$$

from which we can extract the (p)reheating temperature $T_{\rm rh}$ relevant for baryogenesis. Note, as we stressed before, our linearized results here neglect back-reaction of the excited modes onto the background condensates; this limitation should be kept in mind. We summarize which fields can preheat the Universe individually and table the corresponding value $T_{\rm rh}$ in Table II. The impact of $T_{\rm rh}$ on the geometric baryogenesis will be discussed shortly.

8 Baryogenesis

The baryon asymmetry of the Universe is characterized, in its entropic version, by the parameter

$$\eta_B = \frac{n_b - n_{\bar{b}}}{s}, \tag{8.1}$$

where $n_b - n_{\bar{b}}$ is the difference between the baryon and anti-baryon number density and s the comoving entropy density of the SM plasma. The best fit of CMB anisotropy puts the contraint [73]

$$\eta_B = (8.70 \pm 0.11) \times 10^{-11} \qquad (95\%\ \text{CL}). \tag{8.2}$$

Besides and for completeness, the observed abundances of all the Big Bang Nucleosynthesis (BBN) isotopes today coincide within the range value [74]

$$8.2 \times 10^{-11} \leqslant \eta_B \leqslant 9.2 \times 10^{-11} \qquad (95\%\ \text{CL}), \tag{8.3}$$

as all the light element abundances depend on η_B, compatible with the CMB measurement.

The SM Higgs mass measurement of 125 GeV favors a smooth electroweak crossover at temperatures around 180 GeV $\gtrsim T \gtrsim$ 130 GeV. At first glance, this might jeopardize an electroweak baryogenesis scenario as the Sakharov conditions impose that baryon number and C/CP-violating processes occur in a non-equilibrium environment [75]. However, by carefully analyzing the transport equations for all SM species during the EWPT, it was shown in Refs. [3, 15] that the difference between chirality sources and sphaleron washout yields an out-of-equilibrium configuration even for the crossover; the chiral anomaly of the SM provides a baryon+lepton violating process, which is then sufficient to generate the BAU. The anomaly expresses the fact that the $B+L$ charges, the $U(1)_Y$ helicity, and the weak sphaleron are connected as

$$\Delta N_B = \Delta N_L = N_g \left(\Delta N_{\rm CS} - \frac{g'^2}{16\pi^2}\, \Delta \mathcal{H}_Y \right), \tag{8.4}$$

where the factor $N_g = 3$ is the number of fermion generations. Under the thermal fluctuation of the $SU(2)_L$ gauge fields, the Chern-Simons number $N_{\rm CS}$ is diffusive, resulting in the rapid washout of both lepton N_L and baryon N_B numbers. In contrast, a helical primordial magnetic field acts as a source, and a net baryon asymmetry can remain after the EW phase transition. These two observations open the possibility of a baryogenesis mechanism within the SM electroweak theory although physics beyond the SM is needed to provide a strong enough CP violation at a higher-dimensional operator level. Indeed, the SM CP-violating term from the CKM matrix phase is too small to induce a significant baryon asymmetry at a low energy scale. In our scenario, the dim-6 interaction term $\epsilon^{\mu\nu\rho\sigma} B_{\mu\nu} B_{\rho\sigma} R_J$ fulfills this role.

The proper modelling of the epoch 160 GeV $\gtrsim T \gtrsim$ 130 GeV is critical for an accurate prediction of the relic BAU. We will rely on a mechanism that introduces a time-dependent (temperature-dependent) weak mixing angle $\theta_W(T)$ which enters an additional source of the baryon number into the kinetic equation, see Refs. [3, 15]. The angle behavior is confirmed by analytic calculations [76], and numerical lattice simulations [77]. We follow Refs. [15, 16] and model it with a smooth step function

$$\cos^2\theta_W = \frac{g^2}{g_Z^2} + \frac{g'^2}{2g_Z^2}\left(1 + \tanh\left[\frac{T - T_{\rm step}}{\Delta T}\right]\right), \tag{8.5}$$

which, for 155 GeV $\lesssim T_{\rm step} \lesssim$ 160 GeV and 5 GeV $\lesssim \Delta T \lesssim$ 20 GeV, describes reasonably well the analytical and lattice results for the temperature dependence. We will now present the main lines of this mechanism and refer the reader to Refs. [1, 3, 15, 17–19, 78] and references therein for further background details.

The Boltzmann equation for the baryon-to-entropy ratio η_B reads [15]

$$\frac{d\eta_B}{dx} = -\frac{111}{34}\gamma_{W,\rm sph}\,\eta_B + \frac{3g_Z^2}{16\pi^2}\,\sin(2\theta_W)\,\frac{d\theta_W}{dx}\,\frac{\mathcal{H}_Y}{s}, \tag{8.6}$$

where $x = T/H(T)$ and $\mathcal{H}_Y$ is the hypermagnetic helicity that is initially present. Furthermore, $\gamma_{W,\rm sph} = 6\,\Gamma_{W\rm sph}/T^4$ is the dimensionless transport coefficient for the EW sphaleron, which, for temperatures $T < 161$ GeV, is found from lattice simulations to be [79]

$$\gamma_{W\rm sph} \simeq \exp\left(-147.7 + 107.9\,\frac{T}{130\ \text{GeV}}\right). \tag{8.7}$$

The Boltzmann equation (8.6) has been numerically solved in [15] and the baryon-to-entropy ratio η_B was found to become frozen, i.e. $d\eta_B/dx = 0$, at a temperature $T \simeq 135$ GeV. As expected, this is close to $T \simeq 130$ GeV at which EW sphalerons freeze out. Setting the RHS of Eq. (8.6) to zero and solving for η_B yields

$$\eta_B = \frac{255}{592}\,\frac{g_Z^2}{\pi^3\sqrt{10 g_*}}\,\frac{\mathcal{H}_Y}{(T_{\rm rh}a_{\rm rh})^3}\,\frac{f_{\theta_W}}{M_{\rm P}}\,\frac{T}{\gamma_{W\rm sph}}\bigg|_{T=135\ \text{GeV}}, \tag{8.8}$$

where we used that

$$s = \frac{2\pi^2}{45}\,g_*(T_{\rm rh}a_{\rm rh})^3, \qquad g_* = 106.75. \tag{8.9}$$

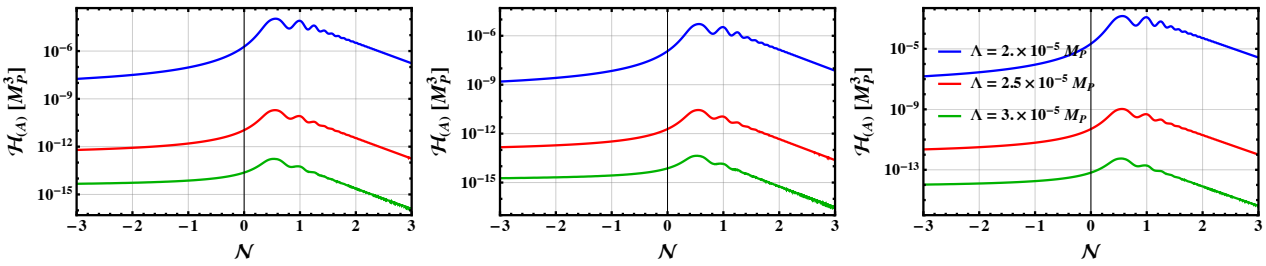

Figure 12. The helicity $\mathcal{H}_A$ for various values of Λ and all the benchmark points BPa, BPb and BPc, from left to right.

The parameter f_{θ_W} encodes all the details on the EWPT dynamics with significant uncertainties

$$f_{\theta_W} = -\sin(2\theta_W)\,\frac{d\theta_W}{d\log T}\bigg|_{T=135\ \text{GeV}}, \qquad 5.6\times 10^{-4} \lesssim f_{\theta_W} \lesssim 0.32. \tag{8.10}$$

Provided that the magnetic induction prevails over the dissipation effects in the plasma between reheating and the EWPT (see hereafter), we can estimate the hypermagnetic helicity at the start of the EWPT as

$$\mathcal{H}_Y = \mathcal{H}_A(a_{\rm rh})\ \cos^2\theta_W, \tag{8.11}$$

where $\mathcal{H}_A$ is the helicity of the EM field defined as

$$\mathcal{H}_A = \frac{1}{a^3}\int dk\,\frac{k^3}{2\pi^2}\sum_{\lambda=\pm}\lambda\left|u_k^\lambda\right|^2 \tag{8.12}$$

that depends on time (or alternatively on the scale factor a or the e-folding number $\mathcal{N}$) and on Λ, see Fig. 12. The Z boson contribution vanishes from $\mathcal{H}_Y$ in Eq. (8.11) because the massive fields are screened or decay away quickly compared to the time scale on which the baryon asymmetry evolves [15]. Because the BD solution (6.23) is the same for both helicities, i.e. $u^+_{k,\rm BD} = u^-_{k,\rm BD}$, the BD vacuum contribution to the helicity vanishes, hence no vacuum subtraction is needed.

We can read the values of $T_{\rm rh}$, $\rho_{\rm rh}$ and $a_{\rm rh}$ from Tab. II. BPa, for which preheating is not evident and the relevant quantities have to be approximated, has been discussed in detail in our previous work, see Ref. [1]. In this work, we base the baryogenesis mechanism on the preheating results detailed in the previous section, and we will, therefore, mainly focus on BPb and BPc. Of course, in all these cases, a detailed calculation of the perturbative reheating in the R^2-Higgs inflation model is needed to further improve on our findings.

The relation (8.11) holds only when the helicity is conserved between reheating and the electroweak crossover. To guarantee that the magnetic induction dominates over dissipation in the plasma, we must require that the magnetic Reynolds number $\mathcal{R}_m$ evaluated at reheating is bigger than unity as

$$\mathcal{R}_m \approx 2\,\alpha_Y\,\frac{c_\sigma}{c_\nu}\,\frac{\rho^q_{B_Y}}{\rho_{\rm rh}}\left(\frac{\ell^q_{B_Y}T_{\rm rh}}{a_{\rm rh}}\right)^2 > 1, \tag{8.13}$$

where $c_\sigma \approx 4.5$ and $c_\nu \approx 0.01$ are respectively the conductivity and the kinematic viscosity factors of the plasma [80, 81] and $\alpha_Y = g'^2/4\pi$. The former equation (as well as Eq. (8.18) hereafter) is valid only for $\mathcal{R}_e < 1$, where

$$\mathcal{R}_e \approx \frac{2\,\alpha_Y^4}{c_\nu^2}\ \log\!\left(\alpha_Y^{-1}\right)^2\,\frac{\rho^q_{B_Y}}{\rho_{\rm rh}}\left(\frac{\ell^q_{B_Y}T_{\rm rh}}{a_{\rm rh}}\right)^2 \tag{8.14}$$

is the electric Reynolds number. In Fig. 13 we show that this regime applies for the relevant values of Λ in BPb and BPc. In the last two expressions, $\rho^q_{B_Y}$ is the quantum hypermagnetic energy density that can be computed as

$$\rho^q_{B_Y} = \rho^q_{A,B}(a_{\rm rh})\ \cos^2\theta_W, \tag{8.15}$$

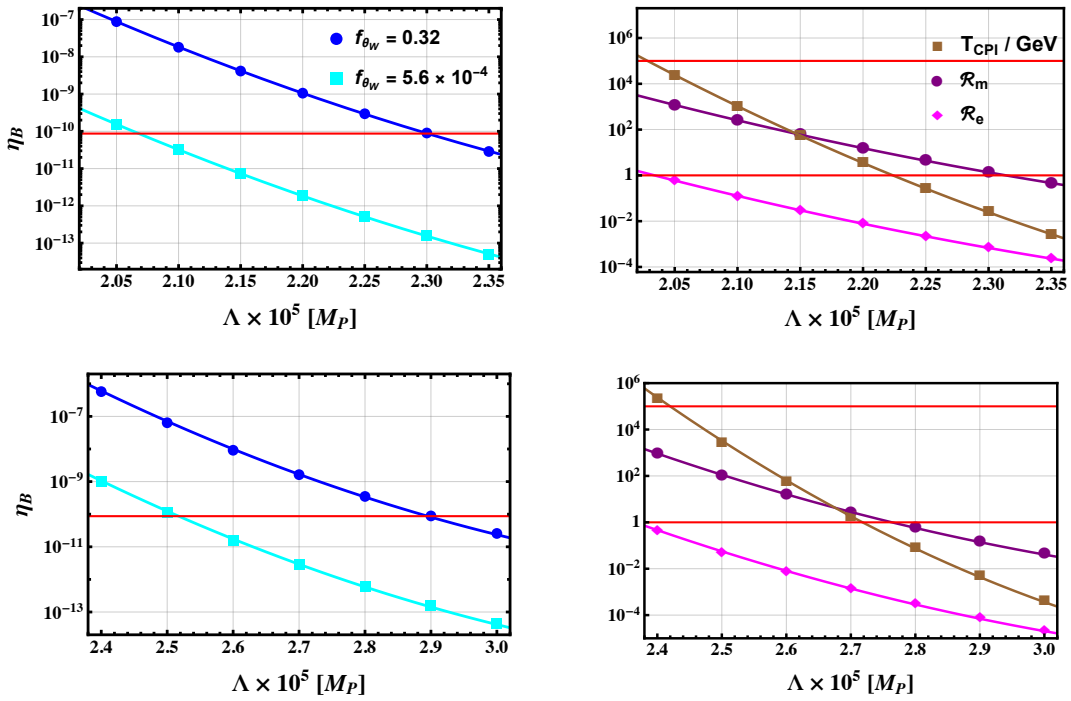

Figure 13. Baryogenesis parameter space for BPb (top) and BPc (bottom). On the left panels we show the asymmetry parameter in function of Λ and f_{θ_W}. The red line must be in between the light and dark blue curves to meet the observational constraint $\eta_B = 8.7 \times 10^{-11}$. On the right panels we display the two contraints, $\mathcal{R}_m > 1$ and $T_{\rm CPI} < 10^5$ GeV in function of Λ. To meet these contraints, both curves must be in between the horizontal red lines. We also display quantity $\mathcal{R}_e$ on which there is no constraint, see text tor detail.

with the EM magnetic energy

$$\rho_{A,B} = \frac{1}{a^4}\int dk\,\frac{k^4}{4\pi^2}\sum_{\lambda=\pm}\left|u_k^\lambda\right|^2, \qquad \rho^q_{A,B} = \rho_{A,B} - \rho^{\rm BD}_{A,B}, \qquad \rho^{\rm BD}_{A,B} = \frac{\rho^{\rm BD}_A}{2}, \tag{8.16}$$

and $\ell^q_{B_Y}$ is the hypermagnetic characteristic size given by

$$\ell^q_{B_Y} = \frac{2\pi}{\rho^q_{A,B}\,a^3}\left[\int dk\,\frac{k^3}{4\pi^2}\sum_{\lambda=\pm}\left|u_k^\lambda\right|^2 - \int dk\,\frac{k^2}{4\pi^2}\right], \tag{8.17}$$

where we performed a vacuum subtraction. Note that $\ell^q_{B_Y} = \ell^q_B$.

The last constraint arises from the CP-odd term present in the magnetohydrodynamics description of the plasma. As the energy configuration in the gauge sector is more favorable than in the fermion sector [82], a helicity cancellation is induced because of the fermion asymmetry back-transformation into helical gauge fields with opposite sign. This phenomenon is called chiral plasma instability (CPI). Thus, one must ensure that all fermion asymmetry created alongside the helical field during inflation is erased by the action of the weak sphaleron for 10^{12} GeV $\gtrsim T \gtrsim$ 130 GeV. Hence to preserve the helicity in the gauge sector, before the CPI can happen, we must require that $T_{\rm CPI} \lesssim 10^5$ GeV, where [17, 82]

$$T_{\rm CPI} \approx \frac{4\alpha_Y^5}{\pi^4 c_\sigma}\log\left(\alpha_Y^{-1}\right)\left(\frac{2133}{481}\right)^2\frac{\mathcal{H}_Y^2}{H(t_{\rm end})\,T_{\rm rh}^4\,\sqrt{a_{\rm rh}^9\,a(t_{\rm end})}}. \tag{8.18}$$

Using Eqs. (8.8), (8.13), (8.18) and the values from Table II, we display in Fig. 13 the baryogenesis parameter space. The following ranges on Λ meet all the constraints and hence yield a successful BAU:

$$\begin{aligned} 2.07\times10^{-5}M_{\rm P} \lesssim \Lambda \lesssim 2.30\times10^{-5}M_{\rm P} \qquad &\text{for BP}b, \\ 2.52\times10^{-5}M_{\rm P} \lesssim \Lambda \lesssim 2.76\times10^{-5}M_{\rm P} \qquad &\text{for BP}c. \end{aligned} \tag{8.19}$$

We observe that the smaller the reheating temperature, the smaller the coupling Λ needs to be to achieve the BAU. This is in agreement with our result for the BPa in Ref. [1] although there the reheating temperature was left as a free parameter.

9 Summary and Outlook

In this work, we studied the implications of the preheating on gravity assisted baryogenesis in R^2-Higgs inflation, namely how preheating can impact on baryogenesis at the electroweak crossover from the production of helical hypermagnetic fields. To this end, we adopted the doubly-covariant formalism for both inflationary dynamics and gauge field production. We derived the equations of motion and energy densities for the inflaton, Higgs background fields, and relevant perturbations at linear order. This includes the inflationary fields, the $W^{\pm}$, Z bosons, the photon, and the three Goldstone fields. The Coulomb gauge was used, as the unitary gauge becomes ill-defined at Higgs zero-crossings. Hence, the Goldstone bosons remained dynamical in our discussion. The preheating is governed by the field-space manifold, the dynamics of the background condensates, the respective effective masses and the coupled metric perturbations.

We primarily focused on R^2 and mildly mixed R^2-Higgs-like regimes, however expressions and the formalism can be applied to other regimes of ξ_R and ξ_H. We highlight different phenomenological possibilities by identifying three benchmark points: a deep R^2-like scenario with $\xi_H \approx 10^{-3}$ (BPa), $\xi_H \approx 1$ (BPb) and a mixed R^2-Higgs scenario with $\xi_H \approx 10$ (BPc) (see Tab. I). We find that the Higgs quanta and transverse modes of the W boson can preheat the Universe for BPc for $\xi_H \approx 10$, while the Z boson can provide successful preheating for both BPb and BPc. The Goldstone sector can also preheat for BPb and BPc. We find that for both BPb and BPc, the Goldstone bosons can preheat the Universe faster than any other field: at $\mathcal{N} \approx 3$ and $\mathcal{N} \approx 1.8$, respectively (see Fig. 7). In all cases, preheating never happens for BPa unless Λ is small. We remark that our results for preheating are in good agreement with previous studies in this model [26, 28], however, we find that $\xi_H \approx 1$ is also sufficient for preheating of the ϕ_3 field at $\mathcal{N} \approx 3$. This is caused predominantly by the spikes in $\omega^2_{(I)}$ due to the presence of the $\mathcal{E}_{(I)}$ term for the Goldstones as also discussed in Ref. [52].

We find that the value of Λ, required for baryogenesis does depend on ξ_H indirectly via the reheating temperature. We identify a window around $\Lambda \sim 2.2\,(2.6) \times 10^{-5}\,M_{\rm P}$ for $\xi_H \approx 1\,(10)$ where the observed baryon asymmetry of the Universe can be achieved. As preheating happens earlier for larger ξ_H, leading to larger reheating temperature, a larger value of Λ is required for successful baryogenesis. However, our analysis also reveals that sufficiently small values of Λ could lead to gauge preheating as found in Fig. 5 and Fig. 8 for BPa. Nevertheless, based on earlier findings from Ref. [1] and pending further investigation into fermion-gauge boson backreaction, we expect the inclusion of the Schwinger effect to significantly impact our results. Importantly, incorporating the Schwinger effect is unlikely to alter the successful sourcing of baryon number density (see also Refs. [1, 20]). Moreover, the relevance of the Schwinger effect dramatically depends on the value of the fermion masses at high values of the background Higgs field, and so on the mechanism for the generation of fermion masses at high scales. For instance a particular Froggatt-Nielsen mechanism was presented in Ref. [83] where there is no Schwinger effect for the Standard Model at inflationary scales, while reproducing the fermion spectrum at electroweak scales. In that case, small values of Λ are disfavored as they tend to overproduce the baryon asymmetry.

Our work systematically builds upon previous studies [1, 19, 83] by explicitly computing, for the first time, the reheating time, temperature, and energy without taking them as effective parameters in the model. One remaining uncertainty regarding the baryogenesis mechanism, which we leave for future work, concerns the specific dynamics of the electroweak crossover, particularly the evolution of the weak mixing angle from zero to its low-energy value. In the present analysis, we ensured that the helicity generated during reheating is preserved until the electroweak scale by carefully considering the plasma's Reynolds number and verifying that the chiral plasma instability does not impact our results. We also remark that for our preheating dynamics, we adopted a naive effective approach related to how decays impact the produced quanta instead of incorporating them in the EoMs directly. Furthermore, we have also not discussed how the produced particles backreact on both the background condensates (see Ref. [56]). In addition, we have ignored fermions from the picture to a large extent; they can impact significantly via the Schwinger effect as discussed in [1, 19, 20, 83]. This requires a first principle derivation of all EoMs retaining terms beyond the linear order in this doubly covariant formalism including fermions and gauge bosons. This is beyond the scope of the current work and we leave a dedicated analysis of non-linear effects for future work.

Acknowledgments

We thank Evangelos Sfakianakis for helpful discussions. YC acknowledges funding support from the Initiative Physique des Infinis (IPI), a research training program of the Idex SUPER at Sorbonne Université. CE is supported by the UK Science and Technology Facilities Council (STFC) under grant ST/X000605/1, the Leverhulme Trust under Research Project RPG-2021-031 and Research Fellowship RF-2024-300\9, and by the Institute for Particle Physics Phenomenology Associateship Scheme. The work of MQ is supported by the grant PID2023-146686NB-C31 funded by MICIU/AEI/10.13039/501100011033/ and by FEDER, EU. IFAE is partially funded by the CERCA program of the Generalitat de Catalunya.

A Gauge boson spectra

We provide the spectra for the Z, W and photon for illustration in comparison to corresponding BD-spectra. This is utilized to evaluate the corresponding energy densities for the respective fields. See main text for details.

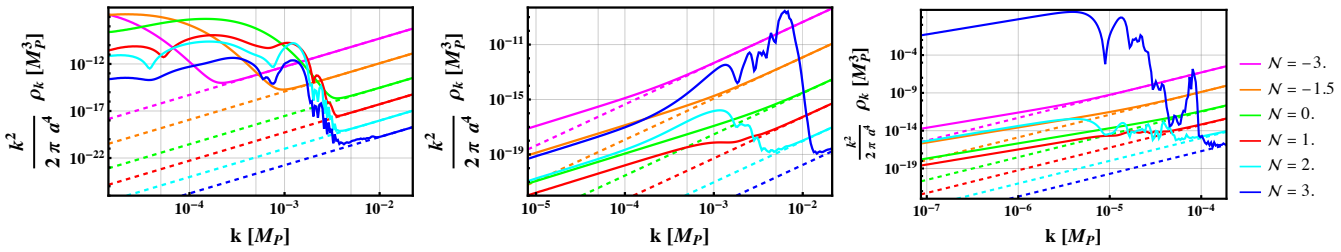

Figure 14. Spectra of the transverse mode of the Z boson and the corresponding BD spectra for different values of $\mathcal{N}$.

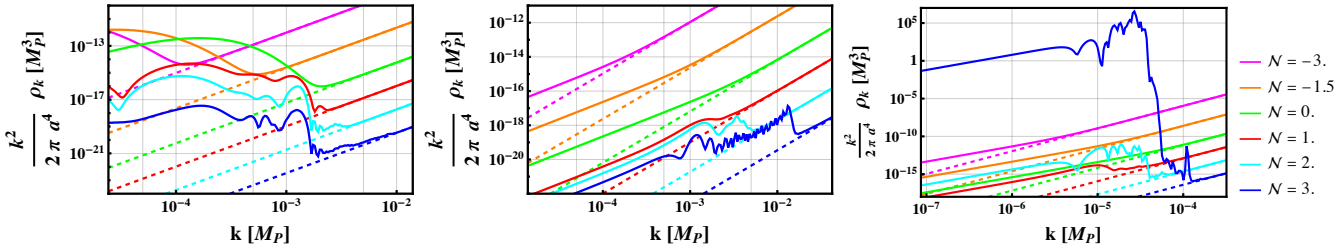

Figure 15. Same figure as Fig. 14 but for the transverse W boson.

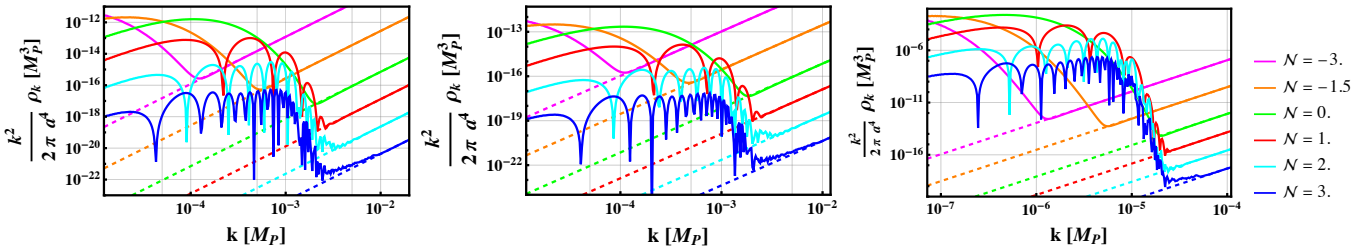

Figure 16. Same figure as Fig. 14 but for the photon.

[1] Y. Cado, C. Englert, T. Modak, and M. Quirós, Phys. Rev. D **109**, 043026 (2024), arXiv:2312.10414 [astro-ph.CO].
[2] M. E. Shaposhnikov, Nucl. Phys. B **287**, 757 (1987).
[3] K. Kamada and A. J. Long, Phys. Rev. D **94**, 063501 (2016), arXiv:1606.08891 [astro-ph.CO].
[4] R. Durrer, O. Sobol, and S. Vilchinskii, Phys. Rev. D **106**, 123520 (2022), arXiv:2207.05030 [gr-qc].
[5] R. Durrer, O. Sobol, and S. Vilchinskii, Phys. Rev. D **108**, 043540 (2023), arXiv:2303.04583 [gr-qc].
[6] O. Savchenko and Y. Shtanov, JCAP **10**, 040 (2018), arXiv:1808.06193 [astro-ph.CO].
[7] K. Subramanian, Rept. Prog. Phys. **79**, 076901 (2016), arXiv:1504.02311 [astro-ph.CO].

[8] R. Durrer and A. Neronov, Astron. Astrophys. Rev. **21**, 62 (2013), arXiv:1303.7121 [astro-ph.CO].
[9] M. M. Anber and L. Sorbo, JCAP **10**, 018 (2006), arXiv:astro-ph/0606534.
[10] K. Bamba, Phys. Rev. D **74**, 123504 (2006), arXiv:hep-ph/0611152.
[11] K. Bamba, C. Q. Geng, and S. H. Ho, Phys. Lett. B **664**, 154 (2008), arXiv:0712.1523 [hep-ph].
[12] M. M. Anber and L. Sorbo, Phys. Rev. D **81**, 043534 (2010), arXiv:0908.4089 [hep-th].
[13] M. M. Anber and E. Sabancilar, Phys. Rev. D **92**, 101501 (2015), arXiv:1507.00744 [hep-th].
[14] Y. Cado and E. Sabancilar, JCAP **04**, 047 (2017), arXiv:1611.02293 [hep-ph].
[15] K. Kamada and A. J. Long, Phys. Rev. D **94**, 123509 (2016), arXiv:1610.03074 [hep-ph].
[16] D. Jiménez, K. Kamada, K. Schmitz, and X.-J. Xu, JCAP **12**, 011 (2017), arXiv:1707.07943 [hep-ph].
[17] V. Domcke, B. von Harling, E. Morgante, and K. Mukaida, JCAP **10**, 032 (2019), arXiv:1905.13318 [hep-ph].
[18] Y. Cado, B. von Harling, E. Massó, and M. Quirós, JCAP **07**, 049 (2021), arXiv:2102.13650 [hep-ph].
[19] Y. Cado and M. Quirós, Phys. Rev. D **106**, 055018 (2022), arXiv:2201.06422 [hep-ph].
[20] Y. Cado and M. Quirós, Phys. Rev. D **106**, 123527 (2022), arXiv:2208.10977 [hep-ph].
[21] A. Salvio and A. Mazumdar, Phys. Lett. B **750**, 194 (2015), arXiv:1506.07520 [hep-ph].
[22] Y. Ema, Phys. Lett. B **770**, 403 (2017), arXiv:1701.07665 [hep-ph].
[23] S. Pi, Y.-l. Zhang, Q.-G. Huang, and M. Sasaki, JCAP **05**, 042 (2018), arXiv:1712.09896 [astro-ph.CO].
[24] D. Gorbunov and A. Tokareva, Phys. Lett. B **788**, 37 (2019), arXiv:1807.02392 [hep-ph].
[25] A. Gundhi and C. F. Steinwachs, Nucl. Phys. B **954**, 114989 (2020), arXiv:1810.10546 [hep-th].
[26] M. He, R. Jinno, K. Kamada, S. C. Park, A. A. Starobinsky, and J. Yokoyama, Phys. Lett. B **791**, 36 (2019), arXiv:1812.10099 [hep-ph].
[27] D. Y. Cheong, S. M. Lee, and S. C. Park, JCAP **01**, 032 (2021), arXiv:1912.12032 [hep-ph].
[28] M. He, R. Jinno, K. Kamada, A. A. Starobinsky, and J. Yokoyama, JCAP **01**, 066 (2021), arXiv:2007.10369 [hep-ph].
[29] M. He, JCAP **05**, 021 (2021), arXiv:2010.11717 [hep-ph].
[30] A. A. Starobinsky, Phys. Lett. B **91**, 99 (1980).
[31] A. A. Starobinsky, Sov. Astron. Lett. **9**, 302 (1983).
[32] A. Vilenkin, Phys. Rev. D **32**, 2511 (1985).
[33] M. B. Mijic, M. S. Morris, and W.-M. Suen, Phys. Rev. D **34**, 2934 (1986).
[34] K.-i. Maeda, Phys. Rev. D **37**, 858 (1988).
[35] F. L. Bezrukov and M. Shaposhnikov, Phys. Lett. B **659**, 703 (2008), arXiv:0710.3755 [hep-th].
[36] A. O. Barvinsky, A. Y. Kamenshchik, and A. A. Starobinsky, JCAP **11**, 021 (2008), arXiv:0809.2104 [hep-ph].
[37] F. Bezrukov, A. Magnin, M. Shaposhnikov, and S. Sibiryakov, JHEP **01**, 016 (2011), arXiv:1008.5157 [hep-ph].
[38] F. Bezrukov, Class. Quant. Grav. **30**, 214001 (2013), arXiv:1307.0708 [hep-ph].
[39] A. De Simone, M. P. Hertzberg, and F. Wilczek, Phys. Lett. B **678**, 1 (2009), arXiv:0812.4946 [hep-ph].
[40] F. L. Bezrukov, A. Magnin, and M. Shaposhnikov, Phys. Lett. B **675**, 88 (2009), arXiv:0812.4950 [hep-ph].
[41] A. O. Barvinsky, A. Y. Kamenshchik, C. Kiefer, A. A. Starobinsky, and C. F. Steinwachs, Eur. Phys. J. C **72**, 2219 (2012), arXiv:0910.1041 [hep-ph].
[42] B. L. Spokoiny, Phys. Lett. B **147**, 39 (1984).
[43] T. Futamase and K.-i. Maeda, Phys. Rev. D **39**, 399 (1989).
[44] D. S. Salopek, J. R. Bond, and J. M. Bardeen, Phys. Rev. D **40**, 1753 (1989).
[45] R. Fakir and W. G. Unruh, Phys. Rev. D **41**, 1783 (1990).
[46] L. Amendola, M. Litterio, and F. Occhionero, Int. J. Mod. Phys. A **5**, 3861 (1990).
[47] D. I. Kaiser, Phys. Rev. D **52**, 4295 (1995), arXiv:astro-ph/9408044.
[48] J. L. Cervantes-Cota and H. Dehnen, Nucl. Phys. B **442**, 391 (1995), arXiv:astro-ph/9505069.
[49] E. Komatsu and T. Futamase, Phys. Rev. D **59**, 064029 (1999), arXiv:astro-ph/9901127.
[50] Y. Akrami et al. (Planck), Astron. Astrophys. **641**, A10 (2020), arXiv:1807.06211 [astro-ph.CO].
[51] M. P. DeCross, D. I. Kaiser, A. Prabhu, C. Prescod-Weinstein, and E. I. Sfakianakis, Phys. Rev. D **97**, 023526 (2018), arXiv:1510.08553 [astro-ph.CO].
[52] Y. Ema, R. Jinno, K. Mukaida, and K. Nakayama, JCAP **02**, 045 (2017), arXiv:1609.05209 [hep-ph].
[53] E. I. Sfakianakis and J. van de Vis, Phys. Rev. D **99**, 083519 (2019), arXiv:1810.01304 [hep-ph].
[54] F. Bezrukov, D. Gorbunov, C. Shepherd, and A. Tokareva, Phys. Lett. B **795**, 657 (2019), arXiv:1904.04737 [hep-ph].
[55] J. Garcia-Bellido, D. G. Figueroa, and J. Rubio, Phys. Rev. D **79**, 063531 (2009), arXiv:0812.4624 [hep-ph].
[56] F. Bezrukov and C. Shepherd, JCAP **12**, 028 (2020), arXiv:2007.10978 [hep-ph].
[57] D. G. Figueroa, A. Florio, T. Opferkuch, and B. A. Stefanek, SciPost Phys. **15**, 077 (2023), arXiv:2112.08388 [astro-ph.CO].
[58] H. Jeong, K. Kamada, A. A. Starobinsky, and J. Yokoyama, JCAP **11**, 023 (2023), arXiv:2305.14273 [hep-ph].
[59] J.-O. Gong and T. Tanaka, JCAP **03**, 015 (2011), [Erratum: JCAP 02, E01 (2012)], arXiv:1101.4809 [astro-ph.CO].
[60] D. I. Kaiser, E. A. Mazenc, and E. I. Sfakianakis, Phys. Rev. D **87**, 064004 (2013), arXiv:1210.7487 [astro-ph.CO].
[61] H. Kodama and M. Sasaki, Prog. Theor. Phys. Suppl. **78**, 1 (1984).
[62] V. F. Mukhanov, H. A. Feldman, and R. H. Brandenberger, Phys. Rept. **215**, 203 (1992).
[63] K. A. Malik and D. Wands, Phys. Rept. **475**, 1 (2009), arXiv:0809.4944 [astro-ph].
[64] J. Elliston, D. Seery, and R. Tavakol, JCAP **11**, 060 (2012), arXiv:1208.6011 [astro-ph.CO].
[65] M. Sasaki, Prog. Theor. Phys. **76**, 1036 (1986).
[66] V. F. Mukhanov, Sov. Phys. JETP **67**, 1297 (1988).
[67] M. A. Amin, M. P. Hertzberg, D. I. Kaiser, and J. Karouby, Int. J. Mod. Phys. D **24**, 1530003 (2014), arXiv:1410.3808 [hep-ph].

[68] M. P. DeCross, D. I. Kaiser, A. Prabhu, C. Prescod-Weinstein, and E. I. Sfakianakis, Phys. Rev. D **97**, 023528 (2018), arXiv:1610.08916 [astro-ph.CO].
[69] G. N. Felder, L. Kofman, and A. D. Linde, Phys. Rev. D **64**, 123517 (2001), arXiv:hep-th/0106179.
[70] K. D. Lozanov and M. A. Amin, JCAP **06**, 032 (2016), arXiv:1603.05663 [hep-ph].
[71] F. Bezrukov, D. Gorbunov, and M. Shaposhnikov, JCAP **06**, 029 (2009), arXiv:0812.3622 [hep-ph].
[72] V. Domcke and K. Mukaida, JCAP **11**, 020 (2018), arXiv:1806.08769 [hep-ph].
[73] N. Aghanim et al. (Planck), Astron. Astrophys. **641**, A6 (2020), [Erratum: Astron.Astrophys. 652, C4 (2021)], arXiv:1807.06209 [astro-ph.CO].
[74] R. L. Workman et al. (Particle Data Group), PTEP **2022**, 083C01 (2022).
[75] A. D. Sakharov, Pisma Zh. Eksp. Teor. Fiz. **5**, 32 (1967).
[76] K. Kajantie, M. Laine, K. Rummukainen, and M. E. Shaposhnikov, Nucl. Phys. B **493**, 413 (1997), arXiv:hep-lat/9612006.
[77] M. D'Onofrio and K. Rummukainen, Phys. Rev. D **93**, 025003 (2016), arXiv:1508.07161 [hep-ph].
[78] Y. D. Cado, Baryogenesis and Inflation from the Higgs sector, Ph.D. thesis, Barcelona, Autonoma U. (2023).
[79] M. D'Onofrio, K. Rummukainen, and A. Tranberg, Phys. Rev. Lett. **113**, 141602 (2014), arXiv:1404.3565 [hep-ph].
[80] G. Baym and H. Heiselberg, Phys. Rev. D **56**, 5254 (1997), arXiv:astro-ph/9704214.
[81] P. B. Arnold, G. D. Moore, and L. G. Yaffe, JHEP **11**, 001 (2000), arXiv:hep-ph/0010177.
[82] M. Joyce and M. E. Shaposhnikov, Phys. Rev. Lett. **79**, 1193 (1997), arXiv:astro-ph/9703005.
[83] Y. Cado and M. Quirós, Phys. Rev. D **108**, 023508 (2023), arXiv:2303.12932 [hep-ph].